Toward Optimal Operation of Multienergy Home-Microgrids for Power Balancing in Distribution Networks: A Model Predictive Control Approach

Der Fakultät für Elektrotechnik und Informationstechnik

der Technischen Universität Dortmund

vorgelegte

Dissertation

zur Erlangung des akademischen Grades

Doktor der Ingenieurwissenschaften (Dr.-Ing.)

von

M. Sc. Diego I. Hidalgo Rodríguez

aus

Bogotá D.C., Kolumbien

Dortmund, 2020

Referent: Prof. Dr.-Ing. Johanna Myrzik

Korreferent: Prof. Dr.-Ing. Timm Faulwasser

Abstract

End-users in energy systems are becoming heterogeneous with the increasing installation of distributed energy resources in residential buildings. They can behave as electricity consumers, as electricity producers, as energy storage units, or they can be just self-sufficient. This heterogeneity implies that the energy system is undergoing certain paradigm changes. This dissertation defines home-microgrid as a residential building with integrated distributed energy resources. It suggests the optimal operation of home-microgrids as a backbone for the operation of future distribution power systems.

Therefore, the work at hand presents an optimal and scalable operation strategy for home-microgrids using model predictive control. The proposed strategy can coordinate the operation of a single home-microgrid or the operation of a group of interconnected home-microgrids.

This research pays particular attention to multienergy home-microgrids. It, consequently, provides a detailed description of the modeling and optimization of a photovoltaic-heat pump home-microgrid and a photovoltaic-combined heat and power home-microgrid.

Another main focus of this research is the investigation of coordination strategies for interconnected home-microgrids, namely decentralized, centralized, and hierarchical-distributed coordination strategies. In this context, the work presents the use of the alternating direction method of multipliers to improve the performance of hierarchical-distributed coordination strategies.

Finally, this dissertation introduces a framework for the co-simulation of electrical networks with penetration of home-microgrids. The simulation results show the functionality of the framework and enable the evaluation of the effects of the coordination of home-microgrids on a generic low-voltage grid.

Through simulation experiments, this work concluded that using the l_2-norm in the objective function enables an improvement in local power balancing for home-microgrids. Moreover, the work showed the use of model predictive control for storage sizing purposes. The research also concluded that the sharing problem formulation of the alternating direction method of multipliers could handle binary variables within a hierarchical-distributed operation strategy for interconnected home-microgrids. In the end, with the co-simulation framework's help, the work showed that a local power balancing results in a reduction of network power losses.

Kurzfassung

Mit der zunehmenden Durchdringung von dezentralen Energieanlagen in Wohngebäuden werden die Endnutzer in Energiesystemen immer heterogener. Dies bedeutet, dass Sie Stromverbraucher, Stromerzeuger, Energiespeicher oder einfach nur autark sein können. Diese Heterogenität impliziert, dass sich das Energiesystem einem Paradigmenwechsel unterzieht. In dieser Dissertation wird Home-Microgrid als ein Wohngebäude mit integrierten, dezentralen Energieanlagen definiert. Diese Dissertation schlägt den optimalen Betrieb von Home-Microgrids als Grundlage für den Betrieb zukünftiger Verteilnetze vor.

Daher wird in dieser Dissertation eine optimale und skalierbare Betriebsstrategie für Home Microgrids unter Verwendung eines modellprädiktiven Regelungsansatzes vorgestellt. Diese Strategie kann den Betrieb eines einzelnen Home Microgrid oder den Betrieb einer Gruppe von miteinander verbundenen Home Microgrids koordinieren.

Diese Arbeit richtet ein besonderes Augenmerk auf multienergie Home-Microgrids. Die Arbeit liefert daher eine detaillierte Beschreibung der Modellierung und Optimierung eines Photovoltaik-Wärmepumpen-Home-Microgrids und eines Photovoltaik-Home-Microgrids mit Kraftwärmekopplungsanlage.

Ein weiterer Schwerpunkt dieser Forschung ist die Untersuchung von Koordinationsstrategien für vernetzte Home-Microgrids, nämlich dezentralisierte, zentralisierte und hierarchisch-verteilte Koordinationsstrategien. In diesem Zusammenhang stellt die Dissertation die Anwendung der “Alternative Direction Method of Multipliers” für eine verbesserte hierarchisch-verteilte Koordinationsstrategie vor.

Zum Schluss wird in dieser Arbeit ein Framework für die Co-Simulation von elektrischen Netzen mit Durchdringung von Home-Microgrids präsentiert. Die Simulationsergebnisse zeigen die Funktionalität des Frameworks und ermöglichen die Bewertung der Auswirkungen der Koordination von Home-Microgrids auf ein generisches Niederspannungsnetz.

Preface

It has been a long journey, a journey full of incredible people, exciting learning and research experiences, and personal development. It had some stressful days, sleepless nights, manuscript rejections, and frustration feelings. Still, in the end, it was a worthy journey. Doing a doctorate was for me not merely writing a dissertation on some research topic. Doing a doctorate implied learning new methods, attending great conferences, working with some great students, writing research papers, doing teaching activities, reading many articles, writing paper reviews, working on an interdisciplinary research project, and exchanging ideas with colleges. I am happy to say that so was my doctorate, and I enjoy it.

As I said, this journey was full of learning. Learning optimization methods, how to code them, write them, and explain them. I am glad I was allowed to work with mathematical optimization and model predictive control throughout this research. This is one of the most significant features of my doctorate. Learning optimization methods and applying them to practical problems. I enjoyed reading optimization papers, reading optimization books, and watching optimization lectures from top university professors. I also enjoyed attending two PSCC conferences and one IFAC World Congress, where I had the chance to participate in live talks of leading researchers in optimization and model predictive control.

I want to encourage young researchers in the power and energy community to be curious and brave and take the challenge to learn new methods and apply them to their research topic. It is worthwhile.

This work is dedicated to my sons, Luis Diego and Lucas Felipe. They gave me the motivation and the strength to continue and finish this doctorate. To their mother, for taking care of our children, also over the weekends, while I was programming and writing, thank you. Thanks to my brother, a great economics researcher, to support me, have an ear for me, give me advice, and read and comment on my thesis. To my parents and my sister in Colombia, thank you for encouraging me from abroad.

Special thanks to my *Doktormuter* Prof. Johanna Myrzik. She appeared twice in my career at decisive moments. She allowed me to write my master thesis in her research group. Years later, she allowed me to join the group as a research assistant. I admire how she leads her group, always demanding academic excellence and taking care of her research assistants' personal or familiar situations.

I am also thankful to my second examiner Prof. Timm Faulwasser. Not just for examining my thesis, but because his final comments and hints helped me to improve the document. I also want to say thank you to Prof. Christian Rehtanz, Dr. Ulf Häger, and all my colleges from ie3. It was a great time in the institute with many exchange opportunities.

Thanks to all the students that I had the opportunity to supervise. I learned a lot from you.

I had a fantastic experience working on the interdisciplinary research project *KoRiSim*. There, I had the opportunity to work with Fabian Adelt, Sebastian Hoffmann, and Prof. Johannes Weyer. Thanks to all of them.

I would like to thank my former colleges and supervisors, especially Prof. Martin Braun, Dr. Tanja Kneiske, Dr. Jan von Appen, and Dr. Fabian Niedermeyer from Fraunhofer IWES in Kassel. My research journey started there.

Finally, I also want to mention my head of department in the STEAG Dr. Daniel Lehmann, and my colleges Lars Wenning, Dr. Eran Schweitzer, and Michel Brack. Thanks for supporting me in the final stage of this journey.

Diego I. Hidalgo Rodríguez

Dortmund, November 2020.

Nomenclature

Acronyms

ABMS Agent-based modeling and simulation
ADMM Alternating direction method of multipliers
Aux Auxiliary gas Boiler
Batt Battery
CCU Central coordination unit
CHP Combined heat and power
DER Distributed energy resources
DG Distributed generator
DHW Domestic hot water
DSO Distribution system operator
EMS Energy management system
EWH Electrical water heater
FIT Feed-in tariff
H-MG Home microgrid
HP Heat pump
LC Local controller
LM Local meter
LP Linear programming
MFH Multi-family house
MG Microgrid
MILP Mixed integer linear programming
MPC Model predictive control
PCC Point of common coupling
PV Photovoltaic
QP Quadratic programming
RES Renewable energy sources
SFH Single-family house
SH Space heating
SM Smart meter
SOC State of charge
TES Thermal energy storage

Indices

el	Electrical quantity
gas	Chemical quantity
k	Time step $\in \mathbb{N}_{\geq 0}$
th	Thermal quantity

Parameters[1]

α Weighting factor for power peaks
α^{dd} Iteration step size for dual decomposition
β Weighting factor for thermal comfort
Δt MPC sample time $\in \mathbb{N}_{\geq 0}$ (min)
η^{Aux} Efficiency coefficient auxiliary gas boiler $\in (0, 1]$
$\eta^{\mathrm{Batt,char}}$ Charging efficiency coefficient battery $\in (0, 1]$
$\eta^{\mathrm{Batt,dis}}$ Discharging efficiency coefficient battery $\in (0, 1]$
$\eta^{\mathrm{Batt,sd}}$ Self-discharge coefficient battery $\in (0, 1]$
η^{Ewh} Efficiency electrical heater $\in (0, 1]$
$\eta^{\mathrm{Tes,char}}$ Charging efficiency coefficient TES $\in (0, 1]$
$\eta^{\mathrm{Tes,dis}}$ Discharging efficiency coefficient TES $\in (0, 1]$
$\eta^{\mathrm{Tes,sd}}$ Self-discharge coefficient TES $\in (0, 1]$
$\eta_{\mathrm{el}}^{\mathrm{Chp}}$ Electrical efficiency coefficient CHP $\in (0, 1]$
$\eta_{\mathrm{th}}^{\mathrm{Chp}}$ Thermal efficiency coefficient CHP $\in (0, 1]$
γ Regularization factor for power peaks in ADMM
Φ Solar radiation (kW/m^2)
ρ Augmented Lagrangian parameter
A_w Window area facing south (m^2)
$A_{\mathrm{th}}^{Chp,up}$ State matrix for CHP thermal start-up behavior
$B_{\mathrm{th}}^{Chp,up}$ Input matrix for CHP thermal start-up behavior
$C^{\mathrm{Chp,fit}}$ Feed-in-Tariff for CHP (EUR ct)
$C^{\mathrm{Chp,up}}$ Costs for CHP start-up (EUR)
$C^{\mathrm{Pv,fit}}$ Feed-in-Tariff for PV (EUR ct)
c_i Heat capacity of the room air (kWh/°C)
c_m Heat capacity of the large heat-accumulating medium in a building (kWh/°C)
C_{el} Electricity costs (EUR)
C_{gas} Gas costs (EUR)
COP Coefficient of Performance for HP
N_p Prediction horizon $\in \mathbb{N}_{\geq 0}$ (time steps)
$p_{\mathrm{el}}^{\mathrm{Load}}$ Household load ($\mathrm{kW_{el}}$)
$p_{\mathrm{th}}^{\mathrm{Dhw}}$ Power demand domestic hot water ($\mathrm{kW_{th}}$)
$p_{\mathrm{th}}^{\mathrm{Sh}}$ Power demand for space heating ($\mathrm{kW_{th}}$)
p_{el}^{Pv} Total power output PV-Inverter (kW_{el})
pl Share of the solar radiation which is directly affecting $T^{\mathrm{m}} \in (0, 1]$
r_a Resistance against heat transfer from the house air to ambient air (°C/kW)
r_i Resistance against heat transfer between the house air and the large heat-accumulating medium (°C/kW)
T Temperature (°C)

Variables[1]

λ Lagrange multiplier

b^{Aux} On/Off Status auxiliary gas boiler $\in \{0, 1\}$. On(1)/Off(0)

$b^{\text{Batt,char}}$ Battery charging status $\in \{0, 1\}$. Charging(1)/Discharging(0)

$b^{\text{Chp,down}}$ Shut-down status CHP $\in \{0, 1\}$. Shut-down(1)/other operation status(0)

$b^{\text{Chp,up}}$ Start-up status CHP $\in \{0, 1\}$. Start-up(1)/other operation status(0)

b^{Chp} On/Off status CHP $\in \{0, 1\}$. On(1)/Off(0)

b^{Ewh} On/Off Status electrical heater. On(1)/Off(0) $\in (0, 1]$

b^{Hp} On/Off Status heat pump. On(1)/Off(0) $\in (0, 1]$

$p_{\text{el}}^{\text{Batt,char}}$ Battery charging power (kW_{el})

$p_{\text{el}}^{\text{Batt,dis}}$ Battery discharging power (kW_{el})

$p_{\text{el}}^{\text{Chp}}$ Electrical power output CHP (kW_{el})

$p_{\text{el}}^{\text{Ewh}}$ Electrical heater electrical power consumption (kW_{el})

$p_{\text{el}}^{\text{Grid,exp}}$ Total power exported to the grid (kW_{el})

$p_{\text{el}}^{\text{Grid,imp}}$ Total power imported from the grid (kW_{el})

$p_{\text{el}}^{\text{Hp}}$ Electrical power input HP (kW_{el})

$p_{\text{gas}}^{\text{Aux}}$ Power input auxiliary gas boiler (kW_{gas})

$p_{\text{gas}}^{\text{Chp}}$ Power input CHP (kW_{gas})

$p_{\text{th}}^{\text{Aux}}$ Power output auxiliary gas boiler (kW_{th})

$p_{\text{th}}^{\text{Chp}}$ Thermal power output CHP (kW_{th})

$p_{\text{th}}^{\text{Ewh}}$ Generated thermal power electrical water heater kW_{el}

$p_{\text{th}}^{\text{Hp}}$ Thermal power output HP (kW_{th})

$p_{\text{th}}^{\text{Tes,char}}$ TES charging power (kW_{th})

$p_{\text{th}}^{\text{Tes,dis}}$ TES discharging power (kW_{th})

SoC^{Batt} Battery state of charge (%)

SoC^{Tes} TES state of charge (%)

T^{m} Temperature of the large heat-accumulating medium in the house

T^{room} Room air temperature

u Input vector

x State vector

y Output vector

$\boldsymbol{P}_{h,el}^{\text{G}}$ Power exchange between a H-MG and the main grid over the whole prediction horizon $\in \mathbb{R}^{N_p}$

[1] All variables and parameters are in $\mathbb{R}_{\geq 0}$ unless something different is stated

Contents

Abstract III

Preface V

Nomenclature VII

1. Introduction 1
- 1.1. Challenges of the energy transition . . . 1
- 1.2. A bottom-up approach based on the cellular energy system concept . . . 4
- 1.3. Home-microgrid as the smallest unit of the power system . . . 6
- 1.4. Model predictive control . . . 9
- 1.5. Research questions and contributions . . . 22
- 1.6. Structure of this work . . . 24

2. Flexible power operation of a photovoltaic-heat pump home-microgrid 27
- 2.1. Introduction . . . 27
- 2.2. Problem formulation . . . 28
- 2.3. Simulation results and discussion . . . 36
- 2.4. Summary of the chapter . . . 42

3. Economic operation of a photovoltaic-combined heat and power home-microgrid 44
- 3.1. Introduction . . . 44
- 3.2. System description and problem formulation . . . 45
- 3.3. Simulation results and discussion . . . 53
- 3.4. Summary of the chapter . . . 61

4. Coordination strategies for optimal operation of interconnected home-microgrids 62
- 4.1. Introduction . . . 62
- 4.2. System description . . . 64
- 4.3. Decentralized coordination strategy . . . 69
- 4.4. Centralized coordination strategy . . . 73
- 4.5. Hierarchical-distributed coordination strategy based on dual decomposition 73
- 4.6. Simulation results and discussion . . . 76
- 4.7. Summary of the chapter . . . 82

5. A hierarchical-distributed coordination strategy for interconnected home-microgrids using the ADMM sharing problem 83
- 5.1. Introduction . . . 83
- 5.2. ADMM sharing problem formulation . . . 84

5.3. ADMM implementation . . . 86
5.4. Simulation results and discussion . . . 89
5.5. Summary of the chapter . . . 99

6. A co-simulation framework for electrical networks and home-microgrids 100
6.1. Introduction . . . 100
6.2. Co-simulation framework . . . 101
6.3. Simulation results and discussion . . . 106
6.4. Summary of the chapter . . . 110

7. Summary, conclusions and outlook 111
7.1. Limitations and outlook . . . 112

Bibliography 115

Appendix A. Mathematical optimization background 126
A.1. Convexity . . . 126
A.2. Optimization problems . . . 127
A.3. Duality . . . 127
A.4. Optimality conditions . . . 128
A.5. Decomposition of optimization problems . . . 129

Appendix B. Two rooms building model for application in MPC schemes 135
B.1. Introduction . . . 135
B.2. Model description . . . 135
B.3. Numerical Results . . . 141
B.4. Conclusion . . . 141

Appendix C. Closed-form analytical solution for the $\bar{z}$-update 145

Appendix D. Objective gap for ADMM and dual decomposition 147

Appendix E. Primal residual and dual residual open-loop behavior for ADMM approaches 149

Appendix F. Scientific activity record 153

1. Introduction

Electrical power systems are undergoing several concurrent paradigm changes. Small decentralized power sources are replacing big centralized power plants. Power generators' connection is no longer exclusive for high voltage networks; it also takes place at medium and low voltage networks. End-users in electrical networks are not just net electricity consumers; they can now generate their electricity and store it. Such changes bring challenges and opportunities for electrical power systems, and this work approaches some of them.

This work considers the optimal operation of home-microgrids as a backbone for future distribution power systems' operation. It aims to present an optimal and scalable operation strategy for home-microgrids using model predictive control. The proposed strategy can coordinate a single home-microgrid or a group of interconnected home-microgrids.

Accordingly, this chapter briefly describes the challenges of the energy transition. It proposes a home-microgrid as the smallest controllable distributed energy resource. The chapter highlights the relevance of the optimal operation of home-microgrids for the operation of future power systems. It follows by describing the model predictive control concept and gives a literature review on its application for microgrid operation. Next, the chapter lists the work's research questions and contributions. The last section provides an overview of the content and structure of this dissertation.

1.1. Challenges of the energy transition

There is a worldwide consensus of governments about the importance of reducing greenhouse gas (GHG) emissions and moving towards a more secure, competitive, and sustainable energy system. The European Commission sets the target of lowering GHG emissions by 80% to 95% by 2050 compared to 1990 levels [1]. According to the guideline 2009/28/EG of the European Parliament and Council, achieving this target implies, among others, two main measures: the utilization of all possible renewable energy sources (RES) and the improvement of energy efficiency. In this context, the guideline also sees the reduction of transmission losses as an essential aspect, and it points out the necessity of storage systems for the successful integration of renewable energies [2].

Following this line of action, the *Bundesregierung* (German government) has adopted climate and energy policy programs. The "Energy Concept 2010" [3] and the "Climate Protection Plan 2050" [4] agreed upon in November 2016 include commitments to reduce GHG emissions at least 55% by 2030, and at least 80-95% by 2050 (in each case below 1990 levels), and to expand renewable energies and energy efficiency by 2050. Consequently, the *Bundesregierung* committed to increasing the share of RES in end-energy consumption

to 18% by 2020, and 60% by 2050. Furthermore, the share of electricity generation from RES in gross electricity consumption should rise to 35% by 2020, and 80% by 2050.

The building sector also plays a vital role in the "Climate Protection Plan 2050". This sector generates around one-third of GHG emissions, mainly for heating purposes. By 2050, buildings' primary energy demand is to be reduced by 80 percent compared to 2008. The "Climate Protection Plan 2050" also states that the provision of electricity and heat from RES can only contribute to the decarbonization of other sectors if:

1. the energy demand in all sectors is reduced significantly and permanently ("efficiency first"),
2. the direct use of renewable energies take place in all sectors if technically possible and economically viable, and
3. electricity from RES is used efficiently for heating, transport, and industry (sector coupling).

The *Bundesregierung* has launched with the "National Action Plan for Energy Efficiency" (short NAPE in German) a strategy to increase the energy efficiency in the building sector through the promotion of energy-related modernization and the use of heat pumps and mini combined heat and power (mini CHP) systems, among other measures [5]. Also, the "Renewable Energy Act" (short EEG in German) promotes clean electricity production by providing a special feed-in tariff (FIT) for the electricity produced from RES [6]. The "Combined heat and power act" (KWKG) defines a different FIT, which supports the use of combined heat and power (CHP) plants for the efficient generation of electricity and heat [7].

Following these incentives, such low carbon electricity technologies are rapidly penetrating electrical power systems, particularly at the distribution grid level. According to [8], when this research started in 2015, 20 of 900 German distribution system operators were hosting over 75% of the installed RES in Germany. It means that RES' installation occured at some particular distribution network areas, as shown in Figure 1.1.

Household owners are increasingly installing rooftop photovoltaic plants (PV) and mini CHP plants. Energy-efficient power-to-heat appliances, namely heat pumps, are replacing old fossil-fuel-burning heating appliances in single and multi-family houses. The rapid penetration of PV, the electro-mobility, and the increasing number of heat pumps and mini-CHP plants may bring electrical distribution power systems to their limits [9].

Next to the known challenge posed by the increasing fluctuating, decentral, and weather-dependent power generation from RES, there are further challenges for the operation of electrical power systems.

Distribution power systems now face reverse power flows due to the simultaneous feed-in of PV plants and mini CHP plants during low consumption periods. Figure 1.2 presents

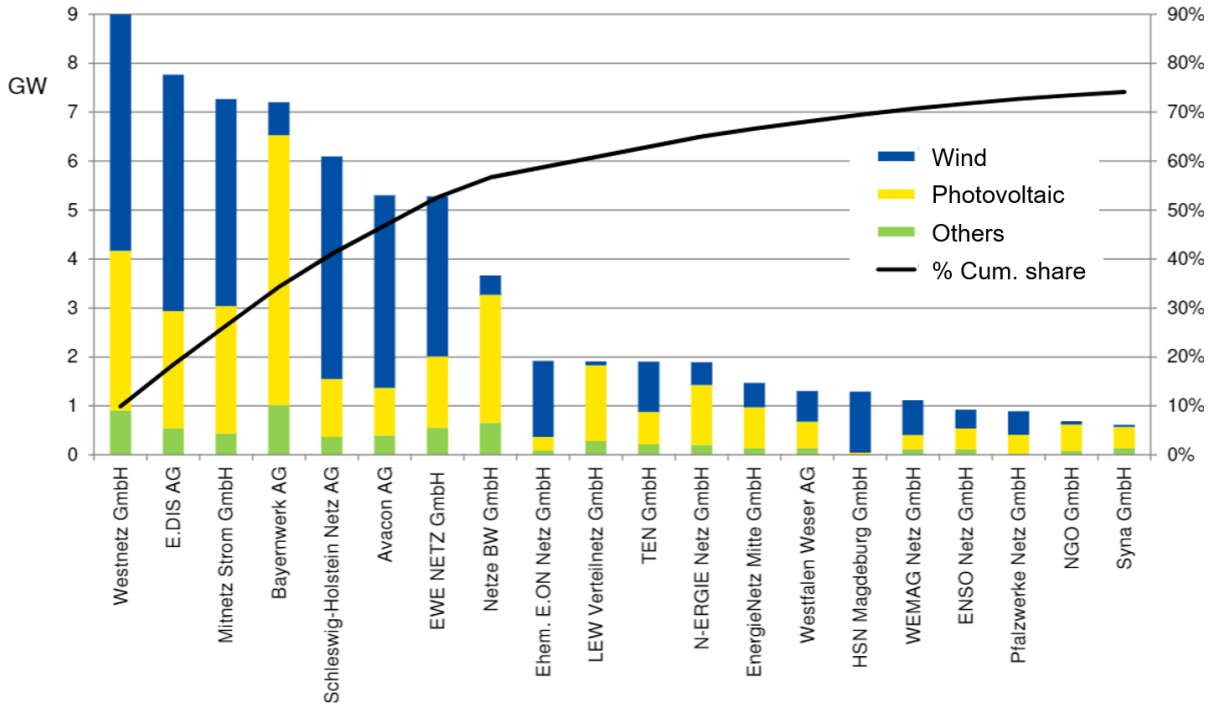

Figure 1.1.: Penetration of RES in German distribution networks[8]

historical operational data from a high/medium voltage substation in Southern Germany. It shows an increment of reverse power flows over the years. Notice that, at least for the last year, reverse power flows also occur during winter. Such circumstance leads to technical issues such as [10]:

- Overvoltage in medium voltage networks, and overloading of electrical equipment.
- Malfunction of protection devices, as they were not designed for this situation.
- Congestion in sub-transmission and transmission networks.
- Increment of power losses: surplus power goes from a low-voltage network, through a medium-voltage network to the high-voltage network, back to the consumers in a different low-voltage network.

Furthermore, the activation of heat pumps at times of high electricity demand can overload existing electrical infrastructure [12]. Thus, distribution power networks require additional actions to guarantee uninterrupted regional electricity supply and system stability.

To minimize rather than maximize network expansion through the use of these technologies (PV, mini CHP, heat pumps, et al.), a proper intelligent deployment of their inherent flexibilities is necessary.

In this context, flexibility means adjusting the power consumption/feed-in of a system at a defined time and location according to the network situation. System's flexibility capability results from the maximum permissible changes in its power profile without

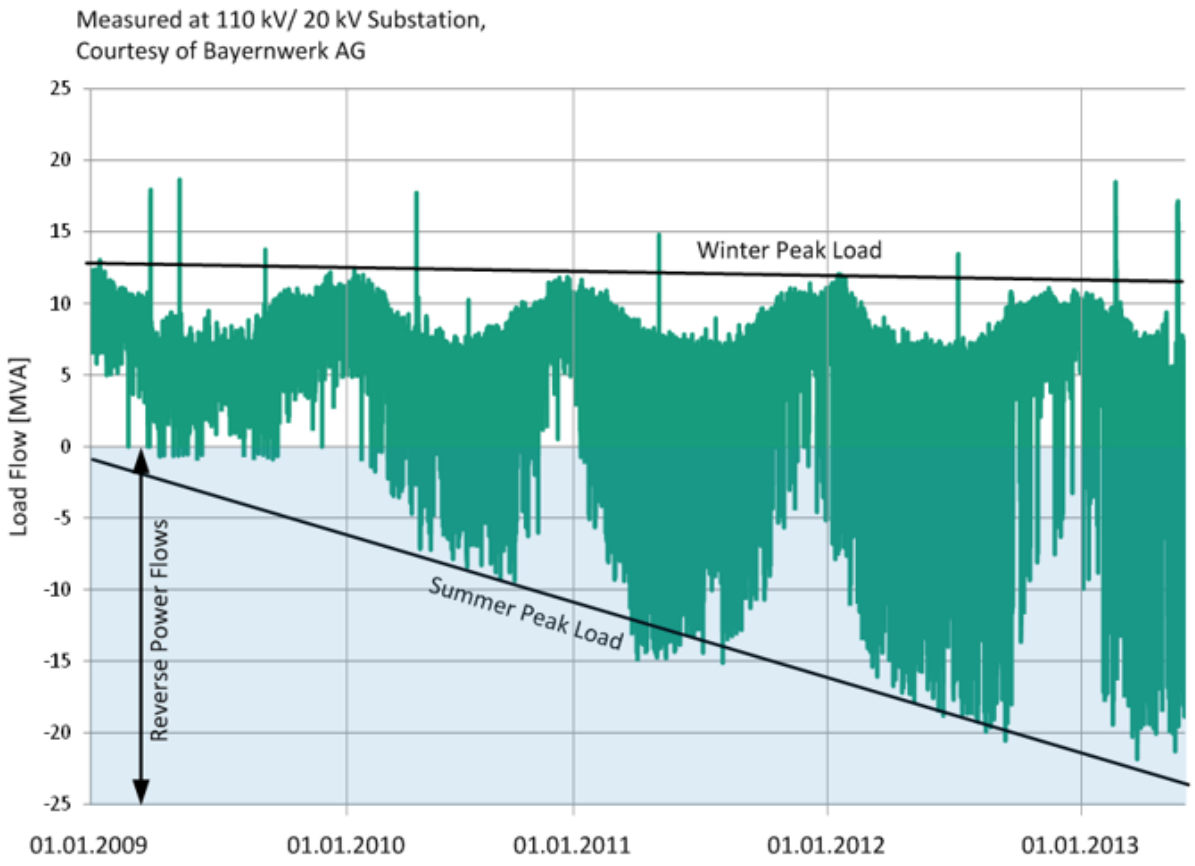

Figure 1.2.: Evolution of reverse power flows over the years at a high/medium voltage substation in Southern Germany [11]

compromising its primary purpose (e.g., heat supply). Here, mini-CHP and heat pumps as sector coupling technologies are suitable for relieving low and medium voltage networks. Energy storage systems are also crucial for increasing flexibility. Besides electrical batteries, thermal energy storage (TES) units serve as time-decoupling units between the electricity and heating sectors and add flexibility to the demand side.

Figure 1.3 depicts a qualitative example of the targeted and coordinated use of batteries and heat pumps for modifying the resulting power profile at the local network transformer[1].

1.2. A bottom-up approach based on the cellular energy system concept

The present work follows the cellular approach proposed by the Power Engineering Society of the German Association for Electrical, Electronic and Information Technologies

[1] This work uses the consumer sign convention where consumed power is positive and generated power is negative

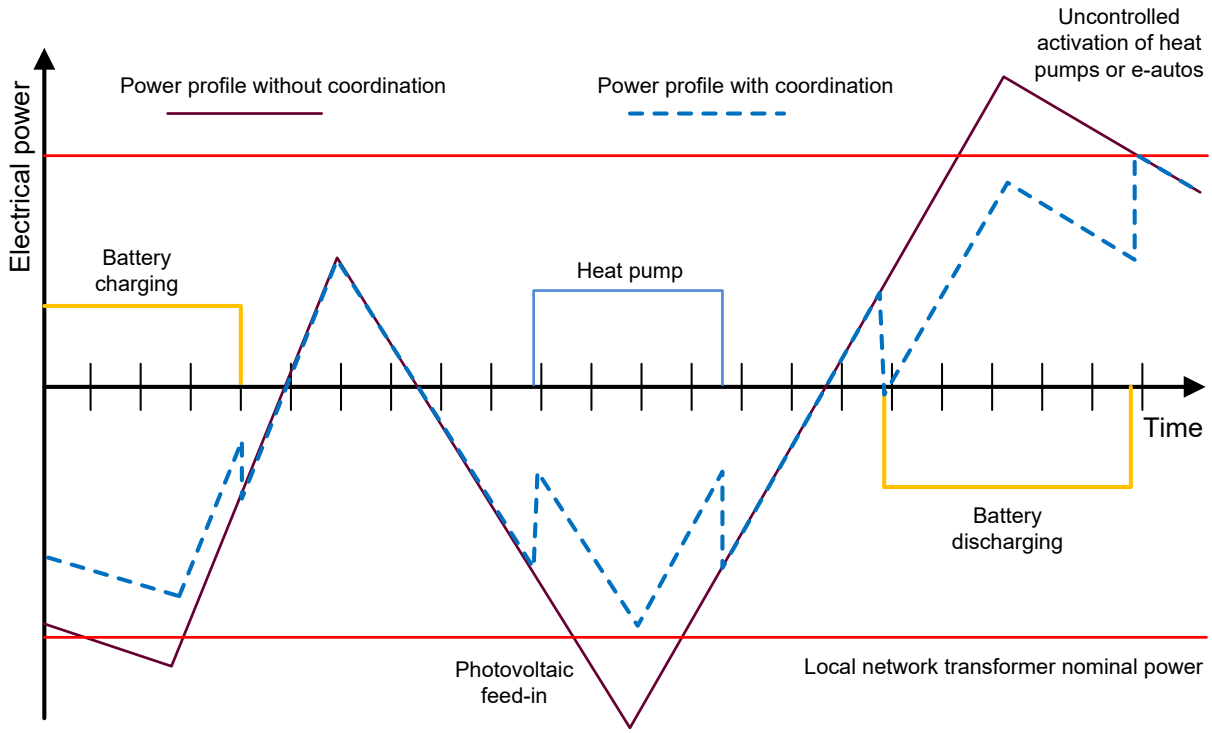

Figure 1.3.: Example of the use of local flexibilities to avoid transformer overloading

(VDE-ETG in German) in the studies "The Cellular Approach" [13] and "Cellular Energy System" [9]. This approach gives a new organizational model for energy supply suitable for managing multiple decentralized energy systems. The cellular energy system concept proposes to balance energy supply and demand at a regional and local level.

Based on the principle of subsidiarity, such a system- and grid-friendly balance of generation and consumption must occur at the lowest possible voltage level. This principle says that any unbalance or problem in the power system is primarily to be tackled directly at the problem's source. Corrective actions in the nearest upstream/downstream network areas should occur only secondarily.

The improved local energy balance would allow better use of existing infrastructure, the rapid expansion of renewable energies, and the relief of electrical transmission grids from grid stabilization actions. In this context, the purpose of the cellular approach is to optimize the electricity grid's expansion and increase energy efficiency at the local, regional, and supra-regional levels.

The cellular approach's central component is the energy cell, which consists of the infrastructure for different energy sectors (electricity, gas, and heat). An energy management system (EMS) organizes the balancing of generation and consumption in an energy cell. If possible, it cooperates with neighboring cells (neighboring EMS) using all available energy forms (electrical, chemical, and thermal). The cellular approach does not aim at achieving the highest possible degree of self-sufficiency. Instead, it seeks to enable an

optimal exchange with neighboring, subordinate, or superimposed cells using the existing infrastructure [9].

The concept of cooperative energy cells is similar to the concept of energy collectives or communities, where groups of end-users can coordinate their energy utilization [14–17]. The European Committee of the Regions points out that local energy communities can play an essential role in the energy transition. They can promote the development of sustainable energy technologies to benefit local communities and the European Union as a whole. Furthermore, the Committee states that the introduction of local energy communities can improve the efficiency of managing energy at the community level [18].

Other authors refer to the concept of local aggregation of distributed energy resources (DER) given the coordination of both supply-side and demand-side as *microgrids* [19, 20]. Accordingly, the term *networked microgrids* or *interconnected microgrids* denotes a group of microgrids that exchange power with each other in order to achieve a common goal [21].

1.3. Home-microgrid as the smallest unit of the power system

This work uses the term *home-microgrid* (H-MG) to refer to a group of generators, loads, and storage systems located inside a family house (end-user level). Through proper coordination, these energy resources can respond to variable network conditions as a single flexible unit. Analog to an energy cell, the main properties of a H-MG are:

- its ability to balance power supply and demand within the house, and
- its ability to share power with neighboring home-microgrids.

Here, the local energy management system, or home-microgrid controller, plays a key role in enabling the coordination of internal energy resources and simultaneously handling power exchange with neighboring home-microgrids. The home-microgrid controller can get and send information from/to relevant energy resources inside a H-MG; it aggregates this information and communicates only aggregated data to the outside world [9].

1.3.1. Home-microgrid controller

References [9] and [22] provide a comprehensive description of requirements for a so-called energy cell management system. For a home-microgrid controller (H-MG controller), the same requirements are valid. Therefore, an H-MG controller has to:

- be able to record, process, and manage all relevant information from loads, generators storage systems inside an H-MG,
- be equipped with algorithms that enable the H-MG to operate in various scenarios with the best possible optimization of its consumption,
- automatically regulate all power flows within the H-MG,
- negotiate power supply and demand with neighboring H-MGs, and
- exchange data and information with H-MG controllers from neighboring H-MGs, energy market participants, and load and weather forecasting systems.

Moreover, according to [23] such an energy management system can achieve the following goals:

- Distribution network optimization by coordinating fluctuating RES and loads. Here, load shifting and short-term storage can reduce generation and load peaks in low-voltage networks. This peak reduction might improve voltage profile and power utilization in the local grid.
- Use of decentralized generated green electricity directly on site.
- Relief of the medium-voltage networks through local coordination in the low voltage network.
- Targeted regulation of power feed-in by self-consumption or charging of storage systems in the event of overvoltage.

The authors in [9] also differentiate between cell manager and cell cluster manager. As these concepts are of high relevance for the present work, they are adapted as follows:

Local H-MG Controller (Cell Manager): It has control over a limited, locally linked infrastructure that can include generators, consumers, and storage systems.

Central Coordination Unit (Cell Cluster Manager): It manages several local H-MG controllers

The local H-MG controller and the central coordination unit (CCU) are responsible for their respective network nodes. A network node can be, for example, the house connection of an H-MG, the local transformer station of a low-voltage network, or a 20 kV substation.

Figure 1.4 illustrates the bottom-up approach followed in this dissertation. It focuses on flexibilities at the end-user and low-voltage network level to improve local power balance in distribution networks.

Finally, the authors in [9] propose developing agent-based energy management systems and developing models to simulate cellular energy systems' behavior as roadmaps to advance the cellular approach.

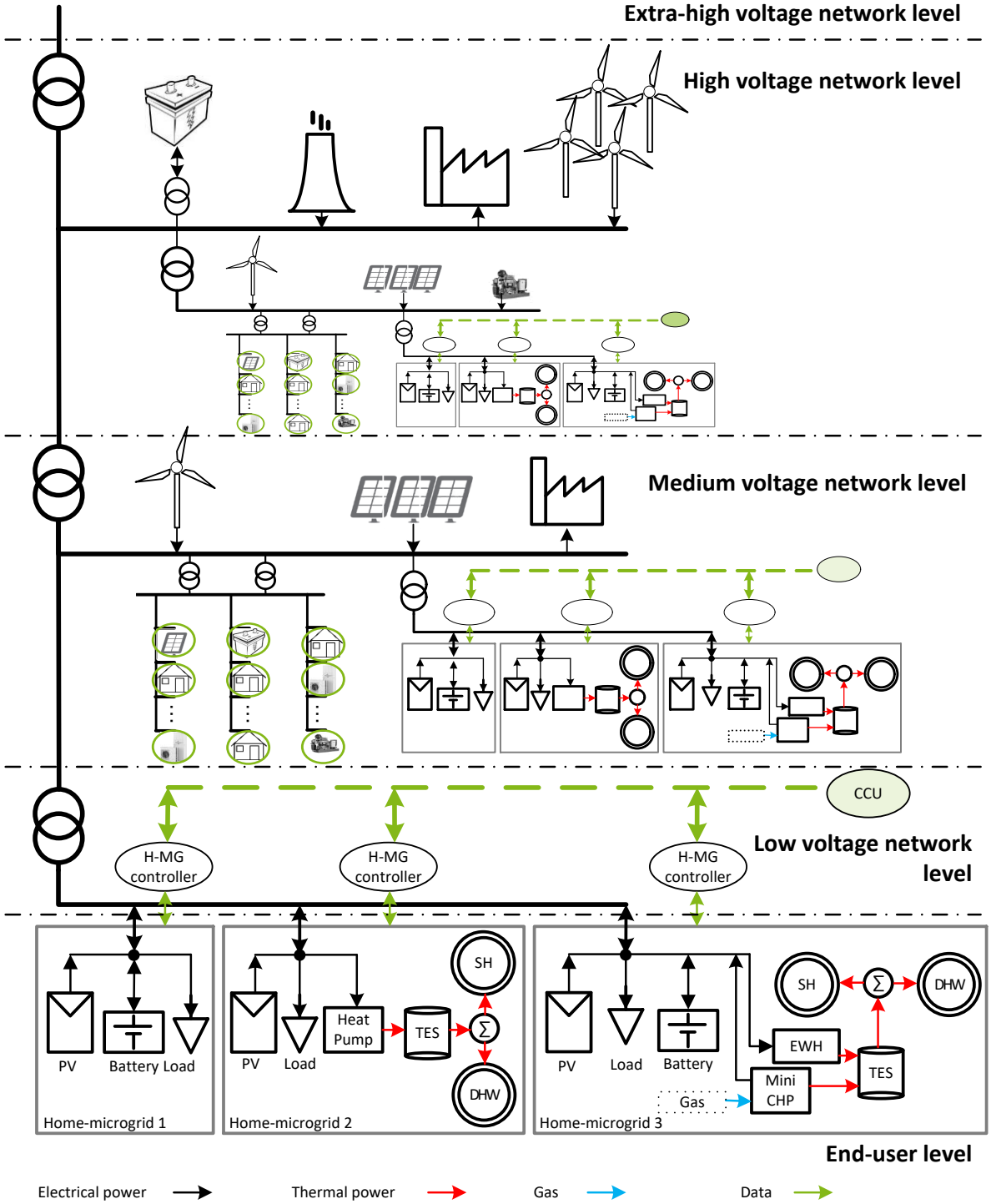

Figure 1.4.: A bottom-up approach: Power balancing starts at end-user and low voltage network levels (based on [9])

From here, the conclusion is that the design and implementation of an optimal operation strategy to enable flexible power supply and power consumption of H-MGs is an actual topic for investigation. Advanced coordination strategies might be appropriate for this task. An advanced coordination strategy optimizes the interaction between generators, storage units, and flexible loads at the end-user level by managing both thermal and electrical power flows. Within the power and energy research community, approaches based on numerical optimization methods are very promising [24–31]. These approaches are attractive because they explicitly consider system operation through mathematical models and include operational constraints and operational goals in the problem formulation. Within this framework, model predictive control (MPC) is gaining relevance due to its prediction nature and its robustness against uncertainties [24]. Researchers are using MPC for the operation and control of transmission and distribution grids, and also for the operation and coordination of interconnected microgrids [32–35].

1.4. Model predictive control

Model Predictive Control (MPC) is a concept from control theory, which is being used increasingly in industry. It originated in the late seventies and has grown substantially since then. MPC optimizes the future behavior of a system by computing optimal trajectories for its inputs within a receding horizon control scheme (RHC). This optimization is performed within a finite time window by applying numerical optimization techniques [36]. According to Camacho and Bordons [37], the main ideas in MCP are :

- explicit utilization of a model for the prediction of the process output at future points in time (horizon);
- computation of a control sequence that minimizes an objective function; and
- receding strategy, so that the horizon moves at each point in time towards the future, involving the application of the first control signal of the sequence calculated at each step.

The day-to-day work planning activity example of predictive control presented in the book of Wang [38] helps to understand the basic ideas in the design of MPC. In this example, there is a working team, which needs to complete a given set of tasks. The rule is that they always make a schedule for the next 8 hours, but they only implement the activities for the first hour. They repeat this scheduling activity for every hour until they fulfill all the tasks.

The day starts at 9 o'clock in the morning. The team determines the required hour-by-hour activities for the next 8 hours in order to achieve the goal in the best possible way. They take into account resources and limitations. As a result, the team gets a list of projected activities from 9 o'clock to 5 o'clock, and they start working by just

implementing the activities for the first hour of the plan. At 10 o'clock, the team evaluates what they have done, and uses this updated information for planning the activities for the next 8 hours. They continue by implementing just the first hour of activities. The length of time for the planing always remains the same, i.e., 8 hours. Every hour, they repeat the same planning process (new projected activities for the next 8 hours) and the same implementation process until they achieve the objective.

Accordingly, the central aspects of MPC are:

1. *Moving horizon window*: a time window from an arbitrary initial time k_i to $k_i + N_p$. Where N_p is the length of the window, which remains constant, and k_i is the starting time for the optimization window. In the previous example, $N_p = 8$ hours, as the length of the time window was 8 hours. k_i starts at $k_i = 9:00$ hours and increases on an hourly basis.

2. *Prediction horizon*: it determines how far in the future, the planning process requires a prediction. This parameter corresponds to N_p.

3. *Receding horizon control*: the planning process calculates the optimal trajectory of the input variables for the whole moving horizon window; however, the implementation process takes just the first element of this trajectory and neglects the rest of the trajectory.

4. *Model*: a way for predicting what might occur.

5. *Measurement*: to accurately predict the future, the planning process also requires information at time k_i. The vector $x(k_i)$ denotes this information, which should be directly measured or estimated.

6. The optimal decisions (the trajectory of input variables) are related to an objective function. The planning process finds the optimal decisions by minimizing this objective function (also called cost function) within the optimization window.

To find optimal input trajectories for a process, there exist approaches based on numerical optimization techniques such as open-loop and closed-loop optimization. The so-called *open-loop optimization* uses a precomputed control trajectory to control a real process without any feedback. However, in any control application the performance of a control strategy is subject to uncertainties (unforeseen disturbances or model-plant-mismatch) [39]. Therefore, and especially for energy systems with RES, an open-loop optimization strategy might not meet the expected results. For example, if it is necessary to charge a battery system up to a certain state of charge (SOC) based on a forecast for PV generation, the storage might end at a completely different SOC than the precomputed one. This is due to the discrepancy between the predicted PV production and the real PV generation.

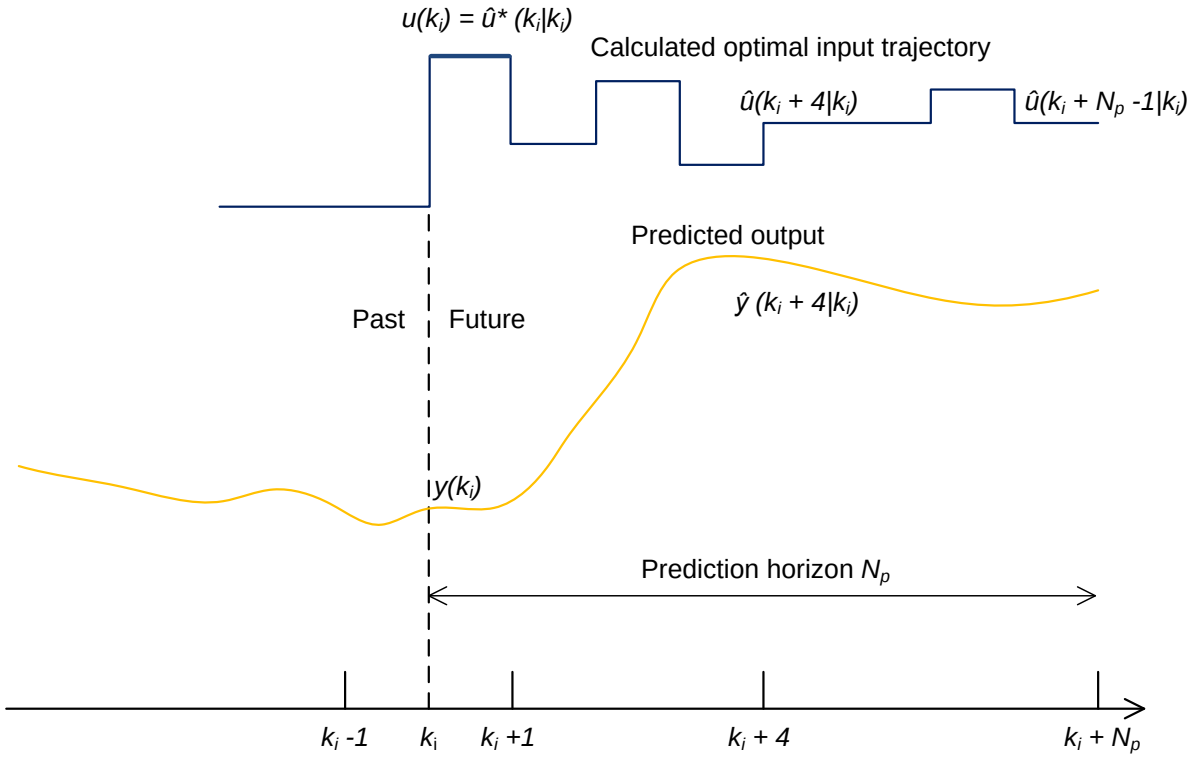

Figure 1.5.: MPC's principle

By measuring the real process throughout time development, and thanks to its *closed-loop optimization* nature, MPC will adjust the control inputs online to obtain a better performance. Thus, if during the charging process of the battery, the actual PV generation differs from the original PV forecast, MPC will adapt to the new situation and will compute and follow a new optimal trajectory.

MPC's objective function can be a linear function or a non-linear function, and its formulation can be as an economic cost function [28], as a set-point tracking function [27] or as a function for driving the system to a particular state [40]. The optimization problem is considered from any arbitrary initial time k_i to a final time $k_i + N_p$. To predict the future behavior of the system, MPC considers a model of the process and forecasts for disturbances. Figure 1.5 illustrates MPC's principle over time. Optimal trajectories for the controllable input variables have to be found, which minimize a predefined objective function within the considered time window. At the start of the time window, MPC gets initial values of the state variables, together with a forecast for disturbances over the whole prediction horizon. Then the optimization problem is solved. Once an optimal solution (input trajectory) is available, MPC implements just the first element of the solution and discards the rest. In the next time step, the time window moves one step forward, and the process starts again with updated information on the measured variables and on the forecast for disturbances [37, 38].

To summarize, the general steps for the implementation of MPC in discrete time are

[37, 39]:

1. Measure or estimate the actual state of the system $x(k_i)$.
2. Predict and optimize the future outputs $\hat{y}(k_i + k \mid k_i)$ for $k = 1 \ldots N_p - 1$, within a finite moving horizon window of N_p steps. The notation indicates the value of $\hat{y}$ at the instant $k_i + k$ calculated at point in time k_i. These predicted outputs are dependent on the known state values up to instant k_i and on the computed future optimal control trajectory $\hat{u}(k_i + k \mid k_i)$ for $k = 0 \ldots N_p - 1$. This optimal control trajectory is found by solving an open-loop optimization problem, given a determined objective function, starting at the state $x(k_i)$.
3. Implement the first optimal control action $\hat{u}^*(k_i \mid k_i)$ in the real process and disregard the rest. This is because at the next sampling instant, the state $x(k_i + 1)$ will be already known and, therefore, $\hat{u}(k_i + 1 \mid k_i + 1)$ will be in principle different from $\hat{u}(k_i + 1 \mid k_i)$ because of this new information.
4. Move the moving horizon window one time step forward and repeat the procedure with $k_i = k_i + 1$.

1.4.1. MPC formulation

To illustrate MPC's basic formulation, this work adapts the introduction to the basic principle of MPC presented in the work of Faulwasser et al [41] and the basic formulation given in the work of Maciejowski (see [42] page 41). For this purpose, this work considers a time-invariant discrete-time model of a system in the form

$$x(k+1) = Ax(k) + Bu(k) + Ed(k), \qquad x(0) = x_0 \in \mathcal{X}_0, \tag{1.1a}$$

$$y(k) = Cx(k), \tag{1.1b}$$

where $x \in \mathbb{R}^n$ is an n-dimensional state vector, $u \in \mathbb{R}^m$ is an m-dimensional input vector, and $d \in \mathbb{R}^l$ is an l-dimensional disturbance vector. $A \in \mathbb{R}^{n \times n}$ is the system matrix, $B \in \mathbb{R}^{n \times m}$ is the input matrix, $E \in \mathbb{R}^{n \times l}$ is the disturbance matrix, x_0 is an initial state vector, and $k \in \mathbb{Z}$ is the discrete-time variable. The output vector is given by $y \in \mathbb{R}^p$, and the output matrix is given by $C \in \mathbb{R}^{p \times n}$. The compact sets $\mathcal{U} \subset \mathbb{R}^m$ and $\mathcal{X} \subset \mathbb{R}^n$ restrict inputs and states respectively. An objective function given by

$$J = \sum_{k=k_i}^{k_i+N_p-1} f(x(k), u(k)), \tag{1.2}$$

describes the performance requirements associated to system (1.1) with a continuous stage cost function $f : \mathcal{X} \times \mathcal{U} \to \mathbb{R}$.

Normally, an MPC scheme implies solving the following optimization control problem in a receding horizon fashion

$$\underset{\hat{\boldsymbol{u}}}{\text{minimize}} \sum_{k=k_i}^{k_i+N_p-1} f\left(\hat{x}\left(k \mid k_i\right), \hat{u}\left(k \mid k_i\right)\right) \tag{1.3a}$$

subject to

$$\hat{x}\left(k+1 \mid k_i\right) = A\hat{x}\left(k \mid k_i\right) + B\hat{u}\left(k \mid k_i\right) + E\hat{d}\left(k \mid k_i\right), \tag{1.3b}$$

$$\hat{y} = C\hat{x}\left(k \mid k_i\right), \tag{1.3c}$$

$$\hat{x}\left(k_i \mid k_i\right) = x_0, \tag{1.3d}$$

$$\hat{u}\left(k \mid k_i\right) \in \mathcal{U}, \quad \hat{x}\left(k \mid k_i\right) \in \mathcal{X}, \tag{1.3e}$$

$$\forall k \in \{k_i, \ldots, k_i + N_p - 1\}. \tag{1.3f}$$

The problem is to be solved at each time step, from any arbitrarily initial time step k_i until a final time step. The prediction horizon is given by $N_p \in \mathbb{N}_{\geq 0}$. System behavior and additional operation constraints are represented in (1.3b)-(1.3f). The embedded model in MPC's optimization problem predicts the future behavior of system (1.1) based on measurements up to time k_i, and, if required, on knowledge of the inputs only up to $u\left(k_i - 1\right)$, as the solution for the optimal values of the next input vector $u\left(k_i\right)$ is not yet available. $\hat{u}\left(k_i + i \mid k_i\right)$ indicates the future assumed value of the input u at time $k+i$ computed at time k_i. $\hat{x}\left(k_i + i \mid k_i\right)$ denotes[2] the prediction of state variables x made at time k_i, assuming the realization of some sequence of inputs $\hat{u}\left(k_i + j \mid k_i\right)$ and some sequence of disturbances $\hat{d}\left(k_i + i \mid k_i\right)$ for $j = 0, 1, \ldots, i-1$. This work assumes that the equations in (1.1) determine real system's behavior. Since MPC's model uses the same equations, the predictions will be consistent with the assumed linear model. When forecasting errors in the disturbances are present, or parameters in the system matrix or the input matrix are wrongly estimated, mismatches between MPC's prediction and real system occur.

Let $\hat{u}^*\left(k_i \mid k_i\right)$ denote the first element of the optimal input solution for the optimal control problem (1.3). Then, accordingly to MPC, just the first element of this optimal input sequence is implemented with

$$u\left(k_i\right) = \hat{u}^*\left(k_i \mid k_i\right), \tag{1.4}$$

and the next state of the closed-loop system is obtained as

$$x\left(k_i + 1\right) = Ax\left(k_i\right) + Bu\left(k_i\right) + Ed\left(k_i\right), \tag{1.5a}$$

$$y\left(k_i\right) = Cx\left(k_i\right). \tag{1.5b}$$

[2]For the sake of compact formulation, this work does not use this notation when postulating optimization problems in the upcoming chapters. For optimization strategies that work under an MPC scheme, the reader needs to keep the meaning of this notation in mind.

For the next time step, i.e., $k_i = k_i + 1$, the initial state is updated as $x_0 = x(k_i)$. If the actual state $x(k_i)$ cannot be directly measured, it must be estimated using measurements from $y(k_i)$.

The interested reader can refer to the book of Maciejowski [42] and the book of Camacho and Bordons [37] for further background information on MPC. This work formulates MPC's optimization problems as mixed-integer linear programming problems (MILP) or mixed-integer quadratic problems (MIQP). Appendix A gives a general theoretical background on mathematical optimization which is required to understand and follow concepts and formulations presented in this dissertation. For more information on numerical optimization methods, the reader can also refer to the work of Boyd and Vandenberghe in [36].

One advantage of MPC is that its implementation can take place at different layers of a control hierarchy structure. It means that MPC can be present in the low-level controllers of an automation system, and it can also reside in the supervisory and management level [43]. This work considers MPC at the energy management level of a home automation system (HAS), and it does not investigate low-level control loops. The MPC-controller sends power set-points to the low-level controllers, and this work assumes that they can track the given set-points. Figure 1.6 shows a schematic structure of MPC for a H-MG.

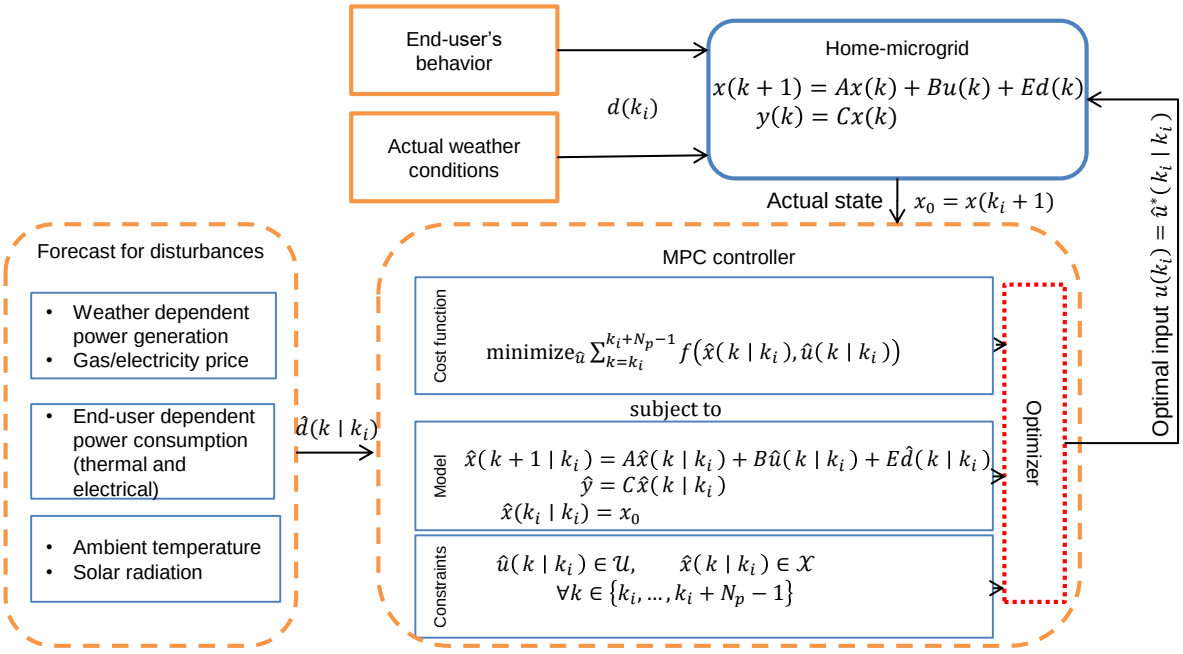

Figure 1.6.: Basic principle of model predictive control for Home-microgrids (based on [27, 44])

1.4.2. Review on MPC and optimization approaches for multienergy home-microgrids

This section provides a literature review on MPC for the operation of multienergy systems at the end-user level, i.e., at buildings and microgrid (MG) levels. Subsequently, the section presents the main contributions of this work.

According to Parisio et al. [24], three main aspects make MPC attractive for MG operation:

- as MPC is based on predictions and future behavior of the system, it is suitable to coordinate systems, which greatly dependent on forecasts of demand and RES generation;
- due to MPC's inherent feedback mechanism, uncertainties can be handled with more robustness; and
- MPC can handle MG operation constraints, such as storage capacity and distributed generators (DG) limits.

For these reasons, MPC has drawn the attention of the power system community in recent literature. Faulwasser and Engelmann [45] identified two main branches of research on MPC for energy systems.

1. MPC for fast time scales (a few seconds): Voltage and frequency stabilization.
2. MPC for slow time scales (15 minutes to 1 hour): Energy management and generator dispatch using price-based objectives.

This literature review focuses on the second research branch, specifically on MPC's use for the operation of multienergy microgrids and buildings. It does not aim at providing a complete extensive review of the existing literature on this topic, but rather at presenting a structure of the leading research topics in this area.

Parisio et al. in [24] propose a well-developed mixed-integer linear programming (MILP) approach for modeling and optimizing the operation of a campus MG. They consider unit commitment, economic dispatch, energy storage, sale and purchase of energy to/from the main grid, and curtailment schedule for a MG composed by RES, CHP units, electricity storage units, flexible and non-flexible loads. The authors conclude that the MPC-MILP operation scheme is able to economically optimize the operation of the MG and save money when compared to other existing operation approaches. MG's thermal balance constraints (i.e. thermal demand and heat storage) are disregarded in the formulation. If thermal flexibilities are considered within the scheme, the results may vary.

In the work of Houwing et al. [28], the use of MPC for the demand response (DR) of a micro combined heat and power system (μ-CHP) is presented. The authors formulate

the optimization problem as a MILP, where thermal comfort satisfaction is defined as a constraint for the optimization problem, given a thermal demand prediction. A different way to consider thermal comfort satisfaction is to include a building's thermal model in the optimization problem and define upper and lower room temperature boundaries as constraints, as proposed in the works of Chen, Oldewurtel, Ali, and Sossan [25, 26, 29, 46]. A load management strategy using MPC for PV with electrical heaters was investigated by Zong et al. [27], in which the thermal comfort satisfaction issue was treated as a temperature set point tracking problem using the l_1-norm (see [36] for further information) in the objective function to minimize absolute deviations of the actual room temperature to the given set-point temperature. Another characteristic of the operation strategy adopted in the cited references is that, the DR activity was defined as the minimization of operation costs with an assumption that the utility offers a variable price signal.

An interesting example for the application of MPC including thermal flexibilities in a residential setting is presented in the work of Sossan et al. [47]. The authors apply MPC to shift the electricity consumption of a freezer for demand response purposes. Simulation results are supported by lab experiments showing the ability of MPC to exploit the freezer as flexible electrical load. Further thermal flexibilities can be utilized if building space heating is considered within the MPC structure. As example, Oldewurtel et al. in [25] present a stochastic MPC tractable formulation for the building application domain, taking into account uncertainty in weather predictions. Even though energy flexibility related topics - e.g., demand response or self-consumption with RES generation - are not directly addressed in the paper, it provides a general basis for including space heating into the MPC formulation. In the work of Costanzo et al. [48], the authors present a case study where the thermal inertia of the building is considered for the operation of a building climate control system for demand response applications. Here, MPC is used as reference to evaluate data-driven control approaches.

A different application for (DR) with thermal energy storage and direct electric space heating appliance is illustrated in the work of Ali et al. [46]. The authors present a linear programming (LP) formulation to shift power demand from peak price periods to the cheapest hours without sacrificing user comfort. The simulation results show that the thermal energy storage together with thermal inertia of the house can offer much flexibility in DR control. Because the authors considered the system for an open loop optimization, assuming perfect knowledge of prices and weather for the scheduling horizon, the impact of uncertainties is not addressed in that work.

MPC is also used for an appliance scheduling case under dynamic electricity prices in the work of Chen et al. [26]. The thermal mass of the building is integrated into the optimization problem and user's comfort range is modeled by the predicted mean vote index. Impact of uncertainties coming from user's comfort range and electricity price forecast are also assessed. Due to the fact that the work focuses on flexible loads, distributed generators (PV or CHP) are not examined in the scheme.

When DGs are integrated in the optimization, the complexity of the problem increases. A real lab demonstration of MPC implementation for active load management of heater's power consumption together with PV and wind generation is reported in the work of Zong et al. [27]. Here, the authors uses the potential of residential optimization to support the penetration of RES and improve the use of the existing distribution grid infrastructure. Weather forecast and prediction of dynamic electricity price are integrated. The lab results demonstrate that MPC strategy with weather and price predictions improves the matching of demand and supply. Robustness of MPC against uncertainty in measurements and prediction is left as future work.

Houwing et al. in [28] investigates the extent to which demand response with time-varying tariffs and mini fuel cell CHP leads to reduced energy costs for households when compared to standard heat-led control. An MPC strategy is proposed for enabling demand response of the mini CHP systems. The authors show that demand response with mini CHP lowers variable costs for households. However, trade-off between economic performance and uncertainties is neither quantified nor discussed.

In [29], Sossan et al. evaluate the added value for a consumer to have the capability to choose the most convenient source for providing space heating to a building according to a dynamic electricity price. This energy replacement is achieved using MPC as operation strategy using dynamic models of the considered elements. The authors propose a new model for a fuel-cell CHP obtained using a system identification grey-box approach based on experimental measurements. The simulation results show that the predictive energy replacement strategy reduces the operation costs of the system and is able to provide a larger amount of regulating power to the grid. The flexibility of such a MG setting can be enhanced if a second generator (e.g. PV) and a second storage system (e.g. battery) are incorporated.

This is the case presented in the work of Kriett and Salani [30]. Here, a generic MILP model within an MPC scheme is proposed, which minimizes the operating costs of a residential MG. The proposed strategy aims at finding the minimum cost operating schedule of both electrical and thermal supply and demand in a residential MG. The residential setting covers photovoltaic plants, CHP, thermal storage, battery, controllable loads and non-controllable loads. The authors quantify cost reduction that result from minimum cost control by comparison with other benchmark models on the basis of a case study, revealing the performance of the minimum cost control strategy. They discuss the utilization levels of selected units to provide further insight into the effects of minimum cost control on residential MG operation. The authors also confirm the optimality of the presented results as well as its robustness to changes in estimated costs parameters. Nonetheless, robustness to errors in forecasts and model mismatches are not attended. Furthermore, the presented case study does not involve DGs with different FIT.

Next, in the work of Zhang et al. [31] a MILP problem is formulated for the optimal operation of a grid-connected residential MG composed by RES (wind and solar), a CHP,

energy storage units (battery and water tank), electrical vehicle, and flexible loads. The MILP problem is integrated into an MPC framework to reduce negative impacts of forecast errors. A case study which considers forecast uncertainties is implemented for evaluating the performance of the proposed method. Moreover, a further sensitivity analysis is realized in order to discuss the impacts of energy storage units on the MG operation. The authors take into account forecast uncertainties coming from RES generation, load demand and electricity price. Issues such as impacts of uncertainties coming from storage model mismatches, DGs with different FIT, and the self-consumption problematic are not included in the investigation.

Gupta et al. [49] consider a single building with the objective of introducing an algorithm that increases the thermal comfort of building users while simultaneously reducing energy costs through load management. The algorithm takes into account the requirements of each user regarding room temperature together with the thermal interactions of the different building areas. Hence, an optimal temperature set-point is to be found for all building areas. In large buildings, however, users may have different perceptions of comfort. It is therefore not trivial to determine a temperature set-point that is acceptable for every user. Thus, a method for joint temperature control in rooms with many users is presented. Among other things, this method uses price feedback to reach a consensus between users (increase comfort, reduce energy costs) and the building operator (thermal management system). Each user is represented as an agent in the simulation, transmitting feedback signals to the building operator via sensors or smartphone apps. The algorithm achieves a temperature set-point that minimizes the sum of the community discomfort of the users and thereby lowers the overall energy costs of the building. This target value is then used by a control structure with proportional feedback and an adaptive control component to bring the building to the desired temperature level. The developed solution works only with agents without MPC. The solution assumes that users think energy-efficiently.

In the work of Chen et al. [50] a single building is also examined, but this time an MPC strategy is used as the control method. Building users are modeled as agents and thermal sensitivity is considered in detail. They use a data-driven dynamic heat sensitivity model. The goal is to minimize energy consumption while maintaining thermal comfort. The presented MPC algorithm is designed to determine the probability of a violation of thermal comfort limits. Under this consideration a balance between energy saving and thermal comfort shall be achieved. It is assumed that a feedback channel exists through which users can transmit their personal perception to the control system. To calibrate the model, user data is continuously recorded. This includes the perception of the different users with regard to actual thermal situation. The simulation results show that the MPC algorithm, which is based on user feedback, provides better results for thermal comfort and energy consumption than one based on the theoretically determined thermal comfort.

The assessment of several buildings in a network is the focus in the work of Mai et al.

[51]. Here the important agents are the building itself, a building aggregator and the energy supplier. This is a centralized MPC concept. The building aggregator developed in the paper coordinates the heating, ventilation and air conditioning (HVAC) loads of commercial buildings and sends the resulting power flexibility to the energy supplier. This allows flexible and fast responding power reserves to be made available, which in turn enables the energy supplier to control the power over a wide area within the grid. For this purpose, a contractual framework is created between commercial buildings, the aggregator and the supplier, which can maximize and reward the reserves of power flexibility provided by commercial buildings. The authors formulate a robust, centralized MPC algorithm that can both maximize aggregator's profit and minimize the payments of a participating building. Furthermore, the comfort limits of the building are not violated while the systems are available to the network as a fast control reserve. Another contribution is the presentation of a suitable, detailed building model. Although the simulation results are system-specific, they also reveal the need for further investigation. Since the building users are not considered in detail, significant knowledge about behaviour of building users in commercial buildings and the effects on the building temperature when providing system services must be obtained.

Larsen et al. in [52] developed a distributed MPC concept for the coordination of several households with controllable loads (washing machines) within a local network area. The idea is to solve the optimization problem in a distributed way by dividing the problem into several subproblems so that the calculations take place at each household level. Each household is treated as an agent and thus a reduction on computation effort is achieved. Within the network, the decisions for switching on the washing machine are made and the exchange of information regarding a specific topology is coordinated. By exchanging price information with a few neighbors within an information network and taking into account their own local information, each household makes its own decision on when to purchase energy. By exchanging information with neighbors, it is also possible to match and coordinate the switch-on times of the washing machines with the overall demand within the network, thus reducing the overall peak load in the network. The scalability of the algorithm remains the biggest challenge in this approach.

In another paper [34], Larsen et al. further develop the distributed MPC concept. The main focus of the work is on the integration of mini CHP plants into the supply network. In order to avoid a central structure, an information network is presented where each agent (household) has only local information about the system for decision making. A fully distributed MPC algorithm is used in combination with the presented information network. At the beginning, the topology of the information network is defined so that the prosumers can exchange the energy price information with their neighbors within the selected information network topology. The agents of the information network are a subset of the agents of the supply network. The aim is to minimize the difference between generation and consumption within the information network by locally determining the on/off status of the mini CHP plant. Thus, the local energy production and demand

should be coordinated in order to avoid transport losses. One question that remains unanswered is the organisation of the information network model. One possibility is for the DSO to take over this task. Another possibility would be to introduce the role of the aggregator. It could then manage the flexibility of the various information networks.

Worthmann et al. consider in [35] a network of residential energy systems, each of them consisting of PV, battery storage, and non-flexible loads. They present three MPC-based approaches to flatten the network's aggregate power usage: centralized, decentralized, and distributed. The proposed distributed control methodology is a hierarchical-distributed control approach as it requires a central coordination unit. It does not rely on any know decomposition method for optimization problems (see [53]). The results show that the centralized MPC-based approach gives the best performance but suffers from scalability problems. The decentralized MPC-based approach does not present scalability issues. However, this approach does not lead to network-wide optimum. The hierarchical-distributed MPC scheme shows a compromise between these two extremes, as limited information exchange occurs between subsystems, and the optimization problem remains local.

A cooperative distributed MPC for wind farms is the focus of the work of Spudić et al. [54]. They present a fully distributed MPC approach, where each wind turbine computes its optimal input by taking into account local information and communicating to neighboring turbines only. In terms of the required number of iterations, they compare the performance of the distributed MPC using two distributed optimization techniques: dual decomposition and the alternating direction method of multipliers (ADMM). The authors conclude that ADMM outperforms dual decomposition significantly. Compared to a centralized MPC approach, ADMM achieves a good performance after ten iterations for the studied case. After 100 iterations, ADMM's performance is virtually the same as with the centralized MPC. The paper indicates that the scalability of the distributed MPC needs further investigation.

The recent paper of Parisio et al. [55] focuses on designing an energy management system for urban districts consisting of multiple multienergy microgrids. They present an MPC-based cooperative energy management system that optimizes, via aggregators, energy users' flexibility. The proposed energy management framework requires solving a certain number of MILP problems. The authors argue that commonly used distributed optimization methods, e.g., fast gradient techniques, dual decomposition, ADMM, do not apply to MILP problems. Therefore, the authors propose a kind of heuristic-based algorithm for the coordination task. As an outlook, the authors indicate that the approach's scalability needs to be improved and that stochastic approaches are needed to address uncertainties more effectively.

Moret and Pinson introduce the concept of energy collectives in [14]. They present a distributed structure, where all end-users communicate with a central node that coordinates the energy exchange process. The authors present the corresponding convex optimization problem and its decomposition using ADMM and give simulation results for an energy

collective of 15 participants. Here, the authors do not consider binary variables formulation, and they see scalability and robustness towards more extensive and more realistic test cases as future challenges.

A hierarchical distributed MPC with ADMM for large-scale energy systems is the topic in the work of Braun et al. [56]. The authors propose a variant of the ADMM algorithm. A central entity needs to solve an optimization problem that does not require detailed information about the subsystems and is independent of the number of subsystems. Each subsystem solves an optimization problem that depends on a single quantity broadcast from the central entity and local information. They implement the approach for a network of RES. With the help of simulation results, the authors demonstrate how the use of the algorithm optimizes the network's operation. The authors do not consider binary variables in their formulation, and the case study does not include multienergy systems. As an outlook, the authors say that the generalization of the approach to consider nonlinear and nonconvex systems remains an open issue.

Hans et al. [33] also deal with a hierarchical distributed economic MPC implementation using ADMM. They investigate how to increase the renewable infeed from MGs by using a transmission network for allowing the exchange of energy between MGs. For this purpose, they propose a hierarchical distributed scheme that allows optimizing the operation of multiple interconnected MGs. The optimization model considers loads, thermal generators, wind generation, PV generation, battery systems, and a linearized DC power flow model for the transmission network. The economic objective function includes generators' costs and electricity prices. The authors consider binary variables in the formulation, and in the end, they use ADMM to decompose a MIQP. To deal with the binary variables, they use a relaxation step and a mixed integer update step in the hierarchical distributed MPC algorithm. Extending the approach for more complex MGs (e.g., multienergy MGs) and investigating the mixed-integer update feasibility are seen as the next steps.

Finally, Stoyanova et al. [57] investigate three MPC strategies for cooperative energy management of household electro-thermal devices, namely a hierarchical distributed MPC, a distributed MPC, and a combined method. The authors conclude that the combined method achieves better integration of RES.

In summary, this literature review allows to identify two main MPC research trends for multienergy microgrids:

1. MPC for the operation of single buildings or microgrids. Here, the cited authors indicate that future research paths are the development of more detailed building thermal models, more detailed appliance models, and more detailed models for user-behavior and the development of robust and stochastic MPC strategies for handling uncertainties.

2. MPC for the operation of interconnected buildings/microgrids. Here, the research outlook is the design of fully distributed or hierarchical distributed coordination

strategies, where scalability towards large-scale systems and robustness against uncertainties play a significant role.

The dissertation at hand focuses on the use of MPC for the optimal operation of single multienergy H-MGs, and on the use of MPC for the hierarchical-distributed coordination a group of interconnected multienergy H-MGs. It considers the energy balance at both building level and neighborhood level. This work differs from the presented literature by investigating the formulation of optimization problems for local balancing when heterogeneous distributed energy resources - e.g., heat pumps, CHP, battery, TES, and PV - at the end-user level are involved. It also differs from the previous research by designing a suitable hierarchical-distributed strategy to coordinate the operation of such heterogeneous flexible resources using the ADMM sharing problem with binary variables. In addition, this work provides a framework to co-simulate electrical distribution networks with H-MGs.

1.5. Research questions and contributions

As previously stated, this work follows a bottom-up approach that pursues the improvement of local balancing in low voltage networks by using flexibilities from H-MGs (end-user). Accordingly, this work aims at answering the following research questions:

1. What is a suitable approach for the optimal management of power flows within an H-MG? The use of flexibilities from H-MGs implies an optimal operation inside the H-MG. An end-user will only agree to provide flexibility for improving balancing with its neighbors, just if it does not affect its comfort and costs. Therefore, an approach to operate H-MGs optimally must consider end-user restrictions and objectives, and find the best solution accordingly. Finding the best solution requires not only looking into actual information but also taking future information into account. Doing this allows considering uncertainties from weather-dependent power generation and human-behavior-dependent power consumption.

2. How to model and describe flexibilities at the end-user side in a systematic way, and how to formulate optimization criteria for each H-MG? It is necessary to correctly represent the energy conversion and energy storage process inside the H-MG as well as the involved interactions between components. Such a modeling demands a certain level of detail to fully characterize the flexibility of a unit, but it also needs a certain level of abstraction as these models are intended to run in an energy management system. Moreover, it is also essential to carefully decide which dynamics to consider and how to treat end-user comfort. End-user comfort can be a hard constraint, or it can be a soft constraint with a high penalty. Finally, the formulation of an operation

target for minimization or maximization is fundamental to evaluate the optimality of the operation.

3. How to coordinate a group of interconnected heterogeneous H-MGs? An optimal local balancing between H-MGs requires a coordination strategy, which takes into account local consumption and local generation of each H-MG and the state of their respective internal components. If an H-MG has an electrical power surplus at a given point of time, its local management system can decide to store this surplus for later usage within the H-MG. It can also decide to supply a neighboring H-MG, which has high electrical demand at that time. For this purpose, a handful of coordination strategies are viable. One option is to let each local H-MG controller decide, based on its operation goal, what to do without any knowledge on power consumption/injection of its neighboring H-MGs expecting a natural simultaneity between total generation and total consumption of the group of H-MGs. Another option is to collect and manage all information centrally and to have just one global controller that decides on the power flows of all H-MGs. This implies that this global controller has the knowledge on the status on every single component and it has the right to manipulate every internal component of a H-MG as desired. A different option is to have a central controller that does not possess the information from every single component but rather aggregated information per H-MG. This central controller sends coordination signals to incentive local H-MG controllers to adapt their resulting power profile to improve local balancing between H-MGs.

4. How to design a scalable coordination strategy for interconnected H-MGs, which accounts for limitations on information exchange in large scale energy systems? When coordinating a large number of interconnected H-MGs, scalability is crucial. A suitable coordination strategy must restrict information exchange, while ensuring an optimal (or close to optimal) operation. The strategy must also consider data privacy issues and it needs to be consonant with the structure of the local H-MG controllers.

5. How to integrate the developed models for H-MGs and the proposed operation strategies with a power grid model in a simulation environment? The simulation of the behavior of a complex system composed by interconnected heterogeneous H-MGs, local controllers, central controller, and electrical and information networks is not straightforward. The simulation environment must support a bottom-up process in order to be consistent with the modeling approach, and it has to support a modular development.

1.5.1. Statement of contributions

The purpose of this work is to present an optimal and scalable operation strategy for H-MGs. The proposed strategy can coordinate the operation of a single H-MG or the

operation of a group of interconnected H-MGs. This work investigates the formulation of optimization problems for MPC when heterogeneous distributed energy resources at the end-user level are involved. Also, it proposes a suitable hierarchical-distributed strategy to coordinate the operation of such multienergy H-MGs. Furthermore, the work presents a framework to simulate large-scale systems consisting of H-MGs together with electrical networks. More specifically, the main contributions of this work include:

1) an optimization problem for the optimal operation of a photovoltaic-heat pump H-MG considering heat pump operational characteristics, thermal dynamics of the building and a thermal energy storage unit (see [58]),

2) an optimization problem for the economic operation of a photovoltaic-combined heat and power H-MG considering a thermal model for the dynamic behavior of the mini CHP and the evaluation of the impact of battery size and TES size on the economic operation (see [59, 60]),

3) a problem formulation for the MPC based centralized coordination of interconnected H-MGs taking into account costs minimization and peak power reduction (see [61]),

4) the design and implementation of a hierarchical-distributed MPC strategy for distributed coordination of interconnected H-MGs using the alternating direction method of multipliers sharing problem with binary variables, and

5) a co-simulation framework to assess the impact of operation strategies of H-MGs on electrical distribution networks (see [62]).

The referenced peer-review publications support these claimed contributions.

1.6. Structure of this work

The remaining part of this work starts with the analysis of a single-family H-MG in Chapter 2. For single-family houses, the combination of roof-top PV plants and heat pumps with TES is already economically attractive. The flexibility from the coupling of the electricity sector and the heat sector, together with the storage capability of the building envelope and the TES, make these kinds of systems interesting for local balancing. The chapter, therefore, investigates an MPC-based optimal operation of a PV-heat pump H-MG. It presents the corresponding optimization problem and gives conclusive simulation results regarding the most appropriate objective function formulation. Subsequently, Chapter 3 focuses on a multi-family H-MG. Such buildings can have a gas-based cogeneration plant for electricity and heat supply, and a roof-top PV plant for increasing self-sufficiency. For the same purpose, a heat storage unit (TES) and a battery storage unit can complement the residential setting. The chapter proposes and simulates an economic MPC for the operation of these systems, which handles the inherent uncertainties.

As the capacity of storage units is a determining factor for the degree of flexibility of an H-MG, the dimensioning of these units, with economic feasibility as the main driver, requires special care. In this context, the concept of MPC is also useful not just in the operation phase but also in the dimensioning phase, where simulations that include uncertainties deliver additional insights regarding the optimal size. The chapter also evaluates the impact of storage capacity on the total costs of the H-MG.

The work continues looking at the coordination of interconnected H-MGs. The goal here is to design and evaluate coordination strategies for improving local balancing between H-MGs, while also having regard to their local economic operation. Accordingly, the assessment of three different MPC architectures - centralized, decentralized, and hierarchical-distributed - for the coordination of a group of interconnected H-MGs is the topic of Chapter 4. Distributed optimization techniques are intrinsic to MPC-based hierarchical-distributed strategies. In this respect, the alternating direction method of multipliers is a promising approach, which is the topic of Chapter 5. The chapter aims to present, evaluate, and discuss a novel hierarchical-distributed coordination strategy for interconnected H-MGs based on the ADMM sharing problem. The co-simulation of complex energy systems is the subject of Chapter 6. It describes a simulation framework to co-simulate H-MGs and coordination strategies, together with power distribution networks. The chapter presents an overview on the simulators that form the framework, their main tasks, and how they communicate with each other. The simulation of a generic low voltage network with H-MGs serves as example to show the functionality of the framework. Finally, Chapter 7 recapitulates the dissertation's content, gives concluding remarks, and suggests further research paths.

2. Flexible power operation of a photovoltaic-heat pump home-microgrid

This chapter investigates model predictive control problem formulations for the flexible operation of a photovoltaic-heat pump home-microgrid. Two flexible operation strategies using model predictive control are proposed and thoroughly evaluated. The simulation results indicate that the problem formulation always poses a trade-off between the comfort of the inhabitants, peak power reduction at the point of common coupling, and computation time for the optimizer. For the presented case in this chapter, a quadratic objective function shows the most promising results.

The content of this chapter is adapted from [58]: D. I. Hidalgo Rodríguez, J. Hinker, and J. M. Myrzik, "On the problem formulation of model predictive control for demand response of a power-to-heat home microgrid," in *19th Power Systems Computation Conference*. Genoa, Italy, 2016.

2.1. Introduction

This chapter investigates a H-MG which combines a HP, a TES and a PV plant. It represents a single family house (SFH). The objective is to minimize extreme power peaks (in generation and consumption) at the point of common coupling (PCC) between the H-MG and the distribution grid. This type of flexible operation could be promoted by the distribution system operator (DSO), by requiring limitations on PV feed-in at the PCC. In doing so, the DSO avoids reverse power flows from the low voltage to the medium voltage grid as well as large consumption peaks, which are normally not desired in the grid operation. For an energy retailer this kind of flexible operation could also be interesting if electricity tariff based on demand rates on peak power consumption is desired. To achieve this flexible operation, this chapter proposes to minimize the instantaneous difference between PV generation and house electricity consumption (household load and heat pump consumption). For thermal comfort satisfaction, it follows the idea of temperature set-point tracking problem as discussed in [27], but the chapter investigates an alternative problem formulation, namely the use of the l_2-norm in the objective function for flexible operation and thermal comfort satisfaction. Even though the l_2-norm in the objective function is usual for control purposes, this investigation pays special attention to its residuals and resulting implications for local balancing. The chapter presents a benchmark of the l_2-Norm - against the l_1-Norm and against a classical heat-led operation - with respect to the resulting peak power at the PCC, resulting mean absolute thermal comfort error and resulting mean CPU time.

To sum up, the purpose of this chapter is two-fold. First, the aim is to formulate three operation strategies for flexible operation of residential PV-heat pump systems. Second, using numerical simulation, these three formulations are compared in terms of peak power reduction, thermal comfort and CPU time. The contribution of this chapter will specifically be on:

1. focusing on residential PV-Heat pump systems and formulating the optimization problem for such systems considering heat pump operational characteristics, thermal dynamics of the house and a thermal energy storage unit, and
2. providing conclusive results on the best problem formulation for these specific systems by comparing three operating strategies using MPC for this kind of systems.

The chapter is organized as follows: First, the model description for the PV-HP-TES system and the formulation of the optimization problem for MPC are presented. Then, three operational strategies are developed and formulated as objective functions. Evaluation criteria and simulation setup are presented next. In the end, numerical results are illustrated and discussed.

2.2. Problem formulation

In this section dynamics and constraints for the MPC are formulated, followed by the description of the objective functions for each operation strategy. Finally, indicators for evaluation and simulation setup are defined. One advantage of MPC is that the concept can be implemented at different layers of an automation system i.e. MPC can be used at the low controller level or at the supervisory level [43]. In this chapter, MPC is considered at the supervisory level of the home energy management. Low level control loops are not investigated. MPC determines optimal power set-points and sends them to the low level controllers. It is assumed that these controllers are able to track the given set-points. Figure 2.1 shows an MPC schematic structure for a photovoltaic-heat pump H-MG.

The MPC strategy is applied to dynamic models of a single family house (SFH) and a TES. Measurement data for PV, load and weather from a field test in Germany serve as input data. The goal of MPC is to find a future trajectory for the TES and the HP, over a finite prediction horizon, to minimize the instantaneous difference between PV generation and electrical consumption (household loads plus HP). This is done by shifting the operation times of the heating appliance using the flexibility provided by the TES and the storage capacity of the house.

In the upcoming subsections, models used in the optimization problem to represent the main thermal characteristics of the considered system are presented. For the formulations below the relative time within the prediction horizon is indicated with $k \in \{k_i, ..., k_i + N_p - 1\}$, where k_i denotes the initial time step for the optimization.

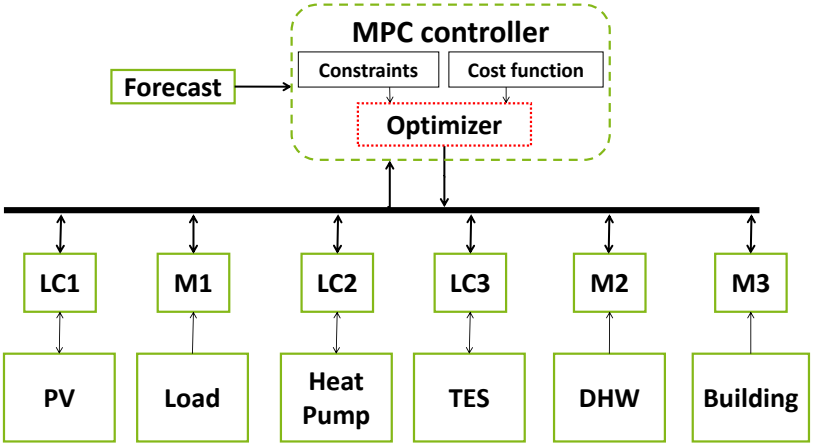

Figure 2.1.: Information flows and structure of the whole setup including H-MG components and MPC controller (with LC# as local controllers, and M# as measurement devices).

2.2.1. Heat pump model

In [63], the economic addressable market for HPs and μ-CHP in Germany is estimated, concluding that for SFH, heat pumps are more cost efficient.

The heating system is assumed to be monovalent, consisting of just the HP as heating source without auxiliary boiler. The HP is directly connected to the TES, which feeds the residential heating circuit.

Figure 2.2 shows a schematic representation of the considered system.

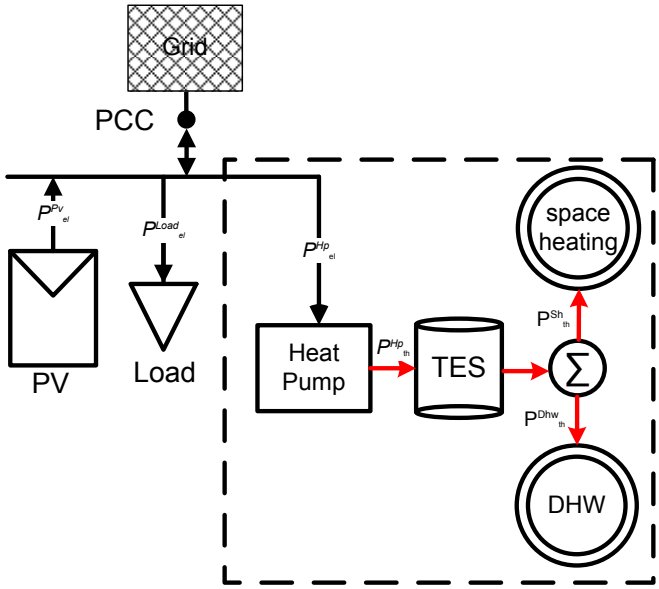

Figure 2.2.: Overview of the system components in the H-MG setting

The relationship between the generated thermal power and consumed electrical power in a HP is given by the coefficient of performance (COP) as

$$p_{th}^{\mathrm{Hp}}(k) = p_{el}^{\mathrm{Hp}}(k) \cdot COP, \tag{2.1}$$

where $p_{th}^{\mathrm{Hp}}(k)$ denotes the generated thermal power, and $p_{el}^{\mathrm{Hp}}(k)$ is the consumed electrical power.

In this work a brine/water HP is considered. Brine/water HPs use heat from the ground as source, at a relative constant temperature over the year [64]. Therefore, a constant COP for the entire year is assumed, neglecting variations due to weather conditions. The HP is driven by a frequency inverter, which implies that it can be modulated. The operation range of the HP is given by

$$b^{\mathrm{Hp}}(k) \cdot p_{el}^{\mathrm{Hp,min}} \leq p_{el}^{\mathrm{Hp}}(k) \leq b^{\mathrm{Hp}}(k) \cdot p_{el}^{\mathrm{Hp,max}}, \tag{2.2}$$

$$b^{\mathrm{Hp}}(k) \in \{0, 1\}, \tag{2.3}$$

here, the binary variable $b^{\mathrm{Hp}}(k)$ is used to indicate the ON/OFF status of the HP. The inequality restricts the operation of the HP to its maximum allowable power $p_{el}^{\mathrm{Hp,max}}$ and minimum allowable power $p_{el}^{\mathrm{Hp,min}}$.

2.2.2. House thermal model

There exist detailed building models for MPC applications in the literature (see for example the work of Oldewurtel [25] and Appendix B). As the focus of this chapter is on the formulation of the objective function, the thermal behavior of the house is represented by a simple model as proposed in [65] which has already been used for demand side management with heating systems in [66–68]. The storage capacity of the house is dominated by the air in the room and a large heat-accumulating medium, composed mainly by the walls and the floor. The thermal behavior is given by

$$\begin{bmatrix} T^{\mathrm{m}}(k+1) \\ T^{\mathrm{room}}(k+1) \end{bmatrix} = A \cdot \begin{bmatrix} T^{\mathrm{m}}(k) \\ T^{\mathrm{room}}(k) \end{bmatrix} + B \cdot \begin{bmatrix} T^{\mathrm{Amb}}(k) \\ p_{th}^{\mathrm{Sh}}(k) \\ \Phi^{\mathrm{Solar}}(k) \end{bmatrix}, \tag{2.4}$$

where the states of the system are T^{m}, the temperature of the large heat-accumulating medium in the house, and T^{room}, the house air temperature. Model inputs are outside ambient temperature T^{Amb}, solar radiation Φ^{Solar} and the space heating power p_{th}^{Sh}. As mentioned before, this work uses the discrete-time version of MPC, hence the discrete-time

matrices A and B in (2.4) are obtained by discretizing the continuous-time matrices

$$A^{\text{cont}} = \begin{bmatrix} -\frac{1}{r_i \cdot c_m} & \frac{1}{r_i \cdot c_m} \\ \frac{1}{r_i \cdot c_i} & -\left(\frac{1}{r_i \cdot c_i} + \frac{1}{r_a \cdot c_i}\right) \end{bmatrix}, \tag{2.5}$$

$$B^{\text{cont}} = \begin{bmatrix} 0 & 0 & \frac{A_w \cdot pl}{c_m} \\ \frac{1}{r_a} & \frac{1}{c_i} & \frac{A_w(1-pl)}{c_i} \end{bmatrix}, \tag{2.6}$$

with MPC's sample time. These matrices are composed of building physical parameters, such as the heat capacity of the large heat-accumulating medium c_m, heat capacity of the room air c_i, the resistance against heat transfer from the house air to ambient air r_a, and r_i as the resistance against heat transfer between the house air and the large heat-accumulating medium. Besides, other parameters like the window area facing south A_w, and the share of the solar radiation which is directly affecting T^{m} (as pl) are also considered.

2.2.3. Thermal energy storage model

As shown in Figure 2.2 besides building's thermal storage capabilities for space heating, the H-MG has an an extra TES. A simple TES model for MPC strategies is given in [28, 69]. Based on these references, the evolution of the energy state of charge over the time is determined with

$$SoC^{\text{Tes}}(k+1) = \eta^{\text{Tes,sd}} \cdot SoC^{\text{Tes}}(k) + \left(p_{th}^{\text{Tes,char}}(k) - p_{th}^{\text{Tes,dis}}(k)\right) \cdot K^{\text{Tes}}, \tag{2.7}$$

where $SoC^{\text{Tes}}(k)$ is the TES' state of charge relative to its capacity in percentage points (0% is empty, and 100% is full). $K^{\text{Tes}} = \Delta t/(60 \cdot Cap^{\text{Tes}}) \times 100$. Δt is the MPC sample time and Cap^{Tes} is the total energy capacity of the TES. $\eta^{\text{Tes,sd}}$ is the self-discharge coefficient.

$p_{th}^{\text{Tes,char}}(k)$ and $p_{th}^{\text{Tes,dis}}(k)$ denote the thermal charging and discharging power respectively. They are given by:

$$p_{th}^{\text{Tes,char}}(k) = P_{th}^{\text{Hp}}(k) \cdot \eta^{\text{Tes,char}}, \tag{2.8}$$

$$p_{th}^{\text{Tes,dis}}(k) = \frac{p_{th}^{\text{Sh}}(k) + p_{th}^{\text{Dhw}}(k)}{\eta^{\text{Tes,dis}}}, \tag{2.9}$$

with $\eta^{\text{Tes,char}}$ and $\eta^{\text{Tes,dis}}$ denoting charging and discharging efficiency respectively. $p_{th}^{\text{Dhw}}(k)$ is the domestic hot water consumption. For TES, it is possible to charge and discharge thermal power simultaneously. The state of charge is also bounded to its allowable limits with

$$SoC^{\text{Tes,min}} \leq SoC(k)^{\text{Tes}} \leq SoC^{\text{Tes,max}}. \tag{2.10}$$

With equations (2.1) to (2.10) all dynamics and constraints for the MPC are defined. The next subsection describes the objective functions that define the different operation modes.

2.2.4. Objective functions

Three operation strategies are contrasted. The first strategy is heat-led operation strategy which serves as reference. The second strategy seeks a flexible operation of the H-MG by using the $l1$-norm in the objective function. The third and last strategy aims as well at a flexible operation of the H-MG but uses the $l2$-norm in the objective function.

2.2.4.1. Heat-led operation

In this operation strategy the only objective is to satisfy thermal comfort. The HP and the TES are operated in a way that the given temperature set-point is satisfied. For this purpose the objective function is

$$J_1\left(\boldsymbol{T}^{\mathrm{Room}}, \boldsymbol{p}_{\boldsymbol{el}}^{\mathbf{Hp}}\right) = \beta\Big(\sum_{k=k_i}^{k_i+N_p-1} |T^{\mathrm{Setpoint}}(k) - T^{\mathrm{Room}}(k)|\Big), \tag{2.11}$$

and this work uses the relaxation presented in the work of Boyd [36] to treat the l_1-norm problem as a linear programming problem.

2.2.4.2. Flexible power operation DR-l_1

In this operation strategy there are two objectives: the minimization of deviations of the room temperature to the desired set point temperature and the minimization of peak power flows at PCC. As positive and negative deviations have to be minimized, the absolute value of the difference is formulated in the objective function using the l_1-norm as

$$\begin{aligned} J_2\left(\boldsymbol{T}^{\mathrm{Room}}, \boldsymbol{p}_{\boldsymbol{el}}^{\mathbf{Hp}}\right) = \alpha\Big(&\sum_{k=k_i}^{k_i+N_p-1} |p_{el}^{\mathrm{Pv,ac}}(k) - p_{el}^{\mathrm{Load}}(k) - p_{el}^{\mathrm{Hp}}(k)|\Big) \\ &+\beta\Big(\sum_{k=k_i}^{k_i+N_p-1} |T^{\mathrm{Setpoint}}(k) - T^{\mathrm{Room}}(k)|\Big). \end{aligned} \tag{2.12}$$

2.2.4.3. Flexible power operation DR-l_2

Similar to the previous operation strategy, deviations in thermal comfort and peaks at PCC have to be minimized. Here, not the absolute difference is considered but instead the

square of the difference is used. This is done using the squared l_2-norm in the objective function with

$$J_3\left(\boldsymbol{T}^{\text{Room}}, \boldsymbol{p}_{\boldsymbol{el}}^{\mathbf{Hp}}\right) = \alpha\Big(\sum_{k=k_i}^{k_i+N_p-1}\left(p_{el}^{\text{Pv,ac}}(k) - p_{el}^{\text{Load}}(k) - p_{el}^{\text{Hp}}(k)\right)^2\Big) + \beta\Big(\sum_{k=k_i}^{k_i+N_p-1}\left(T^{\text{Setpoint}}(k) - T^{\text{Room}}(k)\right)^2\Big). \tag{2.13}$$

Table 2.1 summarizes all three considered objective functions.

Table 2.1.: Three operation strategies

Operation strategy	**Motivation**
heat-led (see (2.11))	Thermal comfort is the only objective so the heating system will act accordingly. As there is no trade-off, this is the **reference** scenario.
DR-l_1 (see (2.12))	Thermal comfort and the net energy flow at the PCC are evaluated in an integrated, **linear** l_1-norm metric. The weights of the two components can be defined at will. (default weights: $\alpha = 0.5, \beta = 0.5$)
DR-l_2 (see (2.13))	Like DR-l_1, but with a **squared** l_2-norm metric. (default weights: $\alpha = 0.5, \beta = 0.5$)

To summarize, MPC problem's formulation for these operation strategies, i.e., $n \in \{1, 2, 3\}$, is

$$\underset{\hat{\boldsymbol{u}}_a}{\text{minimize}} \quad J_n\left(\boldsymbol{T}^{\text{Room}}, \boldsymbol{p}_{\boldsymbol{el}}^{\mathbf{Hp}}\right) \tag{2.14a}$$

subject to

$$\boldsymbol{T}^{\text{Room}}, \boldsymbol{T}^{\text{Tm}} \in \mathcal{P}^{\text{House}}, \tag{2.14b}$$

$$\boldsymbol{p}_{el}^{\text{Hp}}, \boldsymbol{p}_{th}^{\text{Hp}}, \boldsymbol{b}^{\text{Hp}} \in \mathcal{P}^{\text{Hp}}, \tag{2.14c}$$

$$\boldsymbol{p}_{th}^{\text{Tes,char}}, \boldsymbol{p}_{th}^{\text{Tes,dis}} \in \mathcal{P}^{\text{Tes}}, \tag{2.14d}$$

$$\forall k \in \{k_i, \ldots, k_i + N_p - 1\}. \tag{2.14e}$$

Where the set $\mathcal{P}^{\text{House}}$ is given by (2.4), $\mathcal{P}^{\text{Hp}}$ is defined by (2.1)-(2.3), and $\mathcal{P}^{\text{Tes}}$ is given by (2.7)-(2.10). The vectors $\boldsymbol{T}^{\text{Room}}$, $\boldsymbol{T}^{\text{Tm}}$, $\boldsymbol{p}_{el}^{\text{Hp}}$, $\boldsymbol{p}_{th}^{\text{Hp}}$, $\boldsymbol{b}^{\text{Hp}}$, $\boldsymbol{p}_{th}^{\text{Tes,char}}$, and $\boldsymbol{p}_{th}^{\text{Tes,dis}} \in \mathbb{R}^{Np}$, and

the decision variables vector is $\hat{\boldsymbol{u}}_a = \left[\boldsymbol{p}_{el}^{\mathrm{Hp}\intercal}, \boldsymbol{b}^{\mathrm{Hp}\intercal}\right]^{\intercal}$.

2.2.5. Evaluation criteria and scenario

To evaluate the performance of the three operation strategies, these are compared with regard to customer comfort, power peak reduction as well as computational effort. The evaluation is based on a 30 day long simulation with a time resolution of 10 Minutes (ΔT =10 min) from an initial simulation time k_{ini} to a final simulation time N. The objective is to guarantee thermal comfort to the inhabitants as well as to operate in a flexible way.

As a first approach, a 1°C difference in temperature is assumed to be equally important as a 1kW difference at the PCC. Thus, to perform a fair comparison of all simulations, the setting of the weighting factors is $\alpha = 0.5$ and $\beta = 0.5$. Although the optimal value of these parameters is a whole optimization problem in itself and therefore falls out of the scope of this work, these values will be briefly discussed as follows:

For the sensitivity of people to a change in the temperature, the international standard ISO 7730 [70] can be utilized to evaluate the corresponding neutral temperature levels that go along with a minimum of dissatisfaction. Typical household conditions and building category *Class A* gives a desirable, comfortable temperature of 21.0°C and an appropriate allowed temperature variation of roughly 1.0K. The linear combination of temperature and power, through the coefficients α and β in the objective function, directly depends on the magnitude of the power and temperature values.

The assessment of simulation results uses the following performance indicators as a basis. The results section will refer to them when evaluating the strategies.

2.2.5.1. Local PV usage

To quantify the local usage of PV two indicators are defined: a self-consumption quota and a self-sufficiency quota. First the amount of PV power, which is instantaneously and directly used by the local loads at each time step is calculated using:

$$p_{el}^{\mathrm{Pv,used}}(k) = \min\{p_{el}^{\mathrm{Pv,ac}}(k), p_{el}^{\mathrm{Hp}}(k) + p_{el}^{\mathrm{Load}}(k)\} \tag{2.15}$$

The self-consumption quota q^{sc} is calculated as the ratio of total PV used to total PV generated for the whole simulation period as expressed below:

$$q^{\mathrm{sc}} = \frac{\sum_{k=k_{ini}}^{N} p_{el}^{\mathrm{Pv,used}}(k)}{\sum_{k=k_{ini}}^{N} p_{el}^{\mathrm{Pv,ac}}(k)} \tag{2.16}$$

The self-sufficiency quota q^{ss} is calculated as the ratio of total PV used to total electrical consumption for the whole simulation period as expressed below:

$$q^{\mathrm{ss}} = \frac{\sum_{k=k_{ini}}^{N} p_{el}^{\mathrm{Pv,used}}(k)}{\sum_{k=k_{ini}}^{N} p_{el}^{\mathrm{Hp}}(k) + p_{el}^{\mathrm{Load}}(k)} \tag{2.17}$$

2.2.5.2. Mean thermal comfort

The temperature mean absolute error (MAE) serves as key performance indicator for customer comfort. The mean error is given by:

$$MAE = \frac{1}{N} \sum_{k=k_{ini}}^{N} |T^{\mathrm{Setpoint}}(k) - T^{\mathrm{Room}}(k)| \tag{2.18}$$

within the simulated time, all time steps are treated equally so that the absolute error is evaluated by giving the mean for the absolute temperature error between set point and actual room temperature.

2.2.5.3. Further indicators

Since every time step is of different computational effort, the mean of the CPU time for each optimization has to be evaluated as well. For the evaluation of the flexible operation strategies DR-l_1 and DR-l_2, the maximum value and the minimum value of all observations of the electrical power at PCC are compared.

2.2.6. Simulation setup for a single family house H-MG

Building physical characteristics are taken from [71], for a SFH with an area of 140m^2, constructed in 1990 with low thermal modernization. Weather data consist of ambient temperature and global radiation, which are used as disturbance inputs for the building thermal model. Time series data for weather and PV power generation are for Germany for 30 days of April. Profiles for electrical household load, and DHW are taken from the VDI guideline 4655 [72] for a SFH with an annual thermal consumption of 136kWh/(m^{2}a) and an annual electrical consumption (without HP) of 5000kWh/a according to [73]. Profiles are obtained for 30 days in 10 min resolution. A temperature set-point is given, which varies according to the hour in the day. From 22.00 to 6.00, the temperature is set to 18°C, whereas during the day (i.e. from 6.00 to 22.00) a room temperature of 21°C is desired.

For this case study, MPC requires a forecast for PV generation, ambient temperature, electrical load demand, and DHW consumption. The implemented MPC uses a simple

Table 2.2.: Parameters for Simulation

Parameter	**Value**	**Parameter**	**Value**
COP	3	$\eta^{\text{Tes,sd}}$	0.01 (%/hrs)
N_p	12 (hrs)	Δt	10 (min)
c_i	1.35 (kWh/°C)	Cap^{Tes}	11.50 (kWh)[1]
c_m	11.20 (kWh/°C)	$p_{el}^{\text{Hp,min}}$	1 (kW_{el})
$p_{el}^{\text{Hp,max}}$	5 (kW_{el})	$\eta^{\text{Tes,char}}$	0.9
r_i	0.60 (°C/kW)	$\eta^{\text{Tes,dis}}$	0.92
r_a	4.21 (°C/kW)	$SoC^{\text{Tes,min}}$	0 (%)
A_w	2 (m^2)	$SoC^{\text{Tes,max}}$	100 (%)
pl	0.5	$p_{el}^{\text{Pv,nom}}$	7.5 (kW_{p})

[1]as for a typical water tank with 500l and $\Delta T = 20\text{K}$

one-day persistence forecast for PV generation and ambient temperature, which assumes that the current day's PV production and ambient temperature are the same as those from the day before. A seven-day persistence forecast is used for electrical load consumption and domestic hot water consumption, as they are dependent on end-user weekday behavior. It means that the MPC assumes that these consumptions are the same as those from one week before.

Table 2.2 gives the parameters used for the simulation. The implementation is done in Python using Pyomo [74, 75] as modeler, and CPLEX [76] as solver.

2.3. Simulation results and discussion

In this section numerical simulation results are presented and discussed. First a qualitative analysis for two exemplary days is given considering interactions and side-effects of the considered operation strategies. Next, a 30 day study is discussed based on performance indicators, TES usage and local PV usage.

Figure 2.3 contrasts the three target values for the three operation strategies using the two exemplary days. The first row shows the coincidence of set point room temperature and actual temperature achieved. The second row gives information about the activity of the heat pump and the electrical power flow from the PV. Finally, the third row shows the delta of consumption and PV in-feed. Note that (just as discussed in (2.12)) this is not just the delta of PV electricity generation and heat pump consumption as there is a household load included.

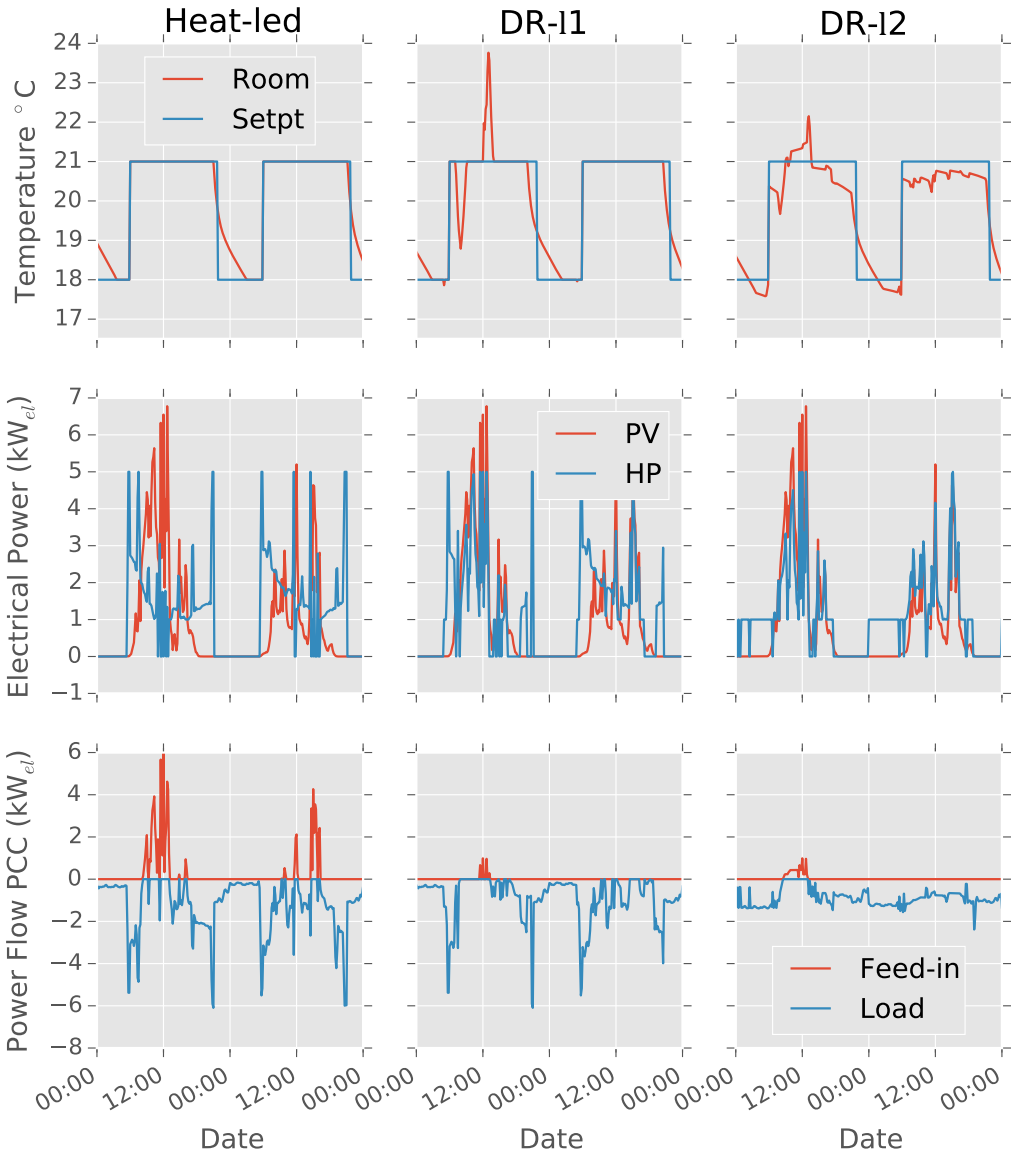

Figure 2.3.: Exemplary day profiles for temperature, electrical consumption, and PCC power flow

2.3.1. Thermal comfort

In Figure 2.3, it can be seen that for the heat-led operation, the room temperature follows the given set-point quite well. During the setback period at night, the room temperature gradually decreases showing the expected behavior of the dynamic building model. Although a complete match of the curves might be expected at first sight, the simple reason for the remaining discrepancy at setback times is that cooling is not possible for the chosen system.

For the DR-l_1 strategy, there are some spiky temperature over- and undershoots visible that even reach temperatures of 20 degrees. As a consequence, the temperature comfort cannot be guaranteed satisfactorily, but depends on the actual occupancy and the personal

thermal sensation of inhabitants. This might not pose a big problem as the spikes are only momentary.

Looking at the temperature profile for the DR-l_2 strategy, the fluctuation becomes present over the whole heating time frame, which therefore makes the restrictions of the whole system and the necessity of a detailed analysis much clearer. There is a clear deterioration in performance concerning the temperature control quality. Another aspect to notice is that even during the setback period, there are undershoots that might not be expected beforehand. It also becomes clear that during the morning time when the heating period starts again, such deviations are no problem at all: the capacity of the heat pump fits the corresponding heat consumption quite well and is able to quickly counterbalance the undershoots that result from the system operation at night. However, the temperature deviation can be as high as two degrees, although normally in the range of 0.5 degrees.

2.3.2. Side-effects of the operation strategies

In the second subplot of Figure 2.3, electrical profiles for PV generation and electrical consumption of the heat pump are illustrated. Under the heat-led operation the heat pump is operated with a power level that is sufficient to just cover the thermal demand (or as much of it as possible), while the PV generation profile is completely ignored. In the example shown, the heat pump reduces its electrical power consumption around noon, although there is a clear peak in the PV generation. This results in large peaks at the PCC for both electrical consumption and feed-in.

For the DR-l_1 strategy the temperature set point is well tracked, even in direct comparison with the reference scenario. However, it has to be noticed that the temperature sag is visible at an earlier point of time. This is because the optimization according to the objective function has to care about both the temperature and the peak power at the PCC at the same time. As there is no PV generation in the evening, it is more favorable to lower the heat pump activity than to invest high power to achieve higher temperatures. For the temperature peak, the operation strategy dictates to rather use the given power from PV generation and accept the overshoot than to have high power flows at the PCC. It can be stated that the heat pump runs more often and at higher average powers than in the reference scenario. That is because the TES is loaded whenever there is power from PV generation but no instant space heating demand. However, even though the heat pump is operated in a smarter way than before, short activation times of the heat pump are present at full power. Although this is appreciated during periods of high solar radiation, this is also visible for the night times. This clearly affects the balance of demand and in-feed at the PCC. On the one hand, peaks are clearly reduced at the generation side to less than 1kW. So, the optimization by the l_1-norm achieves a significant improvement of the correlation between activation of the heat pump and the given power from PV

generation. On the other hand, this operation strategy is not able to gain much flexibility by charging the TES, because the heat pump is already running for long periods.

Using the DR-l_2 operation strategy, the deviation of the room temperature rises although the quadratic approach behind the squared l_2-norm generally favors smaller values in comparison to the l_1-norm. However, looking at the electrical profiles at the PCC, it can be seen that the correlation between PV generation and heat pump operation significantly improves the power flow at the PCC. Therefore, large activation peaks of the heat pump at times of no PV generation are effectively avoided when employing the squared l_2-norm, which is a clear advantage of the squared l_2-norm. Another important factor is that in contrast to the DR-l_1 strategy, the heat pump is only operated at minimal power (roughly 1kW) when there is no solar radiation present. So, the charging of the TES is bound in a more restrictive way than for the DR-l_1 strategy. Here, the MPC-algorithm anticipates the heat demand of the day and tries to include the TES without overburdening the power budget at the PCC. In fact, this results in a flat power flow profile at the PCC as it can be seen in the third subplot.

2.3.3. Extensive 30 day study

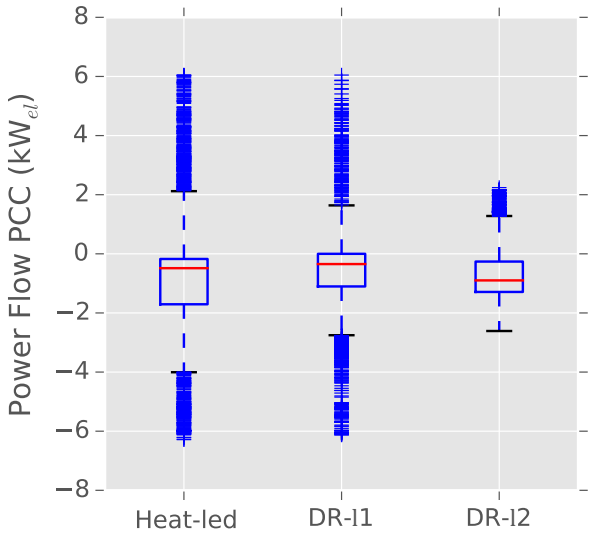

Figure 2.4.: Resulting power flows over the PCC

To provide a better analysis, a quantitative evaluation is done for 30 days simulation in April. The distribution of all observations for net power at the PCC is displayed in box plots in Figure 2.4. It can be seen how the DR-l_2 operation strategy is able to reduce peaks from heat-led and peaks from DR-l_1. What is not directly visible from the above discussion is to what extent the TES is used by the operation strategies. It should again be stated that the TES usage is not an objective itself. In this regard, Figure 2.5 shows a discrete histogram of the TES charging states. The heat-led strategy does not make proper

use of the capabilities of the TES, as the state of charge (SoC) shows a dramatic peak at zero and mostly lies below 40%. This is possible because the heat pump operation is only limited by its technical maximum power of 5 kW, which does not pose a big constraint on the target to follow the heat temperature with the given building.

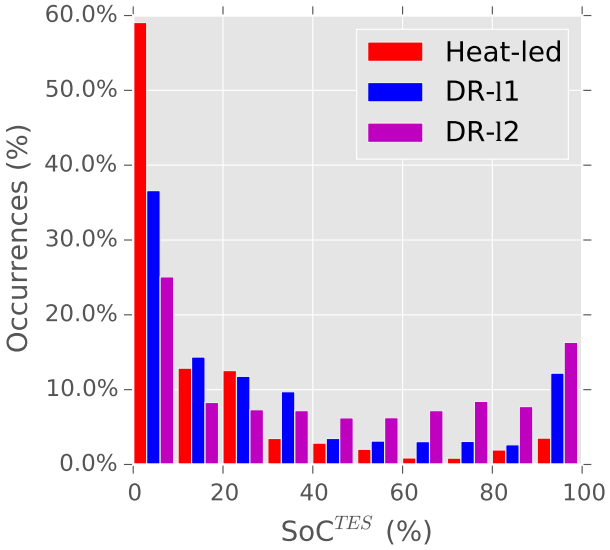

Figure 2.5.: Histogram of TES usage

For the operation strategy DR-l_2, the situation is completely different: the peak at $SoC^{\text{Tes}} = 0$ is only half as high as for the reference scenario, and the tail is much more balanced along the whole spectrum. On the contrary, there is a small but noticeable peak at $SoC^{\text{Tes}} = 100\%$, which signifies that the optimizer had to deal with a constraint here. Even though the question of the right TES size cannot be answered directly from this finding, the side-effects of optimiziation strategy and chosen boundary conditions becomes clear now, and is subject to further evaluations in the future. Next, Table 2.3 summarizes the resulting performance indicators for all strategies.

As mentioned before, DR-l_2 achieves a significant reduction in max and min peaks at PCC. However, there are two important aspects to discuss here, namely the increments in MAE and mean CPU time. The distribution of CPU time for all runs shows a large number of occurrences with a duration of around 1 min, and some extreme cases when the optimization takes 9 min or more, as illustrated in Figure 2.6.

It can be seen that for the considered strategy with a probability of 75% the computational time for the optimization using this operation mode will take less than 1 min. On the other hand there is 21% of probability that the computation time will take 9 min or more. In the simulation, a time limit for the optimization of 540 sec was set, and if this time was reached, available results provided by the solver at that moment were used. This long computation times can be explained by the complexity of the MIQP problem. The relative *mipgap* tolerance is 0.01, meaning that the solver only stops when it finds

Table 2.3.: Performance indicators with adjusted weights

Indicator	**Heat-led** (-)	**DR-l_1** ($\alpha = 0.5$ $\beta = 0.5$)	**DR-l_2** ($\alpha = 0.5$ $\beta = 0.5$)	**DR-l_2** ($\alpha = 0.5$ $\beta = 1.0$)	**DR-l_2** ($\alpha = 0.5$ $\beta = 1.5$)
Mean absolute error (MAE, °C)	0.21	0.32	0.55	0.41	0.36
Mean CPU time (sec)	0.05	0.06	125.87	133.73	128.97
Max peak PCC (kW_{el})	6.05	6.05	2.24	2.69	2.96
Min peak PCC (kW_{el})	-6.29	-6.13	-2.61	-2.61	-2.61

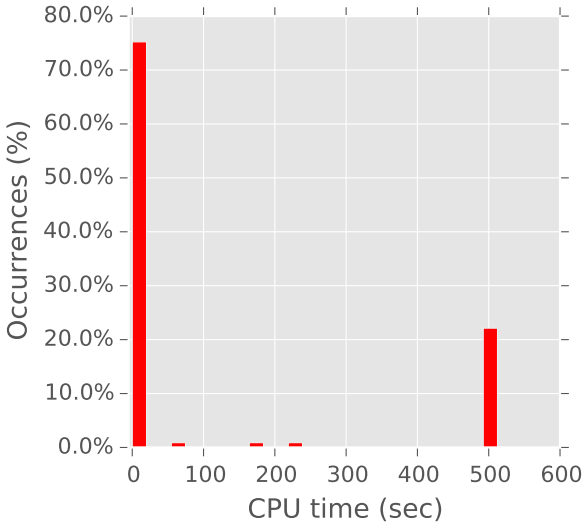

Figure 2.6.: Variation of CPU time (for DR-l_2-strategy)

a feasible integer solution proved to be within 1% of optimal. If after 9 minutes, this *mipgap* has not been reached, the optimization was stopped, and available results were used. Even though the available results are still not the optimal, they are good enough to be used, compared to the results obtained with heat-lead and with DR-l_1. In this chapter, the optimization is done every 10 minutes, and the resulting optimal value is sent as set-point to the lower controllers. In this case, getting the optimization results in 9 minutes is an issue and must be further investigated for implementation purposes.

On the other hand, an MAE of almost 0.6°C may be not acceptable in practical situations. By adjusting the weight of β in the objective functions i.e. prioritizing comfort over peak reduction, smaller deviations can be reached. Resulting indicators for adjusted β values are presented in Table 2.3. From this table it can be concluded that by adjusting β to 1,

the temperature error is around 0.45°C, which is a more realistic value to be admissible by customers. Also, even when thermal comfort weight β is three times larger than peak reduction weight, resulting maximal and minimal power peaks at PCC are still lower than the ones obtained by heat-led and DR-l_1 operations.

Self-consumption quota and self-sufficiency quota are also calculated and analyzed in Table 2.4. In theory a self-consumption quota of 100% is always possible. With a flexible demand management operation, the self-consumption quota improves around 28 percentage points in comparison to the heat-led operation. As expected, the DR-l_2 operation presents the highest self-consumption quota.

Table 2.4.: Energy indicators

Indicator	**Heat-led**	**DR-l_1**	**DR-l_2**
q^{sc} (%)	55.93	82.91	84.99
q^{ss} (%)	33.02	49.26	50.57
Energy import (kWh)	295.31	114.47	100.57
Energy export (kWh)	760.49	572.39	556.67

The self-sufficiency quota depends on the total PV production, total household load consumption and total heat pump electrical consumption. For the considered dates there is a total PV-production of 670kWh and a total household load consumption of 380kWh. The heat pump electrical consumption varies for each operation strategy, with a total consumption of 754kWh, 747kWh and 745kWh for the heat-led, DR-l_1 and DR-l_2 respectively. This is explained due to the fact that in heat-led mode thermal comfort is well satisfied, which means that thermal energy produced by the heat pump is higher. As the flexible management operation strategies have a second objective to optimize, the thermal comfort is reduced, which results also in a reduction in the thermal production and accordingly in the electrical consumption of the heat pump. For the heat-led operation there is a theoretical maximum self-sufficiency quota of 59.02%, which means that the heat-led operation achieves a self-sufficiency quota 26 percentage points below its theoretical maximum. For the DR-l_1 and DR-l_2 there are theoretical maximums for self-sufficiency quota of 59.40% and 59.50% respectively. Both strategies achieve a self-sufficiency quotas around ten points below the theoretical maximum.

2.4. Summary of the chapter

This chapter concerned itself with the optimal operation of a power-to-heat H-MG using model predictive control. It presented the particular optimization problem considering a ground source heat pump, the household thermal dynamics, and thermal energy storage. The chapter evaluated three operation strategies that differ in the weight of individual

objectives and the implemented norm. Numerical simulation and performance indicators such as customer comfort, peak power reduction as well as computational effort, helped in the evaluation.

In the first step, using two days as an example, simulation results revealed the interactions of the system components and the working principle of the MPC operation strategies. With the help of this example, it becomes clear that even for smaller interconnected systems, the effects are not always directly foreseeable. Thus, finding the proper weight of individual objectives and the norm is not trivial. Afterward, an extensive 30-day study was conducted to depict the range of electrical power flows at the PCC. Here, the squared l_2-norm was the most promising for peak power reductions, while $l1$-norm and the heat-led mode respectively showed higher and less reliable power flows.

Further steps are the evaluation of MPC sensitivity to uncertainties coming from forecasts and model mismatches, an extension of the approach to multiple systems in a distribution network, including other technologies such as mini-CHP and batteries, and a benchmark between a decentralized MPC approach and a centralized MPC approach for grid operation with flexible H-MGs. The next chapters elaborate on some of these issues.

3. Economic operation of a photovoltaic-combined heat and power home-microgrid

This chapter investigates the economic model predictive control operation of a Home-Microgrid with photovoltaic-combined heat and power storage systems. The purpose of the chapter is to present the problem formulation and quantify the impact of uncertainties. The chapter compares a model predictive control-based strategy with an open loop-based operation, and a perfect forecast based operation. The chapter discusses the effects of having uncertainties in the operation, relaying the benefits of using model predictive control to handle such situations. Additionally, the chapter at hand presents a sensitivity analysis regarding storage size, concluding that the proposed economic model predictive control strategy can be used to reduce total annual costs.

The content of this chapter is adapted from [59]: D. I. Hidalgo Rodríguez and J. M. Myrzik, "Economic model predictive control for optimal operation of home microgrid with photovoltaic-combined heat and power storage system," in *Proceedings of the 20th IFAC World Congress*. Toulouse, France, 2017.

3.1. Introduction

In this chapter, the purpose is to provide new insights regarding H-MGs' operation using an economic MPC approach. Here, economic MPC is a receding horizon control strategy with a stage cost that includes an economic objective function and does not merely penalize the distance to a desired set-point. More specifically, this chapter investigates the impact of mini CHP dynamic behavior prediction and storage size on the economic operation. This chapter includes the following contributions:

1. a thermal model for the dynamic behavior for a commercial internal combustion engine mini CHP in the optimization problem,
2. an analysis on the impact of uncertainties from mini CHP thermal power settling times, PV generation, electrical demand, and thermal demand,
3. a quantification of the added value of MPC compared to an open loop-based optimization strategy, and
4. a sensitivity analysis on the impacts of battery size and TES size on the economic operation.

The chapter is organized as follows: Section 3.2 describes the system under investigation, the optimization problem, operation strategies and simulation setup. Then, simulation results and corresponding discussion are presented in Section 3.3. Finally, Section 3.4 summarizes the main outcomes of the chapter, its limitations and future work.

3.2. System description and problem formulation

A system for a multi-family house (MFH) is investigated, which combines one mini CHP, one TES, one PV plant and one battery, as Figure 3.1 presents. System's operation is formulated as a mixed integer linear programming (MILP) problem within an MPC framework. This section first briefly describes the utilization of MPC for the system under investigation, then it presents correspondent constraints and objective function for the optimization problem, followed by the description of operation strategies and simulation setup.

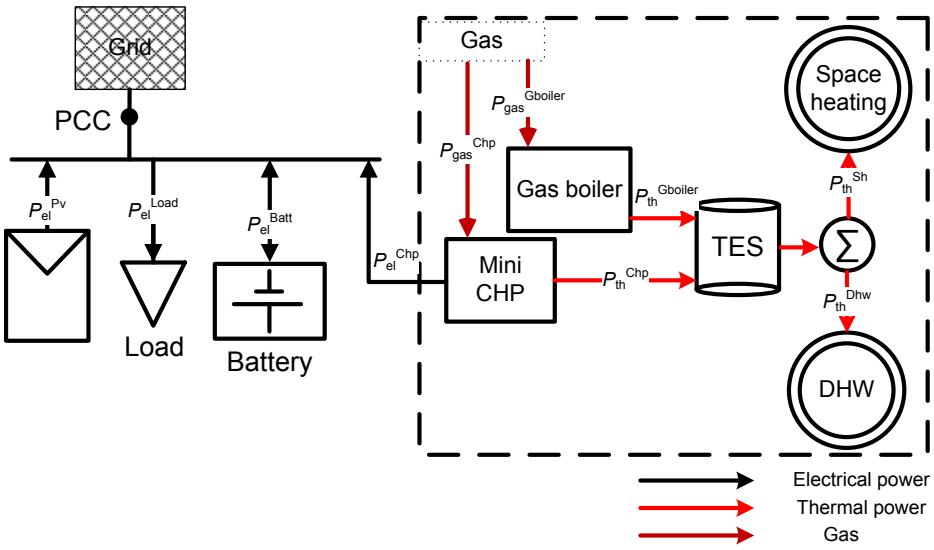

Figure 3.1.: Overview of system components in the home microgrid

3.2.1. MPC for the considered H-MG

For the actual case study, the goal of the proposed economic MPC-based operation is to find a future trajectory for the electrical and thermal power output of the mini CHP, the state of charge of the storage systems, and the thermal power of the auxiliary gas boiler over a given prediction horizon, to minimize operational costs of the H-MG. This is done by shifting operation times of the mini CHP using the flexibility provided by the TES and the battery. The MPC strategy considers dynamic models for CHP thermal behavior and evolution of state of charge of the storage systems, as well as measurement data for PV, load, space heating and domestic hot water for a MFH in Germany. The

MPC is considered at the management level of the H-MG automation system, and power set-points are sent to low level controllers of system's components (see Figure 3.2).

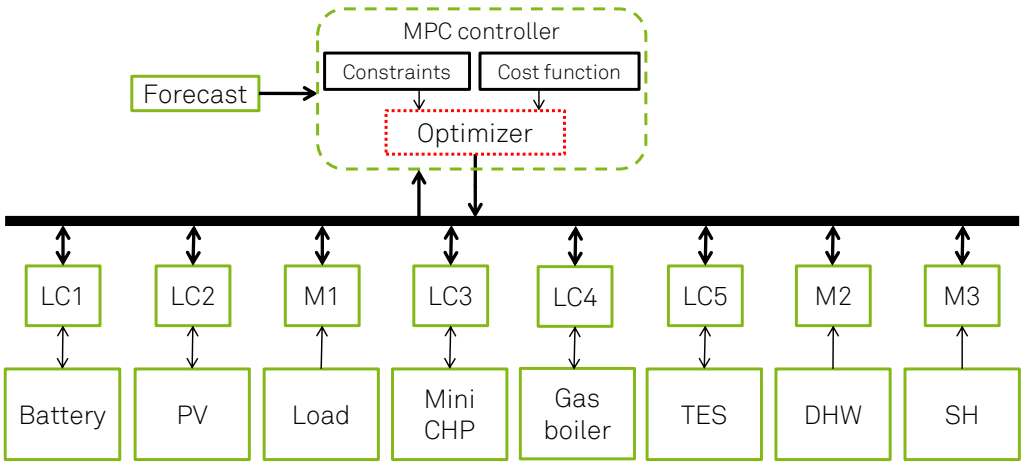

Figure 3.2.: Structure of the whole setup including microgrid components and MPC controller (LC#:local controllers, and M#: measurement devices)

In the following subsections, all equations and inequalities are valid for each time step k, where $k \in \{k_i, \ldots, k_i + N_p - 1\}$.

3.2.2. Mini CHP model

This section describes the modeling for the considered internal combustion engine (ICE) mini-CHP. Reference [30] uses an approximated piece-wise linear model, initially developed for large scale CHPs, to describe the behavior of the CHP considered in that work. Thermal and electrical response times from large scale CHPs may significantly differ from response times of mini-CHPs. The authors in [29] introduce a grey-box data-based model for a fuel cell mini-CHP, which is also used within an MPC scheme. As basic principles of fuel cell mini-CHPs and ICE mini-CHPs are different, the representation of the dynamic response of ICE mini-CHPs needs a specific model. Figure 3.3 depicts the operation of a commercial ICE mini CHP [77]. The brown line indicates the input power, and the red and green line the thermal and electrical output power respectively. It is noticeable that the two outputs present different step response characteristics. While the electrical output reaches the steady state very fast, in a matter of seconds, the thermal output needs more time to reach the steady state. The figure also shows different step response behaviors for the thermal output. According to [77], ICE mini-CHPs present two types of step responses for their thermal output: cold-start response and warm-start response. Depending on how long an OFF status of the mini CHP lasts, it takes more or less time to reach a given nominal power set-point. In the figure, for the first start the mini-CHP needs around 60 minutes to reach its nominal power. This is a cold-start. Then, two

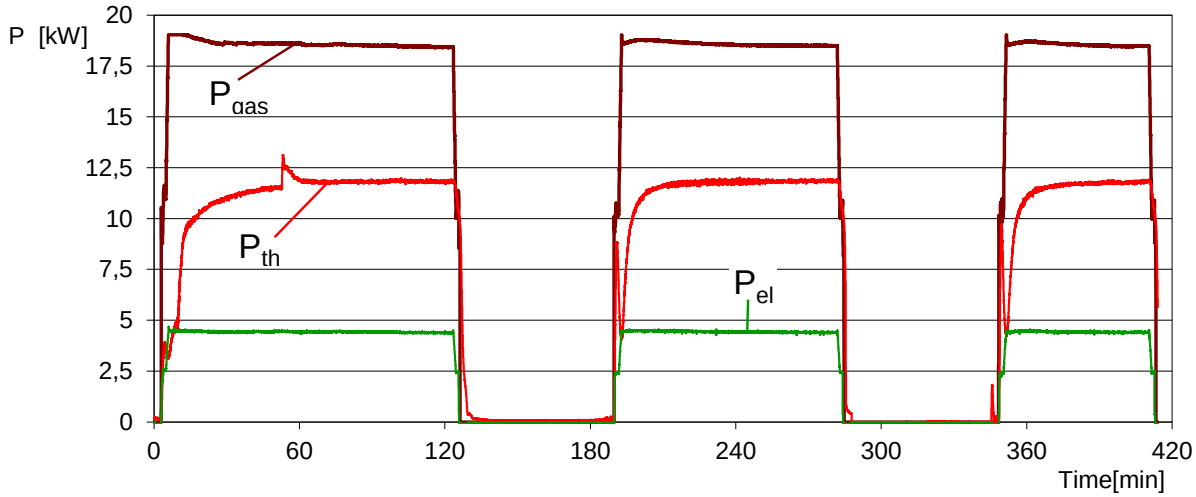

Figure 3.3.: Step responses for a commercial mini CHP (see [77])

consecutives warm-starts occur, one at minute 190 and the next at minute 350. For these warm-starts, it takes for the mini-CHP around 40 minutes to achieve the steady state.

In view of the fact that the dynamic response of the electrical output is faster than the thermal one, and that the settling time of the electrical power output is shorter than the MPC sample, it is reasonably acceptable to describe the relationship between mini CHP power input p_{gas}^{Chp} and electrical power output p_{el}^{Chp} using a steady-state model (static model) as

$$p_{el}^{\mathrm{Chp}}(k) = p_{gas}^{\mathrm{Chp}}(k) \cdot \eta_{el}^{Chp}, \tag{3.1}$$

where p_{gas}^{Chp} is the power input and p_{el}^{Chp} is the electrical power output. The electrical operation range is given by

$$b^{\mathrm{Chp}}(k) \cdot p_{el}^{\mathrm{Chp,min}} \leq p_{el}^{\mathrm{Chp}}(k) \leq p_{el}^{\mathrm{Chp,max}} \cdot b^{\mathrm{Chp}}(k), \tag{3.2}$$

$$b^{\mathrm{Chp}}(k) \in \{0, 1\}, \tag{3.3}$$

with the binary variable $b^{\mathrm{Chp}}(k)$, which is used to limit $p_{el}^{\mathrm{Chp}}(k)$ to its minimum and maximum allowable values when the mini CHP is ON.

However, the thermal output dynamic behavior needs a more detailed model. Therefore, the work at hand uses the data-based model proposed in [78], which reproduces the thermal step-response behavior of an ICE mini-CHP. The model is given as continuous-time transfer function. After a transformation to state space representation and a discretization, the resulting model is

$$p_{th}^{\mathrm{Chp}}(k+1) = A_{th}^{\mathrm{warm}} \cdot p_{th}^{Chp}(k) + B_{th}^{\mathrm{warm}} \cdot p_{gas}^{\mathrm{Chp}}(k). \tag{3.4}$$

The following constraint is used to have a continuous operation of the mini CHP for m_{cont}

steps

$$p_{gas}^{\mathrm{Chp}}(m) = p_{gas}^{\mathrm{Chp}}(m + k_{cont}), \tag{3.5}$$

and this must hold for all $m \in \{k_i, k_i + m_{cont}, \ldots, k_i + N_p - m_{cont} - 1\}$ and for all $k_{cont} \in \{0, \ldots, m_{cont}\}$.

In this work, just the warm start behavior is taken into account. Considering both, cold start and warm start behavior in the optimization problem is beyond the scope of this work and is left as future work.

3.2.3. Electrical battery

The behavior of the battery is described by

$$SoC^{\mathrm{Batt}}(k+1) = SoC^{\mathrm{Batt}}(k) \cdot \eta^{\mathrm{Batt,sd}} + \left(p_{el}^{\mathrm{Batt,char}}(k) \cdot \eta^{\mathrm{Batt,char}} - \frac{p_{el}^{\mathrm{Batt,dis}}(k)}{\eta^{\mathrm{Batt,dis}}} \right) \cdot K^{\mathrm{Batt}}, \tag{3.6}$$

$$SoC^{\mathrm{Batt,min}} \leq SoC^{\mathrm{Batt}}(k) \leq SoC^{\mathrm{Batt,max}}, \tag{3.7}$$

$$0 \leq p_{el}^{\mathrm{Batt,dis}}(k) \leq p_{el}^{\mathrm{Batt,dis,max}} \cdot \left(1 - b^{\mathrm{Batt}}(k)\right), \tag{3.8}$$

$$0 \leq p_{el}^{\mathrm{Batt,char}}(k) \leq p_{el}^{\mathrm{Batt,char,max}} \cdot (b^{\mathrm{Batt}}(k)), \tag{3.9}$$

$$b^{\mathrm{Batt}}(k) \in \{0, 1\}, \tag{3.10}$$

with $K^{\mathrm{Batt}} = \frac{\Delta T}{Cap^{\mathrm{Batt}}} \times 100$. SoC^{Batt} gives the available energy level in the battery in percent. Self-discharge coefficient $\eta^{\mathrm{Batt,sd}}$, charging and discharging efficiencies, $\eta^{\mathrm{Batt,char}}$ and $\eta^{\mathrm{Batt,dis}}$, are also taken into account. Similar to [24], battery power at time k is modeled with two different variables $p_{el}^{\mathrm{Batt,char}}$ for charging, and $p_{el}^{\mathrm{Batt,dis}}$ for discharging to be able to implement separate efficiencies for both processes. To avoid simultaneous battery charging and discharging at a single time step, a binary decision variable $b^{\mathrm{Batt}}(k)$ is used which makes both process mutually exclusive in the optimization problem.

3.2.4. Electrical power balance

The electrical power balance at PCC (see Figure 3.1) is given by the expression

$$p_{el}^{\text{Load}}(k) + p_{el}^{\text{Batt,char}}(k) + p_{el}^{\text{Grid,exp}}(k) = p_{el}^{\text{Chp}}(k) + p_{el}^{\text{Pv}}(k) + p_{el}^{\text{Batt,dis}}(k) + p_{el}^{\text{Grid,imp}}(k), \quad (3.11)$$

as $p_{el}^{\text{Batt,char}}(k)$ and $p_{el}^{\text{Batt,dis}}(k)$ are mutually exclusive, just one of them can be larger than zero at time k. In addition, because costs of power import from the grid are higher than the FIT for $p_{el}^{\text{Grid,exp}}(k)$ in the objective function (see (3.20)), it implies that whenever there is power export to the grid $p_{el,k}^{\text{Grid,imp}}$ is zero. This implies that for this case, there is no need of an additional constraint to set mutual exclusivity between power import and power export.

The constraint below avoids charging the battery from the grid as

$$0 \leq p_{el}^{\text{Grid,imp}}(k) \leq \left(p_{el}^{\text{Load,max}}\right) \cdot \left(1 - b^{\text{Batt}}(k)\right), \quad (3.12)$$

and it is used just for the stand-alone H-MG operation. When the operation of interconnected H-MGs is investigated, the optimization problem does not include this constraint.

3.2.5. Auxiliary gas boiler

The relationship between gas input power and thermal output power is given by

$$p_{th}^{\text{Gboiler}}(k) = p_{th}(k) \cdot \eta^{\text{Gboiler}}, \quad (3.13)$$

with the boiler efficiency $\eta^{Gboiler}$. Similar to the CHP, a binary variable is used here to keep the thermal output power $p_{th}^{\text{Gboiler}}(k)$ within its limits as

$$b^{\text{Gboiler}}(k) \cdot p_{th}^{\text{Gboiler,min}} \leq p_{th}^{\text{Gboiler}}(k) \leq p_{th}^{\text{Gboiler,max}}(k) \cdot b^{\text{Gboiler}}(k), \quad (3.14)$$

$$b^{\text{Gboiler}}(k) \in \{0, 1\}. \quad (3.15)$$

3.2.6. Thermal energy storage

Similar to Subsection 2.2.3, the following TES model is implemented in this chapter. It reproduces the evolution of TES state of charge considering stand-by heat loss coefficient, charging efficiency and discharging efficiency.

$$SoC^{\text{Tes}}(k+1) \quad = \quad SoC^{\text{Tes}}(k) \cdot \eta^{\text{Tes,sd}} + \left(p_{th}^{\text{Tes,char}}(k) - p_{th}^{\text{Tes,dis}}(k)\right) \cdot K^{\text{Tes}}, \quad (3.16)$$

with $K^{\text{Tes}} = \frac{\Delta T}{Cap^{\text{Tes}}} \times 100$,

$$SoC^{\text{Tes,min}} \leq SoC^{\text{Tes}}(k) \leq SoC^{\text{Tes,max}}, \quad (3.17)$$

and the charging-/discharging for TES is given by

$$p_{th}^{\text{Tes,char}}(k) = \left(p_{th}^{\text{Chp}}(k) + p_{th}^{\text{Gboiler}}(k)\right) \cdot \eta^{\text{Tes,char}}, \quad (3.18)$$

$$p_{th}^{\text{Tes,dis}}(k) = \frac{p_{th}^{\text{Sh}}(k) + p_{th}^{\text{Dhw}}(k) + p_{th}^{\text{Lost}}(k)}{\eta^{\text{Tes,dis}}}. \quad (3.19)$$

3.2.7. Objective function

The economic objective function gives the total operation costs for the H-MG over a given time horizon as

$$J_4 = \sum_{k=k_i}^{k_i+N_p-1} C_{gas}\left(p_{gas}^{\text{Chp}}(k) + p_{gas}^{\text{Gboiler}}(k)\right) + C_{el} \cdot p_{el}^{Grid,imp}(k) - C_{Fit} \cdot p_{el}^{\text{Grid,exp}}(k) + C^{\text{Lost}} \cdot p_{th}^{\text{Lost}}(k), \quad (3.20)$$

where k_i is any arbitrary initial time step. C_{gas} is the gas price, C_{el} is the electricity price, C_{Fit} is the feed-in tariff for injected power, and C^{Lost} is the penalty cost for wasting energy in the TES. This function is minimized within the MPC scheme.

To summarize, the optimization problem is stated as

$$\underset{\hat{\boldsymbol{u}}_b}{\text{minimize}} \qquad J_4(\hat{\boldsymbol{u}}_{\boldsymbol{b}}) \quad (3.21a)$$

subject to

$$\boldsymbol{p}_{el}^{\text{Chp}}, \boldsymbol{p}_{th}^{\text{Chp}}, \boldsymbol{b}^{\text{Chp}} \in \mathcal{P}^{\text{Chp}}, \quad (3.21b)$$

$$\boldsymbol{p}_{el}^{\text{Batt,char}}, \boldsymbol{p}_{el}^{\text{Batt,dis}}, \boldsymbol{b}^{\text{Batt}} \in \mathcal{P}^{\text{Batt}}, \quad (3.21c)$$

$$\boldsymbol{p}_{el}^{\text{Imp}}, \boldsymbol{p}_{el}^{\text{Exp}} \in \mathcal{P}^{\text{Grid}}, \quad (3.21d)$$

$$\boldsymbol{p}_{th}^{Gboiler}, \boldsymbol{b}^{\text{Gboiler}} \in \mathcal{P}^{\text{Gboiler}}, \quad (3.21e)$$

$$\boldsymbol{p}_{th}^{\text{Tes,char}}, \boldsymbol{p}_{th}^{\text{Tes,dis}} \in \mathcal{P}^{\text{Tes}}, \quad (3.21f)$$

$$\forall k \in \{k_i, \ldots, k_i + N_p - 1\}. \quad (3.21g)$$

Where the set $\mathcal{P}^{\text{Chp}}$ is given by (3.1)-(3.5), the set $\mathcal{P}^{\text{Batt}}$ is defined by (3.6)-(3.10), the set $\mathcal{P}^{\text{Grid}}$ is defined by (3.11)-(3.12), the set $\mathcal{P}^{\text{Gboiler}}$ is given by (3.13)-(3.15), and the set $\mathcal{P}^{\text{Tes}}$ is defined by (3.16)-(3.19). The vector of decision variables vectors is

$$\hat{\boldsymbol{u}}_b = \begin{bmatrix} \boldsymbol{p}_{gas}^{\text{Chp}} \\ \boldsymbol{p}_{th}^{\text{Gboiler}} \\ \boldsymbol{p}_{el}^{\text{Batt,char}} \\ \boldsymbol{p}_{el}^{\text{Batt,dis}} \\ \boldsymbol{p}_{th}^{\text{Lost}} \\ \boldsymbol{b}^{\text{Chp}} \\ \boldsymbol{b}^{\text{Batt}} \end{bmatrix}, \tag{3.22}$$

where all decision variables vectors are in $\mathbb{R}^{Np}$.

3.2.8. Operation strategies for a photovoltaic-combined heat and power H-MG

To better quantify the advantages or disadvantages of an MPC-based operation for a photovoltaic-combined heat and power H-MG, two further operation strategies are simulated for comparison purposes. The next paragraphs briefly describe the operation strategies.

Perfect forecast strategy : The optimization problem is solved assuming perfect knowledge of the system. It gives the optimal solution and serves as a lower bound for the other strategies. This is the baseline scenario.

MPC-based strategy : Here, uncertainties in thermal behavior of the mini CHP are considered. The mini-CHP model in the optimization problem differs from the real system. The optimization problem is solved for the next 24 hours, but just the set-points for the first hour are sent to the low level controllers. After, one hour, actual states of the system are updated in the model and a new optimization loop starts.

Open loop-based strategy : Similar to the MPC-based strategy, uncertainties in the thermal behavior of the mini CHP are present. The optimization problem is solved for the next 24 hours, and the whole sequence is implemented in the real system. After 24 hours, the procedure is repeated.

Some authors include a terminal constraint to avoid the battery's full discharge at the end of the horizon. This work does not consider such a terminal constraint either for the

MPC-based strategy or for the open loop-based strategy. Therefore, the comparison is made on the same basis.

3.2.9. Simulation setup for a multi-family house H-MG

Time series data in 10 min resolution for space heating, domestic hot water, household load (from the VDI guideline 4655 [72]) and PV power generation (from a field test) are for Germany for one year. The MFH has an annual electrical consumption of 23655.70 kWh/a, and a thermal consumption of 74888.57 kWh/a. The PV plant has an annual energy yield of 8529.24 kWh/a. Table 3.1 gives the parameters used for the simulation. Moreover, for the economic analysis, specific investment costs of 1724 EUR/kWh for a 6 kWh battery, and 1108 EUR/kWh for a 12 kWh battery are assumed. Similarly, total investment costs of 1100 EUR, 1387 EUR, 1546 EUR, and 2300 EUR are used for the 100 liter TES, the 300 liter TES, the 500 liter TES, and the 1000 liter TES respectively. The annual costs per year considers an annuity factor of 0.09. The calculation of the annuity factor uses an interest rate of 5% and a useful life-time of 15 years. The implementation is done in Python using Pyomo [74, 75] as modeler, and CPLEX [76] as solver.

Table 3.1.: Parameters for Simulation

N_p	24 (hrs)	Δt	10 (min)
$p_{el}^{\text{Chp,max}}$	4.5 (kW_{el})	η_{th}^{Chp}	0.633
$p_{el}^{\text{Chp,min}}$	1 (kW_{el})	A_{th}^{warm}	0.088
Cap^{Batt}	12 (kWh)	B_{th}^{warm}	0.577
$p_{el}^{\text{Batt,char,max}}$	6 (kW_{el})	$\eta^{\text{Batt,char}}$	0.9
$p_{el}^{\text{Batt,dis,max}}$	6 (kW_{el})	$\eta^{\text{Batt,sd}}$	0.999
$p_{el}^{\text{Load,max}}$	10 (kW_{el})	$\eta^{\text{Batt,dis}}$	0.92
$p_{th}^{\text{Gboiler,max}}$	40 (kW_{th})	η^{Gboiler}	1
$p_{th}^{\text{Gboiler,min}}$	1 (kW_{th})	$p_{el}^{\text{Pv,nom}}$	9 (kW_p)
C_{el}	28.38 (ct./kWh)	$\eta^{\text{Tes,sd}}$	0.998
Cap^{Tes}	11.50 (kWh)[1]	$\eta^{\text{Tes,char}}$	0.9
C_{gas}	6.52 (ct./kWh)	$\eta^{\text{Tes,dis}}$	0.92
C_{Fit}	12 (ct./kWh)	η_{el}^{Chp}	0.238

[1]as for a typical water tank with 500l and $\Delta T = 20\text{K}$

3.3. Simulation results and discussion

This section present relevant simulation results for the optimal operation of the photovoltaic-combined heat and power H-MG. The section is divided in three parts. First, a qualitative analysis of resulting profiles for one exemplary day helps for further understanding the operation of the system. The second part quantifies the overall impact of uncertainty in the mini CHP model on annual costs. Also, a sensitivity analysis on TES and battery storage sizes shows how costs change if smaller storage systems are used. In the end, the section presents results from annual simulations considering all sources of uncertainties.

3.3.1. Qualitative analysis

Figure 3.4 presents resulting profiles for the system operation. The first subplot contains the electrical profiles of the system, and the second subplot shows resulting thermal profiles. The last subplot depicts storage systems' state of charge. When looking at the electrical power output of the CHP, two operation patterns are visible: one during night and early morning hours, and one different during the day. When there is no PV generation, the CHP runs under an electricity-led strategy, i.e. following the household load in order to reduce electricity costs.

As soon as the MPC predicts the thermal load peak at around 6:00 in the morning (second subplot), the CHP changes to a heat-led operation. It increases the operation point in order to fully charge the TES, so that the coming peak in thermal demand can be covered without using the gas boiler. During PV production hours, the CHP continues under heat-led operation, the electrical load is covered mainly by the PV production, and the electricity surplus is sold into the grid. Due to the high thermal demand during the day, there are just few cases when the TES can be charged (see 10:00 and 14:00 hours). Regarding the battery system, the MPC decides not store the electricity surplus, but to sell it to the grid. Just when the MPC predicts the evening peak in household load around 19:00 hours, it decides to charge the battery at around 13:00 hours to have enough energy to cover the coming peak. As PV generation decreases, the CHP switches again to electricity-led operation.

3.3.2. Impact of a small uncertainty in the thermal behaviour of CHP on annual costs

The second part of this section presents the quantification of the impact of uncertainty in the CHP thermal behavior. For this purpose, two operational costs are compared: the resultant costs for a simulation with optimal operation without uncertainty (perfect

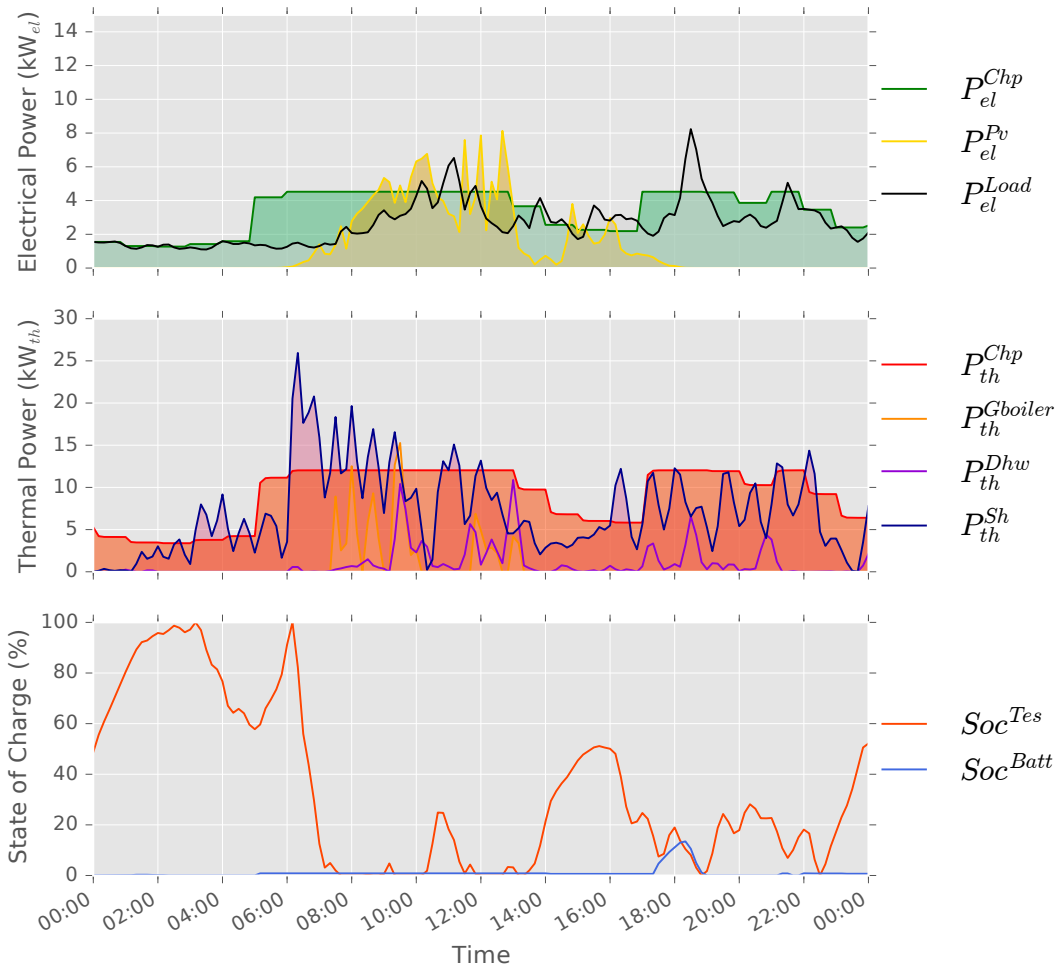

Figure 3.4.: Example of resultant profiles for perfect operation strategy

knowledge of the system) over a year, against the resultant costs for the open loop optimization operation and the MPC operation, also over a year but including uncertainty in the model. Here, it is assumed that the model in the optimization problem is different from the real system, and this is done by decreasing the time constant of the thermal power system of the CHP. The real system behaves as described in Figure 3.3 for the warm start, while the MPC assumes that the mini CHP reaches its nominal thermal power in about 10 minutes. To better illustrate the responses, Figure 3.5 shows the real, and the mini CHP thermal behavior assumed by the MPC. The brown line shows the gas power input set-points sent from the MPC to the mini CHP. The purple line is the thermal power output assumed by the MPC, while the red line denotes the real thermal power output of the mini CHP.

For the perfect optimal operation the resultant annual operational costs are 7470.79 EUR/a. If uncertainties in the thermal behavior of the mini CHP are present, the annual operational costs increase to 7472.18 EUR/a and 7518.10 EUR/a for the MPC-based operation and the open loop optimization-based operation respectively. These resultant costs can be explained as follows: Because the real system responds slower than assumed

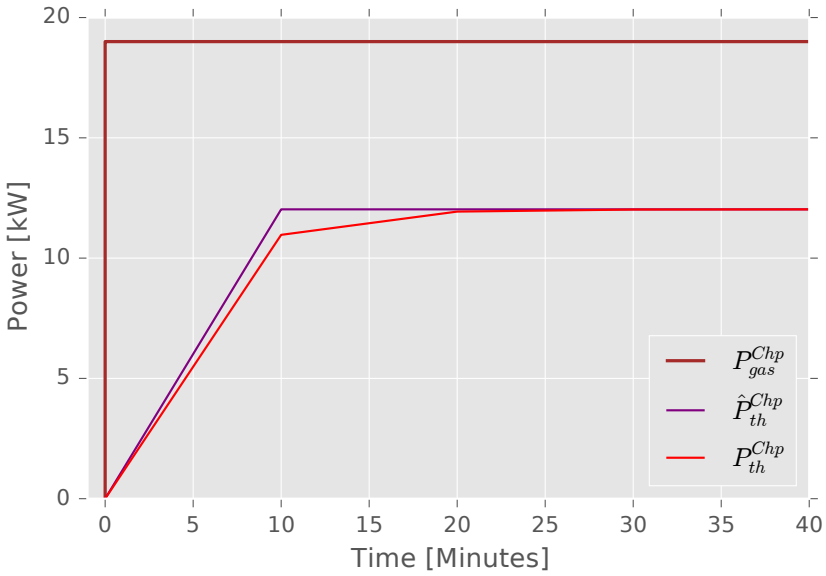

Figure 3.5.: Step responses for the real system and the model in the optimization

by the MPC, this results in the TES receiving less energy than planned when the CHP is running up. On the other hand, when the CHP is running down, slower than assumed by the MPC, the TES receives more energy that initially planned. This may be problematic, if the TES is almost full. In such a situation, the MPC will shut-down the CHP assuming that it will reduce its thermal power very fast, so that the upper limit of the TES will not be reached. In reality, the CHP reduces its thermal power slower than required, meaning that more energy is supplied, leading to an overcharging of the TES. To deal with this issue, the real system has to waste some energy in order to allow further operation, incurring in extra costs. This situation affects the MPC as well, because there may exist situations where in the beginning of MPC's time window the TES is already or almost full, and the CHP is still running down, so that no matter what action the MPC takes, the optimization problem is already infeasible. For this reason, the decision variable P_{th}^{Lost} is included to also enable the MPC to waste some power in order to make the optimization problem feasible. On the contrary, if less energy than expected is given by mini CHP and the storage is almost empty, then the gas boiler has to supply the missing energy. The MPC leads to lower annual operational costs, compared to the open loop strategy, mainly because of its closed loop property, which allows to correct mini CHP schedules every hour. Since the open loop-based operation calculates fixed schedules for the next 24 hours, it must waste more energy due to the presence of uncertainty in the mini CHP thermal behavior. Figure 3.6 gives the net additional operation costs for MPC-based operation and open loop-based operation.

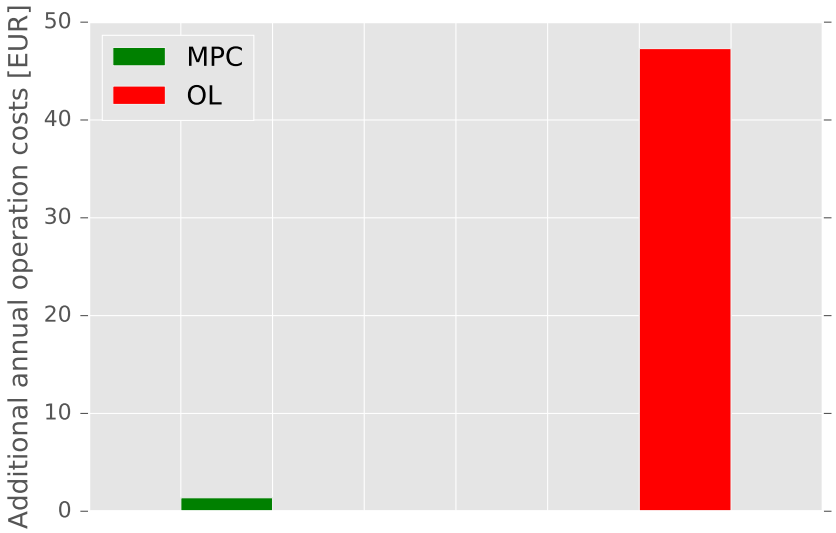

Figure 3.6.: Net additional annual operation costs

3.3.2.1. Sensitivity analysis on storage sizes

Finally, a sensitivity analysis reveals the effects of storage sizes on H-MG operational costs. The baseline is the resultant costs for the perfect operation with 500liter TES and battery capacity of 12 kWh. Simulations over a year with variations of TES volume and battery capacity, recording the corresponding additional operation costs are conducted. The simulation scenarios correspond to TES volumes of 1000 liter, 500 liter, 300 liter and 100 liter, and battery capacities of 12 kWh and 6 kWh, for both operation strategies - MPC-based and open loop-based. Through this experiment, it will be possible to determine how small the storage systems could be, such that under a suitable operation strategy the additional operation costs are still moderated. Figure 3.7 helps to visualize the results of the annual simulations.

As expected, a home microgrid with 1000 liter TES and 12 kWh battery gives the minimum operation costs under MPC-based operation. If the system uses a 100 liter TES with a 6 kWh battery under an open loop-based operation, the operation costs increase by ca. 200 EUR/a compared to the baseline case. This configuration presents the larger additional costs.

In general, for a given configuration, MPC-based operation is always cheaper than the open loop-based. Another aspect worth to mention, is that a system under MPC-based operation with TES-300 liter and 12 kWh battery shows lower operation costs than a system with the same battery size but with larger TES capacity under open loop-based operation.

It is usual that the smaller the storage capacity is, the lower the investment costs are. Therefore, annuity costs, based on investment and operation costs, are shown in Figure 3.8.

Figure 3.7.: Sensitivity analysis on operation costs with different storage capacities for MPC and OL

When considering total annual costs, system configurations with battery sizes of 12 kWh (green) are not attractive anymore. From this chart, the optimal system configuration for a photovoltaic-combined heat and power H-MG is a 1000 liter TES and a 6 kWh battery under an MPC-based operation.

Figure 3.8.: Total annual costs with different storage capacities

3.3.3. Full year simulations considering all sources of uncertainties

The previous section showed resulting operation and investment costs when a small uncertainty in the CHP's thermal behavior was present. However, there are further sources for uncertainties in this kind of system. Uncertainties are present in the CHP's thermal behavior, the forecast for PV generation, the forecast for electrical demand, and the forecast for heat demand - space heating and domestic hot water. This section delivers simulation results considering all these sources of uncertainties in the system.

Similar to the previous section, the analysis considers three operation strategies. The perfect operation strategy does not include any uncertainty, and the optimization assumes perfect knowledge of all uncertain parameters. This approach exemplifies the case of sizing a storage system using historical data as a reference.

The other two strategies are the open-loop operation strategy and the MPC operation strategy (closed-loop). These strategies are usually not used in the design phase of storage systems but during the operation phase. They emulate the operation planning of energy systems, which occurs day-ahead and intra-day. For these two operation strategies, the optimization works with imperfect knowledge of uncertain parameters.

The open-loop operation strategy and the MPC operation strategy require a forecast for PV generation, electrical demand, and thermal demand. As the PV power and the space heating demand are highly weather dependent, the prediction for PV generation and space heating demand includes a simple 1-day persistence forecast. The optimization assumes that the PV generation and the space heating consumption for the current day are the same as from the previous day.

For electrical load consumption and domestic hot water consumption, the prediction uses a 7-day persistence forecast, i.e., the optimization assumes that these consumptions are the same as the ones from one week before (7-day persistence). This assumption is because of the dependency of electrical consumption and DHW consumption on weekdays.

Again, the examination comprises simulations with different storage sizes. It considers TES with 300 liters, 500 liters, and 1000 liters, and battery systems with 6 kWh and 12 kWh. The 100-liter TES is out of the examination because the previous section showed that its operating costs are not competitive. Therefore, there are six possible combinations for storage systems, and each combination requires an annual simulation with a correspondent operation strategy. In the end, a total of 12 annual simulations are necessary.

Figure 3.9 shows the resulting operation costs per year. One interpretation of the chart is that during the design phase, the expectation is that the systems will have operating costs between 6800 EUR and 7000 EUR per year.

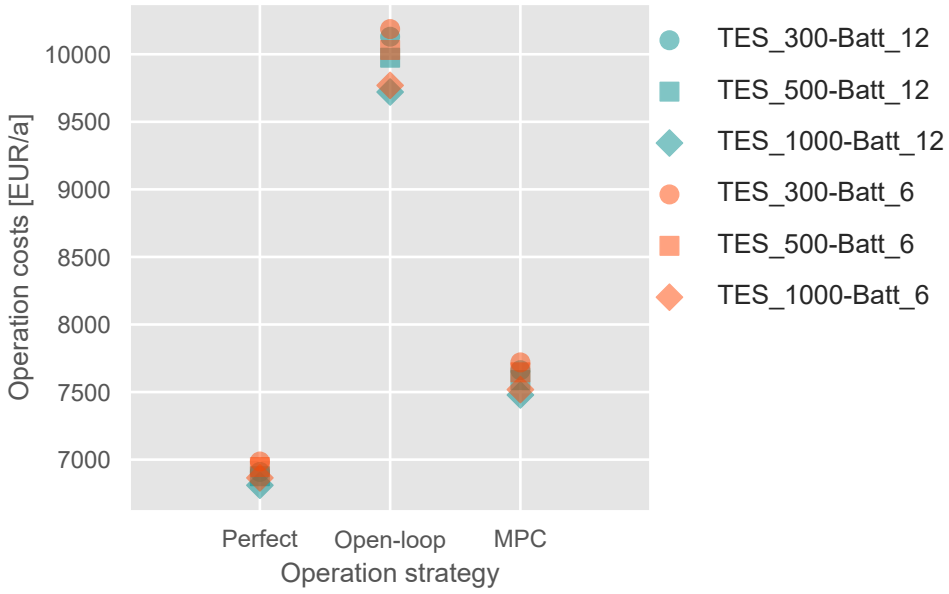

Figure 3.9.: Operation costs considering all uncertainties

However, during the operation phase, these costs could be about 500 EUR up to 3000 EUR higher. The reason for this is the assumption of perfect knowledge of the uncertain parameters during the design phase. In general, MPC gives a cost reduction for a given system configuration of about 2200 EUR/a compared to open-loop. The gap between MPC and perfect operation strategy is around 500 EUR. It is an upper bound for the MCP operation since the strategy used a simple prediction approach for the conducted simulations. If a more accurate prediction is available, this cost gap will be smaller. For all operation strategies, the configuration with the lowest costs is 1000 liters TES and 12 kWh battery, while the configuration 300 liters TES and 6 kWh battery delivers the highest costs.

Figure 3.10 allows the appreciation of the difference in operating costs between system configurations for MPC.

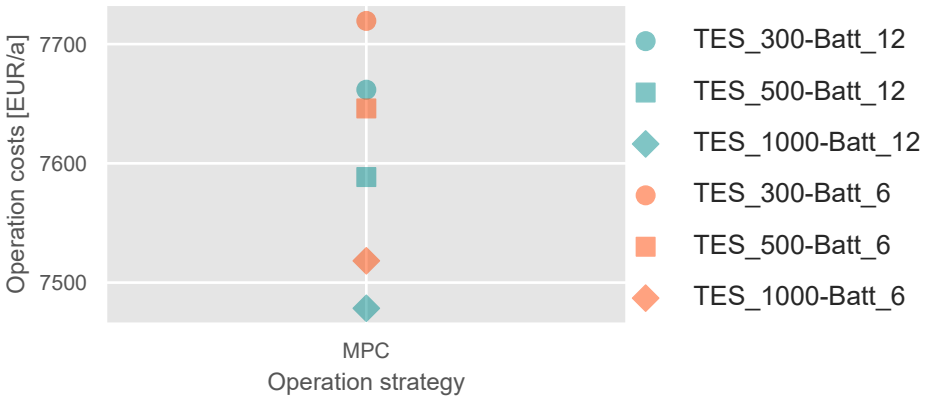

Figure 3.10.: Operation costs for MPC considering all uncertainties

The next lowest operation costs are for the 1000 liters TES with 6 kWh battery, followed by the 500 liters TES with 12 kWh battery. It is also clear that a system with 500 liters TES and 6 kWh battery gives similar operational costs that a system with 300 liters TES and 12 kWh battery.

Next, it is interesting to take a look at the total annual costs in Figure 3.11.

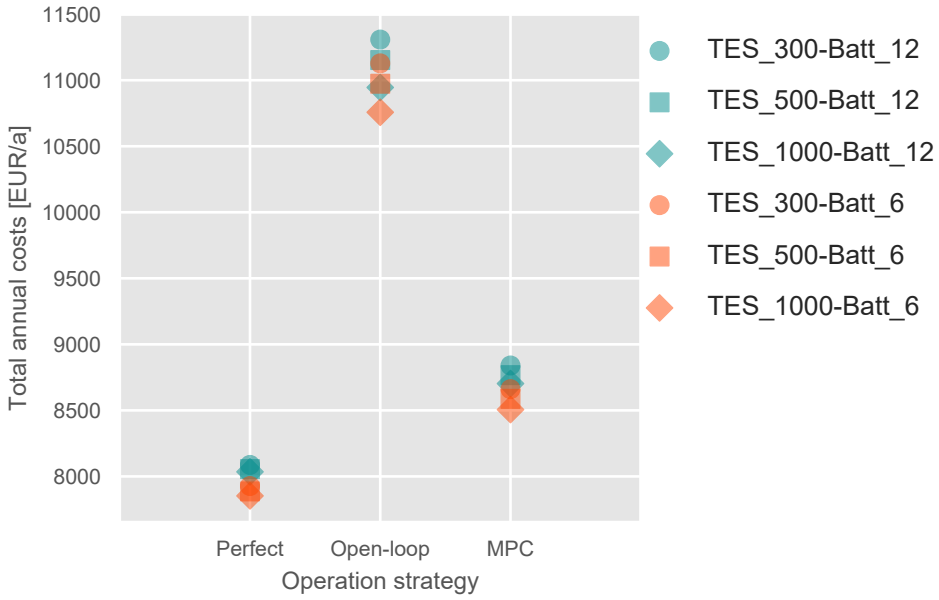

Figure 3.11.: Total annual costs considering all uncertainties

Here again, at least for MPC and the perfect operation strategy, systems containing a 12 kWh battery are not competitive. This situation is not valid for the open-loop operation strategy. Notwithstanding, the analysis will now focus on determining the optimal configuration for the MPC operation strategy. When analyzing the systems with the presence of uncertainties, it becomes clear that the lowest total annual costs are for by a system consisting of a 1000 liters TES and a 6 kWh battery under MPC operation. The larger TES capacity is better exploited by the MPC operation strategy, as already mentioned for the operation cots.

3.4. Summary of the chapter

This chapter investigated the economic MPC operation of an H-MG with photovoltaic-combined heat and power storage systems. The purpose of the chapter was to present the economic MPC problem formulation and investigate the impact of uncertainty coming from the thermal behavior of the mini CHP. The chapter included a comparison of an MPC-based strategy and an open loop-based strategy with a perfect-forecast strategy to quantify the effects of this uncertainty. Additionally, the chapter also presented a sensitivity analysis of storage size. The main consequence of having an imperfect model for the thermal response of the mini CHP is that the TES might be overcharged or undercharged. Therefore the system has to waste energy or use the auxiliary gas boiler to overcome these situations, incurring additional gas costs and inefficient operation. Simulation results showed that, even for a minimal mismatch between the optimization model and the real system regarding the settling time of mini CHP thermal power, resultant additional operating costs are substantially different between the open loop-based operation and the MPC-based operation. While the later one achieves operation costs almost equal to the perfect case, the costs for the open loop-based strategy are notably higher. This outcome confirms the robustness of MPC against uncertainties, as well as its advantages for the operation of H-MGs.

The chapter gave as well a sensitivity analysis regarding the impact of storage size on annual costs. Here, the MPC-based operation enabled a better usage of the storage systems, such that it might be possible to reduce battery size, with a moderate increase in operational costs, but a total reduction in investment costs (smaller storage systems). In the end, the chapter presented simulation results for a whole year considering all sources of uncertainties, namely, thermal CHP behavior, PV generation, and electrical and thermal demand. The results allowed to appreciate the added value of MPC against the open-loop operation strategy. They also indicated that there is still improvement potential for the MPC strategy when employing more accurate prediction approaches.

4. Coordination strategies for optimal operation of interconnected home-microgrids

This chapter presents the formulation and comparison of three different model predictive control coordination strategies for a group of interconnected home-microgrids. First, a decentralized coordination strategy is taken as a reference case, followed by the proposed centralized coordination. Lastly, employing dual decomposition, a hierarchical-distributed strategy is derived from it. The simulation results indicate that the proposed centralized formulation can improve the electrical power balancing among systems, with a reduction in extreme power peaks at the point of common coupling. The hierarchical-distributed strategy also shows an improvement in power profile compared to the decentralized strategy, while solving the global problem in a distributed way. The trade-off among local balancing with peak power reduction, energy bill, and storage losses demands further investigation.

The content of this chapter is adapted from [61]: D. I. Hidalgo-Rodríguez and J. Myrzik, "Optimal operation of interconnected home-microgrids with flexible thermal loads: A comparison of decentralized, centralized, and hierarchical-distributed model predictive control," in *20th Power Systems Computation Conference*. Dublin, Ireland, 2018.

4.1. Introduction

The coordinated operation of interconnected microgrids is a well-studied topic in the recent literature [14, 33–35, 54–57]. Within the context of MPC, several architectures are possible [40, 79]. For a group of H-MGs in a residential area, each H-MG is an independent agent, which tries to minimize its own economic cost function. A H-MG will minimize its total energy bill costs given electricity and gas prices, and feed-in-tariff. These prices can be fixed for the whole year, or dynamic e.g. changing every hour. In a *decentralized coordination strategy* (see Figure 4.1a), each H-MG solves its own optimization problem, based only on knowledge of its own state and forecasts for disturbances affecting only H-MG's individual performance. As there is no coordination between agents, such structure is called a decentralized. In this decentralized strategy, there are many small optimization problems. Furthermore, as each H-MG just uses its own information, there is no need for information exchange, which is an advantage of this strategy. The main disadvantage is that the obtained solution is suboptimal.

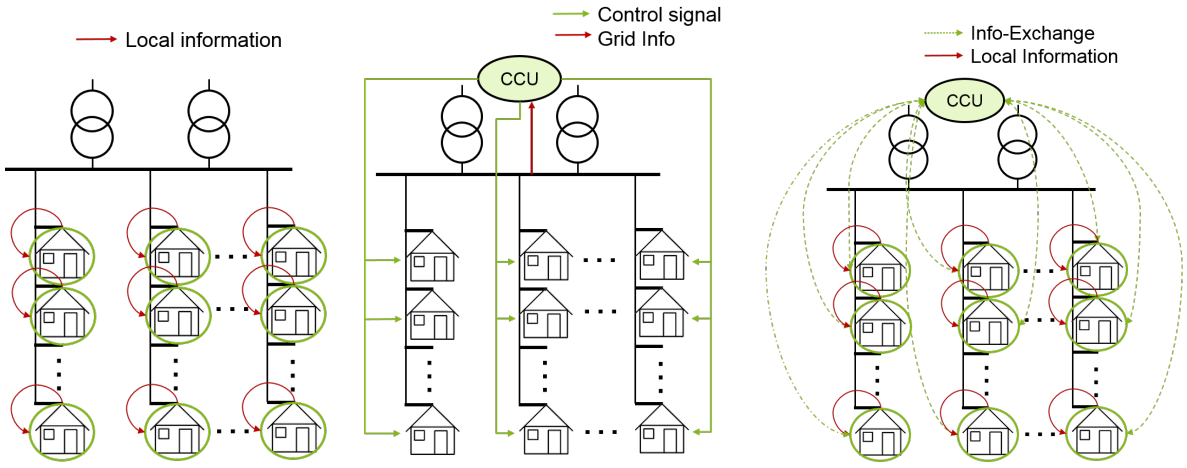

(a) Decentralized architecture (b) Centralized architecture (c) Hierarchical-distributed architecture

Figure 4.1.: Architectures for coordination strategies (CCU: Central Coordination Unit)

From the perspective of the electrical grid, a pure economic operation will result in large power peaks at the residential substation, since there is no incentive to reduce such peaks neither at consumption nor at generation side. This issue reveals the need of some kind of coordination between the H-MGs in order to avoid simultaneous power peaks. One option to tackle this issue is to use a centralized architecture (see Figure 4.1b), where a central unit coordinates all involved H-MGs and has global knowledge of the whole system. A *centralized coordination strategy* implies, therefore, a centralized optimization problem with a global objective function, which consists of two terms: one for the economic operation and, one for penalizing large power peaks. A central entity must have the complete optimization model of the system with information about the state of each H-MG. It solves the optimization problem, based also on disturbance forecasts, and decides about the operation schedule for each H-MG. The advantage of this strategy is that it achieves the optimal solution, as it is assumed that all information is available. On the other hand, it possesses the disadvantage of having to collect all the information from the systems, which subsequently results in a limited scalability of the approach. As this strategy implicates the central unit having knowledge of every model, constraint, parameter and state of each H-MG, the privacy aspect is another disadvantage of the centralized architecture.

Within the architecture for a *hierarchical-distributed coordination strategy* (see Figure 4.1c), a central coordination unit (CCU) gathers just certain local information from each H-MG and coordinates all involved H-MGs through some incentives. Hence, there is no need to reveal all constraints or variables of each H-MG, which helps keeping some privacy issues. In contrast to the centralized coordination strategy, the central unit does not solve a large optimization problem. Instead, this central unit performs simple computations based on the actual state of the system and sends indirect control signals (price signals) to the H-MGs. Each H-MG solves an optimization problem based on this input signal.

The information exchange in this strategy is moderate. Although the solution might be suboptimal, it is still better than the solution from the total decentralized strategy.

The purpose of this chapter is to present and contrast a decentralized MPC operation, a centralized MPC operation, and a hierarchical-distributed MPC operation for a group of interconnected home-microgrids with flexible heating systems. This chapter builds upon the work presented in [58, 59]. Specifically, the main contributions of this chapter include:

1. a new formulation for the centralized MPC optimization problem, taking into account costs minimization and peak power reduction,
2. a description and implementation of the hierarchical-distributed MPC strategy based on dual decomposition, which allows a more distributed implementation of the coordination strategy with less information exchange, and
3. a comparison of the above mentioned strategies against a reference decentralized strategy, providing new insights into the trade-off among local balancing with peak power reduction, energy bill, and storage losses.

The organization of this chapter is as follows. Systems under investigation, and the reference decentralized coordination strategy are described in Section 4.2 and Section 4.3 respectively. The description of the decentralized coordination strategy implies a detailed formulation of local optimization problems for each H-MG. These problem formulations include static and dynamic models of involved subsystems, operational constraints, and local economic objective functions. The Section 4.4 discusses the proposed centralized MPC formulation, while Section 4.5 gives a detailed description of the decomposition technique used for the hierarchical-distributed strategy and introduces the corresponding algorithm. Simulation outcomes are presented and discussed in Section 4.6. Finally, section Section 4.7 sums up the core results and conclusions of the chapter.

4.2. System description

The first part of this section will focus on the description of the considered H-MGs. Each H-MG consists of different types of appliances, generators and/or storage elements, which determine H-MG's electrical flexibility. The work at hand considers three types of H-MGs: H-MGs including a photovoltaic-battery storage system, H-MGs with photovoltaic-heat pump storage system, and H-MGs with an installed photovoltaic-cogeneration storage system. The section gives a compact formulation of set of constraints for battery units, heat pump units, TES units, mini CHP units, electrical water heater units, and electrical balance and power exchange with the grid.

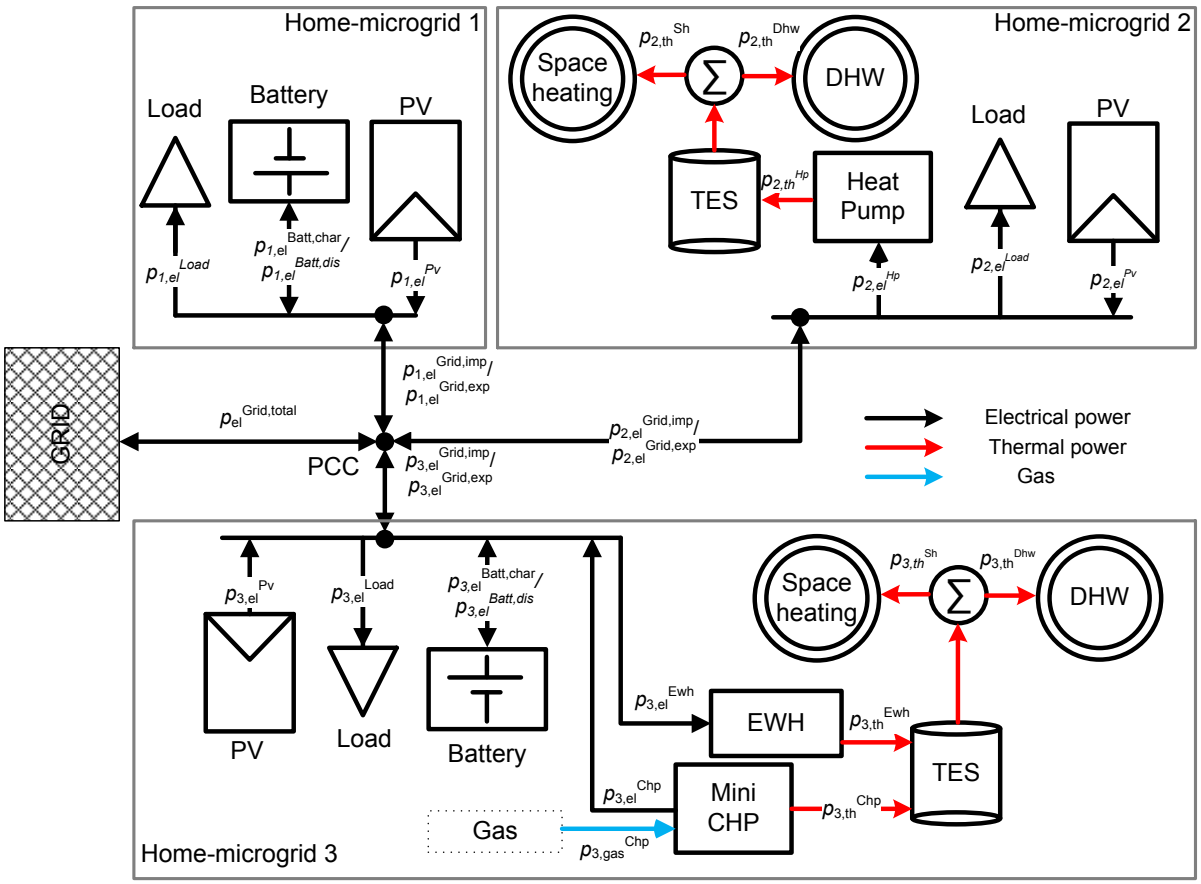

Figure 4.2.: Overview of considered home-microgrids

4.2.1. Considered home-microgrids

Home-microgrids under investigation are residential systems for single or multi-family households. This work focuses on three specific home-microgrids shown in Figure 4.2. The home-microgrid 1 is a photovoltaic-battery system (PV-Battery), which represents a single-family household with an installed PV plant and a battery. The PV plant can charge the battery, inject power to the grid, or feed the residential inflexible loads - in this case fridge, washing-machine, lights, etc. Home-microgrid 2 is a photovoltaic-heat pump system (PV-Heat pump). It also stands for a single-family household and is composed of a PV plant, a heat pump as flexible load, a TES, and further residential inflexible loads. The PV plant can either inject power to the grid or supply the heat pump, which is directly connected to the TES. Here, thermal energy is either stored or used to cover the residential thermal demand, i.e., space heating (SH) and domestic hot water (DHW). Finally, there is home-microgrid 3, which is a photovoltaic-combined heat and power storage system (PV-CHP-Storage) corresponding to a multi-family home-microgrid. It consists of one mini combined heat and power plant (mini CHP), one PV plant, one battery, one electrical water heater (EWH) as flexible load, one TES, and a group of inflexible residential loads. The mini CHP directly feeds a TES with thermal power, which at the same time provides energy to cover space heating and domestic hot water. Additionally, the EWH supplies

thermal power to the TES to cover peaks in the thermal demand. On the electrical side, a PV plant either injects electrical power to the grid, charges the battery or supplies the household loads. Analogously, the electrical power output of the mini CHP can flow to the grid or to the battery and loads.

4.2.2. Models and constraints for the considered technologies

As the previous chapters already described in detail the considered technologies (see Chapter 2 for PV-Heat pump, and Chapter 3 for PV-CHP-Storage), the following descriptions only aim to provide a compact and unified formulation for the coming optimization problems. The formulations are valid for any H-MG with index h, for $h \in \{1, \ldots, H\}$. Where, H denotes the number of interconnected H-MGs.

4.2.2.1. Set of equations for battery units

The set $\mathcal{P}_h^{\text{Batt}}$ describes the behavior of a battery unit. The following equations form this set:

$$SoC_h^{\text{Batt}}(k+1) = SoC_h^{\text{Batt}}(k) \cdot \eta_1^{\text{Batt,sd}} + \left(p_{h,el}^{\text{Batt,char}}(k) \cdot \eta_h^{\text{Batt,char}} - \frac{p_{h,el}^{\text{Batt,dis}}(k)}{\eta_h^{\text{Batt,dis}}} \right) \cdot K_h^{\text{Batt}}, \tag{4.1a}$$

$$SoC_h^{\text{Batt,min}} \leq SoC_h^{\text{Batt}}(k) \leq SoC_h^{\text{Batt,max}}, \tag{4.1b}$$

$$0 \leq p_{h,el}^{\text{Batt,dis}}(k) \leq p_{h,el}^{\text{Batt,dis,max}} \cdot \left(1 - b_h^{\text{Batt}}(k)\right), \tag{4.1c}$$

$$0 \leq p_{h,el}^{\text{Batt,char}}(k) \leq p_{h,el}^{\text{Batt,char,max}} \cdot \left(b_h^{\text{Batt}}(k)\right), \tag{4.1d}$$

$$b_h^{\text{Batt}}(k) \in \mathcal{B}, \tag{4.1e}$$

$$\forall k \in \{k_i, \ldots, k_i + N_p - 1\}. \tag{4.1f}$$

In general, equations (4.1a)-(4.1d) give the evolution of battery's state of charge and its limits, the maximal battery charging and discharging power, as well as the mutual exclusivity for the battery charging and discharging. Normally, $\mathcal{B}$ is $\{0, 1\}$. Just if the binary variables are relaxed, $\mathcal{B}$ is $[0, 1]$.

4.2.2.2. Set of equations for heat pump units

The equations of the set $\mathcal{P}_h^{\text{Hp}}$, which defines the operation of a heat pump, are:

$$p_{h,th}^{Hp}(k) = p_{h,el}^{Hp}(k) \cdot COP_h, \tag{4.2a}$$

$$b_h^{Hp,on}(k) \cdot p_{h,el}^{Hp,min} \leq p_{h,el}^{Hp}(k) \leq b_h^{\text{Hp}} \cdot p_{h,el}^{\text{Hp,max}}, \tag{4.2b}$$

$$b_h^{\text{Hp,on}}(k) - b_h^{Hp,on}(k-1) = b_h^{\text{Hp,up}}(k) - b_h^{\text{Hp,down}}(k), \tag{4.2c}$$

$$b_h^{\text{Hp,up}}(k) + b_h^{\text{Hp,down}}(k) \leq 1, \tag{4.2d}$$

$$t_h^{\text{Hp,ON}} \cdot b_h^{\text{Hp,up}}(k) \leq \sum_{j=k}^{\min\{k+t_h^{\text{Hp,ON}}-1, N_p-1\}} b_h^{\text{Hp}}(k), \tag{4.2e}$$

$$t_h^{\text{Hp,OFF}} \cdot b_h^{\text{Hp,down}}(k) \leq t_h^{\text{Hp,OFF}} - \sum_{j=k}^{\min\{k+t_h^{\text{Hp,OFF}}-1, N_p-1\}} b_h^{\text{Hp,on}}(k), \tag{4.2f}$$

$$b_h^{\text{Hp,on}}(k), b_h^{\text{Hp,up}}(k), b_h^{\text{Hp,down}}(k) \in \mathcal{B}, \tag{4.2g}$$

$$\forall k \in \{k_i, \ldots, k_i + N_p - 1\}. \tag{4.2h}$$

The relationship between consumed electrical power and produced thermal power, and the working range for electrical power are given by equations (4.2a) and (4.2b) respectively. The use of (4.2c) and (4.2d) enables the tracking of heat pump's start-up and shut-down processes. Constraints (4.2e) and (4.2f) guarantee that the HP stays at least $t_2^{\text{Hp,ON}}$ time steps in ON status or $t_2^{\text{Hp,OFF}}$ time steps in OFF status after a start-up or a shut-down process, respectively.

4.2.2.3. Set of equations for TES units

Equations (4.3a), (4.3c), and (4.3d) of the set $\mathcal{P}_h^{\text{Tes}}$ give the progress of TES state of charge over the prediction horizon, and the thermal power balance - which occurs in the TES.

$$SoC_h^{\text{Tes}}(k) = SoC_h^{\text{Tes}}(k) \cdot \eta_h^{\text{Tes,sd}} + \left(p_{h,th}^{\text{Tes,char}}(k) - p_{h,th}^{\text{Tes,dis}}(k)\right) \cdot K_h^{\text{Tes}}, \tag{4.3a}$$

$$SoC_h^{\text{Tes,min}} \leq SoC_h^{\text{Tes}}(k) \leq SoC_h^{\text{Tes,max}}, \tag{4.3b}$$

$$p_{h,th}^{\text{Tes,char}}(k) = p_{h,th}^{\text{Gen}}(k), \tag{4.3c}$$

$$p_{h,th}^{\text{Tes,dis}}(k) = p_{h,th}^{\text{Cons}}(k), \tag{4.3d}$$

$$\forall k \in \{k_i, \ldots, k_i + N_p - 1\}. \tag{4.3e}$$

4.2.2.4. Set of equations for mini CHP units

For a mini CHP unit, the following equations hold:

$$p_{h,el}^{\mathrm{Chp}}(k) = p_{h,gas}^{\mathrm{Chp}}(k) \cdot \eta_{h,el}^{\mathrm{Chp}}, \tag{4.4a}$$

$$b_h^{\mathrm{Chp}}(k) \cdot p_{h,el}^{\mathrm{Chp,min}} \leq p_{h,el}^{\mathrm{Chp}}(k) \leq p_{h,el}^{\mathrm{Chp,max}} \cdot b_h^{\mathrm{Chp}}(k), \tag{4.4b}$$

$$p_{h,th}^{\mathrm{Chp}}(k+1) = A_{h,th} \cdot p_{h,th}^{\mathrm{Chp}}(k) + B_{h,th} \cdot p_{h,gas}^{\mathrm{Chp}}(k), \tag{4.4c}$$

$$b_h^{\mathrm{Chp,on}}(k) - b_h^{\mathrm{Chp,on}}(k-1) = b_h^{\mathrm{Chp,up}}(k) - b_h^{\mathrm{Chp,down}}(k), \tag{4.4d}$$

$$b_h^{\mathrm{Chp,up}}(k) + b_h^{\mathrm{Chp,down}}(k) \leq 1, \tag{4.4e}$$

$$t_h^{\mathrm{Chp,ON}} \cdot b_h^{\mathrm{Chp,up}}(k) \leq \sum_{j=k}^{\min\{k+t_h^{\mathrm{Chp,ON}}-1, N_p-1\}} b_h^{\mathrm{Chp,on}}(k), \tag{4.4f}$$

$$t_h^{\mathrm{Chp,OFF}} \cdot b_h^{\mathrm{Chp,down}}(k) \leq t_3^{\mathrm{Chp,OFF}} - \sum_{j=k}^{\min\{k+t_h^{\mathrm{Chp,OFF}}-1, N_p-1\}} b_h^{\mathrm{Chp}}(k), \tag{4.4g}$$

$$b_h^{\mathrm{Chp,on}}(k), b_h^{\mathrm{Chp,up}}(k), b_h^{\mathrm{Chp,down}}(k) \in \mathcal{B}, \tag{4.4h}$$

$$\forall k \in \{k_i, \ldots, k_i + N_p - 1\}. \tag{4.4i}$$

Equations (4.4a) and (4.4c) respectively consider the electrical and thermal dynamic behavior of the mini CHP. Analogous to the previously described heat pump unit, constraints (4.4c)-(4.4g) assures a minimum ON status or a minimum OFF status after a start-up or a shut-down process. All these equations form the set $\mathcal{P}_h^{\mathrm{Chp}}$.

4.2.2.5. Set of equations for electrical water heater units

Similar to a heat pump unit, the behavior of an EWH is given by the set $\mathcal{P}_h^{\mathrm{Ewh}}$ with the equations:

$$p_{h,th}^{Ewh}(k) = p_{h,el}^{Ewh} \cdot \eta_h^{\mathrm{Ewh}}, \tag{4.5a}$$

$$b_h^{\mathrm{Ewh}}(k) \cdot p_{h,el}^{\mathrm{Ewh,min}} \leq p_{h,el}^{\mathrm{Ewh}}(k) \leq p_{h,el}^{\mathrm{Ewh,max}} \cdot b_h^{\mathrm{Ewh}}(k), \tag{4.5b}$$

$$b_h^{\mathrm{Ewh}}(k) \in \mathcal{B}, \tag{4.5c}$$

$$\forall k \in \{k_i, \ldots, k_i + N_p - 1\}. \tag{4.5d}$$

This work assumes, that an EWH does not have any restriction on ON/OFF status.

4.2.2.6. Set of equations for electrical balance and power exchange with the grid

The set $\mathcal{P}_h^{\text{Grid}}$ comprises:

$$p_{h,el}^{\text{Cons}}(k) + p_{h,el}^{\text{Exp}}(k) = p_{h,el}^{\text{Gen}}(k) + p_{2,el}^{\text{Imp}}(k), \tag{4.6a}$$

$$0 \leq p_{h,el}^{\text{Imp}}(k) \leq \left(p_{h,el}^{\text{Imp,max}}\right) \cdot \left(b_h^{\text{Grid}}(k)\right), \tag{4.6b}$$

$$0 \leq p_{h,el}^{\text{Exp}}(k) \leq \left(p_{h,el}^{\text{Exp,max}}\right) \cdot \left(1 - b_h^{\text{Grid}}(k)\right), \tag{4.6c}$$

$$b_h^{\text{Grid}}(k) \in \mathcal{B}, \tag{4.6d}$$

$$\forall k \in \{k_i, \ldots, k_i + N_p - 1\}. \tag{4.6e}$$

These equations determine the electrical balance within the H-MG, together with the mutual exclusivity for power import and power export.

4.3. Decentralized coordination strategy

The decentralized strategy is the reference coordination strategy for this chapter, in which each H-MG minimizes its own local economic objective function - f_1 for H-MG 1, f_2 for H-MG 2, and f_3 for H-MG 3. There is no central coordination unit and therefore this strategy does not require information exchange between the H-MGs.

As similar problems were already described in detailed in previous chapters (see Chapter 2 for PV-Heat pump, and Chapter 3 for PV-CHP-Storage), the upcoming paragraphs give just a compact overview on the decentralized local optimization problems for each H-MG.

4.3.1. Local optimization problem for a photovoltaic-battery H-MG

This is the first and simplest system, where only the battery offers flexibility. In order to reduce the energy bill, the management system has to decide when to use PV power production to feed the residential loads, when to use it to charge the battery and when to inject to the grid. Additionally, the management system also determines when to discharge the battery to cover the local demand.

The equations below define the optimization problem for the first H-MG.

$$\underset{\hat{\boldsymbol{u}}_1}{\text{minimize}} \qquad f_1\left(\boldsymbol{p}_{1,el}^{\text{Imp}}, \boldsymbol{p}_{1,el}^{\text{Exp}}\right) \tag{4.7a}$$

$$\text{subject to}$$

$$\boldsymbol{p}_{1,el}^{\text{Batt,char}}, \boldsymbol{p}_{1,el}^{\text{Batt,dis}}, \boldsymbol{b}_1^{\text{Batt}} \in \mathcal{P}_1^{\text{Batt}}, \tag{4.7b}$$

$$\boldsymbol{p}_{1,el}^{\text{Imp}}, \boldsymbol{p}_{1,el}^{\text{Exp}}, \boldsymbol{b}_1^{\text{Grid}} \in \mathcal{P}_1^{\text{Grid}}, \tag{4.7c}$$

$$\boldsymbol{p}_{1,el}^{\text{Cons}} = \boldsymbol{p}_{1,el}^{\text{Load}} + \boldsymbol{p}_{1,el}^{\text{Batt,char}}, \tag{4.7d}$$

$$\boldsymbol{p}_{1,el}^{\text{Gen}} = \boldsymbol{p}_{1,el}^{\text{Pv}} + \boldsymbol{p}_{1,el}^{\text{Batt,dis}}, \tag{4.7e}$$

$$\mathcal{B} \in \{0, 1\}. \tag{4.7f}$$

Where the vector of decision variables is

$$\hat{\boldsymbol{u}}_1 = \begin{bmatrix} \boldsymbol{p}_{1,el}^{\text{Batt,char}} \\ \boldsymbol{p}_{1,el}^{\text{Batt,dis}} \\ \boldsymbol{b}_1^{\text{Batt}} \\ \boldsymbol{b}_1^{\text{Grid}} \end{bmatrix}. \tag{4.8}$$

Here, $\boldsymbol{p}_{1,el}^{\text{Batt,char}}$, $\boldsymbol{p}_{1,el}^{\text{Batt,dis}}$, $\boldsymbol{b}_1^{\text{Batt}}$, and $\boldsymbol{b}_1^{\text{Grid}}$ are in $\boldsymbol{R}^{N_P}$.

f_1 denotes the local economic objective function with the continuous variables $p_{1,el}^{\text{Imp}}(k)$ and $p_{1,el}^{\text{Exp}}(k)$ describing power import and power export exchange with the main grid.

4.3.2. Local optimization problem for a photovoltaic-heat pump H-MG

For this H-MG, the goal is to minimize electricity costs by shifting operation times of the heat pump using the flexibility provided by the TES.

The electrical power output of the heat pump and the binary variable for the ON/OFF status of the heat pump, are the main decision variables of the optimization problem.

Domestic hot water consumption, space heating demand, PV generation, and household load consumption are inputs that cannot be controlled, and therefore are considered as disturbances. As their future values are uncertain, a forecast for them is needed.

The equations below define the optimization problem for H-MG 2.

$$\underset{\hat{\boldsymbol{u}}_2}{\text{minimize}} \qquad f_2\left(\boldsymbol{p}_{2,el}^{\text{Imp}}, \boldsymbol{p}_{2,el}^{\text{Exp}}\right) \tag{4.9a}$$

subject to

$$\boldsymbol{p}_{2,el}^{\text{Hp}}, \boldsymbol{p}_{2,th}^{\text{Hp}}, \boldsymbol{b}_2^{\text{Hp}} \in \mathcal{P}_2^{\text{Hp}}, \tag{4.9b}$$

$$\boldsymbol{p}_{2,th}^{\text{Tes,char}}, \boldsymbol{p}_{2,th}^{\text{Tes,dis}} \in \mathcal{P}_2^{\text{Tes}}, \tag{4.9c}$$

$$\boldsymbol{p}_{2,el}^{\text{Imp}}, \boldsymbol{p}_{2,el}^{\text{Exp}}, \boldsymbol{b}_2^{\text{Grid}} \in \mathcal{P}_2^{\text{Grid}}, \tag{4.9d}$$

$$\boldsymbol{p}_{2,el}^{\text{Cons}} = \boldsymbol{p}_{2,el}^{\text{Load}} + \boldsymbol{p}_{2,el}^{\text{Hp}}, \tag{4.9e}$$

$$\boldsymbol{p}_{2,el}^{\text{Gen}} = \boldsymbol{p}_{2,el}^{\text{Pv}}, \tag{4.9f}$$

$$\boldsymbol{p}_{2,th}^{\text{Cons}} = \frac{\boldsymbol{p}_{2,th}^{\text{Sh}} + \boldsymbol{p}_{2,th}^{\text{Dhw}}}{\eta_2^{\text{Tes,dis}}}, \tag{4.9g}$$

$$\boldsymbol{p}_{2,th}^{\text{Gen}} = \boldsymbol{p}_{2,th}^{\text{Hp}} \cdot \eta_2^{\text{Tes,char}}, \tag{4.9h}$$

$$\mathcal{B} \in \{0, 1\}. \tag{4.9i}$$

With the vector

$$\hat{\boldsymbol{u}}_2 = \begin{bmatrix} \boldsymbol{p}_{2,el}^{\text{Hp}} \\ \boldsymbol{b}_2^{\text{Hp}} \end{bmatrix}, \tag{4.10}$$

where

$$\boldsymbol{b}_2^{\text{Hp}} = \begin{bmatrix} \boldsymbol{b}_2^{\text{Hp,on}} \\ \boldsymbol{b}_2^{\text{Hp,up}} \\ \boldsymbol{b}_2^{\text{Hp,down}} \end{bmatrix}. \tag{4.11}$$

The local economic objective function is given by f_2. The vectors $\boldsymbol{p}_{2,el}^{\text{Hp}}$, $\boldsymbol{b}_2^{\text{Hp,on}}$, $\boldsymbol{b}_2^{\text{Hp,up}}$, $\boldsymbol{b}_2^{\text{Hp,down}}$, and $\boldsymbol{b}_2^{\text{Grid}}$ are in $\boldsymbol{R}^{N_P}$.

4.3.3. Local optimization problem for a photovoltaic-combined heat and power H-MG

Same as for the previous systems, the goal of the proposed economic operation is to minimize operational costs.

This is achieved by shifting operation times of the mini CHP using the flexibility provided by the battery and the TES.

A compact description of the problem for H-MG 3 is given below:

$$\underset{\hat{\boldsymbol{u}}_3}{\text{minimize}} \qquad f_3\left(\boldsymbol{p}_{3,el}^{\text{Imp}}, \boldsymbol{p}_{3,el}^{\text{Exp}}\right) + \tilde{f}_3\left(\tilde{\hat{\boldsymbol{u}}}_3\right) \tag{4.12a}$$

$$\text{subject to}$$

$$\boldsymbol{p}_{3,el}^{\text{Chp}}, \boldsymbol{p}_{3,th}^{\text{Chp}}, \boldsymbol{b}_3^{\text{Chp}} \in \mathcal{P}_3^{\text{Chp}}, \tag{4.12b}$$

$$\boldsymbol{p}_{3,el}^{Ewh}, \boldsymbol{p}_{3,th}^{Ewh}, \boldsymbol{b}_3^{\text{Ewh}} \in \mathcal{P}_3^{\text{Ewh}}, \tag{4.12c}$$

$$\boldsymbol{p}_{3,th}^{\text{Tes,char}}, \boldsymbol{p}_{3,th}^{\text{Tes,dis}} \in \mathcal{P}_3^{\text{Tes}}, \tag{4.12d}$$

$$\boldsymbol{p}_{3,el}^{\text{Batt,char}}, \boldsymbol{p}_{3,el}^{\text{Batt,dis}}, \boldsymbol{b}_3^{\text{Batt}} \in \mathcal{P}_3^{\text{Batt}}, \tag{4.12e}$$

$$\boldsymbol{p}_{3,el}^{\text{Imp}}, \boldsymbol{p}_{3,el}^{\text{Exp}}, \boldsymbol{b}_3^{\text{Grid}} \in \mathcal{P}_3^{\text{Grid}}, \tag{4.12f}$$

$$\boldsymbol{p}_{3,el}^{\text{Cons}} = \boldsymbol{p}_{3,el}^{\text{Load}} + \boldsymbol{p}_{3,el}^{\text{Ewh}} + p_{3,el}^{\text{Batt,char}}, \tag{4.12g}$$

$$\boldsymbol{p}_{3,el}^{\text{Gen}} = \boldsymbol{p}_{3,el}^{\text{Chp}} + \boldsymbol{p}_{3,el}^{\text{Pv}} + \boldsymbol{p}_{3,el}^{\text{Batt,dis}}, \tag{4.12h}$$

$$\boldsymbol{p}_{3,th}^{\text{Cons}} = \frac{\boldsymbol{p}_{3,th}^{\text{Sh}} + \boldsymbol{p}_{3,th}^{\text{Dhw}} + \boldsymbol{p}_{3,th}^{\text{Lost}}}{\eta_3^{\text{Tes,dis}}}, \tag{4.12i}$$

$$\boldsymbol{p}_{3,th}^{\text{Gen}} = \left(\boldsymbol{p}_{3,th}^{\text{Chp}} + \boldsymbol{p}_{3,th}^{\text{Ewh}}\right) \cdot \eta_3^{\text{Tes,char}}. \tag{4.12j}$$

$$\mathcal{B} \in \{0, 1\}. \tag{4.12k}$$

The decision variables vector is $\hat{\boldsymbol{u}}_3 = \left[\boldsymbol{p}_{3,gas}^{\text{Chp}\intercal}, \boldsymbol{p}_{3,el}^{\text{Ewh}\intercal}, \boldsymbol{p}_{3,el}^{\text{Batt,char}\intercal}, \boldsymbol{p}_{3,el}^{\text{Batt,dis}\intercal}, \boldsymbol{p}_{3,th}^{\text{Lost}\intercal}, \boldsymbol{b}_3\right]^\intercal$, where $\boldsymbol{b}_3$ is given by $\boldsymbol{b}_3 = \left[\boldsymbol{b}_3^{\text{Chp}}, \boldsymbol{b}_3^{\text{Batt}\intercal}, \boldsymbol{b}_3^{\text{Grid}\intercal}\right]^\intercal$, and $\boldsymbol{b}_3^{\text{Chp}} = \left[\boldsymbol{b}_3^{\text{Chp,on}\intercal}, \boldsymbol{b}_3^{\text{Chp,up}\intercal}, \boldsymbol{b}_3^{\text{Chp,down}\intercal}\right]$.

The vectors $\boldsymbol{p}_{3,gas}^{\text{Chp}}$, $\boldsymbol{p}_{3,el}^{\text{Ewh}}$, $\boldsymbol{p}_{3,el}^{\text{Batt,char}}$, $\boldsymbol{p}_{3,el}^{\text{Batt,dis}}$, $\boldsymbol{p}_{3,th}^{\text{Lost}}$, $\boldsymbol{b}_3^{\text{Chp,on}}$, $\boldsymbol{b}_3^{\text{Chp,up}}$, $\boldsymbol{b}_3^{\text{Chp,down}}$, $\boldsymbol{b}_3^{\text{Batt}}$, and $\boldsymbol{b}_3^{\text{Grid}}$ are in $\boldsymbol{R}^{N_P}$. f_3 defines the local economic objective function and $\tilde{f}_3$ defines additional generation costs.

4.3.4. Local objective functions

Finally, the local economic objective function f_h for each H-MG, i.e. $h = 1, 2, 3$, given a fixed electricity price C_{el} and a fixed feed-in tariff C_{fit} is

$$f_h\left(\boldsymbol{p}_{h,el}^{\text{Imp}}, \boldsymbol{p}_{h,el}^{\text{Exp}}\right) = \sum_{k=k_i}^{k_i+N_p-1} C_{el} \cdot p_{h,el}^{\text{Imp}}(k) - C_{fit} \cdot p_{h,el}^{\text{Exp}}(k). \tag{4.13}$$

For any H-MG h containing a CHP unit, the additional generation costs are

$$\tilde{f}_h\left(\tilde{\hat{\boldsymbol{u}}}_h\right) = \sum_{k=k_i}^{k_i+N_p-1} C_{gas} \cdot p_{h,gas}^{\text{Chp}}(k) + C_{start}^{\text{Chp}} \cdot b_h^{\text{Chp,up}}(k) + C^{\text{Lost}} \cdot p_{h,th}^{\text{Lost}}(k). \tag{4.14}$$

4.4. Centralized coordination strategy

This section mainly deals with the design of an optimal centralized coordination strategy for interconnected H-MGs. It extends the decentralized economic coordination to a centralized approach to improve the power exchange between H-MGs. This strategy seeks to lower energy bill, improve power exchange among H-MGs and reduce large power peaks at the point of common coupling (PCC in Figure 4.2). For this purpose, the objective function of the centralized coordination strategy includes a quadratic term for minimizing the instantaneous quadratic difference between power import and power export among H-MGs over the prediction horizon. The centralized optimization problem is then given by:

$$\underset{\{\hat{\boldsymbol{u}}_h\}}{\text{minimize}} \quad \sum_{h=1}^{H} J_h\left(\hat{\boldsymbol{u}}_h\right) + \sum_{k=k_i}^{k_i+N_p-1} \left(p_{el}^{\text{G,total}}(k)\right)^2 \tag{4.15a}$$

$$\text{subject to} \quad \sum_{h=1}^{H} \left(p_{h,el}^{\text{Imp}}(k) - p_{h,el}^{\text{Exp}}(k)\right) = p_{el}^{\text{G,total}}(k) \quad \forall k \in \{k_i, \ldots, k_i + N_p - 1\}, \tag{4.15b}$$

$$\hat{\boldsymbol{u}}_h \in \Upsilon_h \qquad \forall h \in \{1, \ldots, H\}, \tag{4.15c}$$

$$\mathcal{B} \in \{0, 1\}. \tag{4.15d}$$

Where $J_h\left(\hat{\boldsymbol{u}}_h\right) = f_h\left(\boldsymbol{p}_{h,el}^{\text{Imp}}, \boldsymbol{p}_{h,el}^{\text{Exp}}\right) + \tilde{f}_h\left(\tilde{\hat{\boldsymbol{u}}}_h\right)$ for $h = 1, \ldots, H$. H denotes the number of interconnected H-MGs. For the current case, $H = 3$ and $\tilde{f}_1\left(\tilde{\hat{\boldsymbol{u}}}_1\right) = \tilde{f}_2\left(\tilde{\hat{\boldsymbol{u}}}_2\right) = 0$. The set Υ_h include all the local constraints defined for the decentralized problems, i.e., $\{\Upsilon_1, \Upsilon_2, \Upsilon_3\} = \{(4.7b) - (4.7e), (4.9b) - (4.9h), (4.12b) - (4.12j)\}$.

4.5. Hierarchical-distributed coordination strategy based on dual decomposition

This strategy builds upon the centralized optimization problem presented before. The idea now, is to perform the optimal coordination in a more distributed way. This is achieved by breaking the global optimization problem down, by means of dual decomposition, to smaller subproblems that can be solved possibly in parallel. Because of the presence of binary variables in the local optimization problems, the resulting subproblems are non-convex. On that account, these variables are first relaxed, and the separable dual problem is then solved by sub-gradient iterations. Once convergence of the sub-gradient iterations is established, an additional method to recover feasible primal solutions from the dual problem completes the procedure. If the reader is new to the concept of dual decomposition, Subsection A.5.1 in Appendix A provides a detailed description of decomposition with constraints by means of dual decomposition which may be helpful in order to understand the upcoming formulations. This section illustrates the decomposition and recovering

process, states the resulting optimization subproblems, and concludes by presenting the hierarchical-distributed coordination algorithm.

The idea behind this coordination strategy is to decompose the centralized primal problem, shown in (4.15), into local smaller subproblems in order to solve them possibly in parallel. The centralized problem would be easily separable, except for the quadratic term in the objective function, which cannot be decomposed. For this reason, it is proposed to use dual decomposition, where the global centralized problem is solved by working with the dual problem and by manipulating the dual variables [80]. Accordingly, the first step is to form the partial lagrangian associated to the centralized problem (4.15). It will be shown later that all binary variables from (4.15) will be relaxed, and therefore it is possible to form the partial lagrangian. The partial lagrangian is

$$\begin{aligned}\mathcal{L}\left(\hat{\boldsymbol{u}}, \boldsymbol{p}_{el}^{\mathbf{G,total}}, \boldsymbol{\lambda}\right) = &\sum_{h=1}^{H} J_h\left(\hat{\boldsymbol{u}}_h\right) + \sum_{k=k_i}^{k_i+N_p-1} \left(p_{el}^{\mathrm{G,total}}(k)\right)^2 + \\ &\sum_{k=k_i}^{k_i+N_p-1} \lambda(k) \left(\sum_{h=1}^{H} \left(p_{h,el}^{\mathrm{Imp}}(k) - p_{h,el}^{\mathrm{Exp}}(k)\right)\right) - \\ &\sum_{k=k_i}^{k_i+N_p-1} \lambda(k) \cdot p_{el}^{\mathrm{G,total}}(k),\end{aligned} \tag{4.16}$$

and shows a relaxation of the coupling constraint from the centralized problem, which is now accounted in the objective by adding it as a weighted term. Here $\hat{\boldsymbol{u}} = [\hat{\boldsymbol{u}}_1^\intercal, \ldots, \hat{\boldsymbol{u}}_H^\intercal]^\intercal$ denotes the local decision variables, $\boldsymbol{p}_{el}^{\mathrm{G,total}} = \left[p_{el}^{\mathrm{G,total}}(k_i) \ldots, p_{el}^{\mathrm{G,total}}(k_i + N_p - 1)\right]^\intercal$ is the vector of coupling variables and $\boldsymbol{\lambda} = [\lambda(k_i), \ldots, \lambda(k_i + N_p - 1)]^\intercal$ is the vector of lagrange multipliers. A subgradient iterative method helps to solve the dual problem which is now separable. The solution of the dual problem gives a lower bound for the original centralized problem.

4.5.1. Subproblems for H-MGs and central coordination unit

To compute the dual problem in parallel, each H-MG must find the optimal power grid profile $\boldsymbol{P}_{h,el}^{\mathrm{G}}$ that minimizes

$$\left(\hat{\boldsymbol{u}}_h^{l+1}, \boldsymbol{p}_{h,el}^{\mathrm{G},l+1}\right) := \underset{\hat{\boldsymbol{u}}_h, \boldsymbol{p}_{h,el}^{\mathrm{G}}}{\operatorname{argmin}} \left(J_h\left(\hat{\boldsymbol{u}}_{\boldsymbol{h}}\right) + \sum_{k=k_i}^{k_i+N_p-1} \lambda(k)^l \cdot p_{h,el}^{\mathrm{G}}(k) \right) \tag{4.17a}$$

subject to

$$\hat{\boldsymbol{u}}_h \in \Upsilon_h, \qquad \forall h \in \{1, \ldots, H\}, \tag{4.17b}$$

$$\mathcal{B} \in [0, 1]\,. \tag{4.17c}$$

where $\boldsymbol{p}_{h,el}^{\mathrm{G}} = \left[p_{h,el}^{\mathrm{Imp}}(k_i) - p_{h,el}^{\mathrm{Exp}}(k_i), \ldots, p_{h,el}^{\mathrm{Imp}}(k_i+N_p-1) - p_{h,el}^{\mathrm{Exp}}(k_i+N_p-1)\right]^{\intercal}$. In general, the objective value obtained by dual decomposition with subgradient iterations converges to the solution of the centralized problem [80]. However, since there are binary variables in the formulation, there is not guaranty for such convergence. Tackling this issue requires a relaxation of constraints involving binary variables. Therefore, within the hierarchical-distributed coordination strategy each H-MG has to firstly solve (4.17) subject to the same constraints as in the respective decentralized problems, but changing the domain of the binary variables to $[0, 1]$. Furthermore the central coordination unit (CCU) has to find the optimal $\boldsymbol{p}_{el}^{G,total}$ that minimizes

$$\boldsymbol{p}_{el}^{\mathrm{G,total},l+1} \coloneqq \underset{\boldsymbol{p}_{el}^{\mathrm{G,total}}}{\operatorname{argmin}} \left(\sum_{k=k_i}^{k_i+N_p-1} \left(p_{el}^{\mathrm{G,total}}(k)\right)^2 - \sum_{k=k_i}^{k_i+N_p-1} \lambda(k)^l \left(p_{el}^{\mathrm{G,total}}(k)\right) \right), \tag{4.18}$$

by adjusting the dual variable $\lambda(k)$ to coordinate its decision with the decisions of the H-MGs using a subgradient iteration. The subgradient update is given by

$$\boldsymbol{\lambda}^{l+1} = \boldsymbol{\lambda}^{l} + \alpha^{\mathrm{dd}} \left(\sum_{h=1}^{H} \boldsymbol{p}_{h,el}^{\mathrm{G},l+1} - \boldsymbol{p}_{el}^{\mathrm{G,total},l+1} \right), \tag{4.19}$$

where α^{dd} designates the iteration step size. In this work, the hierarchical-distributed strategy employes $\alpha^{\mathrm{dd}} = 0.5/l$ as iteration step size.

4.5.2. Recovering primal feasible solutions

One limitation of dual decomposition is that the solution to the dual problem does not automatically produces the optimal primal decision variables, but only the optimal value of the primal centralized problem. This situation is aggravated in the present case, since it is solving a relaxed version of the original problem. Hence, the dual decomposition method needs to be complemented by a method for recovering primal feasible solutions. For this purpose, after a convergence for the subgradient iterations is found, problem (4.17) is solved again with $\boldsymbol{\lambda}^{l_{max}}$ and the original constraints, i.e. without relaxation on binary variables as

$$\left(\hat{\boldsymbol{u}}_h, \boldsymbol{p}_{h,el}^{\mathrm{G}}\right) \coloneqq \underset{\hat{\boldsymbol{u}}_h, \boldsymbol{p}_{h,el}^{\mathrm{G}}}{\operatorname{argmin}} \left(J_h\left(\hat{\boldsymbol{u}}_{\boldsymbol{h}}\right) + \sum_{k=k_i}^{k_i+N_p-1} \lambda(k)^{l_{max}} \cdot p_{h,el}^{\mathrm{G}}(k) \right) \tag{4.20a}$$

subject to

$$\hat{\boldsymbol{u}}_h \in \Upsilon_h, \qquad \forall h \in \{1, \ldots, H\}, \tag{4.20b}$$

$$\mathcal{B} \in \{0, 1\}. \tag{4.20c}$$

4.5.3. Disturbance forecasts

Inputs from photovoltaic generation, domestic hot water and space heating consumption, and household load are handled as disturbances in the MPC structure. To handle such uncertainties, the MPC needs a forecast for their values over the considered prediction horizon. Existing methods to perform such a forecast based on historical data include polynomial regression and artificial neural networks among others. As the focus of the present work lays in the formulation and simulation of different coordination strategies, the development of an advanced forecast algorithm to predict disturbances is out of the scope of this work. Instead, the implemented MPC uses a straightforward prediction of disturbances based on persistence. For strong weather-dependent uncertainties -i.e PV generation and space heating consumption- a one-day persistence forecast is employed, and for behavior-dependent uncertainties, like household electrical load and domestic hot water consumption, a seven-day persistence forecast is used.

4.5.4. Algorithm

The steps below in Algorithm 1 give a description of the algorithm for the hierarchical-distributed coordination strategy based on dual decomposition.

Algorithm 1 MPC based hierarchical-distributed algorithm using dual decomposition

1: **Initializing**. Given k_i and $\boldsymbol{\lambda}^1 = 0$, each H-MG $h = 1, 2, 3$ measures its actual states, and gets forecast for disturbances
2: **Sub-gradient iterations**. **For** $l = 1, \ldots, l^{max}$ **do**

- Each H-MG solves the relaxed problem (4.17), and communicates $\boldsymbol{P}_{h,el}^{\mathrm{G},l+1}$ to the CCU
- CCU solves (4.18), updates the lagrange multipliers (4.19), and broadcasts $\boldsymbol{\lambda}^{l+1}$

3: **Recovering primal feasible solutions**. Each H-MG solves (4.17) again with $\boldsymbol{\lambda}^{l_{max}}$ and original constraints without relaxation
4: **Implementation**. Implement first element of the feasible solution vector, increment $k_i = k_i + \Delta t$, and go to 1

4.6. Simulation results and discussion

This section presents relevant results for the three different MPC operation strategies based on a simulation for 7 days in winter. The same simulation setup as in Chapter 2 and Chapter 3 is used. The problem is solved using Pyomo [74, 75] as modeler and CPLEX [76] as solver. The analysis is first conducted from a H-MG perspective and then

from a main grid perspective. First, from a H-MG's perspective, the decentralized and the centralized strategy are analyzed. Figure 4.3 presents power import and power export at each H-MG for the decentralized and the centralized strategy.

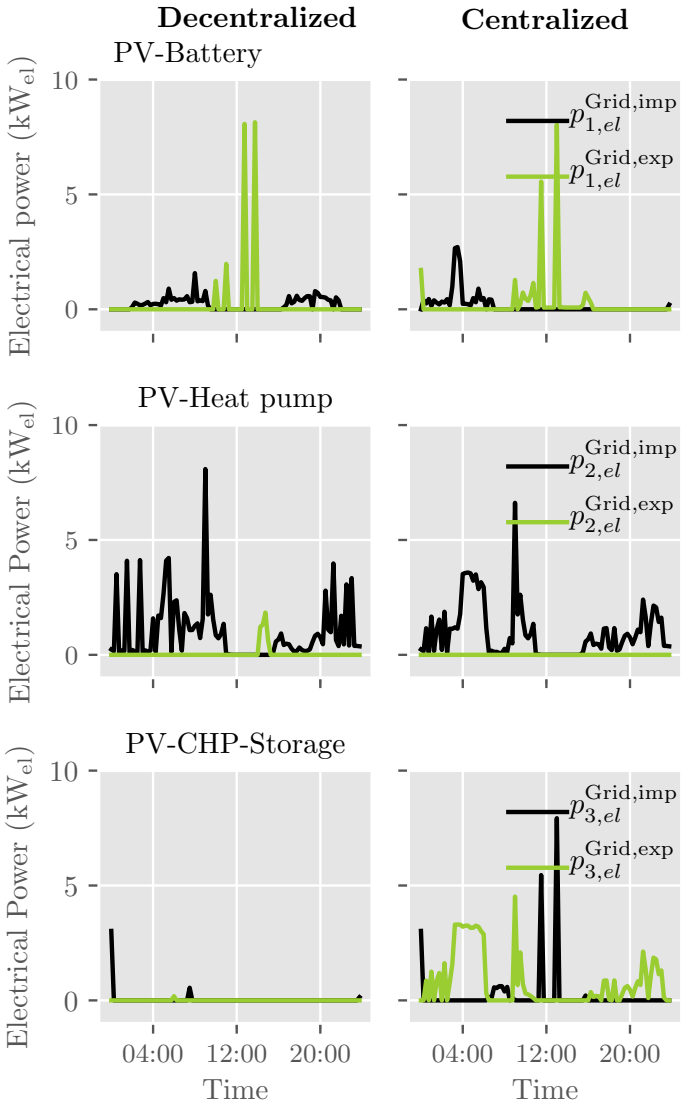

Figure 4.3.: Resultant electrical power profiles for decentralized and centralized strategy

Looking at the upper left subplot under a pure economic operation, the PV-Battery system imports electrical power during morning and afternoon hours and injects PV surplus to the grid around noon. With the centralized strategy, this system now contributes in a small portion to balance the demand of H-MG 2 and also shifts the injection peaks so that they can be absorbed by H-MG 3. Under the decentralized strategy, the PV-Heat pump H-MG (center left subplot) mainly imports power from the grid in order to supply the heat pump and the household loads, with a very large peak of approximately 8 kW_{el} around 8:00 o'clock. For this specific day, the grid receives just a small amount of PV power from this system. For the centralized case, the PV-Heat pump system also presents some changes in its operation that can be seen in the center right subplot. Using the flexibility

from the TES, the heat pump avoids running at high power resulting in a reduction of consumption peaks. H-MG 3 has a minimal interaction with the grid when working in the decentralized mode, as shown in the lower left subplot. Except two import peaks, this H-MG almost supplies itself during this day. This behavior completely changes under the centralized coordination, as the lower right subplot displays. Now, this H-MG actively imports and exports power. Electrical power export is mostly for balancing the demand of the PV-Heat pump system, while electrical power import occurs in order to absorb surplus from H-MG one. It can be appreciated how the proposed centralized formulation optimally coordinates power exchange between systems, so that extreme power peaks at consumption and generation at the PCC are reduced.

The convergence of the dual decomposition approach is now discussed. The objective value obtained with the hierarchical-distributed strategy ($J^{\text{Hierar}-\text{dist}}$), and the one obtained with the centralized strategy (J^{Cent}), versus the iteration count l are shown in Figure 4.4. The plot shows that $J^{\text{Hierar}-\text{dist}}$ converges to the optimal objective value (green line) from the centralized operation strategy. This confirms that the implementation of the hierarchical-distributed strategy is working as expected, and after a certain number of iterations the results obtained with the hierarchical-distributed strategy are acceptable.

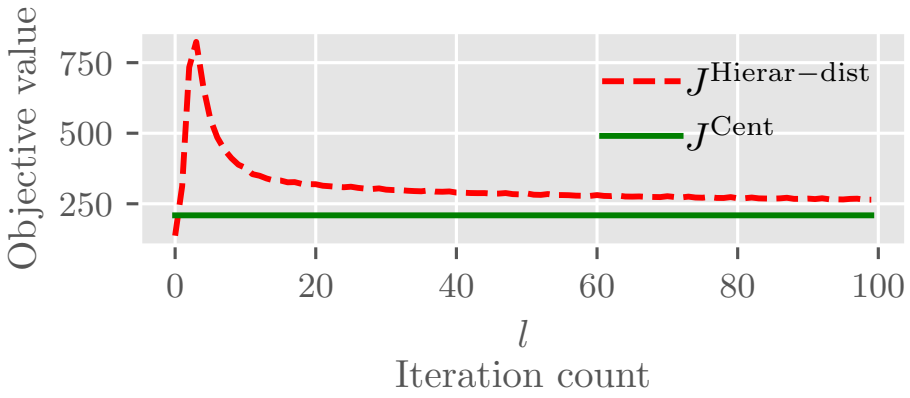

Figure 4.4.: Convergence of objective value for dual decomposition algorithm

To continue the analysis from a main grid perspective, resultant power profiles at the PCC for all strategies are presented in Figure 4.5. As under the decentralized strategy (purple line), each H-MG minimizes its own economic objective function, without caring about power exchange among neighbors, this strategy gives a volatile power profile with large peaks at consumption and generation. In contrast, the centralized strategy (green line) presents an almost regular power profile reducing extreme peaks at generation and consumption. This fact confirms the effect of adding the additional quadratic peak reduction term in the objective function of the centralized problem. For the hierarchical-distributed strategy, it is decided to use 30 as the maximum number of iterations. The orange line displays the resulting power profile.

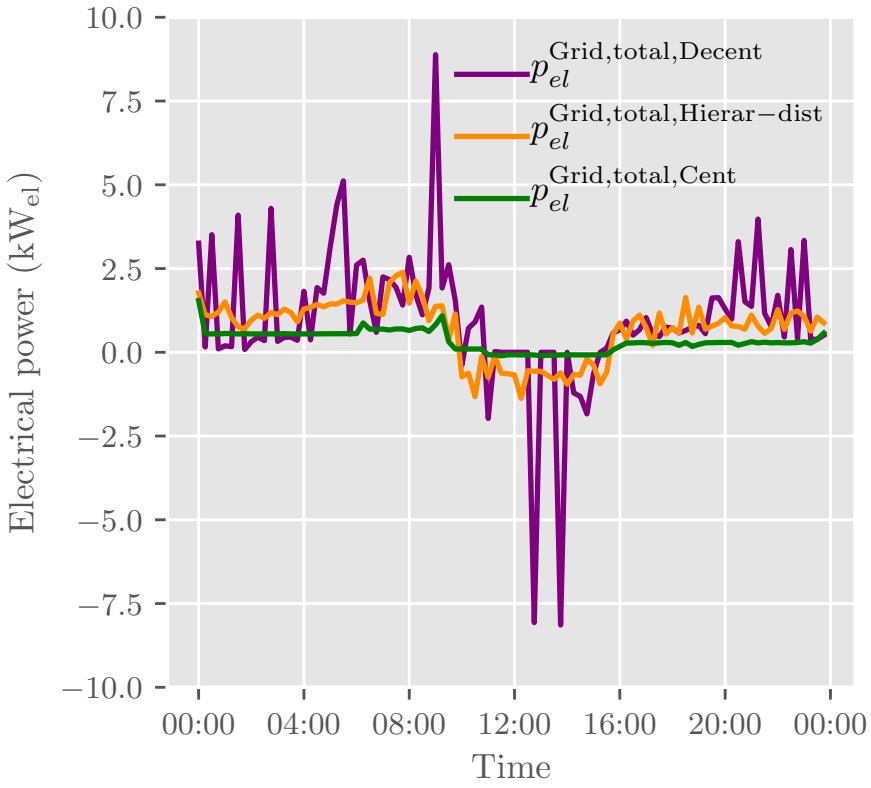

Figure 4.5.: Comparison of electrical power profiles for all considered coordination strategies

Since an arbitrary limit for iterations is set in order to speed up the computation, results of the hierarchical-distributed strategy are not as good as the ones obtained with the centralized strategy. Notwithstanding, they show a considerable improvement compared to the decentralized coordination from the point of view of reduction of large peaks.

Observations for $p_{el}^{G,total}$ for a simulation over 7 days in winter are shown in Figure 4.6. Again, all three different strategies are simulated. For the decentralized strategy, the distribution shows large peaks at consumption and generation side, approximately at 9 kW$_{el}$ and -7.5 kW$_{el}$ respectively, while most of the observations lie between 0 kW$_{el}$ and 5 kW$_{el}$. The centralized strategy gives a narrower distribution, where most of the values are between 0 kW$_{el}$ and 1 kW$_{el}$. The hierarchical-distributed strategy also results in a compact distribution, with maximum peaks around 3 kW$_{el}$ and -2 kW$_{el}$. Although this strategy does not give the same narrow power band as the centralized one, it does reduce the extreme power peaks from the decentralized strategy. The advantage of the hierarchical-distributed strategy is that it does not require the central coordination unit to solve a global optimization problem, therefore, there is no need to collect all the information from H-MGs - e.g. state of charge of batteries, load consumption, PV production, etc. - in a central instance. Instead, individual optimization problems are solved locally and in parallel by the H-MGs and the CCU, and only the expected power profile at the house connection point and prices (lagrange multipliers) have to be communicated.

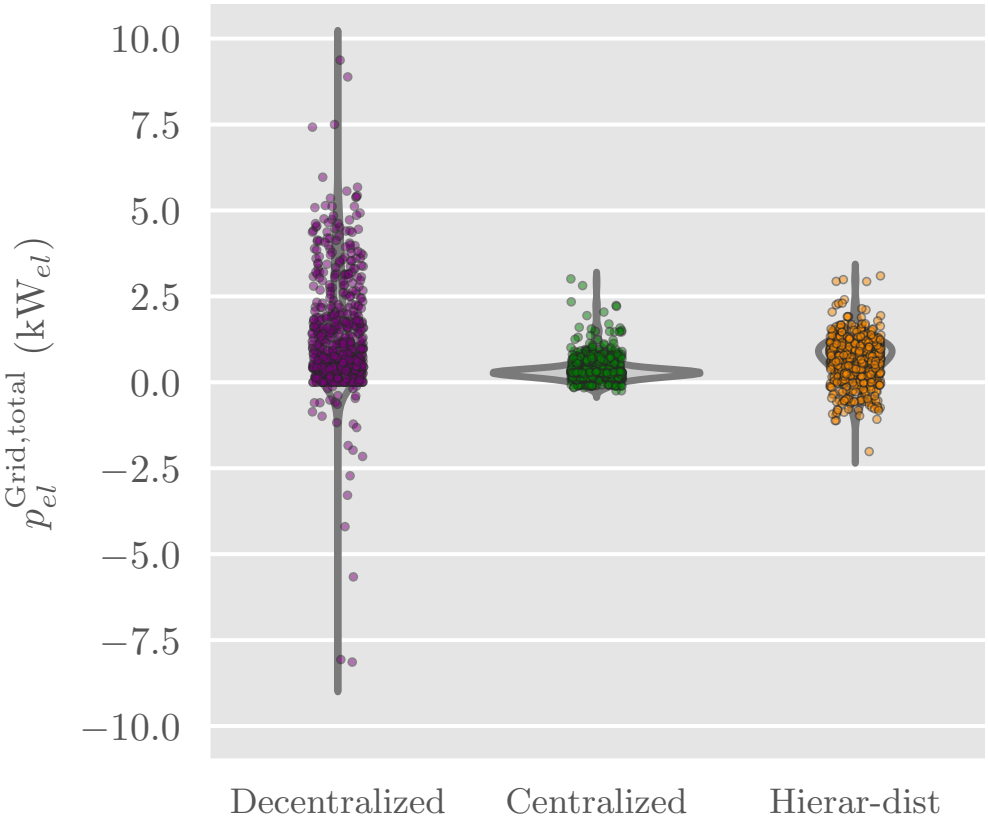

Figure 4.6.: Distribution of $p_{el}^{\text{Grid,total}}$ over 7 days under the different strategies

Energy efficiency is another important aspect to evaluate. For this purpose, storage losses in [kWh] due to self-discharge, charging, and discharging are also quantified by determining the difference in net energy input and output over the 7 days. They are visualized in Figure 4.7. In general, for all strategies, losses in TES are larger than resultant losses in battery systems. Moreover, under the centralized and the hierarchical-distributed strategy, losses in TES increase. For battery systems, this situation is not entirely evident.

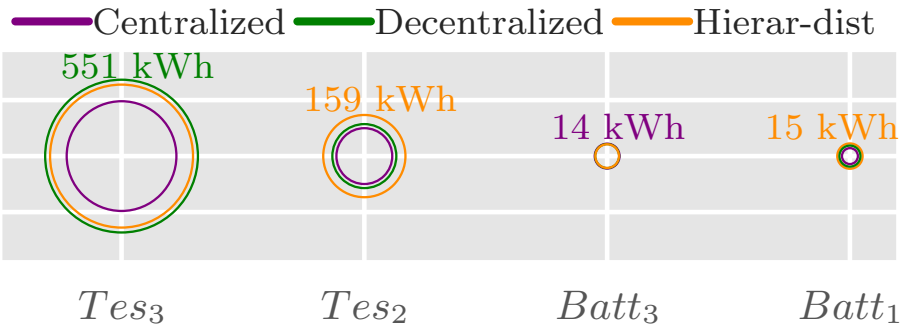

Figure 4.7.: Resulting storage losses for the different strategies over 7 days

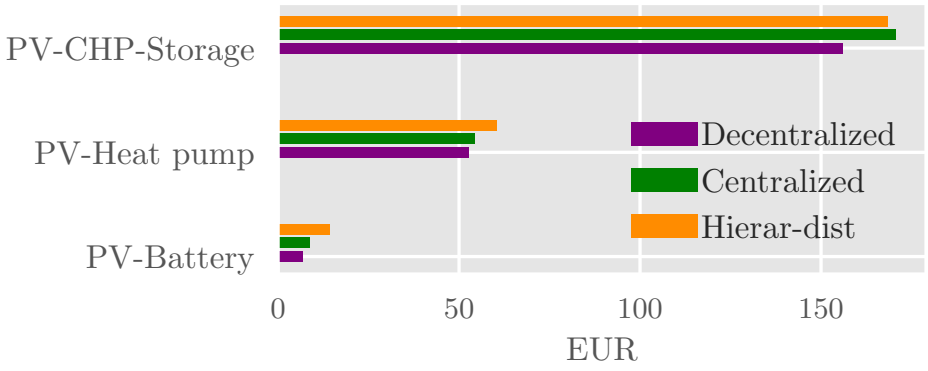

Figure 4.8.: Resulting costs for the different strategies over 7 days

Total energy bill for all H-MGs for the 7 days are calculated and presented in Figure 4.8. Operation under the centralized strategy, or under the hierarchical-distributed strategy implies an increment in energy bill. This is because under these strategies, power peak reduction at PCC is also taken into account in the objective function.

4.7. Summary of the chapter

This chapter introduced three coordination strategies for a group of interconnected H-MGs. First, it presented a reference decentralized MPC operation, which involved the formulation of local optimization problems for each H-MG, i.e., without considering the exchange of power with neighboring H-MGs. Within this kind of operation, each H-MG tries to minimize its operation costs, including energy bills, by using its installed flexibility. The investigation comprised three main possible H-MG configurations: a photovoltaic-battery system corresponding to a single-family house, a photovoltaic-heat pump storage system also corresponding to a single-family house, and a photovoltaic-cogeneration storage system corresponding to a multi-family house. Accordingly, optimization problems for each H-MG configuration were stated, considering the respective static and dynamic models, and constraints. The chapter then moved to the investigation of the optimal operation of a group of interconnected H-MGs, where the goal was, besides minimization of operating costs, that the H-MGs exchange power between them and reduce extreme power peaks at the main connection point (PCC). Thereupon, the chapter continued with the development and description of a hierarchical-distributed optimization approach, which handles the optimal operation of a group of interconnected H-MGs in a more distributed fashion than the centralized approach does. All three strategies were simulated and contrasted for seven days in winter. The results demonstrated that the proposed centralized formulation was able to improve the electrical power balancing between systems while reducing extreme peaks at the generation and consumption side at the PCC.

5. A hierarchical-distributed coordination strategy for interconnected home-microgrids using the ADMM sharing problem

This chapter looks at the optimal operation of a group of interconnected home-microgrids using a model predictive control based hierarchical-distributed strategy with the "Alternating Direction Method of Multipliers" (ADMM). It gives the mathematical formulation for the optimal operation of such a system as an ADMM sharing problem. It investigates two approaches to deal with binary variables in the presented ADMM implementation. The chapter also examines termination conditions for the ADMM algorithm, and in the end, it proposes a new termination condition.

5.1. Introduction

This chapter concerns itself with a novel hierarchical-distributed coordination of interconnected H-MGs. The chapter improves the previous presented dual decomposition based strategy by applying the alternating direction method of multipliers (ADMM). ADMM is an algorithm for large scale distributed optimization which combines the properties of dual decomposition and augmented Lagrangian methods [81]. Subsection A.5.2 in Appendix A provides the theoretical description of ADMM, while this chapter focuses only on ADMM's implementation for the considered case. More specifically, this chapter makes use of the ADMM sharing problem formulation, as presented in [81], to tackle the issue of coordinating interconnected H-MGs. Building upon the centralized coordination strategy presented in Section 4.4, the chapter shows how to formulate such a centralized problem as an ADMM sharing problem and elaborates on the ADMM implementation. As the original centralized problem includes binary variables in its formulation, handling the involved non-convexity becomes an issue when implementing ADMM. On that account, the chapter proposes and investigates two approaches to deal with binary variables, namely:

1) solving a relaxed version of the original subproblems and subsequently recovering primal feasible solutions (ADMM-feasible), and

2) solving the original non-convex subproblems without any relaxation (ADMM-unrelax).

Moreover, the chapter pays special attention to termination conditions for ADMM, since it turns out that deciding when to terminate an ADMM algorithm is not straightforward. In this context, the chapter examines state-of-the-art termination conditions for ADMM

and proposes a new termination condition which exploits the properties of the MPC concept. More specifically, the contributions of this chapter are:

1. an ADMM sharing problem formulation for hierarchical-distributed coordination of interconnected H-MGs,
2. conclusive results on the best approach to handle binary variables within the current ADMM implementation, and
3. a simple yet effective new termination condition for the presented ADMM implementation.

The remainder of this chapter is organized as follows: The first section introduces the problem formulation, going from the centralized problem to the hierarchical-distributed ADMM updates. The second section gives an overview of the ADMM implementation, paying special attention to the handling of the binary variables and ADMM's termination condition. The second section ends by presenting the hierarchical-distributed MPC algorithm based on ADMM. The third and last section shows and discusses the simulation results.

5.2. ADMM sharing problem formulation

Let the vector $\boldsymbol{p}_h^{\mathrm{G}} \in \boldsymbol{R}^{N_p}$, which is dependent on the vector of decision variables $\hat{\boldsymbol{u}}_h$, denotes the power exchange between a H-MG h and the main grid over a prediction horizon N_p. Formally,

$$\boldsymbol{p}_h^{\mathrm{G}} = \left[p_{h,el}^{\mathrm{Imp}}(k_i) - p_{h,el}^{\mathrm{Exp}}(k_i), \ldots, p_{h,el}^{\mathrm{Imp}}(k_i + N_p - 1) - p_{h,el}^{\mathrm{Exp}}(k_i + N_p - 1)\right]^{\intercal},$$

where $p_{h,el}^{\mathrm{Imp}}$ and $p_{h,el}^{\mathrm{Exp}}$ are continuous variables that depend on the decision variables and k_i is the actual time step. The centralized coordination problem (4.15) defined in Section 4.4 can be rewritten as:

$$\begin{aligned}
\underset{\{\hat{\boldsymbol{u}}_h\}}{\text{minimize}} \quad & \sum_{h=1}^{H} J_h\left(\hat{\boldsymbol{u}}_h\right) + g\left(\sum_{h=1}^{H} \boldsymbol{p}_h^{\mathrm{G}}\right) && && \text{(5.1a)}\\
\text{subject to} \quad & \hat{\boldsymbol{u}}_h \in \Upsilon_h, && \forall h \in \{1, \ldots, H\}, && \text{(5.1b)}\\
& \mathcal{B} \in \{0, 1\}. && && \text{(5.1c)}
\end{aligned}$$

Where the local cost function J_h and the shared objective g define the objective function. The problem is constrained by the set of local constraints Υ_h. The argument for g is the sum of local variables $\boldsymbol{p}_h^{\mathrm{G}}$ over all H-MGs such that

$$g\left(\sum_{h=1}^{H} \boldsymbol{p}_h^{\mathrm{G}}\right) = \frac{\gamma}{N_p} \| \sum_{h=1}^{H} \boldsymbol{p}_h^{\mathrm{G}} \|_2^2, \tag{5.2}$$

with a regularization parameter γ.

Problem (5.1) is a shared problem. Here, each H-MG h adjusts its individual power consumption/injection $\boldsymbol{p}_h^{\mathrm{G}}$ to minimize its own energy costs J_h as well as the shared objective $g\left(\sum_{h=1}^{H} \boldsymbol{p}_h^{\mathrm{G}}\right)$, which involves improving balancing between H-MGs and reducing extreme power peaks at the reference node in the main grid. This problem can be formulated in ADMM form by copying the local public variables $\boldsymbol{p}_h^{\mathrm{G}}$ to $\boldsymbol{z}_h$ as follows (see subsubsection A.5.2.2 in Appendix A and Chapter 7.3 in [81] for further information):

$$\begin{aligned}
\underset{\{\hat{\boldsymbol{u}}_h\}}{\text{minimize}} \quad & \sum_{h=1}^{H} J_h\left(\hat{\boldsymbol{u}}_h\right) + g\left(\sum_{h=1}^{H} \boldsymbol{z}_h\right) && && \text{(5.3a)}\\
\text{subject to} \quad & \boldsymbol{p}_h^{\mathrm{G}} - \boldsymbol{z}_h = 0, && \forall h \in \{1, \ldots, H\}, && \text{(5.3b)}\\
& \hat{\boldsymbol{u}}_h \in \Upsilon_h, && \forall h \in \{1, \ldots, H\}, && \text{(5.3c)}\\
& \mathcal{B} \in \{0, 1\}. && && \text{(5.3d)}
\end{aligned}$$

According to Boyd et al. [81], the ADMM algorithm to find the solution to such a sharing problem consists of the iterations:

$$\left(\hat{\boldsymbol{u}}_h^{l+1}, \boldsymbol{p}_h^{\mathrm{G},l+1}\right) := \underset{\hat{\boldsymbol{u}}_h}{\operatorname{argmin}}\left(J_h\left(\hat{\boldsymbol{u}}_{\boldsymbol{h}}\right) + (\rho/2)\left\|\boldsymbol{p}_h^{\mathrm{G}} - \boldsymbol{p}_h^{\mathrm{G},l} + \bar{\boldsymbol{p}}^{\mathrm{G},l} - \bar{\boldsymbol{z}}^{l} + \mathbf{a}^{l}\right\|_2^2\right), \tag{5.4}$$

$$\bar{\boldsymbol{z}}^{l+1} := \underset{\bar{\boldsymbol{z}}}{\operatorname{argmin}}\left(g\left(H\bar{\boldsymbol{z}}\right) + \frac{H\rho}{2}\left\|\bar{\boldsymbol{z}} - \mathbf{a}^{l} - \bar{\boldsymbol{p}}^{\mathrm{G},l+1}\right\|_2^2\right), \tag{5.5}$$

$$\mathbf{a}^{l+1} := \mathbf{a}^{l} + \bar{\boldsymbol{p}}^{\mathrm{G},l+1} - \bar{\boldsymbol{z}}^{l+1}, \tag{5.6}$$

where

$$g\left(H\bar{\boldsymbol{z}}\right) = \frac{\gamma}{N_p}\left\|H\bar{\boldsymbol{z}}\right\|_2^2. \tag{5.7}$$

$\hat{\boldsymbol{u}}_h$ is the vector of local decision variables (private and public) of H-MG h, and $\boldsymbol{p}_h^{\mathrm{G}}$ is a vector dependent on local public variables of the same H-MG. $\mathbf{a}$ can be seen as a coordination mechanism sent by the CCU and $\bar{\boldsymbol{z}}$ as the global variable. ρ is the augmented Lagrangian parameter. Only the CCU has knowledge on the global variable. At each iteration process every single H-MG h, for $h = 1, \ldots, H$, computes its $\hat{\boldsymbol{u}}_h$-update in (5.4) in parallel and builds and communicates its respective $\boldsymbol{p}_h^{\mathrm{G},l+1}$. For the $\bar{\boldsymbol{z}}$-update step, the CCU first collects all $\boldsymbol{p}_h^{\mathrm{G},l+1}$ to form the averages and then solves (5.5). It is an unconstrained minimization problem with N_p variables, whose closed-form analytical solution is given by the following expression (see Appendix C):

$$\bar{\boldsymbol{z}}^{l+1} = \frac{\rho\left(\mathbf{a}^{l} + \bar{\boldsymbol{p}}^{\mathrm{G},l+1}\right)}{\frac{2\gamma}{N_p}H + \rho}, \tag{5.8}$$

where

$$\bar{\boldsymbol{p}}^{\mathrm{G}} = \frac{\sum_{h=1}^{H} \boldsymbol{p}_h^{\mathrm{G}}}{H}. \tag{5.9}$$

The optimal value of $\bar{\boldsymbol{z}}$ depends on the coordination mechanism $\mathbf{a}$ and the average of powers of all subsystems $\bar{\boldsymbol{p}}^{\mathrm{G}}$. With this information the CCU can calculate the $\mathbf{a}$-update in (5.6). Finally, the CCU broadcasts the new value of $\bar{\boldsymbol{p}}^{\mathrm{G},l+1} - \bar{\boldsymbol{z}}^{l+1} + \mathbf{a}^{l+1}$ to all H-MGs.

The reader may refer to subsubsection A.5.2.2 in Appendix A for a detailed step by step deduction of the presented ADMM algorithm for the sharing problem.

5.3. ADMM implementation

This work approaches the ADMM implementation from a global perspective where a central collector coordinates the jobs of a set of H-MGs. The central collector broadcasts $\bar{\boldsymbol{z}}$ and $\mathbf{a}$ to the H-MGs, wait until they finish their local computations, collects all $\boldsymbol{p}_h^{\mathrm{G}}$, and updates $\bar{\boldsymbol{z}}$ and $\mathbf{a}$.

To implement ADMM each H-MG h must store its current value of $\hat{\boldsymbol{u}}_h$. Furthermore, it must be capable of solving its local optimization problem and have access to the required local information for defining J_h. It is necessary to have a global aggregator (CCU), which acts as a central collector and its main tasks are averaging local public variables, updating the global variable, and computing and broadcasting the coordination mechanism. Furthermore, all subsystems (H-MGs) have to be synchronized, i.e. updating local variables must occur before conducting global aggregation, and the latest available global variable and coordination mechanism are to be used for the local updates. Similar requirements are also valid for the implementation of the dual decomposition approach.

As mentioned earlier, for the considered case the ADMM implementation also demands to answer two questions: how to cope with the non-convex problems and when to terminate the algorithm. The following subsections treat these subjects in detail.

5.3.1. Approaches for handling the mixed-integer nature of the subproblems within the ADMM algorithm

ADMM is well suited to work for distributed convex optimization problems [81]. For non-convex problems (in this case a problem with binary variables), ADMM can converge to

non-optimal points. This work investigates two approaches for handling binary variables within the ADMM algorithm:

1. **ADMM-feasible**. It is based on similar case studies discussed in [33] and [34] and implies carrying out two additional steps, namely relax and recover. It firstly consists in relaxing all binary constraints in the local subproblems, such that the relaxed variables are constrained by the real interval between 0 and 1. Once the algorithm's solution satisfies the defined termination condition or the algorithm reaches the maximum allowed iteration counts, the resulting solution vector may not be feasible i.e. the solution for the binary variables is not necessarily boolean. As a consequence, this approach requires an additional step to recover feasible solutions. This is done by solving the $\hat{\boldsymbol{u}}_h$-update with the original binary constraints and last available information.

2. **ADMM-unrelax**. Based on the work in [82], this approach proposes to perform all ADMM steps without any relaxation with the hope that the algorithm will converge. If it converges, the point of convergence may be a good point - compared against the global optimum. Furthermore, the resulting solution will be already feasible and can be implemented directly. The advantage of this approach is the sparing of the relaxation and recovery steps.

5.3.2. Termination condition for the ADMM algorithm

The primal residual norm and the dual residual norm are normally used to check termination condition in ADMM applications. The primal residual norm $\|r^l\|_2$ at an iteration count l is:

$$\|r^l\|_2 = \|\boldsymbol{p}^{\mathrm{G},l} - H\bar{\boldsymbol{z}}^l\|_2, \tag{5.10}$$

where $\boldsymbol{p}^{\mathrm{G},l} = \sum_{h=1}^{H} \boldsymbol{p}_h^{\mathrm{G},l}$. This can be seen as the l_2-norm of the vector difference between the sum of H-MGs power schedules and the power schedule computed by the CCU. When the l_2-norm of this vector difference is small enough, the algorithm is said to meet the primal residual convergence criterion. The dual residual norm at iteration count l is defined as:

$$\|s^l\|_2 = \|\rho(\bar{\boldsymbol{z}}^l - \bar{\boldsymbol{z}}^{l-1})\|_2, \tag{5.11}$$

when the l_2-norm of the vector difference between two consecutive computations of $\bar{\boldsymbol{z}}$ is small enough, the algorithm is said to meet the dual variable convergence.

The termination criterion is met, when the primal residual norm and the dual residual norm are smaller than a given tolerance. The same tolerance definitions as suggested in [81] are used in this work as reference. Accordingly, the primal tolerance is defined as:

$$\epsilon^{\mathrm{pri}} = \sqrt{N_p H}\epsilon^{\mathrm{abs}} + \epsilon^{\mathrm{rel}} \max\left\{\|\sum_{h=1}^{H} \boldsymbol{p}_h^{\mathrm{G},l}\|_2, \|H\bar{\boldsymbol{z}}^l\|_2\right\}, \tag{5.12}$$

and the dual tolerance as:

$$\epsilon^{\text{dual}} = \sqrt{N_p H}\epsilon^{\text{abs}} + \epsilon^{\text{rel}}\|\rho \mathbf{a}^l\|_2, \tag{5.13}$$

where ϵ^{abs} is an absolute tolerance and ϵ^{rel} is a relative tolerance. The implemented values for these tolerances are $\epsilon^{\text{abs}} = 10^{-4}$ and $\epsilon^{\text{rel}} = 10^{-2}$.

5.3.3. A new termination condition for ADMM

As the considered ADMM implementation works within an MPC framework, checking the whole time window with the primal residual norm is not necessary and inefficient. This work proposes new termination conditions for the considered ADMM implementation. First, by exploiting the principles of MPC where just the first element of the solution vector is implemented and the rest is discarded, a new termination criterion pays special attention to $\|r^l_{k_i}\|_1$, which is the absolute value of primal residual's first element as shown in (5.14). In other words, the termination condition implies that the absolute difference between the sum of electrical powers $p^{\text{G},l}_{h,el}(k_i)$ sent by the H-MGs and the estimated power at reference node at time k_i, computed by the CCU, must be less than a given tolerance.

$$\|r^l_{k_i}\|_1 = \left| \sum_{h=1}^{H} p^{\text{G},l}_{h,el}(k_i) - H\bar{z}^l(k_i) \right|. \tag{5.14}$$

Additionally, the l_∞-norm helps to check the maximum discrepancy between the electrical power profiles from the H-MGs and the estimated power profile from the CCU over the whole prediction horizon, as indicated in (5.15). Then, the termination condition also includes the criterion that a solution is valid only if $\|r^l\|_\infty$ is below a certain tolerance.

$$\|r^l\|_\infty = \max_k \left\{ \left| \sum_{h=1}^{H} p^{\text{G},l}_{h,el}(k) - H\bar{z}^l(k) \right| : k = k_i, \ldots, k_i + N_p - 1 \right\}. \tag{5.15}$$

The dual variable convergence is checked by using the same dual residual norm and the same dual residual tolerance as defined in the previous section in (5.11) and (5.13).

5.3.4. Algorithm for the hierarchical-distributed strategy based on ADMM

Algorithm 2 illustrates the sequence of computations of the algorithm for the hierarchical-distributed coordination strategy based on ADMM.

Algorithm 2 MPC based hierarchical-distributed algorithm using ADMM

1: **Initialize**. CCU broadcasts $\bar{\boldsymbol{p}}^{\mathrm{G},1} - \bar{\boldsymbol{z}}^1 + \mathbf{a}^1 = 0$ to H H-MGs
2: **ADMM Iterations**. **For** $l = 1, \ldots, l^{max}$ **do**

- **LP-relaxation** (optional). If required, each H-MG relaxes its local binary variables
- $\hat{\boldsymbol{u}}_h$**-update**. Each H-MG h recovers its stored value of $\boldsymbol{p}_h^{\mathrm{G},l}$ where $\boldsymbol{p}_h^{\mathrm{G},1} = 0$, solves (5.4) locally and communicates $\boldsymbol{p}_h^{\mathrm{G},l+1}$ to the CCU
- $\bar{\boldsymbol{z}}_h$**-update**. The CCU collects $\boldsymbol{p}_h^{\mathrm{G},l+1}$ from all H-MGs, computes the average $\bar{\boldsymbol{p}}^{\mathrm{G},l+1}$ and solves (5.5)
- $\mathbf{a}_h$**-update**. The CCU computes $\mathbf{a}_h^{l+1}$ from (5.6) and broadcasts $\bar{\boldsymbol{p}}^{\mathrm{G},l+1} - \bar{\boldsymbol{z}}^1 + \mathbf{a}^1$ to all H-MGs
- if termination condition is **True** then **break**

3: **Recovery of primal feasible solutions** (optional). If required, each H-MG solves (5.4) again with the last value sent by the CCU and original unrelaxed variables
4: **Implementation**. Implement first element of the feasible solution vector, wait for $k_i = k_i + \Delta t$, and go to 1

5.4. Simulation results and discussion

The upcoming subsections present and describe simulation results from the hierarchical-distributed operation strategy using ADMM. The simulation setup uses $N_p = 96$, $\Delta t = 15$ min, $\gamma = 100$, and $\rho = 0.5$. The rest of the simulation parameters are the same as in Section 4.4. The first part of the results compares the objective convergence from dual decomposition (see Section 4.5) and ADMM approaches and gives insights into the quality of the solution for the ADMM-feasible approach and the ADMM-unrelax approach. The second part presents the behavior of the ADMM approaches regarding a reference termination condition which uses as basis the primal and dual residual norms and primal and dual tolerances. Finally, the last part shows the performance of the algorithm and the quality of its solution when using the new proposed termination condition.

5.4.1. ADMM objective convergence

To better illustrate the performance of the MPC based hierarchical-distributed coordination strategy using ADMM, the objective convergence of the ADMM algorithm is compared against the objective convergence of the dual decomposition algorithm. For this purpose, it is of interest to evaluate the convergence speed and the evolution of the objective gap for both algorithms, where the objective gap at a given iteration l is defined as $\left|p^l - p^\star\right|$. Here, $p^\star$ denotes the global optimum, i.e. the optimal value found with the centralized coordination strategy described in Section 4.4.

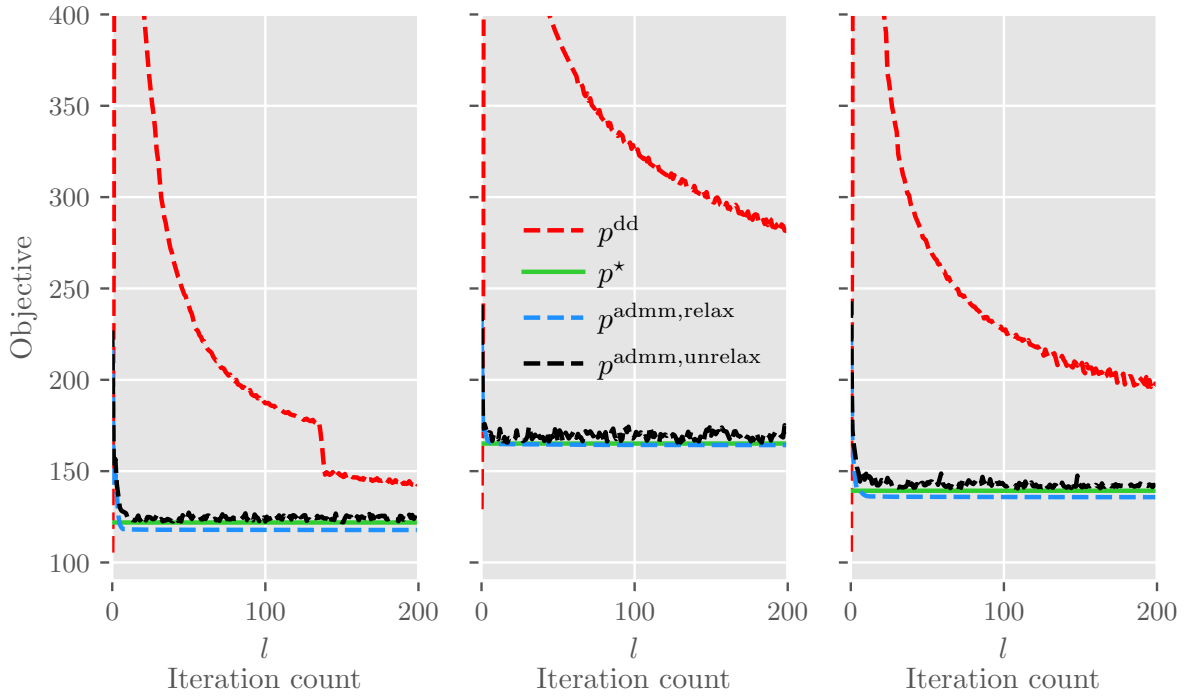

a) Summer b) Transitional c) Winter

Figure 5.1.: Objective value ADMM vs dual decomposition

Simulation experiments are conducted for input data corresponding to three days from different seasons of the year, namely summer, winter, and fall as transitional season. For illustration purposes, one single optimization run is solved for each day - i.e. without receding horizon control - recording the value of the objective at each iteration and the corresponding iteration count. The initial starting values for all simulations are the same. The plots in Figure 5.1 display the evolution of the objective value over the iteration count for both algorithms for the three distinct input data. For the sake of correctness, the ADMM-feasible approach is denoted here by ADMM-relax, since at this point the problems are still relaxed.

The optimal value is given by the green line and the red line denotes the results obtained for dual decomposition. As mentioned above, two approaches are simulated for ADMM. Consequently, the blue dashed line depicts the progress of the objective value for the ADMM-relax approach, whereas the black dashed line shows the evolution of the objective value for the unrelaxed version of ADMM. In general, it becomes clear that the ADMM algorithm converges faster than the dual decomposition algorithm, and that the final objective gap for dual decomposition is considerable higher than the final objective gap for ADMM.

The plots also show that the optimal global value is different for each day, and that the speed of convergence also differs for each day. This implies that the speed of convergence also depends on the input data. For the interested reader Appendix D provides further

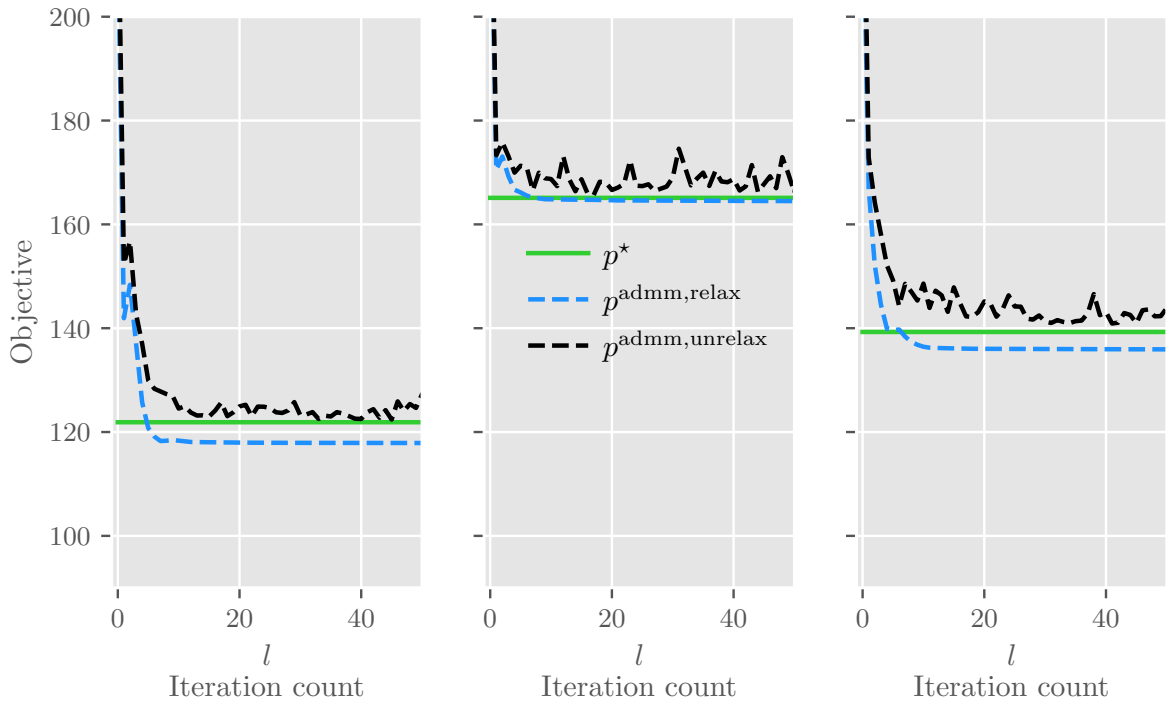

a) Summer b) Transitional c) Winter

Figure 5.2.: Objective value ADMM relax vs ADMM unrelax

information on the objective gap for all considered cases. Figure 5.2 allows a more detailed analysis for the ADMM cases. Compared to the ADMM-relax, the speed of convergence of the ADMM-unrelax is slightly slower - at least for the summer and the winter data. Moreover, the observed objective gap is minimal for both approaches.

Even though at this point the ADMM-relax approach performs well in terms of objective gap and speed of convergence, it may contain infeasible solutions as all binary variables (On/Off status for heat pump, CHP, electric water heater, etc.) are still relaxed. This situation is better appreciated in Figure 5.3, which shows the value of the variables for the On/Off status of the heat pump over the considered time window. As in the previous plots, the green line gives the feasible and optimal solution for the variables, which is either 0 or 1. The blue dot-line represents solution values obtained from the relaxed ADMM (a pre-step of ADMM-feasible) and they can have any value between 0 and 1. Since a decision has to be taken on whether the heat pump must be turned on or off, such relaxed solutions are not feasible.

To complete the picture the relaxed ADMM is complemented by recovering primal feasible solutions from the relaxed solutions. In other words, once the relaxed ADMM is stopped, the last available vector of prices $\boldsymbol{\lambda}^{l_{\max}}$ is used for solving the unrelaxed version of the subproblems so that their solutions are all feasible. This is now the complete ADMM-feasible approach and its solutions are depicted by the orange dash-dot line in the plots.

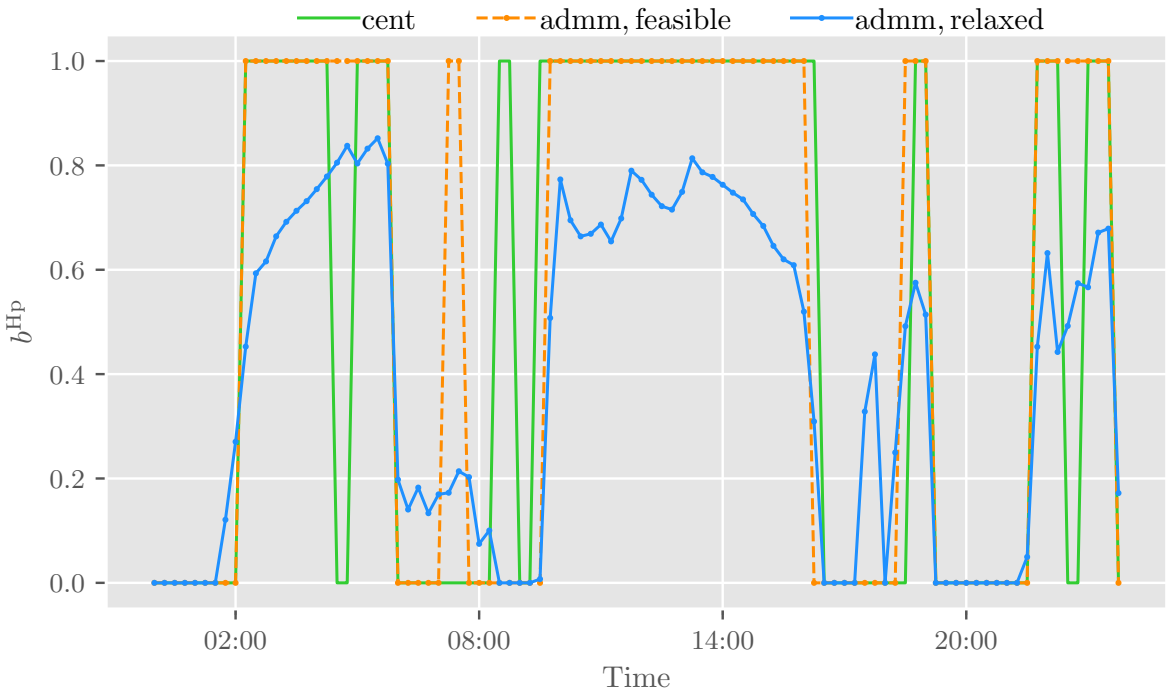

Figure 5.3.: Solution values for On/Off variable of the heat pump

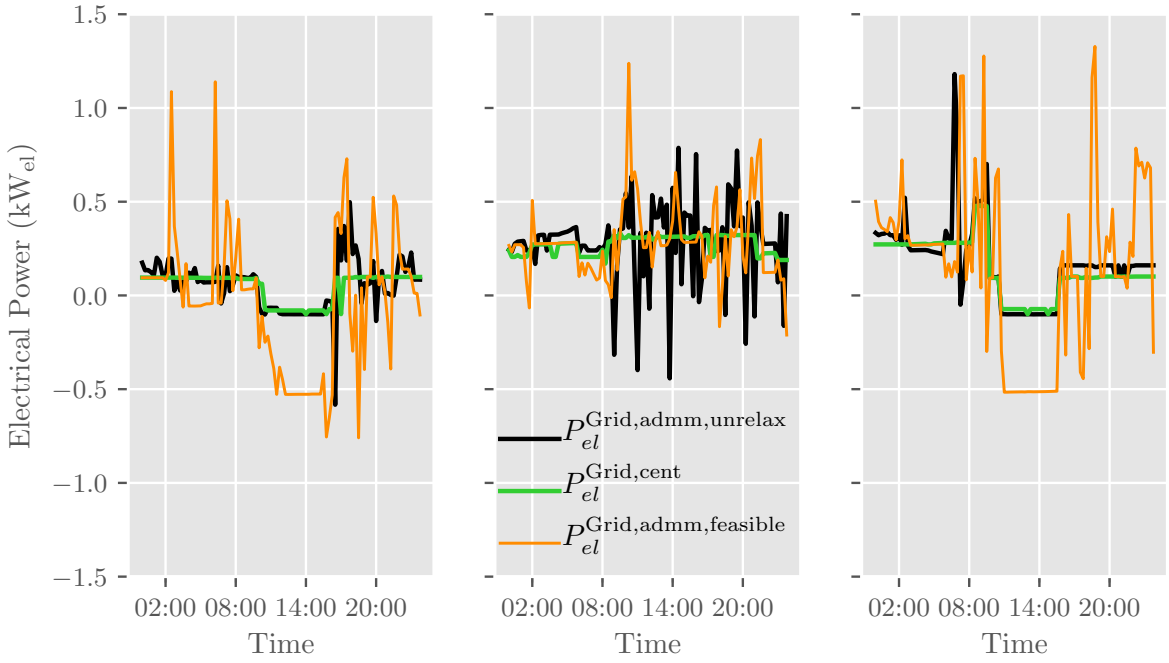

a) Summer b) Transitional c) Winter

Figure 5.4.: Power profiles at reference node: feasible ADMM vs. unrelaxed ADMM

Finally, Figure 5.4 helps to evaluate the effects of recovering feasible solutions from the relaxed problems on the resulting power profile at reference node.

It can be seen that when feasible solutions are recovered from the relaxed ADMM, the resulting $\boldsymbol{p}^{\mathrm{G}}$, indicated by the orange line, shows larger peaks than the power profile from ADMM-unrelax. Although the relaxed and recover approach offers a fast speed of convergence considering objective value, primal residual and dual variable residual (see Appendix E), its final feasible solution yields a power profile which is outperformed by the ADMM-unrelax approach.

This implies that it could be more advantageous to use the ADMM-unrelax approach, as it does not require neither relaxation nor recovering procedures and because its resulting power profile at reference node gives acceptable power peaks. The issue now is to find a proper termination condition for the ADMM approach, such that it does not need a large number of iterations to achieve an acceptable power profile at reference node.

5.4.2. Results for termination condition for ADMM

The results exposed in the previous section illustrate the performance when the respective algorithm iterates until a maximum iteration count is reached. However, it is desirable to stop the algorithm at an early stage if the available solution meets a certain termination condition. A real hierarchical-distributed MPC implementation cannot make use of the objective gap to check a termination condition, as no information regarding the global optimal value - provided by a centralized strategy - is available.

To overcome this situation, the authors in [81] and [14] recommend to monitor the primal residual and dual residual (see (5.10) and (5.11)) in order to establish convergence. The termination criterion is met, when the primal residual norm and the dual residual norm are smaller than a given tolerance.

To check the algorithm's behavior when applying the stopping criterion described in Subsection 5.3.2, Figure 5.5 displays the resulting primal residual norm of new conducted simulations for the ADMM-feasible approach (upper subplot) and the ADMM-unrelax approach (lower subplot). The line in light red denotes the primal tolerance which is different for each approach. It can be seen that the ADMM-feasible meets the primal tolerance for all three scenarios before iteration count 40, such that the algorithm stops before the maximum allowed iteration count. Contrary, the ADMM-unrelax approach does not meet the defined primal tolerance and it stops only when it reaches the maximum number of iterations (200 for this case).

In the sequel, the Figure 5.6 presents the value of the dual residual and the value of the dual tolerance for each iteration count. In contrast to the primal residual, both approaches meet the dual tolerance relatively fast in less than ten iterations.

It is desired to continue with the ADMM-unrelax approach as for practical issues it is better to solve the original problem without having to deal with relaxations inside H-MGs.

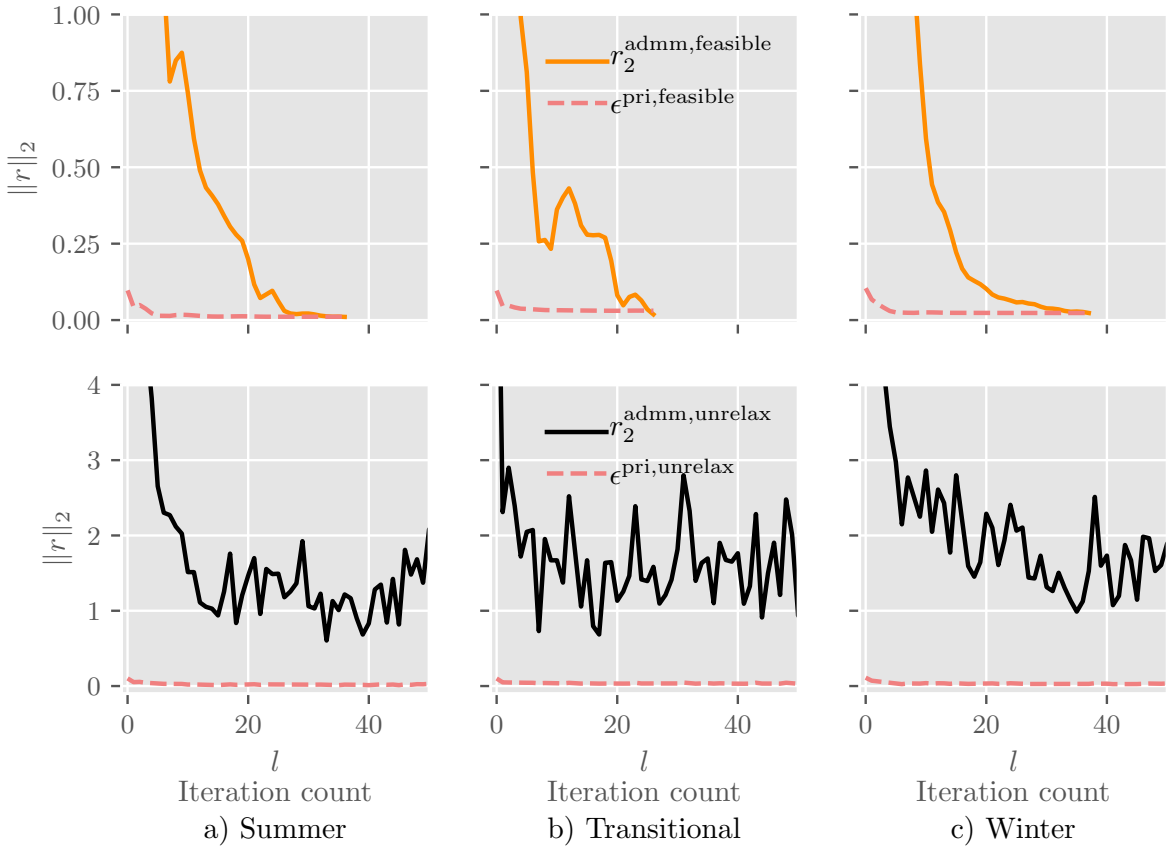

Figure 5.5.: Primal residual norm with implemented termination condition for ADMM-feasible and ADMM-unrelax

It may be hard to coordinate a hierarchical-distributed optimization when sometimes the agents have to send a schedule obtained from a relaxed problem and other times they have to send a schedule obtained from the unrelaxed problem.

Furthermore in terms of power profile at the reference node, the ADMM-feasible approach does not show any clearly advantage over the ADMM-unrelax approach. Nonetheless, a proper termination condition has to be designed for the ADMM-unrelax approach. The next subsection elaborates on this matter.

5.4.3. Results for new termination condition for ADMM-unrelax

Numerical simulations for the same considered cases as in previous section help to demonstrate the effectiveness of the proposed new termination condition for the ADMM-unrelax approach. The optimization loops are embedded in an MPC scheme. Forecast for PV and space heating consist in simple one-day-persistence forecasts, while the forecast for household load and the forecast for domestic hot water use a simple seven-day-persistence forecast.

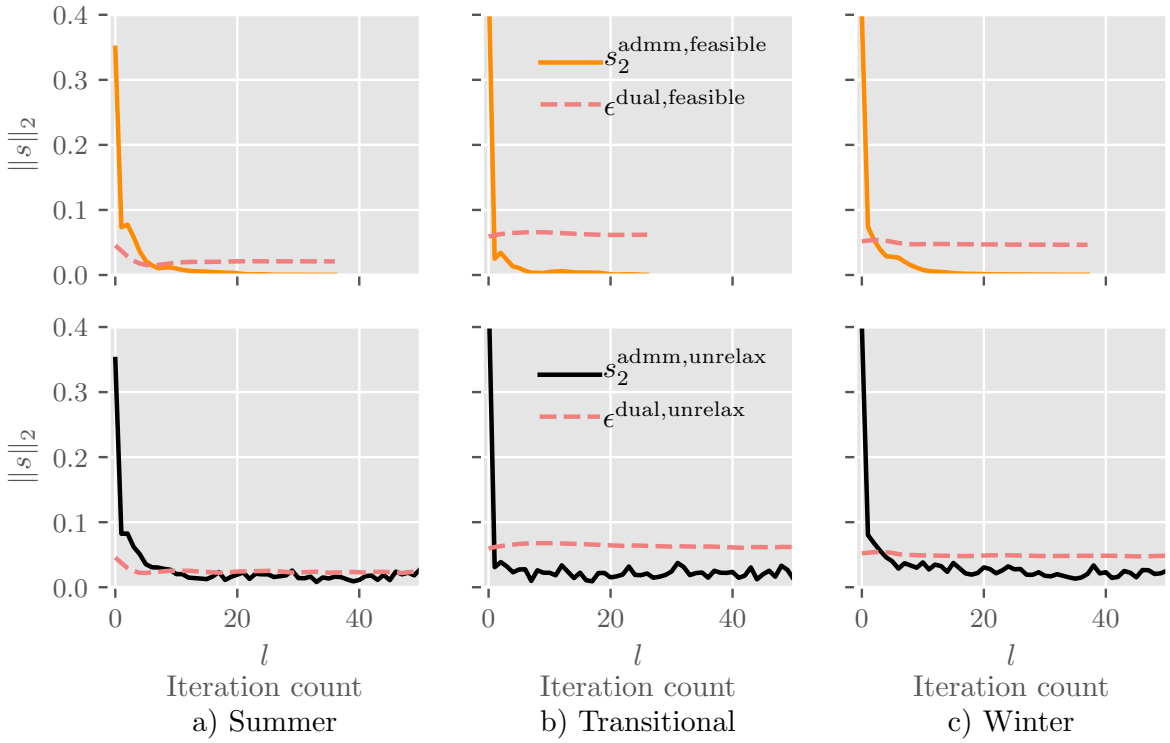

Figure 5.6.: Dual residual norm with implemented termination condition for ADMM-feasible and ADMM-unrelax

Figure 5.7 shows the distribution of the required iterations for the ADMM-unrelax approach with the new proposed termination condition. For comparison purposes, the distribution of iteration counts for the ADMM-feasible approach with termination condition as proposed by [81] is also shown as reference. The median of the iteration counts with the proposed termination condition for a summer day is 2.0, for a transitional day is 2.0 and for a winter day is 5.5, while for the reference termination condition the medians of the distribution are 56.0, 34.0 and 56.5 respectively. In average, to find a solution the ADMM-unrelax approach with the proposed termination condition needs 2.88 iterations in a summer day, 2.96 iterations in a transitional day and 6.01 iterations in a winter day. Accordingly, the ADMM-feasible approach with reference termination condition accounts for an average of 55.53, 40.00 and 64.20 iterations for the evaluated scenarios.

Even though the two approaches cannot be directly compared to each other as they are based in different termination conditions, the objective of the plot is to illustrate the behavior of the iteration counts of the proposed termination condition against the behavior of iteration counts of a state of the art termination condition. It would be also possible to implement the ADMM-feasible approach with the new proposed termination condition, however, as mentioned before, the ADMM-feasible approach is no longer attractive for real application purposes, as it requires further communication effort between the CCU and the H-MGs in order to know if the problem to be solved by the H-MGs has to be relaxed or not.

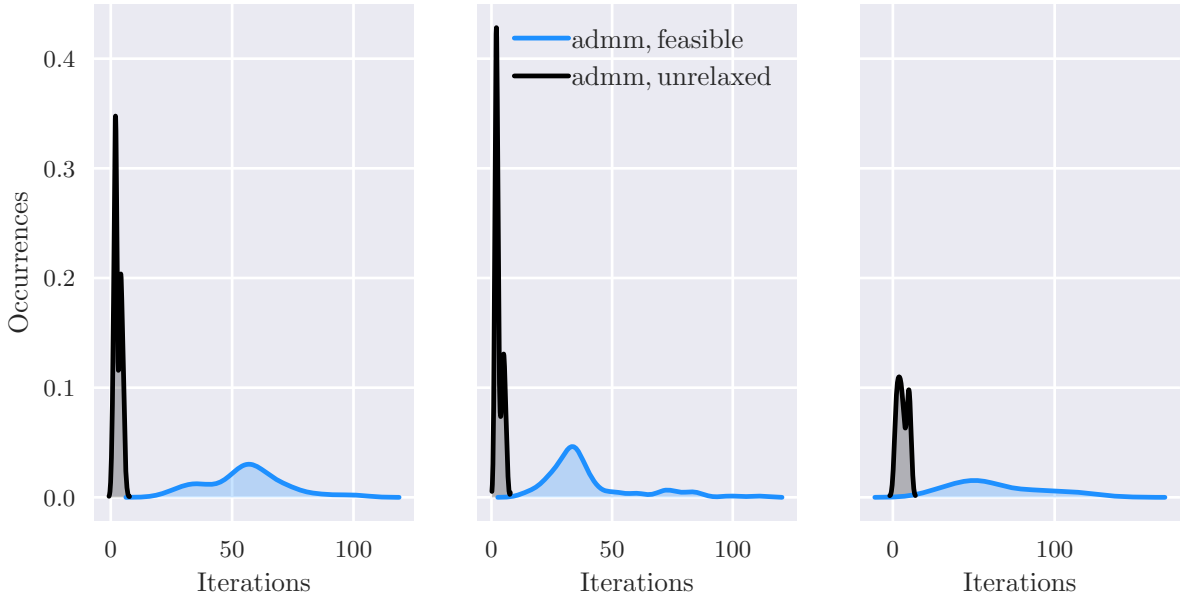

Figure 5.7.: Distribution of iteration counts for ADMM-feasible and ADMM-unrelax

Finally, Figure 5.8 presents the resulting power profile at reference node. It is noticeable that the ADMM-unrelax approach yields similar results as the centralized approach for all three season scenarios. The upper subplot allows a comparison between ADMM-unrelax and ADMM-feasible. Note that it is a zoom over the y-axis. It follows from this subplot that there is no remarkable difference between the profiles resulting from these two approaches.

The lower subplot shows the improvement against the decentralized strategy. For the summer and transitional scenario, the ADMM-unrelax approach is able to reduce extreme power peaks and obtains an almost flat power profile at reference node. For the winter scenario during night and morning hours it is possible to reduce power peaks as well, in the afternoon and evening periods not all peaks can be reduced, nevertheless the large peak around 20:00 hours is reduced by almost 1kW. This situation in the winter scenario is not inherent from the ADMM-unrelax approach as those power peaks are also present with the centralized strategy. As the simulated MPC strategies work with a very simple forecast approach (persistence forecast), it can be expected such power peaks in winter to be reduced if a more accurate forecast method is implemented. This aspect is out of the scope of the present work and must be addressed in a future work.

Based on the presented results it is possible to conclude that the ADMM-unrelax approach offers, from a practical point of view, advantages for implementation over the ADMM-feasible approach because:

- the H-MGs do not need to relax their optimization problems,

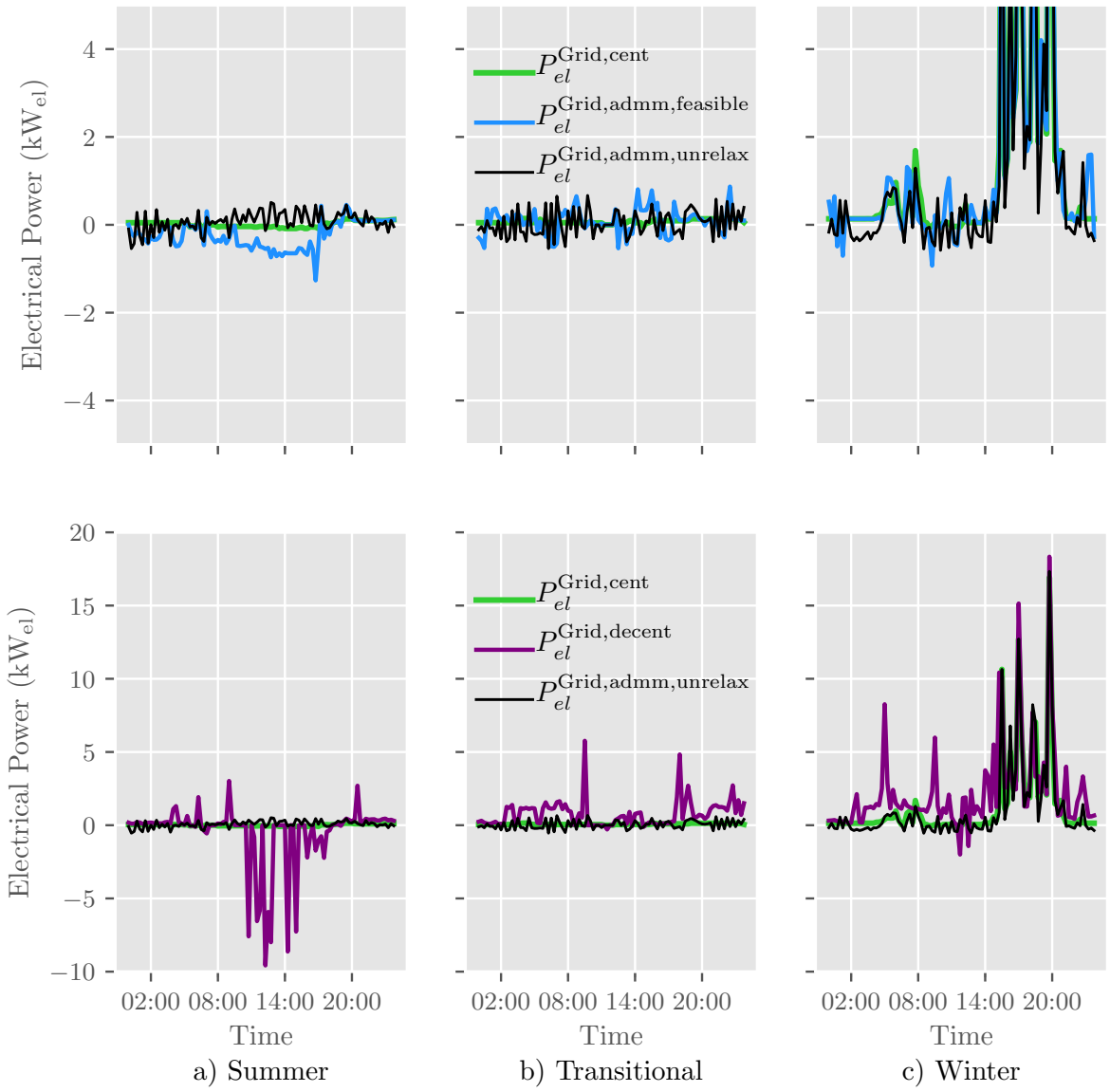

Figure 5.8.: Resulting power profiles at reference node with $P_{el}^{\text{Grid,cent}}$as reference. Upper subplot: ADMM-unrelax vs. ADMM-feasible; lower subplot: ADMM-unrelax vs. Decentralized

- the H-MGs do not need to recover feasible solutions once the iterations are done, and
- the resulting recovered feasible solution from the feasible ADMM approach is not necessarily better than the one obtained working with unrelaxed problems right from the start.

Furthermore, when implemented within an MPC scheme, the ADMM-unrelax approach with a new proposed termination condition delivers results that are competitive to the centralized strategy, while considerably decreasing the iteration counts compared to a state of the art termination condition. Consequently, this work recommends the ADMM-

unrelax approach with the proposed termination condition for laboratory, demonstration and field implementations for hierachical-distributed coordination of H-MGs.

5.5. Summary of the chapter

This chapter looked at the optimal operation of a group of interconnected H-MGs using an MPC based hierarchical-distributed strategy with ADMM. It showed the mathematical formulation for the optimal operation of such a system as an ADMM sharing problem. The chapter examined two approaches to deal with binary variables in the presented ADMM implementation, namely:

1) ADMM-feasible, which solves a relaxed version of the original subproblems with subsequently recovering primal feasible solutions, and

2) ADMM-unrelax, which solves the original non-convex subproblems without any relaxation.

The chapter also investigated termination conditions for the ADMM algorithm. In the end, by taking advantage of the MPC implementation, it proposed a simple yet effective termination condition which allows terminating the ADMM algorithm after a few iterations, while also achieving results similar to that of the centralized operation strategy. The chapter concluded that the ADMM-unrelax is advantageous for implementation purposes because the H-MGs do not need to relax their optimization problems, and they do not need to recover feasible solutions once the iterations are ready. Furthermore, when implemented within an MPC scheme, the ADMM-unrelax approach with a new proposed termination condition gives results that are competitive to the centralized strategy, while considerably decreasing the iteration counts compared to a state of the art termination condition.

6. A co-simulation framework for electrical networks and home-microgrids

This chapter describes a co-simulation tool for evaluating the impact of home-microgrids' operation on electrical distribution networks. Technical aspects of the co-simulation tools are explained in detail. The co-simulation framework described in this chapter was created within the research project 'Collaborative Data and Risk Management for Future Energy Grids - a simulation Study' [83]. The framework was developed by the project team.

The content of this chapter is adapted from [62]: D. Hidalgo-Rodríguez, S. Hoffmann, F. Adelt, J. Myrzik, and J. Weyer, "A socio-technical simulation framework for collaborative management in power distribution grids," in *International ETG Congress 2017*. Bonn, Germany, 2017.

6.1. Introduction

End-users in energy systems are becoming heterogeneous with increasing penetration of distribution energy resources (DER) in distribution grids. Sometimes they behave as electricity consumers, sometimes as producers, sometimes they store energy, or sometimes they are just self-sufficient. This heterogeneity implies that the energy system is a large complex system, and simulating its behavior taking into account inter-dependencies between heterogeneous actors is not a trivial issue. Hence, aiming at simulating this whole large complex system with just one single simulator is not practical. Co-simulation techniques are interesting approaches for such simulation purposes. Within the co-simulation approach, existing simulators are adapted in such a way that they can communicate with each other such that instead of simulating the behavior of the system with one single simulator, many simulators are involved to reproduce the behavior of the system. Consequently, this chapter describes a co-simulation framework for assessing the interactions between H-MGs and electrical distribution networks. The proposed framework is based on design principles of agent-based modeling and simulation (ABMS). The contributions of this chapter are:

1. it presents a co-simulation framework to assess the impact of operation modes of H-MGs on the electrical distribution network, and
2. it shows with the help of simulation results that a coordination of H-MGs brings benefits to the network operation.

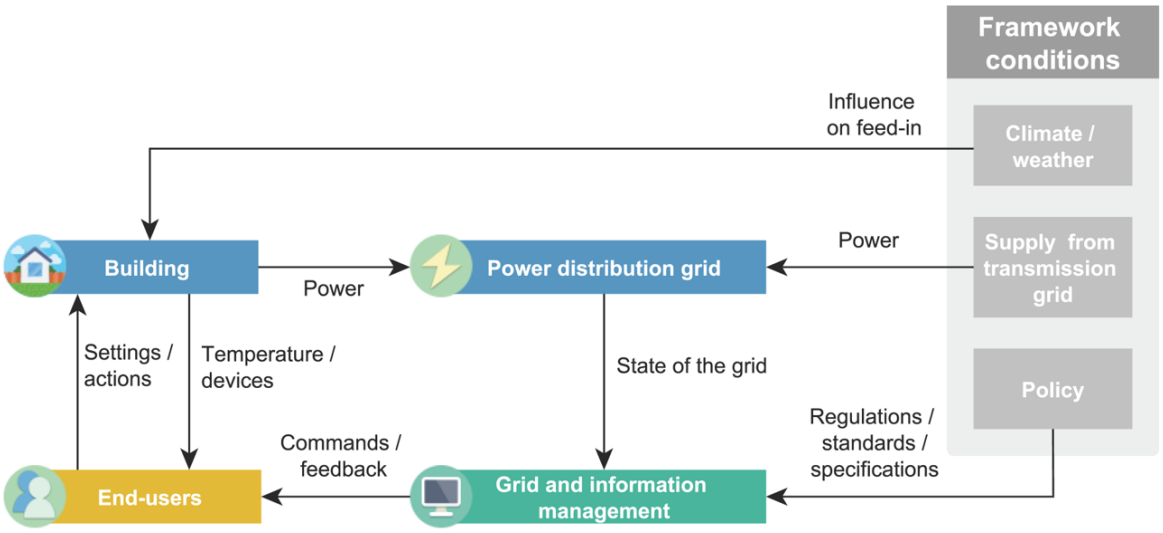

Figure 6.1.: Structure of the overall co-simulation framework and information flows between simulators

The chapter is organized as follows: Section 6.2 introduces the proposed co-simulation framework and describes the involved simulators and their inter-dependencies. Section 6.3 gives a description of the experimental setup consisting of a generic low voltage network for Germany with a certain penetration of H-MGs, and presents corresponding simulation results. Finally, Section 6.4 states concluding remarks and provides insights into next steps.

6.2. Co-simulation framework

As indicated previously, a co-simulation framework may help to understand the (bottom-up) dynamics of complex energy systems and to detect emergent, unintended effects. The proposed co-simulation framework for operation of a power distribution grids is shown in Figure 6.1. It consists of the following simulators.

The *end-user simulator* describes the decision-making of consumers: Based on individual preferences and values, actors decide to switch electricity tariffs, change their energy consumption behaviour or follow recommendations from energy-monitors (e.g. smart meters or mobile applications). These decisions are furthermore translated into load values, which primarily serve as inputs for other simulators (see *building simulator*). The *grid and information management simulator* primarily represents controlling interventions on part of the distribution system operator (DSO) and therefore the standard operating business of grid management. Controlling interventions require comprehensive knowledge of the grid, which is why this module also entails the flow of data and information between

different actors. The simulator for the *power distribution grid* is used for load flow calculations, i.e. the current status of the grid. This status is the result of an equation system; values generated by end-users (i.e. loads), producers (i.e. decentralize feed-in), feed-ins from the transmission grid and DSO commands are inputs for these equations. DSOs, in turn, use the output data from this module to interpret and manage the grid's status.

A high potential for load shifting on end-user level can be found in the heat sector, making the precise modeling of space heating and hot water demand necessary. Therefore, a building simulator is included to represent the actual behavior of a H-MG. This building simulator has to reproduce different technological entities and characteristics (see Figure 2.1 and Figure 3.2), e.g. the energy management system (based on MPC), the type of the building, as well as the technological equipment - i.e., standard gas heating devices, photovoltaic plants, batteries, heat-pumps and mini CHP plants. Framework conditions are externally given and consequently not open to influences from other simulators. They encompass pre-parametrized values and trajectories, e.g. weather/temperature or electricity prices on the European Energy Exchange (EEX). Furthermore, political regulations or feed-in capacity from the transmission grid also represent external inputs. Consequently, framework conditions basically help to characterize scenarios. The emergence of framework conditions is, however, not subject of analysis here (i.e., political negotiations etc.).

This work makes use *MOSAIK* to enable the coupling of multiple simulators [84, 85]. The MOSAIK framework is specific for the co-simulation of cyber-physical systems and smart grid systems, and its goal is to allow the usage of existing simulators in a common context to perform coordinated simulations. MOSAIK pays particular attention to provide flexibility for the configuration of large-scale scenarios. These scenarios serve as test bed to conduct simulation experiments for different control strategies (centralized, distributed, hierarchical distributed, etc.). By means of an application programming interface (API), the connected simulators can communicate with MOSAIK, which schedules the step-wise execution of the simulators and coordinates the data-flow between them. For this purpose, two main modules comprise the MOSAIK framework: the simulator management module and the scheduler module. The simulator management module is in charge of creating connections with the simulators in order to allow data exchange with them. The scheduler module is in charge of coordinating the data exchange between simulators by using a shared simulation clock.

For interaction with the user, MOSAIK uses two fundamental application programming interfaces (API). The Scenario-API enables the user to create instances of models from the connected simulators and to define the communication structure between simulators. By using the functions provided by the Scenario-API, within a scenario script, the user can run a co-simulation process. A second API, the Component-API, arranges a transmission control protocol (TCP) socket and manages the data exchange between simulator and MOSAIK in JSON format. The user needs to implement a Component-API for

each simulator that connects to MOSAIK. There are versions of this API available for different programming languages. The implementation consists of providing a high-level description of the models to be simulated, and their respective variables, as meta data. Additionally, some interface functions are also necessary in order to allow MOSAIK to control the simulator [85].

Consequently, the key challenge is to define relevant information flows between the different simulators. Figure 6.2 illustrates the data flow between simulators over four simulation steps.

At the beginning of the simulation, all H-MGs (instances of building simulator) connected to the power grid send the actual total power consumption/injection at their respective connection node. With this information, the power grid simulator performs a load flow calculation and communicates the resulting power at the main node (reference bus) to the grid manager which using a heuristic algorithm compute individual recommendations for each connected end-user. End-users, in turn, decide whether to accept the recommendation or not and if necessary modify their cost function. For the next simulation step, all H-MGs receive updated cost functions and the cycle repeats until the last simulation step.

The following sub-sections describe the power grid simulator, the building simulator and the grid manager simulator in detail.

6.2.1. Power grid simulator

The goal of the power grid simulator is to represent an electric distribution network within the simulation environment. It includes models of relevant electrical components

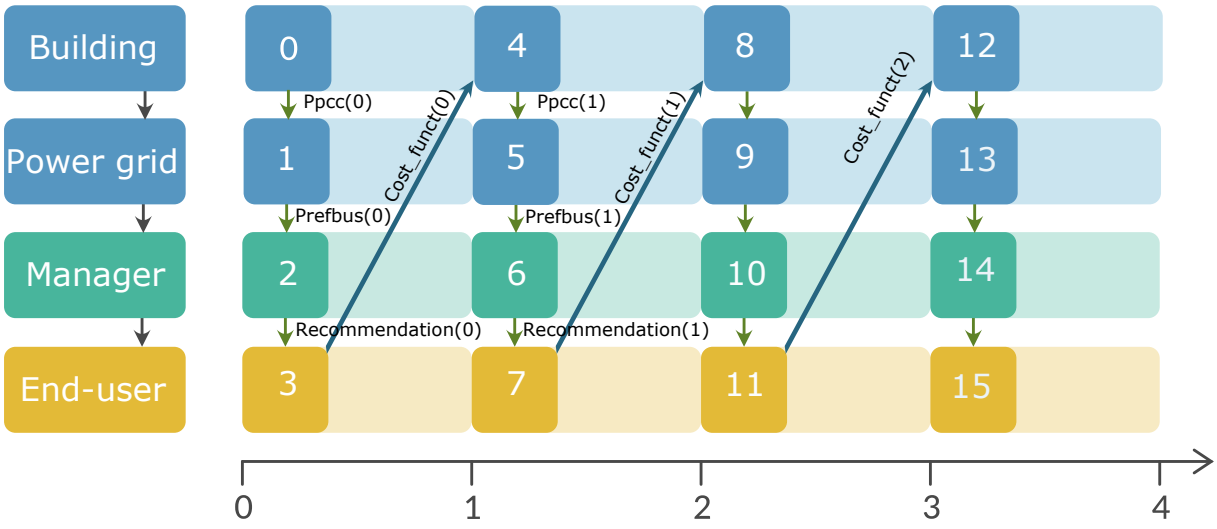

Figure 6.2.: Processing sequence of simulation steps for four simulators (Manager: Grid and information management simulator)

of a power distribution grid such as busbars (nodes), transformers, and lines. Detailed models for loads, storage and generators are not handled in this simulator (see simulator building). It also contains information regarding grid topology i.e. how and through which lines different busbars are interconnected with each other, and which generators, loads and/or transformers are connected to each busbar. A set of nonlinear equations describes the relationship between electrical components in a compact way, and from now on, this is called the power grid model. Values of end-user consumption (loads), power feed-in from distributed generators and overlaying voltage networks, as well as control commands from the DSO serve as inputs for this power grid model. With this information, and based on some initial conditions, the power grid simulator computes a load-flow calculation and provides resulting power flows for each line, and respective voltage magnitudes at each busbar [86]. The output of the simulator would allow to determine if, for the given initial conditions and inputs, voltage and loading values are within safety limits. In the power grid model, it is assumed that only one reference node (slack busbar) exists, and that the remaining nodes are PQ nodes, i.e. nodes with known active and reactive power feed-in/consumption and unknown voltage magnitude and voltage phase. Active and reactive power values are coming from a different simulation instance: the building simulator. Accordingly, in the co-simulation framework the PQ nodes are the coupling points between the power grid simulator and the building simulator. This works makes use of PYPOWER as power grid simulator [87].

6.2.2. Building simulator

The building simulator involves models of H-MGs (flexible and non-flexible residential appliances). These models can be static models - no dependency with previous states, or dynamic models - there is a dependency between actual state and previous state, e.g. a storage unit. Hence, the task of the building simulator is to solve local residential electrical and thermal power flow equations, to give the total electrical power consumed or injected at a specific node, and to compute the resulting state of the dynamic elements (for example state of charge of a thermal energy storage or room temperature of the building). These set of equations describing the behaviour of corresponding building appliances is called the building model. Because of their flexible operation to balance intermittent power from RES, residential heating systems play an important role in the current work. Therefore, heating demand and heating supply in residential systems requires detailed modeling. For accounting the demand, the building model uses some dynamic equations to represent the thermal dynamic behaviour of a residential building. This helps to consider building storage capacities as well. Residential buildings imply two types of objects: single-family houses (see H-MG 1 and H-MG 2 in Chapter 4), and multi-family houses (see H-MG 3 in Chapter 4). Clearly, buildings must contain not just thermal, but also electrical appliances. For example, a single-family house can embrace two energy sectors. In the electrical sector, there can be a rooftop photovoltaic plant, and the normal inflexible

residential loads - lights, refrigerator, washing machine, stove, etc. In the heating sector, an example will be a heat pump with respective thermal energy storage. Here, the heat pump will be the coupling element between the electrical and the heating sector. As residential units can follow different operation schedules, there is an energy management system (EMS), whose task is to compute such operation schedules. Particularly the EMS contains an MPC unit.

Setting of the simulation parameters for the building model, such as type of appliances present in the building, technical characteristics of the appliances, MPC prediction horizon, MPC sample time, etc., happens just once at the beginning of the simulation. The building simulator gets weather input data from the external conditions module, and additionally, data from the end-user simulator serve as input for the model. Specifically, these input data contain information regarding end-user building operation preference (self-consumption or energy costs minimization), and comfort limits (temperature set-points for the heating appliances). With this information, the MPC starts the optimization and concludes by giving the resulting optimal values for electrical consumption of the flexible loads, power generation for the distribution generation units, and charging and discharging power for the storage systems. After balancing electrical power flows within the residential system, the output of the building simulator is the total power consumption/injection of the considered residential setting. This is treated as a single variable, which denotes consumption if the variable is larger than zero, or generation if the variable is negative. This variable is then forwarded to the power grid simulator, which reads the variable as the power at the specific node, where the instance of the building simulator is connected. Once all the solutions from all building simulator instances are available, the power grid simulator can start with its power flow calculation, and a new simulation cycle starts. To sum up building appliances' operation mode may change over time depending on end-user preferences. For instance, end-users may decide to respond to an incentive from the DSO, or change comfort settings. These kinds of actions are computed in the end-user simulator, and are the coupling points between end-user simulator and building simulator.

The python scripts used to conduct the simulations of local H-MGs in previous chapters constitutes the building simulator. For this purpose, an adaptation of the python scripts to fit the structure of MOSAIK was necessary.

6.2.3. Grid and information management simulator

This subsection further elaborates on the logic of the grid and information manager simulator. This simulator receives the resultant power at the reference bus, i.e., the local substation, as an output value from the power grid simulator. It is desired to keep this power within a specific range, such that there are a maximum power limit and a minimum power limit. If the power at the reference bus is above the maximum limit, the grid

manager must try to increase local generation and reduce loads. On the other hand, if the power at the reference bus is below the minimum limit, the grid manager recommends to reduce the local generation and increase loads. If the end-user accepts the recommendation, he/she adapts his/her behavior and forwards it to the building simulator as a cost function. Accordingly, the building simulator will optimize the desired operational objective by adjusting the power at its connection node. Figure 6.3 depicts the logic of the grid manager. This simulator also builds on python as programming language.

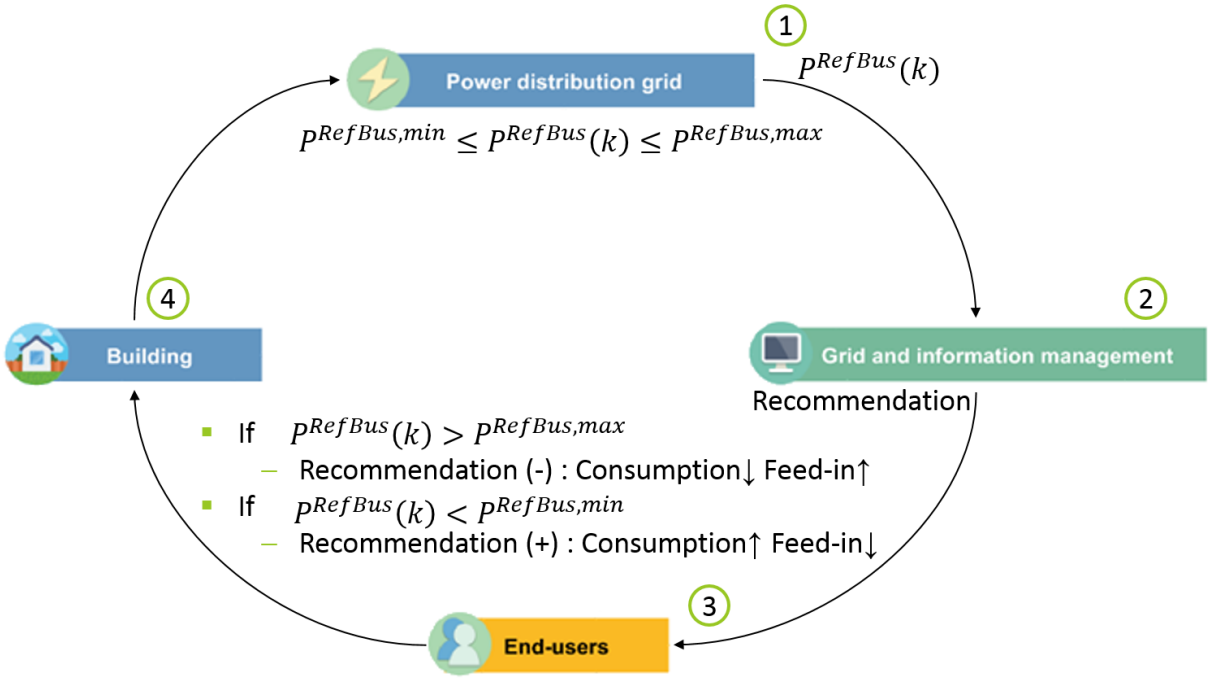

Figure 6.3.: Logic of the grid and information manager simulator

The interested reader can refer to the final report of the KoRiSim project for detailed information on implementation aspects, installation and use instructions of the co-simulation framework [88].

6.3. Simulation results and discussion

This section illustrates the functionality of the co-simulation framework by presenting simulation results for a considered case study. The generic low voltage network in Figure 6.4, presented in [89] and used in [90], serves as the reference network for the study. Its original topology is meshed low-voltage network with open sectioning points and, therefore, it operates as a radial network. It represents the supply of a residential area with single-family households (SFHs) and multi-family households (MFHs). It disposes of 167 house connection points (red nodes) and a local substation of 400 kVA (black reference node).

Consequently, 167 heterogeneous H-MGs populate the network, as described in Table 6.1.

Table 6.1.: Population of H-MGs

H-MG	**Quantity**	**Penetration**
PV	59	35.33%
PV-Battery	17	10.18%
PV-HP	8	4.79%
HP	17	10.18%
Just household load	66	39.52%
$\sum$	167	100%

Figure 6.5 shows the resulting power at the reference node(reference bus). It illustrates in black the case without any control (i.e., the grid manager does not conduct any action), and in red, a situation with activated control where, depending on the grid state, the grid manager actively sends recommendations to the H-MGs.

This plot helps to demonstrate the functionality of the co-simulation framework. From here, it is possible to appreciate that all simulators are communicating with each other such that a coordinated simulation can take place. Furthermore, it also indicates that the simple heuristic coordination algorithm implemented in the grid manager can achieve a reduction in extreme power peaks, both at the consumption and generation side. This situation is better observed in Figure 6.6.

For the simulated week in October, the logic in the grid and information manager reduces the consumption peak from ca. 280 kW to 200 kW, and the generation peak from ca. -180 kW to - 100 kW. Since the simulation considers a model of the electrical network, the impact of such a peak power reduction on the network can be appreciated. Figure 6.7 presents the cumulative network losses over the simulated week. In this case, such a decreasing of extreme power peaks results in a lowering of grid energy losses of around 30%.

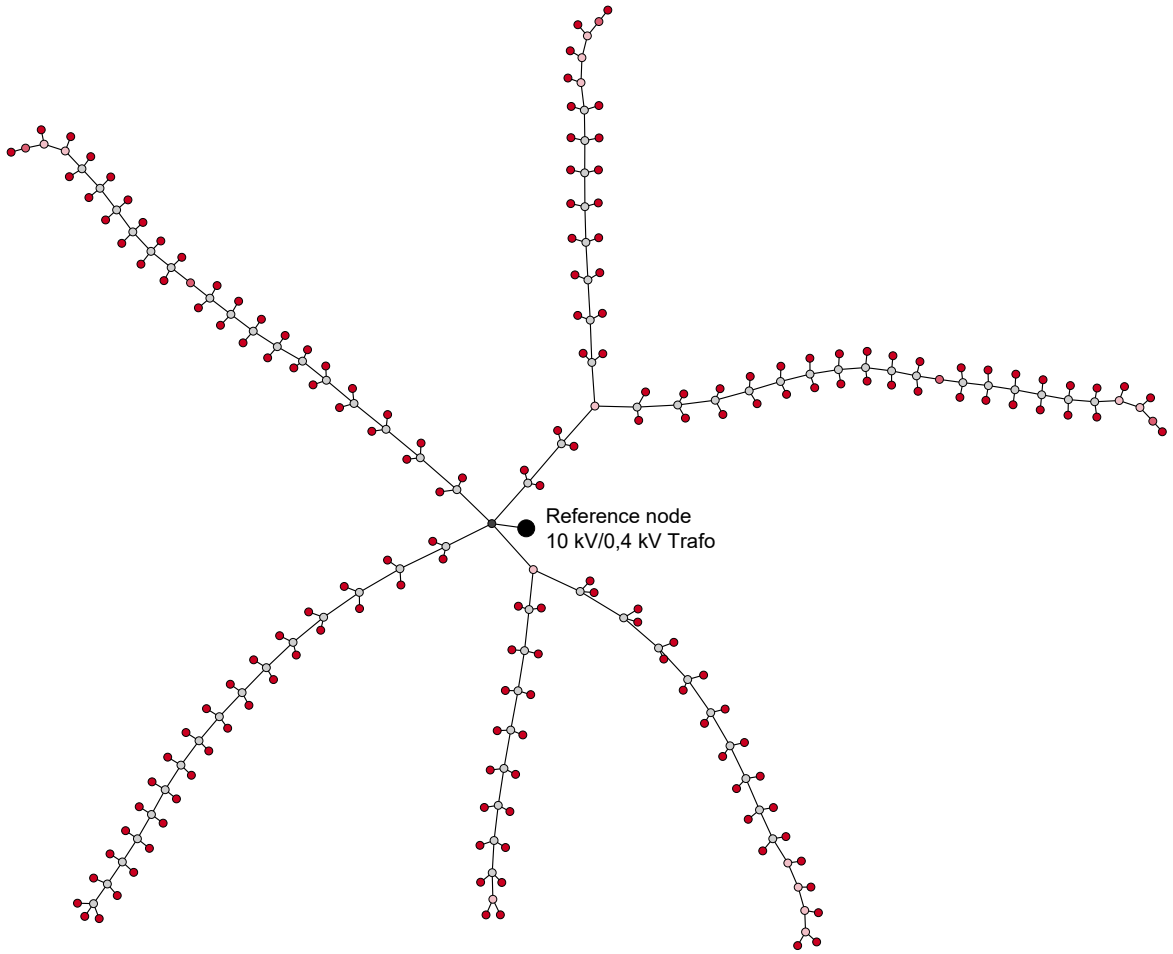

Figure 6.4.: Generic low voltage network for a residential area with SFHs and MFHs (cf. [89, 90])

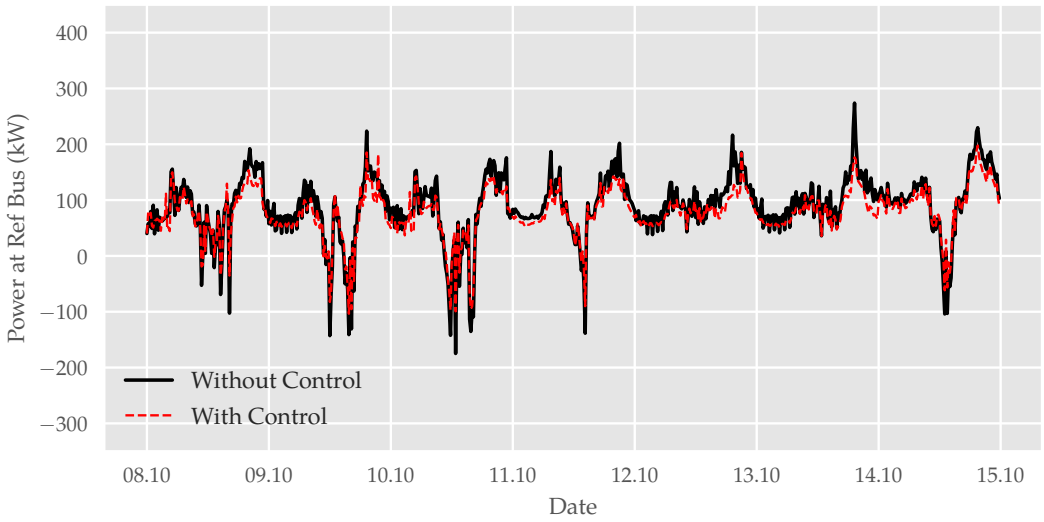

Figure 6.5.: Electrical power profile at reference bus

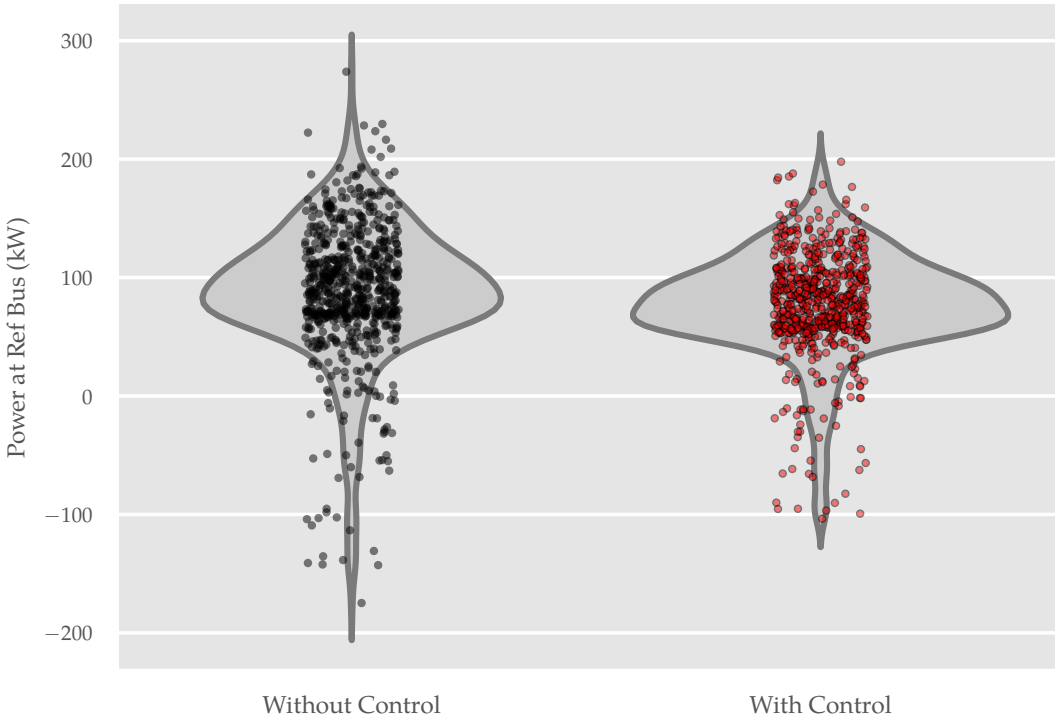

Figure 6.6.: Distribution of power at reference bus

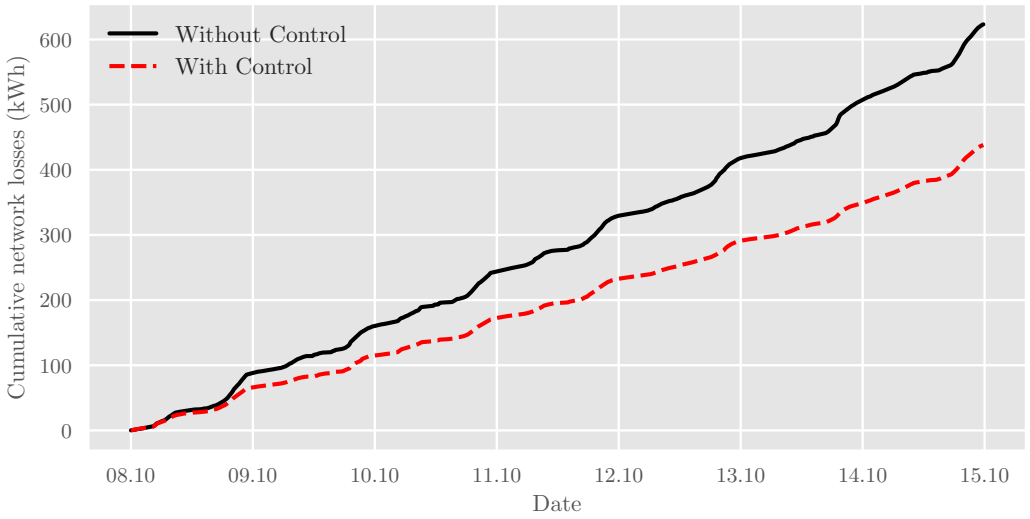

Figure 6.7.: Cumulative network losses

6.4. Summary of the chapter

This chapter presented a framework for the co-simulation of electrical networks with high penetration of H-MGs. The chapter described in detail the involved building simulator, power grid simulator, and grid and information management simulator. It explained the interactions between simulators and demonstrated the functionality of the co-simulation framework employing one-week simulation results. The proposed co-simulation framework supported the evaluation of the impact of coordination strategies on the electrical grid. For the presented case, the results indicated that avoiding extreme power peaks leads to a significant reduction of energy losses on the network.

7. Summary, conclusions and outlook

The work at hand focused on the optimal operation of home-microgrids. For this purpose, the work followed a model predictive control approach, where the formulation of an optimization problem thoroughly embraces main aspects of the operation of the home-microgrid. The optimization runs within a receding horizon control scheme. Consequently, the work provided some background concepts on model predictive control, followed by a literature review on the application of model predictive control for the operation of microgrids. This work paid particular attention to multienergy home-microgrids. It provided a detailed description of the modeling of a photovoltaic-heat pump home-microgrid, and a photovoltaic-combined heat and power home-microgrid.

For the photovoltaic-heat pump home-microgrid, the work considered a ground source heat pump and the thermal flexibility provided by a single-family house with thermal energy storage. For this home-microgrid, the evaluation included a comparison of three operation strategies that differed on the implemented objective function. Here, a flexible operation using the squared l_2-norm in the objective function resulted in a reduction of peaks of electrical power, while not affecting thermal comfort notably.

For the photovoltaic-combined heat and power home-microgrid, the investigation was on the economic operation. The work compared an MPC-based strategy and an open loop-based strategy, against a perfect-forecast strategy to quantify the effects of uncertainties. Simulation results indicated that for minimal uncertainties, the resultant additional operating costs are substantially different between the open loop-based operation and the MPC-based operation. While the MPC-based strategy achieves operation costs almost equal to the perfect case, the costs for the open loop-based strategy are notably higher. The analysis also included a sensitivity analysis regarding the impact of storage size on additional operation costs. Here, the conclusion was that an MPC-based operation enabled a better usage of the storage systems, and it allowed a reduction in investment costs.

The examination of coordination strategies for interconnected home-microgrids was also a central topic. Here, a decentralized coordination strategy, a centralized coordination strategy, and a hierarchical-distributed coordination strategy were the relevant architectures for investigation. Accordingly, a part of the work dealt with the mathematical formulation of these strategies. Numerical simulation results helped to demonstrate how a centralized coordination strategy can improve the power balancing between home-microgrids.

The results showed that a hierarchical-distributed strategy was able to solve the optimization problem with a moderate exchange of information between home-microgrids and the central control unit. For the hierarchical-distributed strategy, the implementation included a dual decomposition approach and an approach with the alternating direction

method of multipliers. The use of ADMM improved the performance of the hierarchical-distributed strategy, which produced results similar to those obtained with the centralized coordination strategy.

The work showed the mathematical formulation for the optimal operation of a group of interconnected home-microgrids as an ADMM sharing problem. Next, the work examined two approaches to deal with binary variables in the presented ADMM implementation. An ADMM-feasible approach solved a relaxed version of the original subproblems with subsequently recovering of primal feasible solutions. In contrast, an ADMM-unrelax approach solved the original non-convex subproblems without any relaxation. The work also investigated termination conditions for the ADMM algorithm. In the end, by taking advantage of the MPC implementation, it proposed a simple yet effective termination condition that allows terminating the ADMM algorithm after a few iterations.

The conclusion was that the ADMM-unrelax is advantageous for practical purposes because the home-microgrids do not need to relax their optimization problems. Also, it is not necessary to recover feasible solutions once the iterations are ready. Furthermore, the ADMM-unrelax approach with a new proposed termination condition provided results that were competitive to the centralized strategy, using a few iteration counts.

The work ended with the presentation of a framework for the co-simulation of electrical networks with home-microgrids. This framework offered the possibility of simulating such a complex system using dedicated individual simulators instead of having a single simulation environment. Here, numerical simulation results showed the functionality of the framework and enabled the evaluation of the effects of the coordination of home-microgrids on a generic low-voltage grid.

7.1. Limitations and outlook

One limitation of the approach used for the optimal operation of a photovoltaic-heat pump home-microgrid, is that the linear combination of temperature and power, through the coefficients α and β in the objective function, directly depends on the magnitude of the power and temperature values. The optimization may lead to different results if the temperature values are in Fahrenheit instead of degrees Celsius. One possible solution to this issue would be a scaling of data (set-points and measurements) before optimization. This work did not handle this aspect.

Future work can include a more detailed model for the thermal dynamics of the building. To accurately represent the inner room temperature and the thermal capacity of the building, such a model has to take into account each wall and room of the house. The consideration of detailed thermal models of the building would result in a more flexible operation of the heat pump, as larger thermal capacity will be available. Still, the

conclusion of this work regarding the $l2$-norm formulation as the best operation strategy will remain valid since a detailed model of the building will only change some of the constraints. The behavior of the objective function will remain the same.

For the photovoltaic-combined heat and power home-microgrid, future work must include a more detailed model of uncertainties in the evaluation, i.e., more detailed forecast models for household load, PV generation, and thermal demand. Also, a sensitivity analysis regarding larger storage systems (TES larger than 1000 liter and battery systems larger than 12 kWh) may provide new insights for determining maximum feasible capacity for such an home-microgrid.

The evaluation performed for the photovoltaic-combined heat and power home-microgrid also indicates an interesting path for future research. The evaluation showed that simulations with MPC are not just for controller and operation design. They are also useful in the planning stage. Usually, when planning energy systems using numerical optimization, the planner assumes perfect knowledge of the system and its inputs. As these systems operate under uncertain conditions, waiting until the operation stage to decide how to deal with such uncertainties can be inefficient. It will be logical to consider all sources of uncertainties right from the planning stage. In this context, simulations using an MPC strategy may help to consider the impact of uncertainties directly in the planning stage and to sketch possible solutions to handle those uncertainties, either with advanced operation strategies or by adjusting the dimensioning of the equipment.

For the operation of interconnected home-microgrids, there are still some limitations that future work needs to address. First, a simulation for a more extended period, e.g., a complete winter season, has to be conducted for a more significant evaluation and comparison of all strategies. The trade-off among local balancing with peak power reduction, energy bill, and storage losses requires further analysis. The scalability of the hierarchical-distributed strategy must also be tested based on the computation burden and the resulting power profiles. Finally, robustness against uncertainties from model mismatches and forecast errors is another issue for further investigation.

In order to exploit the full functionality of the co-simulation framework, further simulation experiments are necessary. They need to involve more advanced coordination strategies (see ADMM) and more extended simulation periods, e.g., seasonal simulation. Also, future analysis can include further grid state information, such as voltage profiles at critical notes and loading of critical lines, to observe the impact of coordination strategies on these network elements.

The scalability of the ADMM based hierarchical-distributed strategy is also an issue that remains open and requires special attention in future research. Moreover, a warm-start technique would improve the performance of the ADMM algorithm, and such an implementation is still required.

Within the scope of the co-simulation framework, an ADMM approach can be realized as a coordination strategy inside the grid manager simulator. It will allow evaluating the advantages and disadvantages of an ADMM based hierarchical-distributed strategy from a grid point of view.

A more formal and generalized approach for handling non-convexities and binary variables within the ADMM-based hierarchical-distributed coordination strategy is also a research outlook. Here, issues such as speed of convergence, proof of stability, and further performance guarantees need to be analyzed and formalized.

Dealing with uncertainties is a crucial topic that this work did not approach in detail. Since the proposed coordination strategies are considerably sensitive to the prediction of disturbances, the improvement of disturbance forecast plays a central role in the performance of MPC-based operation strategies.

Machine learning techniques, e.g., artificial neural networks or polynomial regression methods, are also paths for future research for improving forecasting of disturbances based on historical data. In this context, the performance of forecasting methods should be evaluated within an MPC scheme and not out of it, i.e., the value of the objective function of MPC's optimization problem should be the performance criterion.

Bibliography

[1] European Commission, Energy Roadmap 2050 - Impact Assessment (2011).
URL https://ec.europa.eu 1.1

[2] European Parliament and the Council of the European Union, Directive 2009/28/ec of the European Parliament and of the Council of 23 april 2009 on the promotion of the use of energy from renewable sources and amending and subsequently repealing Directives 2001/77/ec and 2003/30/ec: Directive 2009/28/ec (April 2009).
URL https://eur-lex.europa.eu/eli/dir/2009/28/oj 1.1

[3] Bundesministerium für Wirtschaft und Technologie, Energiekonzept für eine umwelschonende, zuverläsige und bezahlbare Energieversorgung (September/2010).
URL https://www.bmwi.de/Redaktion/DE/Downloads/E/energiekonzept-2010.pdf?__blob=publicationFile&v=5 1.1

[4] Bundesministerium für Umwelt, Naturschutz und nukleare Sicherheit, Klimaschutzplan 2050 - Klimaschutzpolitische Grundsätze und Ziele der Bundesregierung (November 2016).
URL https://www.bmu.de/fileadmin/Daten_BMU/Download_PDF/Klimaschutz/klimaschutzplan_2050_bf.pdf 1.1

[5] Bundesministerium für Wirtschaft und Energie, Nationaler Aktionsplan für Energieeffizienz (Dezember/2014).
URL https://www.bmwi.de/Redaktion/DE/Publikationen/Energie/nationaler-aktionsplan-energieeffizienz-nape.pdf?__blob=publicationFile&v=6 1.1

[6] Bundesministerium für Wirtschaft und Energie, Renewable Energy Sources Act: Res act2014 (2014).
URL http://www.bmwi.de 1.1

[7] Bundesministerium für Wirtschaft und Energie, Gesetz für die Erhaltung, die Mordenisierung und den Ausbau der Kraft-Wärme-Kopplung: Kwkg 2002 (2002).
URL https://www.clearingstelle-eeg.de 1.1

[8] S. Küppers, DSO 2.0 - Entwicklung des Verteilnetzbetriebs durch die Energiewende.
URL https://docplayer.org/20450127-Dso-2-0-entwicklung-des-verteilnetzbetreibers-durch-die-energiewende.html 1.1, 1.1

[9] VDE Verband der Elektrotechnik Elektronik Informationstechnik e.V., Zellulares Energiesystem - Ein Beitrag zur Konkretisierung des zellularen Ansatzes mit Handlungsempfehlungen.

URL https://www.vde.com/resource/blob/1884494/98f96973fcdba70777654d0f40c179e5/studie---zellulares-energiesystem-data.pdf 1.1, 1.2, 1.3, 1.3.1, 1.3.1, 1.4

[10] E. J. Coster, J. M. A. Myrzik, B. Kruimer, W. L. Kling, Integration issues of distributed generation in distribution grids, Proceedings of the IEEE 99 (1) (2011) 28–39. doi:10.1109/JPROC.2010.2052776. 1.1

[11] C. Töbermann, et al., PV-Integrated - Integration großer anteile photovoltaik in die elektrische energieversorgung - neue verfahren für die planung und den betrieb von verteilnetzen: Schlussbreicht (0325224a-d). Laufzeit: 01.10.2010 - 31.12.2014.
URL https://www.iee.fraunhofer.de/de/projekte/suche/2014/pv-integrated.html 1.2

[12] P. Mancarella, C. K. Gan, G. Strbac, Evaluation of the impact of electric heat pumps and distributed CHP on LV networks, in: IEEE PowerTech, IEEE, Trondheim, Norway, 2011, pp. 1–7. doi:10.1109/PTC.2011.6019297. 1.1

[13] VDE Verband der Elektrotechnik Elektronik Informationstechnik e.V., The cellular approach.
URL https://shop.vde.com/en/vde-study-the-cellular-approach 1.2

[14] F. Moret, P. Pinson, Energy Collectives: A community and fairness based approach to future electricity markets, IEEE Transactions on Power Systems 34 (5) (2019) 3994–4004. doi:10.1109/TPWRS.2018.2808961. 1.2, 1.4.2, 4.1, 5.4.2

[15] T. van der Schoor, B. Scholtens, Power to the people: Local community initiatives and the transition to sustainable energy, Renewable and Sustainable Energy Reviews 43 (2015) 666–675. doi:10.1016/j.rser.2014.10.089.

[16] S. Chen, C.-C. Liu, From demand response to transactive energy: state of the art, Journal of Modern Power Systems and Clean Energy 5 (1) (2017) 10–19. doi:10.1007/s40565-016-0256-x.

[17] B. P. Koirala, E. Koliou, J. Friege, R. A. Hakvoort, P. M. Herder, Energetic communities for community energy: A review of key issues and trends shaping integrated community energy systems, Renewable and Sustainable Energy Reviews 56 (2016) 722–744. doi:10.1016/j.rser.2015.11.080. 1.2

[18] The European Committee of the Regions, Opinion of the European Committee of the Regions on models of local energy ownership and the role of local energy communities in energy transition in Europe (March 2019).
URL https://eur-lex.europa.eu/legal-content/EN/TXT/?qid=1584871876006&uri=CELEX:52018IR2515 1.2

[19] N. Hatziargyriou (Ed.), Microgrids: Architectures and control, online-ausg Edition, John Wiley & Sons, Ltd, Chichester, West Sussex, U. K, 2013. 1.2

[20] S. M. Nosratabadi, R.-A. Hooshmand, E. Gholipour, A comprehensive review on microgrid and virtual power plant concepts employed for distributed energy resources scheduling in power systems, Renewable and Sustainable Energy Reviews 67 (2017) 341–363. doi:10.1016/j.rser.2016.09.025. 1.2

[21] M. Shahidehpour, Z. Li, S. Bahramirad, Z. Li, W. Tian, Networked microgrids: Exploring the possibilities of the IIT-Bronzeville grid, IEEE Power and Energy Magazine 15 (4) (2017) 63–71. doi:10.1109/MPE.2017.2688599. 1.2

[22] E. Vaahedi, K. Nodehi, D. Heim, F. Rahimi, A. Ipakchi, The emerging transactive microgrid controller: Illustrating its concept, functionality, and business case, IEEE Power and Energy Magazine 15 (4) (2017) 80–87. doi:10.1109/MPE.2017.2688619. 1.3.1

[23] Netzintelligenz zum anfassen: Das Smart Operator-Projekt.
URL iam.innogy.com 1.3.1

[24] A. Parisio, E. Rikos, L. Glielmo, A model predictive control approach to microgrid operation optimization, IEEE Transactions on Control Systems Technology 22 (5) (2014) 1813–1827. doi:10.1109/TCST.2013.2295737. 1.3.1, 1.4.2, 1.4.2, 3.2.3

[25] F. Oldewurtel, C. N. Jones, A. Parisio, M. Morari, Stochastic model predictive control for building climate control, IEEE Transactions on Control Systems Technology 22 (3) (2014) 1198–1205. doi:10.1109/TCST.2013.2272178. 1.4.2, 2.2.2

[26] C. Chen, J. Wang, Y. Heo, S. Kishore, MPC-Based Appliance Scheduling for Residential Building Energy Management Controller, IEEE Transactions on Smart Grid 4 (3) (2013) 1401–1410. doi:10.1109/TSG.2013.2265239. 1.4.2

[27] Y. Zong, D. Kullmann, A. Thavlov, O. Gehrke, H. W. Bindner, Application of model predictive control for active load management in a distributed power system with high wind penetration, IEEE Transactions on Smart Grid 3 (2) (2012) 1055–1062. doi:10.1109/TSG.2011.2177282. 1.4, 1.6, 1.4.2, 2.1

[28] M. Houwing, R. R. Negenborn, B. de Schutter, Demand response with micro-CHP systems, Proceedings of the IEEE 99 (1) (2011) 200–213. doi:10.1109/JPROC.2010.2053831. 1.4, 1.4.2, 2.2.3

[29] F. Sossan, H. Bindner, H. Madsen, D. Torregrossa, L. Reyes Chamorro, M. Paolone, A model predictive control strategy for the space heating of a smart building including cogeneration of a fuel cell-electrolyzer system, Electrical Power and Energy Systems 62 (2014) 879–889. doi:10.1016/j.ijepes.2014.05.040. 1.4.2, 3.2.2

[30] P. O. Kriett, M. Salani, Optimal control of a residential microgrid, Energy 42 (1) (2012) 321–330. doi:10.1016/j.energy.2012.03.049. 1.4.2, 3.2.2

[31] Y. Zhang, T. Zhang, R. Wang, Y. Liu, B. Guo, Optimal operation of a smart residential microgrid based on model predictive control by considering uncertainties and storage impacts, Solar Energy 122 (2015) 1052–1065. doi:10.1016/j.solener.2015.10.027. 1.3.1, 1.4.2

[32] G. Valverde, T. van Cutsem, Model predictive control of voltages in active distribution networks, IEEE Transactions on Smart Grid 4 (4) (2013) 2152–2161. doi:10.1109/TSG.2013.2246199. 1.3.1

[33] C. A. Hans, P. Braun, J. Raisch, L. Grüne, C. Reincke-Collon, Hierarchical distributed model predictive control of interconnected microgrids, IEEE Transactions on Sustainable Energy 10 (1) (2019) 407–416. doi:10.1109/TSTE.2018.2802922. 1.4.2, 4.1, 1

[34] G. K. H. Larsen, N. D. van Foreest, J. M. A. Scherpen, Distributed MPC applied to a network of households with micro-CHP and heat storage, IEEE Transactions on Smart Grid 5 (4) (2014) 2106–2114. doi:10.1109/TSG.2014.2318901. 1.4.2, 1

[35] K. Worthmann, C. M. Kellett, P. Braun, L. Grüne, S. R. Weller, Distributed and decentralized control of residential energy systems incorporating battery storage, IEEE Transactions on Smart Grid 6 (4) (2015) 1914–1923. doi:10.1109/TSG.2015.2392081. 1.3.1, 1.4.2, 4.1

[36] S. P. Boyd, L. Vandenberghe, Convex optimization, Cambridge University Press, Cambridge, UK and New York, 2004. 1.4, 1.4.1, 1.4.2, 2.2.4.1, A.2

[37] E. Camacho, C. Bordons, Model predictive control, 2nd Edition, Advanced textbooks in control and signal processing, Springer, London, 2007. 1.4, 1.4, 1.4, 1.4.1

[38] L. Wang, Model Predictive Control System Design and Implementation Using MATLAB®, Advances in Industrial Control, Springer, London and Heidelberg, 2009. doi:10.1007/978-1-84882-331-0.
URL http://d-nb.info/996617213/34 1.4, 1.4

[39] S. Gros, Diehl Moritz, Numerical Optimal Control, draft Edition, April 2019.
URL https://www.syscop.de/numericaloptimalcontrol 1.4, 1.4

[40] R. R. Negenborn, J. M. Maestre, Distributed model predictive control: An overview and roadmap of future research opportunities, IEEE Control Systems Magazine 34 (4) (2014) 87–97. doi:10.1109/MCS.2014.2320397. 1.4, 4.1

[41] T. Faulwasser, L. Grüne, M. A. Müller, Economic nonlinear model predictive control, Foundations and Trends® in Systems and Control 5 (1) (2018) 1–98. doi:10.1561/2600000014. 1.4.1

[42] J. M. Maciejowski, Predictive control with constraints, Prentice Hall, Harlow, 2002. 1.4.1, 1.4.1

[43] S. Engell, I. Harjunkoski, Optimal operation: Scheduling, advanced control and their integration, Computers & Chemical Engineering 47 (2012) 121–133. doi:10.1016/j.compchemeng.2012.06.039. 1.4.1, 2.2

[44] J. Siroky, F. Oldewurtel, J. Cigler, S. Privara, Experimental analysis of model predictive control for an energy efficient building heating system, Applied Energy 88 (9) (2011) 3079–3087. doi:10.1016/j.apenergy.2011.03.009. 1.6

[45] T. Faulwasser, A. Engelmann, Toward economic nmpc for multistage ac optimal power flow, Optimal Control Applications and Methods 41 (1) (2020) 107–127. doi:10.1002/oca.2487. 1.4.2

[46] M. Ali, J. Jokisalo, K. Siren, M. Lehtonen, Combining the demand response of direct electric space heating and partial thermal storage using LP optimization, Electric Power Systems Research 106 (2014) 160–167. doi:10.1016/j.epsr.2013.08.017. 1.4.2

[47] F. Sossan, V. Lakshmanan, G. T. Costanzo, M. Marinelli, P. J. Douglass, H. Bindner, Grey-box modelling of a household refrigeration unit using time series data in application to demand side management, Sustainable Energy, Grids and Networks 5 (2016) 1–12. doi:10.1016/j.segan.2015.10.003. 1.4.2

[48] G. T. Costanzo, S. Iacovella, F. Ruelens, T. Leurs, B. J. Claessens, Experimental analysis of data-driven control for a building heating system, Sustainable Energy, Grids and Networks 6 (2016) 81–90. doi:10.1016/j.segan.2016.02.002. 1.4.2

[49] S. K. Gupta, K. Kar, S. Mishra, J. T. Wen, Collaborative energy and thermal comfort management through distributed consensus algorithms, IEEE Transactions on Automation Science and Engineering 12 (4) (2015) 1285–1296. doi:10.1109/TASE.2015.2468730. 1.4.2

[50] X. Chen, Q. Wang, J. Srebric, Model predictive control for indoor thermal comfort and energy optimization using occupant feedback, Energy and Buildings 102 (2015) 357–369. doi:10.1016/j.enbuild.2015.06.002. 1.4.2

[51] W. Mai, C. Y. Chung, Economic MPC of aggregating commercial buildings for providing flexible power reserve, IEEE Transactions on Power Systems 30 (5) (2015) 2685–2694. doi:10.1109/TPWRS.2014.2365615. 1.4.2

[52] G. K. H. Larsen, N. D. van Foreest, J. M. A. Scherpen, Distributed control of the power supply-demand balance, IEEE Transactions on Smart Grid 4 (2) (2013) 828–836. doi:10.1109/TSG.2013.2242907. 1.4.2

[53] S. Boyd, Xiao Lin, Mutapcic Almir, Mattingley Jacob, Notes on decomposition methods.
URL http://stanford.edu/class/ee364b/lectures.html 1.4.2, A.5

[54] V. Spudić, C. Conte, M. Baotić, M. Morari, Cooperative distributed model predictive control for wind farms, Optimal Control Applications and Methods 36 (3) (2015) 333–352. doi:10.1002/oca.2136. 1.4.2, 4.1

[55] A. Parisio, C. Wiezorek, T. Kyntaja, J. Elo, K. Strunz, K. H. Johansson, Cooperative MPC-based energy management for networked microgrids, IEEE Transactions on Smart Grid 8 (6) (2017) 3066–3074. doi:10.1109/TSG.2017.2726941. 1.4.2

[56] P. Braun, T. Faulwasser, L. Grüne, C. M. Kellett, S. R. Weller, K. Worthmann, Hierarchical distributed ADMM for predictive control with applications in power networks, IFAC Journal of Systems and Control 3 (2018) 10–22. doi:10.1016/j.ifacsc.2018.01.001. 1.4.2

[57] I. Stoyanova, E. Gümrükcü, G. Aragon, D. I. Hidalgo-Rodriguez, A. Monti, J. Myrzik, Distributed model predictive control strategies for coordination of electro–thermal devices in a cooperative energy management concept, Optimal Control Applications and Methods 41 (1) (2020) 170–189. doi:10.1002/oca.2528. 1.4.2, 4.1

[58] D. I. Hidalgo Rodríguez, J. Hinker, J. M. Myrzik, On the problem formulation of model predictive control for demand response of a power-to-heat home microgrid, in: 19th Power Systems Computation Conference (PSCC), IEEE, Genoa, Italy, 2016, pp. 1–8. doi:10.1109/PSCC.2016.7541024. 1, 2, 4.1

[59] D. I. Hidalgo Rodríguez, J. M. Myrzik, Economic model predictive control for optimal operation of home microgrid with photovoltaic-combined heat and power storage system, in: Proceedings of the 20th IFAC World Congress, Toulouse, France, 2017. doi:10.1016/j.ifacol.2017.08.2039. 2, 3, 4.1

[60] T. M. Kneiske, M. Braun, D. I. Hidalgo-Rodriguez, A new combined control algorithm for pv-chp hybrid systems, Applied Energy 210 (2018) 964–973. doi:10.1016/j.apenergy.2017.06.047. 2

[61] D. I. Hidalgo-Rodriguez, J. Myrzik, Optimal operation of interconnected home-microgrids with flexible thermal loads: A comparison of decentralized, centralized, and hierarchical-distributed model predictive control, in: 20th Power Systems Computation Conference (PSCC), IEEE, Dublin, Irland, 2018, pp. 1–7. doi:10.23919/PSCC.2018.8442807. 3, 4

[62] D. Hidalgo-Rodriguez, S. Hoffmann, F. Adelt, J. Myrzik, J. Weyer, A socio-technical simulation framework for collaborative management in power distribution grids, in: International ETG Congress 2017, VDE, Bonn, Germany, 2017. 5, 6

[63] L. Spitalny, J. M. A. Myrzik, T. Mehlborn, Estimation of the economic addressable market of micro-CHP and heat pumps based on the status of the residential building sector in germany, Applied Thermal Engineering 71 (2) (2014) 838–846. doi:10.1016/j.applthermaleng.2013.12.027. 2.2.1

[64] F. Wosnitza, H. G. Hilgers, Energieeffizienz und Energiemanagement: Ein Überblick heutiger Möglichkeiten und Notwendigkeiten, Vieweg+Teubner Verlag, 2012. URL https://books.google.de/books?id=_00eBAAAQBAJ 2.2.1

[65] H. Madsen, J. Holst, Estimation of continuous-time models for the heat dynamics of a building, Energy and Buildings 22 (1) (1995) 67–79. doi:10.1016/0378-7788(94)00904-X. 2.2.2, B.1

[66] Y. Zong, L. Mihet-Popa, D. Kullmann, A. Thavlov, O. Gehrke, H. W. Bindner, Model predictive controller for active demand side management with PV self-consumption in an intelligent building, in: 3rd IEEE PES International Conference and Exhibition on Innovative Smart Grid Technologies (ISGT Europe), IEEE, Berlin, Germany, 2012, pp. 1–8. doi:10.1109/ISGTEurope.2012.6465618. 2.2.2

[67] F. Shahnia, M. T. Wishart, A. Ghosh, G. Ledwich, F. Zare, Smart demand side management of low-voltage distribution networks using multi-objective decision making, IET Generation, Transmission & Distribution 6 (10) (2012) 986–1000.

[68] R. Missaoui, G. Warkozek, S. Bacha, S. Ploix, Real time validation of an optimization building energy management strategy based on Power-Hardware-in-the-Loop tool, in: 3rd IEEE PES International Conference and Exhibition on Innovative Smart Grid Technologies (ISGT Europe), IEEE, Berlin, Germany, 2012, pp. 1–7. doi:10.1109/ISGTEurope.2012.6465791. 2.2.2

[69] T. Kashima, S. P. Boyd, Cost optimal operation of thermal energy storage system with real-time prices, in: X.-M. Nguyen (Ed.), 2013 International Conference on Control, Automation and Information Sciences (ICCAIS 2013), IEEE, Nha Trang, Vietnam, 2013, pp. 233–237. doi:10.1109/ICCAIS.2013.6720560. 2.2.3

[70] ISO, ISO 7730: Ergonomics of the thermal environment — Analytical determination and interpretation of thermal comfort using calculation of the PMV and PPD indices and local thermal comfort criteria (2005).
URL https://www.iso.org 2.2.5

[71] C. Nabe, B. Hasche, M. Offermann, et al., Potenziale der Wärmepumpe zum Lastmanagement im Strom und zur Netzintegration erneuerbarer Energien.
URL https://www.bmwi.de/Redaktion/DE/Publikationen/Studien/potenziale-der-waermepumpe.html 2.2.6, B.2, B.2, B.2

[72] VDI, VDI 4655 - reference load profiles of single-family and multi-family houses for the use of CHP system (01.05.2008).
URL https://www.vdi.de/richtlinien 2.2.6, 3.2.9

[73] D. Walberg, Wohnungsbau in Deutschland 2011 - Modernisierung oder Bestandsersatz, Mauerwerk 15 (5) (2011) 294–300. doi:10.1002/dama.201100508. 2.2.6

[74] W. E. Hart, C. Laird, J.-P. Watson, D. L. Woodruff, Pyomo – Optimization Modeling in Python, Vol. 67, Springer US, Boston, MA, 2012. doi:10.1007/978-1-4614-3226-5. 2.2.6, 3.2.9, 4.6

[75] W. E. Hart, J.-P. Watson, D. L. Woodruff, Pyomo: Modeling and solving mathematical programs in python, Mathematical Programming Computation 3 (3) (2011) 219–260. doi:10.1007/s12532-011-0026-8. 2.2.6, 3.2.9, 4.6

[76] IBM, IBM ILOG CPLEX optimization studio.
URL http://www-03.ibm.com/software/products/en/ibmilogcpleoptistud 2.2.6, 3.2.9, 4.6

[77] B. Thomas, Mini-Blockheizkraftwerke: Grundlagen, Gerätetechnik, Betriebsdaten, 2nd Edition, Vogel, Würzburg, 2011. 3.2.2, 3.3

[78] D. I. Hidalgo Rodriguez, L. Spitalny, J. Myrzik, M. Braun, Development of a control strategy for mini CHP plants for an active voltage management in low voltage networks, in: 3rd IEEE PES International Conference and Exhibition on Innovative Smart Grid Technologies (ISGT Europe), IEEE, Berlin, Germany, 2012, pp. 1–8. doi:10.1109/ISGTEurope.2012.6465797. 3.2.2

[79] J. M. Maestre, R. R. Negenborn (Eds.), Distributed Model Predictive Control Made Easy, Vol. 69 of Intelligent Systems, Control and Automation, Springer Netherlands, Dordrecht and s.l., 2014. doi:10.1007/978-94-007-7006-5.
URL http://search.ebscohost.com/login.aspx?direct=true&scope=site&db=nlebk&db=nlabk&AN=662900 4.1

[80] B. Yang, M. Johansson, Distributed optimization and games: A tutorial overview, in: A. Bemporad, M. Heemels, M. Johansson (Eds.), Networked Control Systems, Vol. 406 of Lecture Notes in Control and Information Sciences, Springer-Verlag London, London, 2011, pp. 109–148. doi:10.1007/978-0-85729-033-5{\textunderscore }4. 4.5, 4.5.1, A.5

[81] S. Boyd, N. Parikh, E. Chu, B. Peleato, J. Eckstein, Distributed optimization and statistical learning via the alternating direction method of multipliers, Foundations and Trends® in Machine Learning 3 (1) (2010) 1–122. doi:10.1561/2200000016. 5.1, 5.2, 5.2, 5.3.1, 5.3.2, 5.4.2, 5.4.3, A.5, A.5.2.2, E

[82] R. Takapoui, N. Moehle, S. Boyd, A. Bemporad, A simple effective heuristic for embedded mixed-integer quadratic programming, International Journal of Control 66 (3) (2017) 1–11. doi:10.1080/00207179.2017.1316016. 2

[83] KoRiSim - Kooperatives Informations- und Risikomanagement in zukunftsfähigen Netzen - eine Simulationsstudie. Grant number: BMBF 03ek3547.
URL https://forschung-stromnetze.info/projekte/kooperatives-informations-und-risikomanagement/ 6

[84] mosaik — A flexible Smart Grid co-simulation framework (13.06.2019).
URL https://mosaik.offis.de/ 6.2

[85] C. Steinbrink, A. A. van der Meer, M. Cvetkovic, D. Babazadeh, S. Rohjans, P. Palensky, S. Lehnhoff, Smart grid co-simulation with MOSAIK and HLA: a comparison study, Computer Science - Research and Development 33 (1-2) (2018) 135–143. doi:10.1007/s00450-017-0379-y. 6.2

[86] E. Handschin, Elektrische Energieübertragungssysteme, 2nd Edition, Dr. Alfred Hüthig Verlag Heidelberg, Heidelberg, 1987.
URL https://books.google.de/books?id=OFa5XwAACAAJ 6.2.1

[87] Pypower: Power flow and optimal power flow (opf) solver (28.06.2018).
URL https://pypi.org/project/PYPOWER/ 6.2.1

[88] F. Adelt, S. Hoffmann, D. I. Hidalgo Rodríguez, J. Myrzik, J. Weyer, Kooperatives Informations- und Risikomanagement in zukunftsfähigen Netzen - eine Simulationsstudie (KoRiSim) : KoRiSim: Schlussbericht zu nr. 3.2 (BNBest-BMBF 1998). Laufzeit des Vorhabens: 01.05.2015-31.12.2018. doi:10.2314/KXP:1681046261. 6.2.3

[89] J. Scheffler, Bestimmung der maximal zulässigen Netzanschlussleistung photovoltaischer Energiewandlungsanlagen in Wohnsiedlungsgebieten, Ph.D. thesis, TU Chemnitz, Chemnitz (18 Juni/2002). 6.3, 6.4

[90] L. Spitalny, Analyse der Systemeffizienz beim netzgeführten Betrieb von Wärmeerzeugern im Wohngebäudesektor, Dissertation, TU Dortmund (2016). 6.3, 6.4

Appendices

A. Mathematical optimization background

This appendix gives background concepts on mathematical optimization and provides theoretical support to the main ideas presented in the chapters of this dissertation. By giving foundations and derivations of the methods and approaches used in this research, this appendix aims at facilitating the reader the understanding of the proposed optimization problems. This appendix, however, does not pretend to cover all topics at detailed level as in a textbook. To have a broader insight into this topics the reader should take a look at the referenced literature. The author also recommends to check online courses on mathematical optimization.

The appendix starts defining the structure and elements of an optimization problem together with some basic definitions for mathematical optimization. Next, it handles the basic ideas behind decomposing and pays special attention to the dual decomposition and the ADMM approach, as they are the approaches used in this dissertation.

A.1. Convexity

This works uses convex optimization as approach to formulate and solve the stated optimization problems, as it allows to make use of existing efficient and reliable algorithms to solve them. Before handling the topics regarding optimization problems, definitions for convexity needs to be stated. First of all, a set is convex if the line segment, between two points in the set, is also contained in the set. Formally, a convex set $\mathcal{C}$ can be defined as:

$$\alpha x + (1-\alpha)\, y \in \mathcal{C}, \forall x, y \in \mathcal{C}, \forall \alpha \in [0,1]\,. \tag{A.1}$$

In other words, there should be always a clear line path, without leaving the set, between any two points x and y in the set $\mathcal{C}$. Furthermore, the epigraph of a function f is the set of points lying on or above the function's graph. Then, a function f is convex if its epigraph is a convex set. Formally, a function f is convex if, for a given parameter $\theta \in [0,1]$, the following is true:

$$\theta f\,(x) + (1-\theta)\, f\,(y) \geq f\,(\theta x + (1-\theta)\, y)\,, \tag{A.2}$$

meaning that the value of f at the given linear combination between the two points x and y, lies always on or below the line segment between $f(x)$ and $f(y)$.

A.2. Optimization problems

Following the notation from Boyd. et al. in [36], the standard formulation of an optimization problem is as follows:

$$\underset{x}{\text{minimize}} \quad f_o(x) \tag{A.3a}$$

$$\text{subject to}$$

$$f_i(x) \leq 0, \quad i = 1, \ldots, m, \tag{A.3b}$$

$$h_i(x) = 0, \quad i = 1, \ldots, p, \tag{A.3c}$$

where f_o is the objective function, $x \in \mathbb{R}^n$ is a vector of decision variables, f_i are functions for the corresponding inequality constraints in (A.3b), and h_i are functions for the equality constraints in (A.3c). Problem (A.3) is convex if the following requirements are met:

1. the objective function f_o is convex,
2. the inequality constraint functions f_i are convex, and
3. the equality constraint functions h_i are affine.

An optimization problem is a linear programming (LP) problem, if objective function, inequality constraints and equality constraints are linear expressions. If the decision variables are not continuous but integers, i.e., $x \in \mathbb{Z}$, then the problem is not convex anymore. In this case, the problem becomes a mixed-integer linear programming (MILP) problem . Furthermore, some formulations used in this dissertation also involve a quadratic expression in the objective function and therefore such problems are called mixed-integer quadratic programming (MIQP) problems.

The simplex method and interior point methods (also called barrier methods) are the most common methods used in commercial solvers to solve LP problems. If integer variables are present, then the solver also makes use of linear relaxation and heuristic methods (e.g., branch and bound or branch and cut) to find the optimal solution. For MIQP, interior point and heuristic methods are normally used.

A.3. Duality

Another important concept used in this research is the concept of duality, also called Lagrangian duality. The main idea behind duality, is to formulate and solve a dual problem associated to the primal problem given by (A.3). If certain conditions, which we will describe later, are met when obtaining the solution for both primal and dual problem, then the obtained solution is the global optimum.

The first step to formulate a dual problem is to form the Lagrangian, which implies taking the equality constraints (A.3c) and the inequality constraints (A.3b) to the objective function, weighted with a parameter (Lagrange multiplier). Then, the definition of the Lagrangian associated with the problem (A.3) is:

$$L(x, \lambda, \nu) = f_o(x) + \sum_{i=1}^{m} \lambda_i f_i(x) + \sum_{i=1}^{p} \nu_i h_i(x), \tag{A.4}$$

where λ_i is called the Lagrange multiplier associated to the ith inequality constraint, and respectively, ν_i is called the Lagrange multiplier associated to the ith equality constraint.

The second step to formulate the dual problem is to define the dual function. The dual function g is the infimum of the Lagrangian over x and it is defined as:

$$g(\lambda, \nu) = \inf_x L(x, \lambda, \nu) = \inf_x \left(f_o(x) + \sum_{i=1}^{m} \lambda_i f_i(x) + \sum_{i=1}^{p} \nu_i h_i(x) \right). \tag{A.5}$$

Note that it is a function of λ and ν, not a function of x. It can provide a lower bound on the optimal value f_o^* of the problem (A.3), for each pair (λ, ν). If there are no constraints on the value of λ and ν, it is often the case that the value of the infimum of the Lagrangian is $-\infty$. Thus, in order to find a useful lower bound on the primal objective value, we need to constraint these variables.

The dual problem helps to find the best lower bound on the optimal value of the primal problem, obtained from the dual function, as it explicitly contains the above mentioned constraints on λ and ν. The formulation of the dual problem is given by:

$$\underset{\lambda,\nu}{\text{maximize}} \quad g(\lambda, \nu) \tag{A.6a}$$

$$\text{subject to}$$

$$\lambda \succeq 0, \tag{A.6b}$$

which is a convex optimization problem and we say that the pair (λ, ν) is dual feasible if $\lambda \succeq 0$ and $g(\lambda, \nu) \geq -\infty$. The vectors λ and ν are also referred as the dual variables of the problem (A.3). Furthermore, the term dual optimal refers to the pair (λ^*, ν^*), i.e., the optimal solution of the dual problem (A.6).

A.4. Optimality conditions

The primal problem (A.3) and the dual problem (A.6) provide some important properties and concepts that allow us to define certain conditions in order to establish optimality. The following four conditions are called Karush-Kuhn-Tucker (KKT) conditions, with the triple $\tilde{x}, \tilde{\lambda}, \tilde{\nu}$ representing a solution for the primal and dual problems, respectively.

1. primal feasibility: $f_i(\tilde{x}) \leq 0, i = 1, \ldots, m,\ h_i(\tilde{x}) = 0, i = 1, \ldots, p$
2. dual feasibility: $\tilde{\lambda} \succeq 0$
3. complementary slackness: $\tilde{\lambda}_i f_i(\tilde{x}) = 0, i = 1, \ldots, m$, which implies that either $\tilde{\lambda}_i = 0$ or $f_i(\tilde{x}) = 0$. Since $h_i(\tilde{x})$ is also zero (see primal feasibility), then according to (A.4), $f_o(\tilde{x}) = L\left(\tilde{x}, \tilde{\lambda}, \tilde{\nu}\right)$
4. gradient of Lagrangian with respect to x vanishes: $\nabla_x L = 0$, and therefore the value of the infimum of the Lagrangian over x is equal to the objective value of the dual problem, i.e., $g\left(\tilde{\lambda}, \tilde{\nu}\right) = L\left(\tilde{x}, \tilde{\lambda}, \tilde{\nu}\right)$

thus, $f_o(\tilde{x}) = g\left(\tilde{\lambda}, \tilde{\nu}\right)$. Consequently, if $\tilde{x}, \tilde{\lambda}, \tilde{\nu}$ satisfy these four KKT conditions for a convex problem, then they are global optimal.

A.5. Decomposition of optimization problems

There are several approaches for decomposition of optimization problems. Here, we focus just on the methods used in this dissertation namely, dual decomposition and ADMM. For a broader and detailed introduction to decomposition methods the author recommends to check the material from Boyd et al. in [53] and [81] and also the tutorial on distributed optimization by Yang and Johansson in [80].

A.5.1. Dual decomposition

In this research, we handle the case of the decomposition with constraints, which can be elaborated considering the following optimization problem:

$$\underset{x_1, x_2}{\text{minimize}} \quad f_1(x_1) + f_2(x_2) \tag{A.7a}$$

$$\text{subject to}$$

$$x_1 \in \mathcal{C}_1, \quad x_2 \in \mathcal{C}_2, \tag{A.7b}$$

$$h_1(x_1) + h_2(x_2) \preceq 0, \tag{A.7c}$$

where f_i, h_i, and $\mathcal{C}$ are convex. (A.7c) is a set of coupling constraints, which involve both x_1 and x_2. These coupling constraints can be seen as a capacity restriction on resources shared between two subproblems.

To solve problem (A.7) in a distributed, or hierarchical-distributed way, the first step is to form its separable partial Lagrangian given by:

$$\begin{aligned} L(x_1, x_2, \lambda) &= f_1(x) + f_2(x_2) + \lambda^T (h_1(x_1) + h_2(x_2)), \\ &= \Big(f_1(x_1) + \lambda^T h_1(x_1)\Big) + \Big(f_2(x_2) + \lambda^T h_2(x_2)\Big), \end{aligned} \tag{A.8}$$

and now the problem is separable. We can the define subproblem 1 as:

$$\underset{x_1}{\text{minimize}} \quad f_1(x_1) + \lambda^T h_1(x_1) \tag{A.9a}$$

$$\text{subject to}$$

$$x_1 \in \mathcal{C}_1, \tag{A.9b}$$

and subproblem 2 as:

$$\underset{x_2}{\text{minimize}} \quad f_2(x_2) + \lambda^T h_1(x_2) \tag{A.10a}$$

$$\text{subject to}$$

$$x_2 \in \mathcal{C}_2, \tag{A.10b}$$

with optimal solutions $\tilde{x_1}$ and $\tilde{x_2}$ respectively.

To conclude, the dual decomposition algorithm includes the following steps:

1. Solve subproblem 1 (A.9) and subproblem 2 (A.10) in parallel, finding an optimal $\tilde{x_1}$ and $\tilde{x_2}$.
2. Update dual variables using the projected subgradient with:

$$\lambda := (\lambda + \alpha_k (h_1(\tilde{x}_1) + h_2(\tilde{x}_2))). \tag{A.11}$$

Where α_k is the step size for the subgradient update. $\tilde{x_1}$ and $\tilde{x_2}$ are not necessarily feasible for (A.7) at each iteration, but feasible primal variables can be constructed using projection.

A practical interpretation of dual decomposition for this case is to see the vector λ as prices of resources. Taking into account the revenue or cost from/of resources, the subproblems are solved independently from each other and a master algorithm adjusts the prices at each iteration until the prices converge. Prices on over-demanded resources are increased and prices on under-demanded resources are reduced.

A.5.2. Alternating Direction Method of Multipliers (ADMM)

ADMM is a method which supports decomposition of optimization problems. Consider the optimization problem:

$$\underset{x,z}{\text{minimize}} \quad f(x) + g(z) \tag{A.12a}$$

$$\text{subject to}$$

$$Ax + Bz = c, \tag{A.12b}$$

with f and g convex, two set of decision variables x and z, and a coupling constraint (A.12b). Similar as in dual decomposition, in ADMM we want to form the Lagrangian associated to the problem (A.12) but this time we add an extra quadratic term involving the coupling constraint as follows:

$$L_\rho(x, z, y) = f(x) + g(z) + y^T(Ax + Bz - c) + (\rho/2)\|Ax + Bz - c\|_2^2. \tag{A.13}$$

We denote this expression as augmented Lagrangian, where y is the Lagrange multiplier associated with the coupling constraint and ρ is a weighting parameter for the quadratic expression. As the augmented Lagrangian is not separable with respect to x and y due to this extra quadratic expression, it cannot be minimized over x and z at the same time. Instead, ADMM is an iterative method that uses an alternating optimization minimizing over x with z fixed, and vice versa. The ADMM algorithm includes then three steps within each iteration: x-minimization, z-minimization, and dual update. They are given by:

$$x^{k+1} := \underset{x}{\text{argmin}} L_\rho\left(x, z^k, y^k\right), \tag{A.14}$$

$$z^{k+1} := \underset{z}{\text{argmin}} L_\rho\left(x^{k+1}, z, y^k\right), \tag{A.15}$$

and

$$y^{k+1} := y^k + \rho\left(Ax^{k+1} + Bz^{k+1} - c\right) \tag{A.16}$$

respectively. The superindex k denotes the iteration number.

A.5.2.1. ADMM with scaled dual variables

ADMM can be also expressed in a scaled form which allows a more compact and shorter formulation. In the scaled form, we define the vector $r = Ax + Bz - c$, the scaled dual variable $u_i = (1/\rho)\, y_i$, and combine the linear and quadratic terms in the augmented

Lagrangian (A.13) as follows:

$$\begin{aligned} y^T r + \rho/2 \left\| r \right\|_2^2 =& \sum_i y_i r_i + \rho/2 \sum_i r_i^2 + \sum_i \frac{1}{2\rho} y_i^2 - \sum_i \frac{1}{2\rho} y_i^2 \\ =& \rho/2 \sum_i \left(r_i^2 + \frac{2}{\rho} y_i r_i + \frac{1}{\rho^2} y_i^2 \right) - \sum_i \frac{1}{2\rho} y_i^2 \\ =& \rho/2 \sum_i \left(r_i + y_i \frac{1}{\rho} \right)^2 - \rho/2 \sum_i \left(\frac{y_i}{\rho} \right)^2 \\ =& \rho/2 \sum_i \left(r_i + u_i \right)^2 - \rho/2 \sum_i u_i^2 \\ =& \left(\rho/2 \right) \left\| r + u \right\|_2^2 - \left(\rho/2 \right) \left\| u \right\|_2^2, \end{aligned} \tag{A.17}$$

and now the augmented scaled Lagrangian can be expressed as:

$$\begin{aligned} L_p \left(x, z, u \right) =& f \left(x \right) + g \left(z \right) + \left(\rho/2 \right) \left\| r + u \right\|_2^2 - \left(\rho/2 \right) \left\| u \right\|_2^2 \\ =& f \left(x \right) + g \left(z \right) + \left(\rho/2 \right) \left\| Ax + Bz - c + u \right\|_2^2 + \text{const.} \end{aligned} \tag{A.18}$$

As we want to minimize over x and z the last term in (A.18) can be denoted as a constant. Consequently, ADMM in scaled dual form is:

$$x^{k+1} := \underset{x}{\text{argmin}} \left(f \left(x \right) + \left(\rho/2 \right) \left\| Ax + Bz^k - c + u^k \right\|_2^2 \right), \tag{A.19}$$

$$z^{k+1} := \underset{z}{\text{argmin}} \left(g \left(z \right) + \left(\rho/2 \right) \left\| Ax^{k+1} + Bz - c + u^k \right\|_2^2 \right), \tag{A.20}$$

$$u^{k+1} := u^k + Ax^{k+1} + Bz^{k+1} - c. \tag{A.21}$$

A.5.2.2. Sharing problem in ADMM form

In this dissertation we used the sharing problem as a suitable formulation for a hierarchical-distributed coordination strategy. The sharing problem involves N subsystems with local cost functions and a shared global objective function. The sharing problem as optimization problem can be expressed as:

$$\underset{x}{\text{minimize}} \sum_{i=1}^{N} f_i \left(x_i \right) + g \left(\sum_{i=1}^{N} x_i \right), \tag{A.22}$$

with f_i as a local cost function for each subsystem i, and g as the shared objective. The argument of the shared objective is the sum of the local variables from all subsystems. By copying the local variable x_i into a new variable z_i, the sharing problem can expressed

in ADMM form as:

$$\underset{x,z}{\text{minimize}} \quad \sum_{i=1}^{N} f_i(x_i) + g\left(\sum_{i=1}^{N} z_i\right) \tag{A.23a}$$

subject to

$$x_i - z_i = 0, \quad i = 1, \ldots, N, \tag{A.23b}$$

$$\tag{A.23c}$$

with x_i and $z_i \in \mathbb{R}^n$. Note that there are now N coupling constraints. Accordingly, the scaled ADMM algorithm for problem (A.23) is

$$x_i^{k+1} := \underset{x_i}{\operatorname{argmin}} \left(f_i(x_i) + (\rho/2)\|x_i - z_i^k + u_i^k\|_2^2\right), \tag{A.24}$$

$$z^{k+1} := \underset{z}{\operatorname{argmin}} \left(g\left(\sum_{i=1}^{N} z_i\right) + (\rho/2)\sum_{i=1}^{N}\|z_i - u_i^k - x_i^{k+1}\|_2^2\right), \tag{A.25}$$

$$u_i^{k+1} := u_i^k + x_i^{k+1} - z_i^{k+1}. \tag{A.26}$$

As each z_i has n elements, the z-update in (A.25) implies an optimization over Nn variables. Boyd. et al. in [81] showed that the z-update for the ADMM sharing problem can be reduced to a minimization over n variables. We will elaborate this reduction for the sake of completeness. A possible reformulation for the z-update is:

$$\underset{z_i}{\text{minimize}} \quad g(N\bar{z}) + (\rho/2)\sum_{i=1}^{N}\|z_i - a_i\|_2^2 \tag{A.27a}$$

subject to

$$\bar{z} = (1/N)\sum_{i=1}^{N} z_i, \tag{A.27b}$$

with $\bar{z} \in \mathbb{R}^n$ and $a_i = u_i^k + x_i^{k+1}$. To solve this constrained minimization problem, we first form the Lagrangian associated to (A.27):

$$L(z_i, \bar{z}, a_i, \lambda) = g(N\bar{z}) + \frac{\rho}{2}\sum_{i=1}^{N}\|z_i - a_i\|_2^2 + \lambda^T\left(\bar{z} - \frac{1}{N}\sum_{i=1}^{N} z_i\right), \tag{A.28}$$

and with fixed $\bar{z}$, we find the gradient of the Lagrangian with respect to z_i

$$\nabla_{z_i} L = \rho(z_i - a_i) - \frac{\lambda^T}{N} \tag{A.29}$$

and we set $\nabla_{z_i} L := 0$ to find the optimal solution, which gives

$$z_i := \frac{\lambda^T}{N\rho} + a_i. \tag{A.30}$$

By replacing (A.30) in (A.27b) we have:

$$\begin{aligned}\bar{z} =& \frac{1}{N}\sum_{i=1}^{N}\left(\frac{\lambda^T}{N\rho}+a_i\right)\\ =& \frac{1}{N}\left(\frac{N\lambda^T}{N\rho}+\sum_{i=1}^{N}a_i\right)\\ =& \frac{\lambda^T}{N\rho}+\bar{a},\end{aligned} \tag{A.31}$$

and by solving for $\frac{\lambda^T}{N\rho}$ and replacing again in (A.30) we obtain the optimal solution to problem (A.27) as

$$z_i = \bar{z} - \bar{a} + a_i. \tag{A.32}$$

The z-update becomes now an unconstrained optimization problem over $\bar{z}$

$$\underset{\bar{z}}{\text{minimize}} \quad g\left(N\bar{z}\right) + (\rho/2)\sum_{i=1}^{N}\|\bar{z} - \bar{a}\|. \tag{A.33}$$

By replacing (A.27) in (A.26) the u-update becomes

$$\begin{aligned}u_i^{k+1} &= u_i^k + x_i^{k+1} - a_i^k - \bar{z}^{k+1} + \bar{a}^k\\ &= u_i^k + x_i^{k+1} - u_i^k - x_i^{k+1} - \bar{z}^{k+1} + \bar{u}^k + \bar{x}^{k+1}\\ &= \bar{u}^k + \bar{x}^{k+1} - \bar{z}^{k+1},\end{aligned} \tag{A.34}$$

showing that the u-update does not depend on the individual dual variables u_i from each subsystem i and therefore a global single dual variable u can be used for all subsystems. By substituting z_i, a_i and $\bar{a}$ in the x-update and the z-update respectively, the reduced ADMM algorithm for the sharing problem becomes:

$$x_i^{k+1} := \underset{x_i}{\text{argmin}}\left(f_i\left(x_i\right) + (\rho/2)\left\|x_i - x_i^k + \bar{x}^k - \bar{z}^k + u^k\right\|_2^2\right), \tag{A.35}$$

$$\bar{z}^{k+1} := \underset{\bar{z}}{\text{argmin}}\left(g\left(N\bar{z}\right) + (N\rho/2)\left\|\bar{z} - u^k - \bar{x}^{k+1}\right\|_2^2\right), \tag{A.36}$$

$$u^{k+1} := u^k + \bar{x}^{k+1} - \bar{z}^{k+1}. \tag{A.37}$$

B. Two rooms building model for application in MPC schemes

This appendix presents a two rooms building model for application in MPC schemes, which extends the model presented in Chapter 2. The model is accurate enough to consider each wall and roof within each of the rooms of the building. The thermal model is subjected to real measurements of the solar radiation and ambient temperature. The simulation results indicate the total energy consumed for the required level of comfort. The modeling and simulation work were conducted by Diego Hidalgo and Mohamad Jaber.

B.1. Introduction

The heat dynamics of a two rooms house is represented by the model proposed in [65] which has already been used for demand side management with heating systems. The storage capacity of the house is dominated by the air in the room and composition of materials of the walls and roofs.

Initially, the proposed model [65] was extended such that instead of merely estimating the temperature of the room air and the temperature of the large heat-accumulating medium, it became two rooms building and is now able to estimate each of the wall, roof and room temperatures with respect to their room air and large heat-accumulating medium. Then this model was validated where its stability and speed were checked. Lastly, it was applied to a model predictive control (MPC) scheme were it was subjected to a quadratic optimization problem to control its thermal behavior throughout the year and the total energy consumed was calculated for this building. The controlled part was the space heating system which was built in each room. And the disturbances were the solar radiation and the ambient temperature to ensure realistic values for the model.

B.2. Model description

As illustrated in Figure B.1, there are eleven states in this building which are the wall, roof and room temperatures. All the external walls have windows except the inner wall which does not have. The dotted lines represent the roof of each room. The building is subjected to solar radiation and ambient temperature. Moreover, a space heating power is applied for each room, which distributes heat equally inside the rooms.

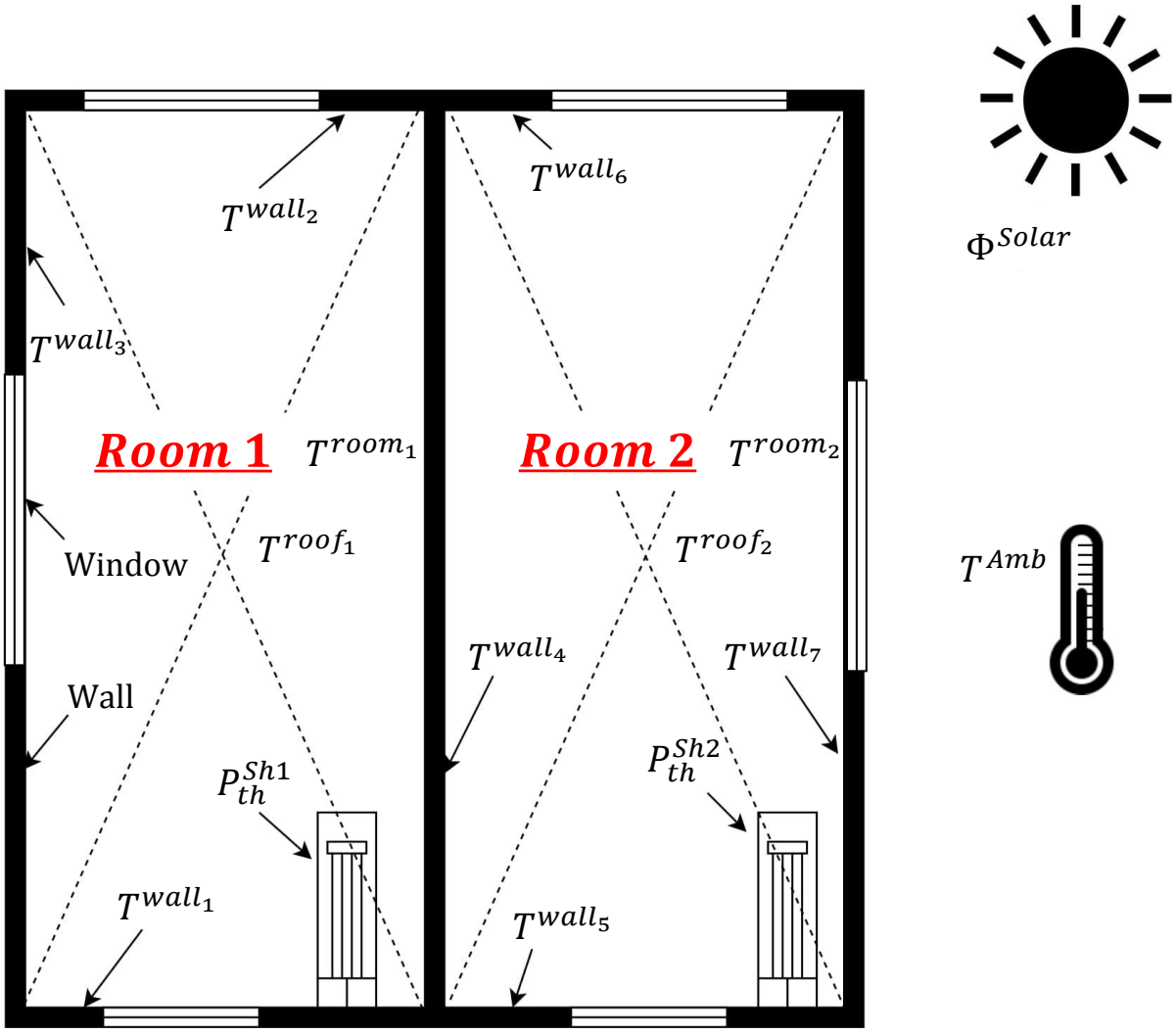

Figure B.1.: Two rooms building (with all the states, inputs and disturbances)

Such model of linear dynamic system can be described in discrete state space form. The structures of the involved matrices and vectors can be shown in (B.1). The states of the system are the temperatures of the each wall, roof and room and is denoted by $\boldsymbol{T_k}$. Model inputs $\boldsymbol{u_k}$ are the space heating power in each room. Disturbances $\boldsymbol{d_k}$ are the outside ambient temperature and solar radiation.

$$\boldsymbol{T_{k+1}} = \boldsymbol{A} \cdot \boldsymbol{T_k} + \boldsymbol{B} \cdot \boldsymbol{u_k} + \boldsymbol{E} \cdot \boldsymbol{d_k}, \tag{B.1}$$

where

$$\boldsymbol{T_k} = \begin{bmatrix} T_k^{wall_1} \\ T_k^{wall_2} \\ T_k^{wall_3} \\ T_k^{roof_1} \\ T_k^{wall_4} \\ T_k^{roof_2} \\ T_k^{wall_5} \\ T_k^{wall_6} \\ T_k^{wall_7} \\ T_k^{room_1} \\ T_k^{room_2} \end{bmatrix}, \tag{B.2}$$

$$\boldsymbol{u_k} = \begin{bmatrix} P_{th,k}^{Sh1} \\ P_{th,k}^{Sh2} \end{bmatrix}, \tag{B.3}$$

and

$$\boldsymbol{d_k} = \begin{bmatrix} T_k^{Amb} \\ \Phi_k^{Solar} \end{bmatrix}. \tag{B.4}$$

The system matrix $\boldsymbol{A} \in \mathbb{R}^{\mathbf{11\times 11}}$ shown in (B.6) is mainly composed of the inverse product of thermal capacitances and thermal resistances illustrated in (B.5). The window is considered part of the wall while applying the calculations. Each of (B.5) is placed such that it is multiplied with its respective wall/roof and room states.

$$\frac{1}{R_n C_n}, \tag{B.5}$$

$$\boldsymbol{A} = [\boldsymbol{M} \quad \boldsymbol{N}], \tag{B.6}$$

where matrices $\boldsymbol{M} \in \mathbb{R}^{\mathbf{11\times 6}}$ and $\boldsymbol{N} \in \mathbb{R}^{\mathbf{11\times 5}}$ are

$$\boldsymbol{M} = \begin{bmatrix} \frac{-1}{R_1C_1} & 0 & 0 & 0 & 0 & 0 \\ 0 & \frac{-1}{R_2C_2} & 0 & 0 & 0 & 0 \\ 0 & 0 & \frac{-1}{R_3C_3} & 0 & 0 & 0 \\ 0 & 0 & 0 & \frac{-1}{R_4C_4} & 0 & 0 \\ 0 & 0 & 0 & 0 & \frac{-1}{R_5C_5} & 0 \\ 0 & 0 & 0 & 0 & 0 & \frac{-1}{R_6C_6} \\ 0 & 0 & 0 & 0 & 0 & 0 \\ 0 & 0 & 0 & 0 & 0 & 0 \\ 0 & 0 & 0 & 0 & 0 & 0 \\ \frac{1}{R_1C_a} & \frac{1}{R_2C_a} & \frac{1}{R_3C_a} & \frac{1}{R_4C_a} & \frac{1}{R_5C_a} & 0 \\ 0 & 0 & 0 & 0 & \frac{1}{R_5C_a} & \frac{1}{R_6C_a} \end{bmatrix}, \tag{B.7}$$

$$\boldsymbol{N} = \begin{bmatrix} 0 & 0 & 0 & \frac{1}{R_1C_1} & 0 \\ 0 & 0 & 0 & \frac{1}{R_2C_2} & 0 \\ 0 & 0 & 0 & \frac{1}{R_3C_3} & 0 \\ 0 & 0 & 0 & \frac{1}{R_4C_4} & 0 \\ 0 & 0 & 0 & \frac{0.5}{R_5C_5} & \frac{0.5}{R_5C_5} \\ 0 & 0 & 0 & 0 & \frac{1}{R_6C_6} \\ \frac{-1}{R_7C_7} & 0 & 0 & 0 & \frac{1}{R_7C_7} \\ 0 & \frac{-1}{R_8C_8} & 0 & 0 & \frac{1}{R_8C_8} \\ 0 & 0 & \frac{-1}{R_9C_9} & 0 & \frac{1}{R_9C_9} \\ 0 & 0 & 0 & -x_1 - y_1 & 0 \\ \frac{1}{R_7C_a} & \frac{1}{R_8C_a} & \frac{1}{R_9C_a} & 0 & -x_2 - y_2 \end{bmatrix}. \tag{B.8}$$

The constant x_1, x_2, y_1, and y_2 are represented in (B.9) and (B.10). x_1 and x_2 shows that each room considers the summation of the inverse product of the thermal resistances of

each wall/roof R_n that is affecting that room and the thermal capacitance of the room air C_a. y_1 and y_2 shows the summation of thermal resistances of inside surfaces of each wall/roof R'_n that has affect on that room and the thermal capacitance of the room air C_a.
Each room takes into account the walls and roof which are straightly affecting it. So x_1 and y_1 are added which affect T^{room_1}. x_2 and y_2 are also added which affect T^{room_2}. In this case, those two states will be similar since the two rooms are identical.

$$x_1 = \sum_{n=1}^{5} \frac{1}{R_n C_a}, \qquad y_1 = \sum_{n=1}^{5} \frac{1}{R'_n C_a}, \tag{B.9}$$

$$x_2 = \sum_{n=5}^{9} \frac{1}{R_n C_a}, \qquad y_2 = \sum_{n=5}^{9} \frac{1}{R'_n C_a}. \tag{B.10}$$

The thermal resistance of each wall/roof R_n is taken from [71], where the product of thermal transmittance or the U-value and the area of each wall/roof is inversely proportional to the thermal resistance as shown in (B.11).

$$R_{n1} = \frac{1}{U_n * (A_n - A_n^w)}, \qquad R_{n2} = \frac{1}{U_n^w * A_n^w}, \tag{B.11}$$

thermal resistances of walls and windows are added in parallel as follows:

$$\frac{1}{R_n} = \frac{1}{R_{n1}} + \frac{1}{R_{n2}}. \tag{B.12}$$

The thermal resistance from the room air to the ambient temperature R'_n was obtained based on [71] in which the coefficient of the inside surface of the wall/roof was divided by the area of each wall/roof.

$$R'_{n1} = \frac{0.13}{A_n - A_n^w}, \qquad R'_{n2} = \frac{0.13}{A_n^w}, \tag{B.13}$$

and their total thermal resistance is shown in (B.14).

$$\frac{1}{R'_n} = \frac{1}{R'_{n1}} + \frac{1}{R'_{n2}}. \tag{B.14}$$

Since [71] can not provide enough information to get the parameters of the thermal capacitance like the number of layers of each wall/roof, the width, the insulating materials, the density etc., assumptions based on specific heat of solids were used for finding the thermal capacitance values. The product of the specific heat capacity, area, width and density of each wall/roof is directly proportional to the thermal capacitance of each wall/roof C_n.

$$C_{n1} = c_p * (A_n - A_n^w) * w * \rho, \qquad C_{n2} = c_p^w * A_n^w * w^w * \rho^w, \tag{B.15}$$

and then the thermal capacitances are added in parallel:

$$C_n = C_{n1} + C_{n2}. \tag{B.16}$$

For the thermal capacitance of the room air C_a, it is directly proportional to the specific heat capacity, density and volume of the room air as illustrated in (B.17). The volume of each room V was calculated based on the dimensions of the rooms (which in this case are identical).

$$C_a = c_p^a * V * \rho^a. \tag{B.17}$$

The input matrix $\boldsymbol{B} \in \mathbb{R}^{\mathbf{11\times 2}}$ and disturbance matrix $\boldsymbol{E} \in \mathbb{R}^{\mathbf{11\times 2}}$ are shown in (B.18). Other parameters like the window area facing south A^w, and the share of the solar radiation (as p) which is directly affecting the walls and rooms are also considered.

$$\boldsymbol{B} = \begin{bmatrix} 0 & 0 \\ 0 & 0 \\ 0 & 0 \\ 0 & 0 \\ 0 & 0 \\ 0 & 0 \\ 0 & 0 \\ 0 & 0 \\ 0 & 0 \\ \frac{1}{C_a} & 0 \\ 0 & \frac{1}{C_a} \end{bmatrix}, \quad \boldsymbol{E} = \begin{bmatrix} 0 & \frac{A_1^w p}{C_a} \\ 0 & \frac{A_2^w p}{C_a} \\ 0 & \frac{A_3^w p}{C_a} \\ 0 & 0 \\ 0 & 0 \\ 0 & 0 \\ 0 & \frac{A_5^w p}{C_a} \\ 0 & \frac{A_6^w p}{C_a} \\ 0 & \frac{A_7^w p}{C_a} \\ x_1 & z_1 \\ x_2 & z_2 \end{bmatrix}, \tag{B.18}$$

x_1 and x_2 were shown in (B.9) and (B.10) are having affect on the ambient temperature T^{Amb}. z_1, and z_2 shown in (B.19), are the summation of the area of the windows with respect to that referred state and the coefficient of the solar radiation p and are hence divided by the thermal capacitance of the room air C_a.

$$z_1 = \sum_{n=1}^{3} \frac{A_n^w(1-p)}{C_a}, \qquad z_2 = \sum_{n=5}^{7} \frac{A_n^w(1-p)}{C_a}. \tag{B.19}$$

In this work, the discrete-time version of MPC is used, hence the continuous-time model is discretized.

B.3. Numerical Results

Since the two rooms are identical, plots for each $T_k^{room_1}$ and $P_{th,k}^{Sh1}$ are only shown. Also, plots for T_k^{Amb} and Φ_k^{Solar} were shown. The total energy consumed per year was 29562.20

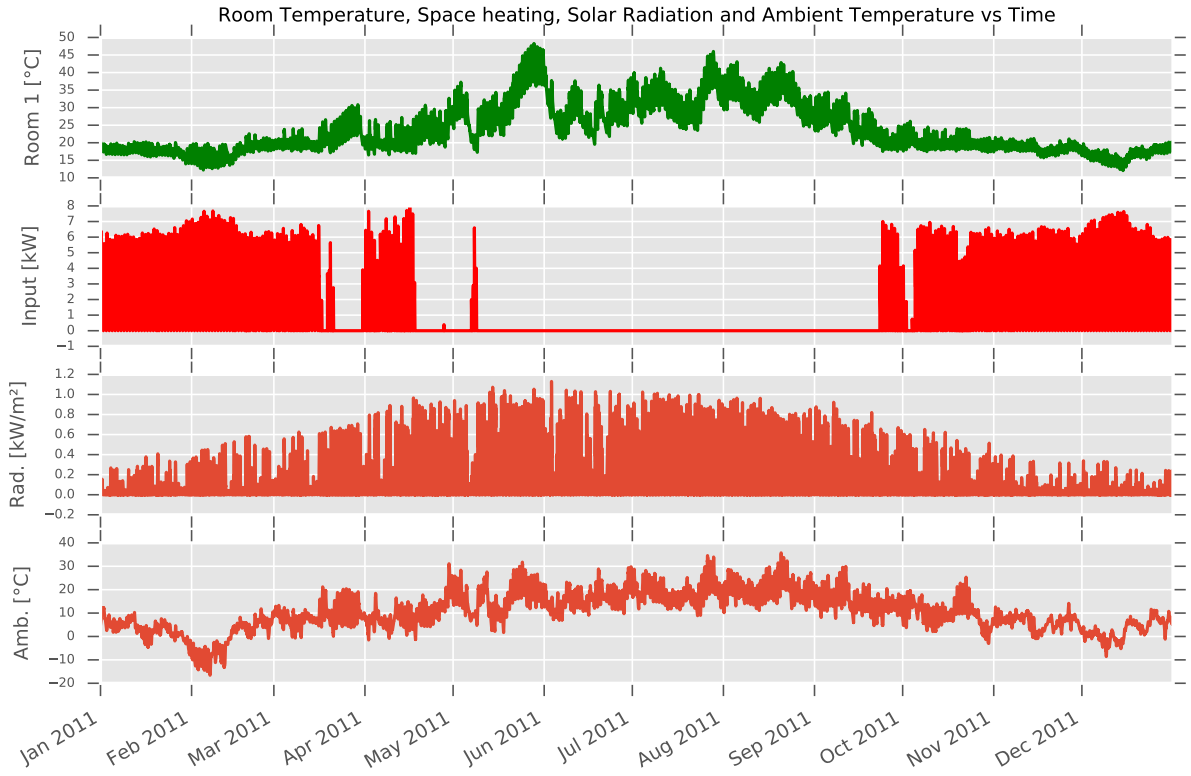

Figure B.2.: One year (Room temperature, Input, Solar radiation and ambient temperature)

kWh, per seven days in winter 1532.42 kWh and per day 178.79 kWh.

B.4. Conclusion

The two rooms building (in this case) were identical. So the trajectories of the room temperature and the space heating system for each room will be the same. For a 140 meter-square area, the total energy shall be close to 21840 kWh for an entire year. The MPC showed a very satisfactory trajectories where it considered real values of disturbances.

From the previously shown results, it was clear that the quadratic optimization problem followed its track well and respected the constraints. Each and every state in the model

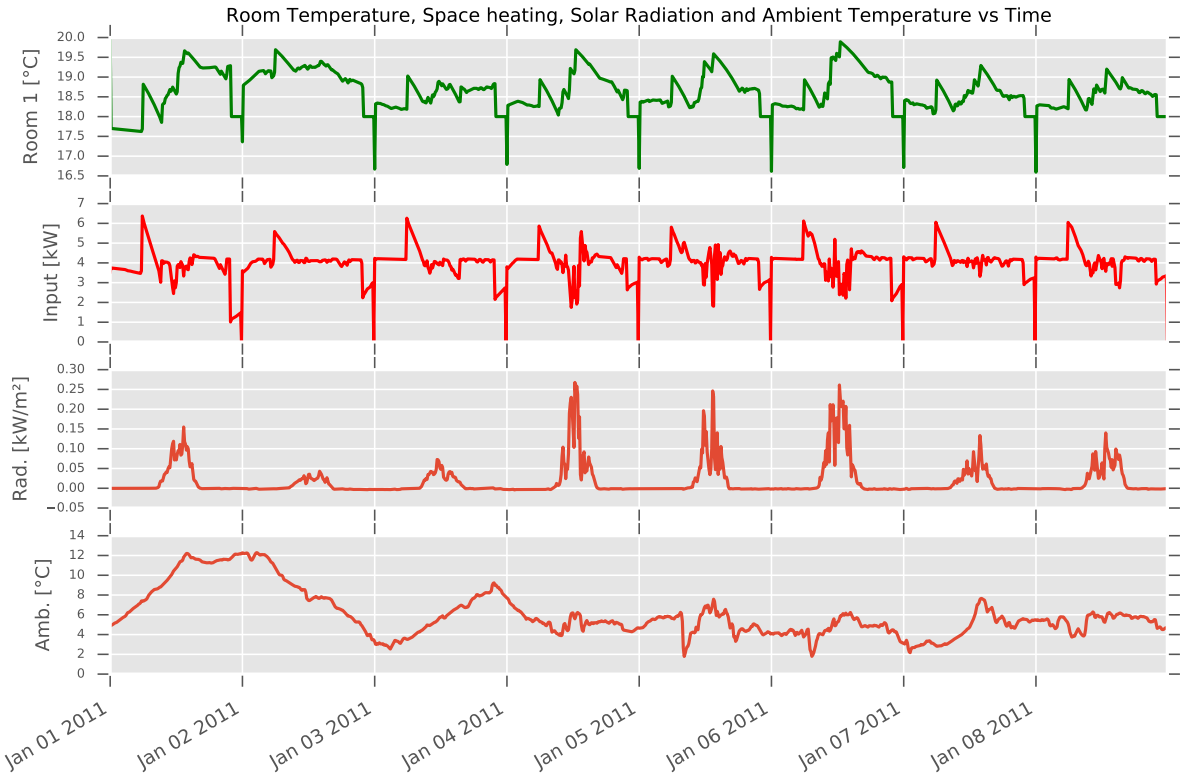

Figure B.3.: Seven days in Winter (Room temperature, Input, Solar radiation and ambient temperature)

such as the walls, roofs and rooms temperature can be estimated and is taken into account while approximating other states. The controlled part, which is the space heating system, maintained to supply room comfort throughout the year and mostly at winter, where the ambient temperature and the solar radiation were so low.

Future work is to consider the floors of the rooms, non-identical rooms for different trajectories, add more rooms and change the heat pump function which supplies the space heating system with thermal energy, in which it will consider the ambient temperature, the inside tank water temperature which will give a varying coefficient of performance. The MPC optimization problem should be updated with the mentioned proposals.

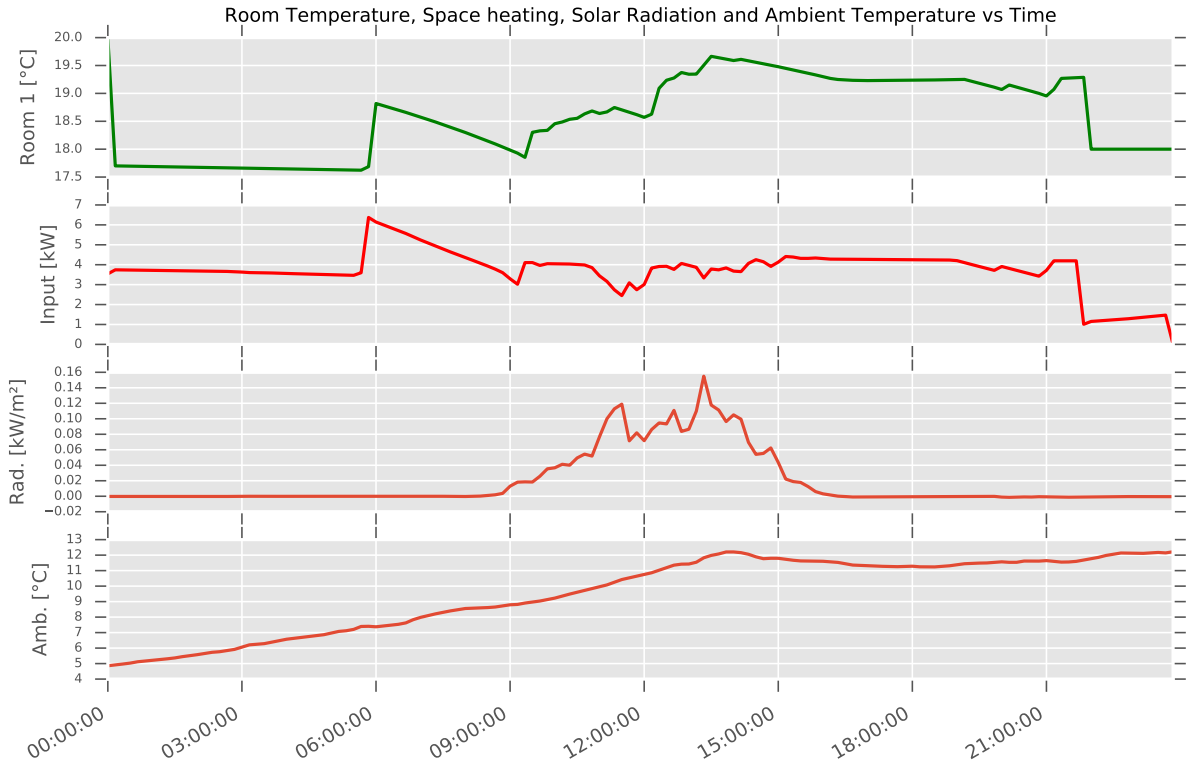

Figure B.4.: One day in Winter (Room temperature, Input, Solar radiation and ambient temperature)

Table B.1.: Nomenclature

Parameter	**Definition**
T^{wall_n}	Temperature of wall n
T^{room_n}	Temperature of room n
T^{roof_n}	Temperature of roof n
P_{th}^{Shn}	Space heating power of room n
Φ_k^{Solar}	Solar radiation
T_k^{Amb}	Ambient temperature
U_n	Thermal transmittance of wall n
U_n^w	Thermal transmittance of window n
A_n	Area of wall n
A_n^w	Area of window n
R_n	Thermal resistance of wall/roof n
R'_n	Thermal resistance of inside surface of wall/roof n
C_n	Thermal capacitance of wall/roof n
C_a	Thermal capacitance of room air n
c_p	Specific heat capacity of wall/roof
c_p^w	Specific heat capacity of window
c_p^a	Specific heat capacity of room air
A_n	Area of wall n
A_n^w	Area of window n
V	Volume of each room
w	Width of wall/roof
w^w	Width of window
ρ	Density of wall/roof
ρ^w	Density of window
ρ^a	Density of room air
p	Solar radiation coefficient

C. Closed-form analytical solution for the $\bar{z}$-update

This appendix elaborates the closed-form analytical solution for the $\bar{\boldsymbol{z}}$-update for the ADMM algorithm presented in Section 5.2. Let the $\bar{\boldsymbol{z}}$-update be defined as:

$$\bar{\boldsymbol{z}} \coloneqq \underset{\bar{\boldsymbol{z}}}{\operatorname{argmin}} \left(g\left(H\bar{\boldsymbol{z}}\right) + \frac{H\rho}{2} \left\| \bar{\boldsymbol{z}} - \boldsymbol{a} - \boldsymbol{b} \right\|_2^2 \right) \tag{C.1}$$

with the vector of variables $\bar{\boldsymbol{z}} \in \boldsymbol{R}^N$, where $\boldsymbol{a} \in \boldsymbol{R}^N$, and $\boldsymbol{b} \in \boldsymbol{R}^N$ are vectors of parameters. For the sake of simplicity, the iterations indices are omitted. The function $g\left(H\bar{\boldsymbol{z}}\right)$ is defined by:

$$g\left(H\bar{\boldsymbol{z}}\right) = \frac{\gamma}{N} \sum_{k=1}^{N} \left(H\bar{z}\left(k\right)\right)^2 \tag{C.2}$$

The objective function in (C.1) can be rewritten as:

$$f\left(\bar{\boldsymbol{z}}\right) = \frac{\gamma}{N} \sum_{k=1}^{N} \left(H\bar{z}\left(k\right)\right)^2 + \frac{H\rho}{2} \sum_{k=1}^{N} \left(\bar{z}\left(k\right) - a\left(k\right) - b\left(k\right)\right)^2 \tag{C.3}$$

The partial derivative of $f\left(\bar{\boldsymbol{z}}\right)$ with respect to $\bar{z}\left(k\right)$ is:

$$\frac{\partial}{\partial \bar{z}\left(k\right)} f\left(\bar{\boldsymbol{z}}\right) = \frac{2\gamma H^2}{N} \bar{z}\left(k\right) + H\rho\left(\bar{z}\left(k\right) - a\left(k\right) - b\left(k\right)\right) \tag{C.4}$$

The minimum value of $f\left(\bar{z}\left(k\right)\right)$ can be found by setting (C.4) to zero:

$$\frac{2\gamma H^2}{N} \bar{z}\left(k\right) + H\rho\bar{z}\left(k\right) - H\rho\left(a\left(k\right) + b\left(k\right)\right) \coloneqq 0 \tag{C.5}$$

Then, the following equality holds for all elements $\bar{z}\left(k\right)$, $a\left(k\right)$ and $b\left(k\right)$:

$$\frac{2\gamma H^2}{N} \bar{z}\left(k\right) + H\rho\bar{z}\left(k\right) = H\rho\left(a\left(k\right) + b\left(k\right)\right) \quad \forall k \in \{1, \ldots, N\}$$

Therefore, in vector notation the closed-form analytical solution for the $\bar{z}$-update can expressed as:

$$\bar{\boldsymbol{z}} = \frac{\rho\left(\boldsymbol{a} + \boldsymbol{b}\right)}{\frac{2\gamma}{N} H + \rho} \tag{C.6}$$

D. Objective gap for ADMM and dual decomposition

This appendix presents detailed results on the convergence comparison between ADMM and dual decomposition discussed in Subsection 5.4.1. Table D.1, Table D.2 and Table D.3 elaborate further on the objective gap for all considered cases. They show the objective gap at some selected iterations for the three cases and each considered scenario (winter, summer, and transitional).

Table D.1.: Objective gap winter

Iteration	$\|p\|^{\text{admm-unrelax}}$	$\|p\|^{\text{admm-relax}}$	$\|p\|^{\text{dual-unrelax}}$
5	12.82	0.63	1497.37
10	6.05	2.47	581.50
50	3.05	3.35	137.19
100	4.28	3.46	88.10
200	1.81	3.51	58.73
500	-	-	42.89
1000	-	-	21.95

Table D.2.: Objective gap summer

Iteration	$\|p\|^{\text{admm-unrelax}}$	$\|p\|^{\text{admm-relax}}$	$\|p\|^{\text{dual-unrelax}}$
5	15.10	3.82	1621.88
10	5.08	3.42	658.45
50	2.76	4.01	120.44
100	2.76	4.08	66.21
200	1.12	4.11	20.99
500	-	-	2.32
1000	-	-	4.89

For all scenarios the relaxed ADMM approach reaches objective convergence around iteration number 10. It is also noticeable, that for this approach the objective gap starts to increase slightly after iteration 10. Therefore, this algorithm should be stopped at this iteration. The relaxed dual decomposition approach shows a poor performance and even after 200 iterations its objective gap is larger than the objective gap reported for the ADMM approaches at iteration number 10. The table also shows that even though the objective gap of ADMM unrelaxed at iteration number 10 is larger than the objective gap of ADMM relaxed, it may be small enough and acceptable for a hierarchical-distributed

Table D.3.: Objective gap transitional

Iteration	$\lvert p\rvert^{\text{admm}-\text{unrelax}}$	$\lvert p\rvert^{\text{admm}-\text{relax}}$	$\lvert p\rvert^{\text{dual}-\text{unrelax}}$
5	4.85	1.56	1365.91
10	3.77	0.26	600.14
50	4.63	0.67	224.03
100	2.74	0.79	163.37
200	5.30	0.85	116.40
500	-	-	78.13
1000	-	-	63.95

MPC application. This issue is further investigated in Section 5.4 taking into account the residual convergence and the dual variable convergence.

E. Primal residual and dual residual open-loop behavior for ADMM approaches

This appendix gives a thoughtful discussion on the results for primal residual and dual residual for the ADMM cases presented in Subsection 5.4.1.

As in real applications for MPC based hierarchical-distributed coordination strategies there is no information regarding the global optimal value, the hierarchical-distributed operation strategy needs a termination condition which does not involve any information about the global optimum, i.e. terminating the algorithm based on the objective gap is not possible. Therefore it is necessary to use the primal residual norm and the dual residual norm described by (5.10) and (5.11) as termination conditions, since they do not rely on information of the global optimal value [81].

Figure E.1 presents the progression of the primal residual norm over iteration count for the ADMM approaches.

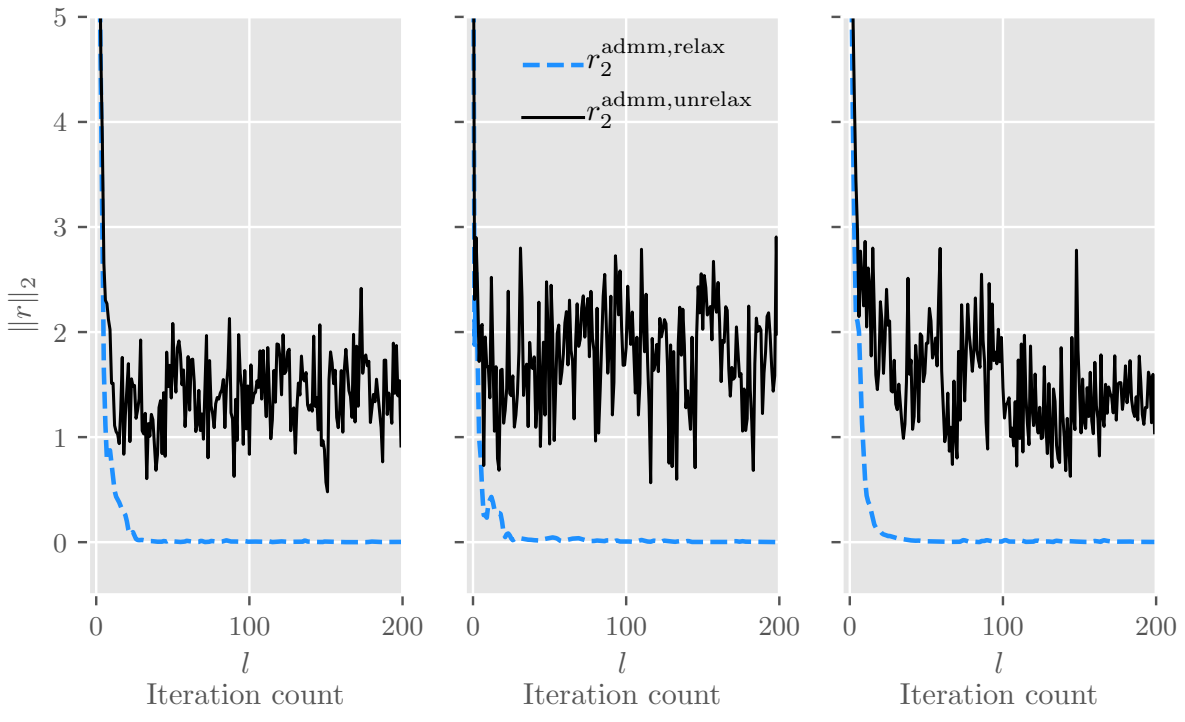

a) Summer b) Transitional c) Winter

Figure E.1.: Primal residual norm

For the relaxed ADMM approach the primal residual norm converges fast to zero, while for the unrelaxed ADMM approach this norm does not show convergence but rather os-

cillates around 1. This implies that the relaxed ADMM approach reaches primal residual convergence and this criterion can be used to stop the algorithm. On the other hand, the unrelaxed ADMM does not meet the primal residual convergence criterion for the considered scenarios and the algorithm has to be stopped after a given maximum number of iterations. Even though the unrelaxed ADMM does not show primal residual convergence, nothing can be said yet regarding the quality of the solution. As the relaxed ADMM is a relaxed version of the original problem and a feasible solution still needs to be recovered, it may happen that the solution from the unrelaxed ADMM approach achieves better results, in terms of objective value, than the recovered solution from the relaxed ADMM approach. This issue is further discussed in Subsection 5.4.1.

In the sequel, Figure E.2 shows the dual residual norm as a function of the iteration count for both ADMM approaches. For the relaxed ADMM approach the dual residual norm rapidly becomes smaller and converges to zero, similar as the primal residual norm. The dual residual norm of the unrelaxed ADMM approach also presents a fast decrease but it does not clearly tends to zero. Nonetheless the values for $\|s\|_2$ could be small enough, such that both approaches might meet the dual variable convergence. This aspect will be further elaborated in the next section.

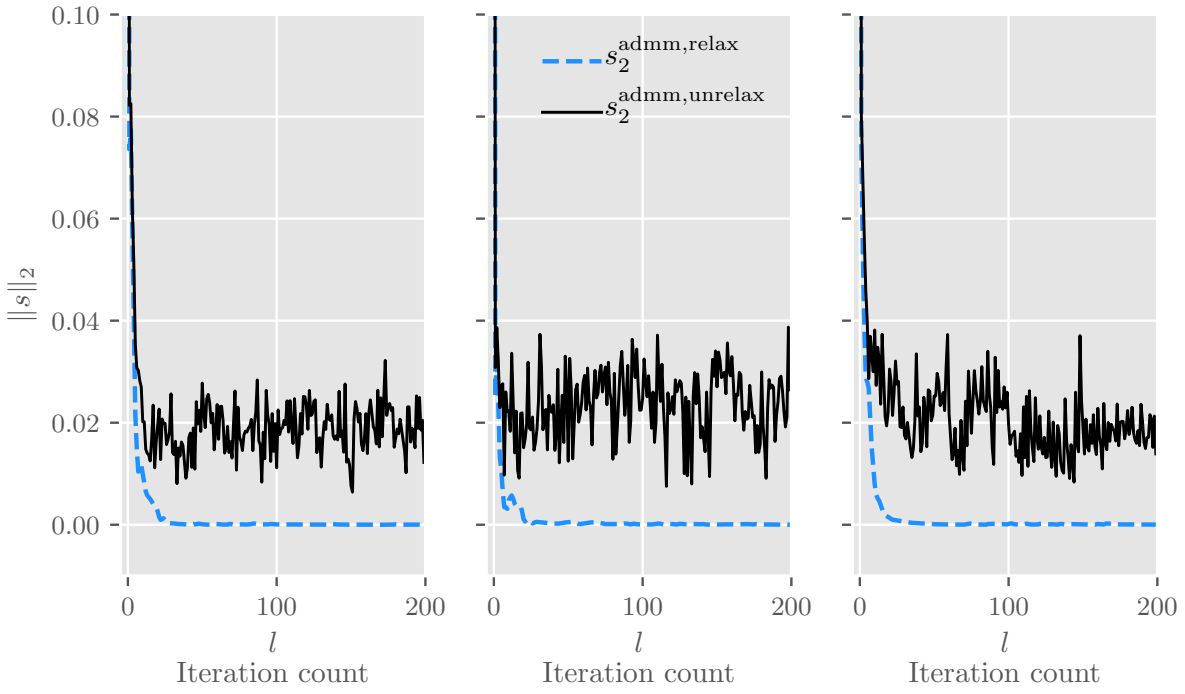

a) Summer b) Transitional c) Winter

Figure E.2.: Dual residual norm

Figure E.3 depicts the resulting power at reference node $\boldsymbol{p}^{\mathrm{G}}$ for relaxed ADMM (black line) and unrelaxed ADMM (dashed blue line). The green line serves as reference denoting the optimal power profile obtained with the centralized coordination strategy, which as

expected, reduces extreme power peaks and improves power balancing between home-microgrids. The figure shows that the relaxed ADMM better fits the optimal power profile at reference node, while the unrelaxed ADMM still presents some minimal peaks below +/- 1 kW_{el}.

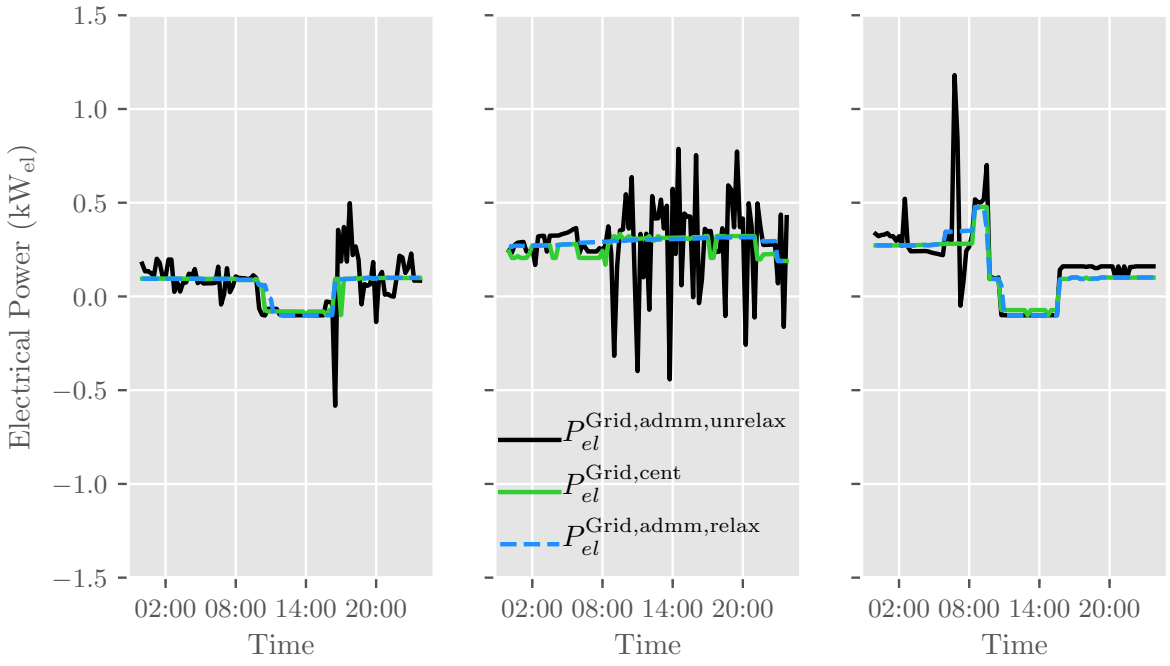

a) Summer b) Transitional c) Winter

Figure E.3.: Power profiles at reference node: relaxed ADMM vs. unrelaxed ADMM

F. Scientific activity record

This appendix lists all publications, bachelor and master thesis that resulted from this research work. The material of the scientific work listed below was (partially) used for this dissertation.

Publications

Journals

1. I. Stoyanova, E. Gümrükcü, G. Aragon, D.I. Hidalgo-Rodríguez, A. Monti, J. Myrzik. "Distributed model predictive control strategies for coordination of electro-thermal devices in a cooperative energy management concept," *Optimal Control Applications and Methods*, vol. 41 (1), pp. 170-189, 2020.
2. T.M. Kneiske, M. Braun, D.I. Hidalgo Rodríguez. "A new combined algorithm for PV-CHP hybrid systems," *Applied Energy*, vol. 210, pp. 964-973, 2018.
3. J. Hinker, C. Hemdkendreis, E. Drewing, S. März, D.I. Hidalgo Rodríguez, J.M.A Myrzik. "A novel conceptual model facilitating the derivation of agent-based models for analyzing socio-technical optimality gaps in the energy domain," *Energy*, vol. 137, pp. 1219-1230, 2017.

Conference papers

1. D.I. Hidalgo Rodríguez, J.M.A. Myrzik. "Optimal Operation of Interconnected Home-Microgrids with Flexbible Thermal Loads: A Comparison of Decentralized, Centralized, and Hierarchical-distributed Model Predictive Control," in *20th Power Systems Computational Conference PSCC*, Dublin-Irland, 2018.
2. D.I. Hidalgo Rodríguez, J.M.A. Myrzik. "Economic Model Predictive Control for Optimal Operation of Home Microgrid with Photovoltaic-Combined Heat and Power Storage Systems," in *Proceedings of the 20th IFAC World Congress*, Toulouse-France, 2017.
3. D.I. Hidalgo Rodríguez, S. Hoffmann, F. Adelt, J.M.A. Myrzik, J. Weyer. "A Socio-Technical Simulation Framework for Collaborative Management in Power Distribution Grids," in *International ETG-Congress 2017: Die Energiewende*, Bonn-Germany, 2017.

4. D.I. Hidalgo Rodríguez, J. Hinker, J. Myrzik."On the Problem Formulation of Model Predictive Control for Demand Response of a Power-to-Heat Home Microgrid," in *19th Power Systems Computational Conference PSCC*, Genoa-Italy, 2016.

5. S. Hoffmann, D.I. Hidalgo Rodríguez, F. Adelt, J. Myrzik, J. Weyer. "Agent-based modelling of the governance of energy transitions," in *International Sustainability Transitions Conference (IST 2016)*, Wuppertal-Germany, 2016.

6. J. Hinker, D.I. Hidalgo Rodríguez, J.M.A. Myrzik, C. Hemkendreis. "A framework for the analysis of societal and energy distribution related interactions in future energy system scenarios," in *11th Conference on Sustainable Development of Energy, Water and Environment Systems (SDEWES 2016)*, Lisbon-Portugal, September 2016.

7. D.I. Hidalgo Rodríguez, L. Spitalny, J. Myrzik and M. Braun."Development of a Control Strategy for Mini CHP Plants for an Active Voltage Management in Low Voltage Networks," in *Proc. 2012 IEEE Innovative Smart Grid Technologies Europe*, Berlin-Germany, 2012.

8. H. Barth, D. Hidalgo, A. Pohlemann, M. Braun, L.H. Hansen and H. Knudsen. "Technical and economical assessment of reactive power provision from distributed generators," in *Proc. 2013 IEEE PowerTech*, Grenoble-France, 2013.

9. A. Kanwar, D.I. Hidalgo Rodríguez, J. von Appen and M. Braun. "A comparative study of optimization- and rule-based control for microgrid operation," in *IEEE PESS*, Dortmund-Germany, 2015.

10. T.M. Kneiske, H. Barth, D. Hidalgo und M. Braun. "Photovoltaik-Wärmepumpen Hybridsysteme," in *VDE Kongress 2012 Smart Grid - Intelligente Energieversorgung der Zukunft*, Stuttgart-Germany, 2012.

11. "Dezentrale Strom- und Wärmespeicherung im Smart Grid," in *FVEE-Jahrestagung*, 2013.

12. "Wärmespeicher: Rolle im Energiesystem der Zukunft," in *FVEE-Jahrestagung*, 2014.

Bachelor and master thesis

1. M. Lüntz. "Wirtschaftliche Optimierung der multimodalen Nutzung von PV-Batterien im Haushalt" (2018); Master thesis Wirtschaftsingenieurwesen.

2. T. Töns. "Optimierung der Leistungsbilanz in Niederspannungsnetzen - eine Vergleichsstudie zwischen einer zentralisiert, hierarchisch-verteilt und dezentral modellprädiktiven Regelungsarchitektur" (2017); Master thesis, Wirtschaftsingenieurwesen.

3. N. Eifert. “Kurzzeitprognoseverfahren der Haushaltslast für lokale Energiemanagementsysteme” (2017); Bachelor thesis, Elektrotechnik und Informationstechnik.
4. D. Hilleringmann. “Bewertung einer netzorientierten Demand Side Management-Strategie von stromgeführten PV-Wärmepumpensystemen in Niederspannungsnetzen” (2016); Bachelor thesis, Wirtschaftsingenieurwesen.
5. C. Hebbeker. “Betriebsführungsstrategien für Strom-Wärmesysteme: Eine Vergleichsstudie zwischen Modellprädiktiver Regelung und regelbasiertem Verfahren” (2016); Bachelor thesis, Wirtschaftsingenieurwesen.

Reviewer activities

- Reviewer for IEEE Transactions on Smart Grid, IEEE Transactions on Power Systems, IEEE Transactions on Sustainable Energy, Automatisierungstechnik, Energy, Applied Energy, IFAC World Congress 2017, and PSCC 2020.